

# **Design and Synthesis of Donor-Acceptor Functionalized Stimuli-Responsive Materials**

**Ph.D. Thesis**

By  
**Ekbote Anupama Vivek**



**DISCIPLINE OF CHEMISTRY  
INDIAN INSTITUTE OF TECHNOLOGY INDORE  
December 2021**



# Design and Synthesis of Donor-Acceptor Functionalized Stimuli-Responsive Materials

**A THESIS**

*Submitted in partial fulfillment of the  
requirements for the award of the degree*

*of*

**DOCTOR OF PHILOSOPHY**

*by*

**Ekbote Anupama Vivek**



**DISCIPLINE OF CHEMISTRY  
INDIAN INSTITUTE OF TECHNOLOGY INDORE**

**December 2021**





# INDIAN INSTITUTE OF TECHNOLOGY INDORE

## CANDIDATE'S DECLARATION

I hereby certify that the work which is being presented in the thesis entitled “**Design and Synthesis of Donor-Acceptor Functionalized Stimuli-Responsive Materials**” in the partial fulfillment of the requirements for the award of the degree of **DOCTOR OF PHILOSOPHY** and submitted in the **DEPARTMENT OF CHEMISTRY, Indian Institute of Technology Indore**, is an authentic record of my own work carried out during the time period from **May 2016** to **December 2021** under the supervision of **Dr. Rajneesh Misra, Professor, Department of Chemistry, IIT Indore**.

The matter presented in this thesis has not been submitted by me for the award of any other degree of this or any other institute.

27/04/2022

**Signature of the student with date  
(EKBOTE ANUPAMA VIVEK)**

-----  
This is to certify that the above statement made by the candidate is correct to the best of my/our knowledge.

27/04/2022

Signature of Thesis Supervisor #1 with date

**(PROF. RAJNEESH MISRA)**

Signature of Thesis Supervisor #2 with date

**(NAME OF THESIS SUPERVISOR)**

-----  
**EKBOTE ANUPAMA VIVEK** has successfully given his Ph.D. Oral Examination held on **27/04/2022**

27/04/2022

Signature of Thesis Supervisor #1 with date

**(PROF. RAJNEESH MISRA)**

Signature of Thesis Supervisor #2 with date

**(NAME OF THESIS SUPERVISOR)**



## ACKNOWLEDGEMENTS

---

---

The work described in this thesis would not have been possible without numerous people who were always there when I required them the most. I take this opportunity to acknowledge them and extend my sincere gratitude for helping me and make this Ph.D. thesis possible.

First and foremost, I would like to express my sincere gratitude to my supervisor Prof. Rajneesh Misra for his continuous support and encouragement during my Ph.D. study and research. I would like to offer my sincere gratitude to him for believing in me from inception to completion and in shaping my career. His dedication, keen interest and above all his overwhelming attitude to help his students has been the solely responsible for completion of my work. He has always guided me to acquire the best out of anything. It's his vigor to perform in adverse situation, which has inspired me to thrive for excellence and nothing less. His exemplary guidance, constant motivation and careful monitoring throughout the journey have helped me greatly in accomplishing this task. I truly dedicate this thesis to him as it would not have been possible without his persistent help, support and kindness.

I express my gratitude to Dr. Shaikh M. Mobin for single crystal X-ray support and his valuable guidance. My sincere thanks also go to my PSPC members Dr. Sanjay Kumar Singh and Dr. Rajesh Kumar for their valuable suggestions and guidance throughout my Ph.D. tenure.

With great respect, I express my sincere thanks and gratitude to Prof. Nilesh Jain [Director (Officiating), Indian Institute of Technology Indore] for his unending support and providing all the facilities at Indian Institute of Technology Indore.

I am grateful to Dr. Biswarup Pathak (Head, Discipline of Chemistry, Indian Institute of Technology Indore) for his suggestions and guidance in various aspects. I am also grateful to Prof. Suman Mukhopadhyay, Dr. Tridib K. Sarma, Dr. Anjan Chakraborty, Dr. Sampak Samanta, Dr. Sanjay Singh, Dr.

Satya Bulusu, Dr. Chelvam Venkatesh, Dr. Amrendra Kumar Singh, Dr. Abhinav Raghuvanshi, Dr. Dipak Kumar Roy, Dr. Selvakumar Sermadurai, Dr. Umesh A. Kshirsagar and Dr. Radhe Shyam Ji for their guidance and help during various activities.

I would like to express my thanks to IIT Indore and Ministry of Human Resource Development (MHRD) for infrastructure and financial help through fellowship.

I would like to acknowledge all my teachers who have taught me in some or the other way since my childhood. I would have never achieved anything without their guidance, blessing and support. I would like to extend my deepest gratitude to Prof. Ashutosh. V. Bedekar, Prof. Neelima D. Kulkarni, Prof. Shailesh R. Shah and Prof. P Padmaja Sudhakar who guided me during my masters and inspired me to pursue a career in research. I would extend my deepest gratitude to Dr. AbdulSajjad Ajmeri for his support and guidance during my M.Sc. dissertation project. I would also like to extend my sincere thanks to Prof. B. V. Kamath, Prof. Prasanna S. Ghalsasi, Prof. Nalini Purohit, Prof. Debjani Chakraborty, Prof. Bhavna M. Trivedi, Prof. Prakash B. Samnani, Prof. Anjali U. Patel, Prof. Shubhangi S. Soman, Dr. Amar Ballabh, Dr. Arpita S. Desai, Dr. Hemant P. Soni and Dr. Vinay K. Singh.

I would also like to thank the technical staff of Sophisticated Instrumentation Center (SIC), IIT Indore, Ms. Sarita Batra, Mr. Kinny Pandey, Mr. Ghanshyam Bhavsar, Dr. Ravinder, Mr. Nitin Upadhyay, Mr. Manish Kushwaha, Mrs. Vinita Kothari and Mr. Rameshwar Dohare for their timely technical support without which it was impossible to continue with my work. I would also like to thank Ms. Anjali Bandiwadekar, Mr. Gati Krishna Nayak, Mr. Rajesh Kumar, Mr. Lala Ram Ahirwar and other library staff and Mr. Prahalad Singh Panwar, Mr. Shailesh Kaushal, Mr. Subha Jana, Mr. Nitin Bhate, and other technical and non-technical staff for their constant help, whenever required.

I owe my deep sense of gratitude to Mr. Kaushik Rajput and Mr. Aditya Puranik for sharing their knowledge and extending constant guidance and motivation during my masters which helped me get through all the competitive exams.

I personally extend my heartiest gratitude to Dr. Thaksen Jadhav, Dr. Bhausahab Dhokale and Dr. Rohit Rai for his constant guidance, help and support in all my ups and downs and during my initial days of the Ph. D. program. I extend my profound thanks to my group members, Dr. Prabhat Gautam, Dr. Ramesh Maragani, Dr. Rekha Sharma, Dr. Yuvraj Patil, Dr. Ramana Reddy Eda, Dr. R. V. Ramana Reddy Dr. Parmeshwar Solanke, Dr. Vijay Singh Parihar, Dr. Gangala Sivakumar, Dr. Shubhra Bikash Maity, Dr. Rami Reddy Eda, Dr. Madhurima Poddar, Dr. Yogajivan Rout, S. Bijesh, Jivan, Manju, Indresh, Faizal, Charu, Dilip, Wazid, Pankaj, Nikhilji, Ramakant, Amit, Nitin Gumber, Vivek, Vinay, Nitin Rajesh, Garima and Renuka for their kind cooperation and cheerful support. for their constant co-operation and help.

It has been wonderful to work with many friends and labmates together during my Ph.D., and I would like to record my thanks to Dr. N. Rajendra, Dr. Bhagwati, Dr. Tamalika, Dr. Shivendra, Dr. Anupam, Dr. Sonam, Dr. Debashish Majee, Dr. Lalit, Dr. Biju, Dr. Pratik, Dr. Meghna, Dr. Aparna, Dr. Suchismita, Dr. Camellia, Dr. Anuradha, Dr. Saptarishi, Dr. Rohit Jadhav, Dr. Pramod Shinde, Dr. Rinki Singh, Dr. Deepika, Dr. Kavita, Dr. Poulami, Dr. Novina, Dr. Priyanka, Dr. Anubha, Dr. Roopali, Dr. Arpan, Dr. Indrani, Dr. Nisha, Dr. Arup, Dr. Kuber, Dr. Preeti, Dr. Neha, Dr. Nishu, Dr. Daisy, Dr. Siddharth, Dr. Soumitra, Dr. Shagufi, Dr. Amit, Dr. Prativa, Ms. Nirali, Ms. Saumya, Mr. Soumya Kanti De, Mr. Mirajjudin, Ms. Richa, Mr. Rahul, Mr. Soumyadeep, Mr. Mahendra, Ms. Bhanu, Mr. Rishi, Mr. Shambhu, Mr. Navdeep, Ms. Ekta, Ms. Neha, Mr. Agnideep, Ms. Isha, Mr. Akshay, Mr. Omkar, Mr. Chinmay, Mr. Suyash, Mr. Rushikesh, Mr. Tirthesh, Ms. Shrayanti, Mr. Kaluram, Mr. Meher, Mr. Laxman, Mr.

Rajesh, Mr. Debanjan, Ms. Ekta Yadav, Ms. Nischal, Ms. Shikha, Mr. Ashwani and Ms. Rajni.

I would also like to extend my heartfelt thanks to Mr. Manojit, Mr. Prashant Mishra, Ms. Varsha Bhardwaj and Ms. Gargi for their timely help and technical support.

I am immensely thankful and obliged to Dr. Chetan Trivedi, Dr. Tushar Mankad, Dr. Shekhar Kulkarni, Dr. Suchitra Nene, Dr. Smita Mhaiskar, Dr. Girish Yeotikar, Dr. Shobha Chamania and Dr. Swati Bansal for their great care and treatment which helped me in my speedy recovery. I would like to express my heart filled thanks to all my friends Ms. Sarehan, Ms. Ankita, Ms. Vatsa, Ms. Puja, Ms. Dharti, Mr. Samrat, Mr. Ankit and Ms. Drashti who relieved me with their fun and love and trusted in me all along. I would also like to thank Late. Mr. Parvinder Singh for his support and guidance.

I thank the Almighty for giving me the strength and patience to work through all these years. My heartfelt regards and gratitude to my family Late Mr. Vishwanath Ekbote, Late Mrs. Shantabai Ekbote, Late Mr. Bhalchandra Garge, Mrs. Shalini Garge, Mr. Suhas Ekbote, Mrs. Meera Ekbote, Late Mr. Datta Ekbote, Mrs. Sunanda Ekbote, Mr. Arun Ekbote, Mrs. Veena Ekbote, Mrs. Jayshri Bakshi, Mrs. Pradnya Joshi, Mr. Uday Garge, Mrs. Madhuri Garge, Late Mrs. Shweta Garge, Mr. Prakash Garge, Mrs. Namrata Kulkarni, Mr. Mayur Kulkarni, and all my lovely cousins Mr. Aditya Ekbote, Mrs. Asavari Oak, Mr. Chinmay Garge, Mr. Viren Garge, Mrs. Pallavi Garge and my sweetest nieces and nephews Aditi, Avani, Arush, Aishwarya, Aditya and Vansh.

No words of thanks can sum up the gratitude that I owe to my father-in-law Mr. Anilkumar Chandratre and mother-in-law Mrs. Vandana Chandratre who extended great support, love and guidance. They always put in their faith in me and helped me patiently in my journey. I am grateful to them for their continuous unparallel love and support always.

My deepest gratitude and heartfelt thanks to my brother Mr. Apoorva Ekbote, my sister-in-law Mrs. Pooja Ekbote and the cutest of all Ms. Anushka Ekbote for their tremendous support and unconditional love. Thank you for believing in me and giving me hope and strength always. You have constantly motivated me to reach my goals and made my days happier.

Finally, my deep and sincere gratitude to the people who mean the most to me my parents and my life partner for their unconditional love and constant support. I am forever grateful to my parents Mr. Vivek Ekbote and Mrs. Kirti Ekbote whose constant love and support kept me motivated and confident. My accomplishments and success are because they believed in me. I am forever indebted to my parents for giving me the opportunities and experience that have made me who I am. Thank you both giving me strength to chase my dream. Lastly, I am grateful to my husband Mr. Krunal Chandratre for his help and support always. He has been a true supporter and has unconditionally loved me during my good and bad times. Thank you for constantly listening to my rant, for believing in me when I was totally uncertain and for being there with me always. This thesis would have never been complete without his optimism and the strength he gave me. No words can express my gratitude and love for you.

**Anupama Ekbote**

**IIT Indore**



**DEDICATED TO  
MY BELOVED PARENTS,  
MY HUSBAND AND MY  
COUNTRY INDIA**

**-Anupama**



## SYNOPSIS

In recent years, the development of luminescent materials which show response to different external stimuli (temperature, pressure, electricity, pH, polarity *etc.*) has gained significant attention considering their utilization in applications such as organic light emitting diodes (OLEDs), information devices, security inks, fluorescent probes, fluorescent sensors, reversible switches, pressure sensors, bioimaging and other optoelectronic devices. Stimuli-responsive materials are new-generation materials which can be constructed by using variety of organic molecules, metal-complexes, metal-organic frameworks and polymeric materials. Mechanochromic materials are stimuli-responsive materials which display reversible changes in their emission on application of mechanical stimuli such as grinding, rubbing, shearing or scratching. In general, majority of the practical applications of stimuli-responsive materials are in the solid state; hence significant amount of solid-state emission is crucial for the design of these materials. The common organic fluorophores such as perylene have been employed in optoelectronic and material devices but their use in the solid-state application is limited due to aggregation caused quenching (ACQ). The organic fluorophores which are often highly emissive in solution state, exhibit ACQ characteristics *i.e.* non-radiative decay of the excited state as an outcome of the extensive  $\pi-\pi$  stacking between the closely lying molecules in the aggregated state. The concept of aggregation-induced emission (AIE) established by Tang *et al.* is beneficial in resolving ACQ and furnishing organic fluorophores with efficient solid-state emission. The AIE luminogens or AIEgens possess a non-planar propeller type structure consisting of rotors attached to a stator that hinder the  $\pi-\pi$  stacking interactions between the molecules on aggregation by the restriction of intramolecular rotations (RIR) resulting in enhanced emission on aggregation or in solid state. The classic examples of AIEgens are tetraphenylethylene (TPE), hexaphenylbenzene (HPB), 9,10-di((E)-styryl)anthracene (DSA) and their functionalized derivatives (Figure 1.).

These AIEgens are non-emissive in solution due to the free rotation of the aromatic rotor rings around the single bond but are highly emissive in solid state *via* RIR. The introduction of AIE active luminogens in conventional organic fluorophores that are usually non-emissive in solid state has proved to be a promising technique for furnishing stimuli responsive materials with efficient solid-state emission. Mechanical stimuli responsive materials or mechanochromic materials usually display physical structural changes such as phase transformation *i.e.* crystalline to amorphous or vice versa or interchange between different crystalline states, E/Z double bond isomerization or conversion between open and closed forms as a response to mechanical force. Reversible mechanochromic behavior is mainly accompanied by morphological transition, changes in molecular conformation and interruption in the molecular stacking interactions. Therefore, subtle changes in the molecular packing and intermolecular interaction by various strategies such as extended  $\pi$  conjugated structures, effective donor-acceptor interaction, inclusion of different substituents (alkyl, aryl, heavy metal or electronegative atoms), positional effects can help in controlling the stimuli-responsive properties. Organic molecules comprising of D-A, D- $\pi$ -A, D-A-D type architecture allow fine tuning of electronic and photophysical properties by use of a variety of donors and acceptors of different strengths. The incorporation of AIE active donors or acceptors render the molecules with conformational flexibility and can function as excellent candidates for design of stimuli-responsive materials suitable for various optoelectronic applications.

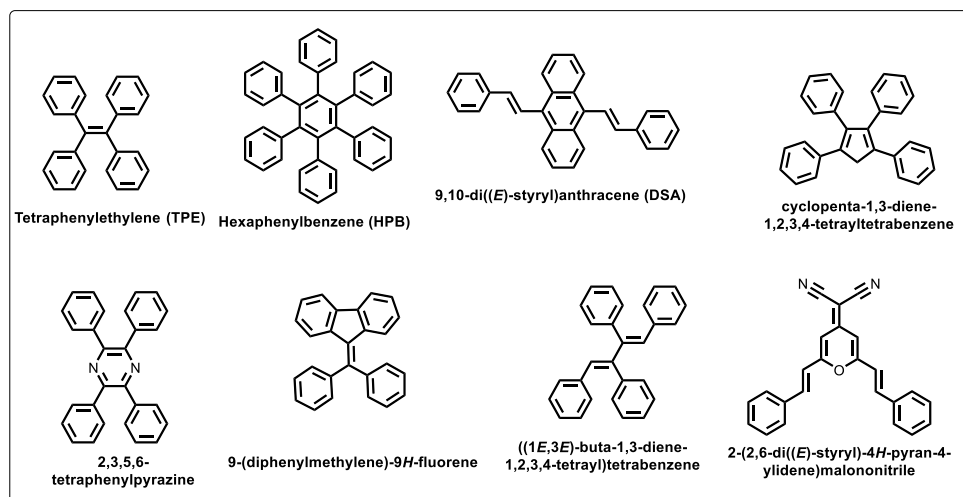


**Figure 1.** Common AIE luminogens and its derivatives.

The following thesis work focuses on the donor-acceptor functionalized luminogens showing stimuli-responsive properties possessing different structures such as D-A, D-A-D, D- $\pi$ -A, D-A-A' encompassing different heterocyclic acceptor moieties (quinoxaline, phenanthroimidazole, benzothiazole and benzothiadiazole) and incorporating AIE active donors like tetraphenylethylene and phenothiazine. The main objectives of this work are as follows:

- To design and synthesize donor-acceptor functionalized organic luminogens exhibiting effective emission in both solution state and solid state.
- To study the AIE, photophysical and stimuli-responsive properties such as solvatochromism, mechanochromism, acidochromism of the designed luminogens using different spectroscopic techniques.
- To explore the effect of use of different donor AIEgens, use of different heterocyclic acceptors to modulate intermolecular interactions, positional isomerism, symmetrical and unsymmetrical substitution on the photophysical, electronic and stimuli-responsive properties.

- To investigate the structural features of the donor and acceptor functionalized luminogens required for inducing stimuli-responsive nature *via* single-crystal X-ray diffraction analysis, powder-X-ray-diffraction analysis and density functional theory (DFT) calculations.

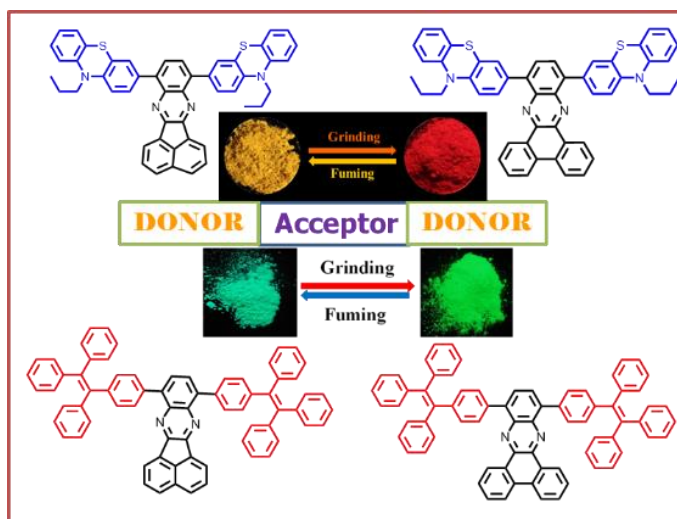
## Chapter 1: Introduction

This chapter discusses about the design strategies for donor-acceptor functionalized stimuli-responsive materials. The chapter also investigates the underlying mechanisms responsible for the stimuli-responsive nature of various materials and their importance in different optoelectronic applications.

## Chapter 2: Materials and experimental techniques

Chapter 2 summarizes the general experimental methods, characterization techniques and details of the instruments used for the characterization.

## Chapter 3: T-shaped donor-acceptor-donor type symmetrical quinoxaline derivatives: Aggregation-induced emission and mechanochromism

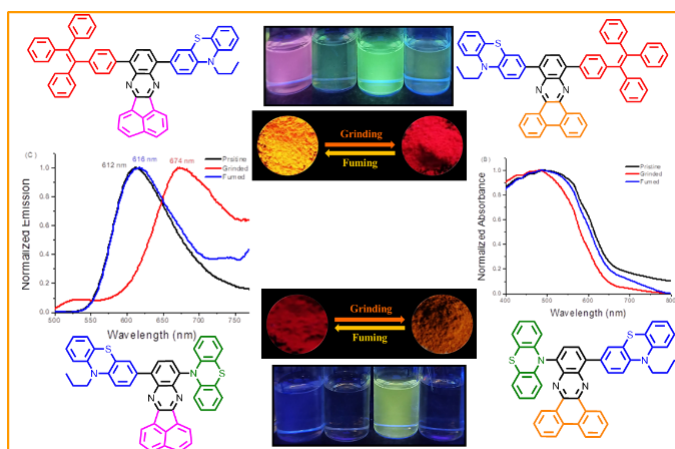


Chapter 3 discusses about the design and synthesis of T-shaped donor-acceptor-donor type phenanthrene-quinoxaline (PQ)-A and acenaphthene-

quinoxaline (AQ)-A' based symmetrical derivatives **PTZ-PQ-PTZ**, **PTZ-AQ-PTZ** and **TPE-PQ-TPE**, **TPE-AQ-TPE** functionalized with phenothiazine (PTZ)-D and tetraphenylethylene (TPE)-D' respectively. The symmetrical quinoxaline derivatives contain two donors TPE and PTZ with contrasting donor character and were synthesized by the Suzuki cross-coupling reaction between TPE/PTZ boronate esters and respective dibromo-quinoxaline derivatives. The effect of substitution of different donors on the solvatochromic, AIE and mechanochromic properties of the symmetrical quinoxaline derivatives were evaluated. The PTZ based symmetrical quinoxaline derivatives **PTZ-PQ-PTZ** and **PTZ-AQ-PTZ** show increased solvent dependent intramolecular charge transfer (ICT) transitions as compared to the TPE derivatives **TPE-PQ-TPE** and **TPE-AQ-TPE** due to the stronger electron-donating nature of PTZ. The symmetrical quinoxaline derivatives **TPE-PQ-TPE**, **TPE-AQ-TPE** and **PTZ-PQ-PTZ**, **PTZ-AQ-PTZ** exhibit strong AIE behaviour due to incorporation of non-planar TPE and PTZ units. The structural features of the quinoxaline derivatives were explored using density functional theory calculation. The PTZ substituted symmetrical quinoxaline derivatives **PTZ-PQ-PTZ** and **PTZ-AQ-PTZ** exhibit reversible mechanochromism between yellow-orange to red colour whereas the TPE substituted quinoxaline derivatives **TPE-PQ-TPE** and **TPE-AQ-TPE** exhibit reversible colour-change from green to yellow and a higher grinding induced spectral shift was observed in PTZ quinoxaline derivatives. The higher conformational flexibility of PTZ in comparison to TPE can account for the increased mechanochromic behaviour of PTZ-quinoxaline derivatives. The powder XRD study of the quinoxaline derivatives reveals that the mechanochromic behaviour is related to a morphological change from crystalline to amorphous. The symmetrical quinoxaline derivatives **TPE-PQ-TPE**, **TPE-AQ-TPE** and **PTZ-PQ-PTZ**, **PTZ-AQ-PTZ** are good solid-state emitters, and the donor-acceptor interaction can be modulated by the use of different donors of contrasting abilities. This work provides

strategy to design stimuli-responsive molecules with distinct properties influenced by donor-acceptor interactions.

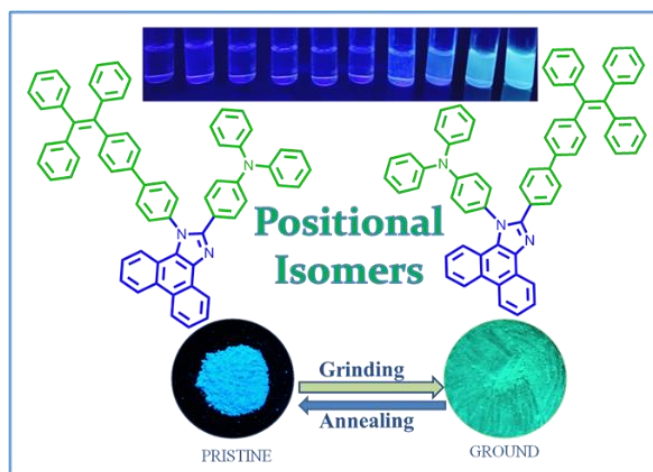
#### Chapter 4: Effect of different donors on mechanochromism of AIE active unsymmetrical D-A-D' type Quinoxaline Derivatives



Chapter 4 summarizes about the design and synthesis of D-A-D'/D-A'-D'' structured unsymmetrical phenanthrene-quinoxaline (**PQ**)-**A** and acenaphthene-quinoxaline (**AQ**)-**A'** derivatives where phenothiazine (PTZ) unit is utilized as donor (D) in combination with tetraphenylethylene (TPE) as donor (D') (**PQ1** and **AQ1**) and N-substituted phenothiazine (N-PTZ) moiety as donor (D'') (**PQ2** and **AQ2**) respectively. The mono-PTZ-substituted bromo intermediate of **PQ** and **AQ** undergoes the Suzuki cross-coupling reaction with TPE boronate ester and Buchwald-Hartwig cross-coupling reaction with PTZ to yield unsymmetrical quinoxaline derivatives **PQ1/AQ1** and **PQ2/AQ2** respectively. The donor-acceptor character of the quinoxaline derivatives can be subtly regulated by unsymmetrical substitution of strong-donor PTZ in combination with donors TPE and N-PTZ and the influence of these structural changes on the photophysical, solvatochromic, AIE and mechanochromic properties have been investigated. The unsymmetrical derivatives show drastic solvatochromic behaviors with highly emissive intramolecular charge transfer (ICT) state in **PQ1** and **AQ1** and quenched twisted intramolecular charge transfer

(TICT) state in **PQ2** and **AQ2** respectively. The unsymmetrical derivatives **PQ1** and **AQ1** incorporating AIEgens PTZ and TPE have efficient solid-state emission and AIE characteristics in contrast to **PQ2** and **AQ2** which are non-emissive in the solid state due to planar N-PTZ moiety. All the unsymmetrical quinoxaline derivatives irrespective of their solid-state emission behavior manifest reversible mechanochromism on application of mechanical stimuli. The reversible mechanochromism involves a phase transformation from crystalline to amorphous which has been studied by powder X-ray diffraction analysis. The presented strategy can help in understanding the influence of different donor-acceptor structures on the AIE and stimuli-responsive characteristics and in further development of donor-acceptor stimuli-responsive materials.

#### **Chapter 5: Stimuli responsive AIE active positional isomers of phenanthroimidazole.**



Chapter 5 discusses about the development of AIE active phenanthroimidazole (PI) based positional isomers **1** and **2** comprising of a triphenylamine (TPA) unit and a tetraphenylethylene (TPE) unit. The positions of triphenylamine (TPA) and tetraphenylethylene (TPE) unit have been interchanged in **1** and **2** and the influence of this change on the AIE and mechanochromism was studied. The phenanthroimidazoles **1** and **2** were synthesized using Suzuki cross-coupling reaction of TPE boronate

ester with iodo-phenanthroimidazoles of TPA and bromo-phenanthroimidazoles of TPA respectively. The PI derivatives **1** and **2** possess significant AIE characteristics by the virtue of propeller orientation of the phenyl rings of the TPE and TPA unit which was further validated by the single crystal X-ray analysis of **1**. Reversible mechanochromism between blue and green color was observed for the phenanthroimidazoles **1** and **2** and the mechanochromic behavior was also studied using the powder X-ray diffraction (PXRD). The PXRD studies demonstrate a phase transition from crystalline to amorphous state associated with the color change. The phenanthroimidazole moiety in combination with TPA and TPE synergistically produces high solid-state emission which can be further employed in optoelectronic applications.

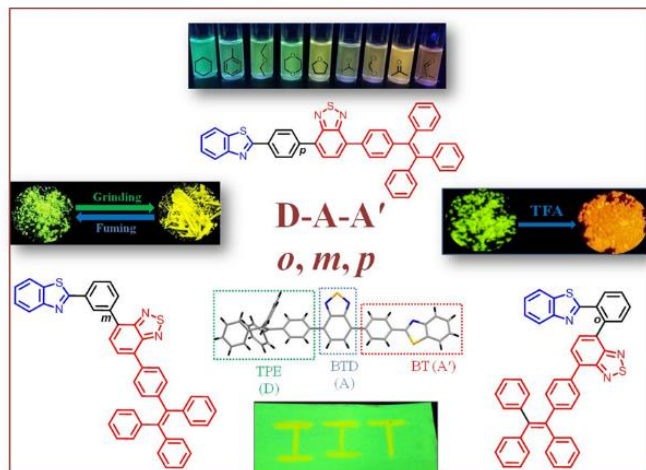
### Chapter 6: Stimuli Responsive Phenothiazine-based Donor-Acceptor Isomers: AIE, Mechanochromism and Polymorphism.



Chapter 6 contributes on the design and synthesis of donor-acceptor (D-A) isomers *p*-PTZ, *m*-PTZ and *o*-PTZ obtained by attaching the phenothiazine (PTZ) moiety at *ortho*, *meta* and *para* positions of the phenyl

benzothiazole (**BT**) unit. This chapter provides in-depth comparison of the structural, photophysical and electronic properties of *p*-**PTZ**, *m*-**PTZ** and *o*-**PTZ** which are influenced as a result of the positional change. The isomers *p*-**PTZ**, *m*-**PTZ** and *o*-**PTZ** were formed by the Suzuki cross-coupling reaction of mono boronate ester of the phenothiazine **PTZ** with corresponding bromo derivatives of phenyl benzothiazole **BT**. The donor-acceptor strength and the molecular packing modes of the isomers can be modulated by attaching the donor **PTZ** at different positions (*para*, *meta* and *ortho*) of the acceptor phenyl **BT** which can result in distinct photophysical and electronic properties. The isomers exhibit contrasting emission properties in different solvents owing to the formation of twisted intramolecular charge transfer (TICT) state. The isomers manifest aggregation-induced emission (AIE) characteristics and reversible mechanofluorochromism (MFC) behavior owing to their twisted structures. The isomers display unique self-reversible color switching mechanism because of the different accessible conformers of **PTZ** moiety. The conformational flexibility of **PTZ** moiety allow the *p*-**PTZ** isomer to occur as polymorphs. The polymorphs of *p*-**PTZ** exhibit structural and morphological difference which were investigated in detail using single crystal X-ray analysis, scanning electron microscopy (SEM) and powder X-ray diffraction (PXRD) studies. The electronic properties of the isomers in ground and excited state were estimated by using the density functional theory (DFT) and time-dependent density function theory (TDDFT) calculations. The isomers were effective in sensing trifluoroacetic acid in solution. The opted design strategy opens possibilities for study of novel stimuli responsive materials.

## Chapter 7: Structure-property relationship in multi-stimuli responsive D-A-A' benzothiazole functionalized isomers.



Chapter 7 discusses about the design and synthesis of multichromophoric D-A-A' positional isomers *p*-BT, *m*-BT and *o*-BT involving benzothiazole (BT)-A', benzothiadiazole (BTD)-A and tetraphenylethylene (TPE)-D formed by incorporating the BTD-TPE moiety at *ortho*, *meta* and *para* positions of the phenyl BT unit. The regio-isomerism in *p*-BT, *m*-BT and *o*-BT is accomplished by exploiting the available *ortho*, *meta* and *para* positions of phenyl BT and allows successful tuning of the acceptor strength and molecular packing. A comparative analysis of the photophysical, AIE and MFC properties of the isomers has been done to investigate the effect of positional change. The *p*-BT and *m*-BT isomers were synthesized by the Suzuki coupling reaction of BTD-TPE with boronate esters of BT; whereas the Stille cross-coupling reaction between stannyl reagent *o*-TBT-BT6 and BTD-TPE was employed for the isomer *o*-BT. The structural aspects of the isomers render molecules with aggregation-induced emission and excellent stimuli-responsive properties such as solvatochromism, mechanochromism, acidochromism, which were studied using emission and absorption spectroscopy. The reversible mechanochromism of the isomers was accompanied by phase transition from crystalline to amorphous and was used to develop rewritable ink free paper. The single crystal X-ray analysis

reveals that the mechanochromism of *p*-BT and *o*-BT synergistically depends on both the flexibility and twisting in the donor and acceptor moieties. The isomers display changes in emission in solution and solid state in response to trifluoroacetic acid. The opted strategy allows modulation of fluorescence properties making them potential stimuli responsive materials with applications in mechano-sensors, security inks and optoelectronic-devices.

### **Chapter 8: Conclusions and Future Scope.**

Chapter 8 summarizes the salient features of the work and provides insights to develop new D-A stimuli responsive materials which can be employed for a wide range of optoelectronic applications.

### **LIST OF PUBLICATIONS**

- [1] **Ekbote, A.**, Mobin, S. M., Misra, R. (2020) Stimuli-responsive phenothiazine-based donor–acceptor isomers: AIE, mechanochromism and polymorphism, *J. Mater. Chem. C*, 8, 3589–3602 (DOI: 10.1039/C9TC05192A)† (Impact Factor = 7.393)
- [2] **Ekbote, A.**, Han, S. H., Jadhav, T., Mobin, S. M., Lee, J. Y., Misra, R. (2018) Stimuli responsive AIE active positional isomers of phenanthroimidazole as non-doped emitters in OLEDs, *J. Mater. Chem. C*, 6, 2077–2087 (DOI:10.1039/C7TC05450E)† (Impact Factor = 7.393)
- [3] **Ekbote, A.**, Mobin, S. M., Misra, R. (2018) Structure–property relationship in multi-stimuli responsive D–A–A' benzothiazole functionalized isomers, *J. Mater. Chem. C*, 6, 10888–10901 (DOI: 10.1039/C8TC04310H)† (Impact Factor = 7.393)
- [4] **Ekbote, A.**, Jadhav, T., Misra, R. (2017) T-Shaped donor–acceptor–donor type tetraphenylethylene substituted quinoxaline derivatives: aggregation-induced emission and mechanochromism. *New J. Chem.*, 41, 9346–9353 (DOI: 10.1039/C7NJ01531C)† (Impact Factor = 3.591)

- [5] Khan, F.,<sup>§</sup> **Ekbote, A.**,<sup>§</sup> Mobin, S. M., Misra, R. (2021) Mechanochromism and Aggregation-Induced Emission in Phenanthroimidazole Derivatives: Role of Positional Change of Different Donors in a Multichromophoric Assembly, *J. Org. Chem.*, 86, 1560–1574 (DOI: 10.1021/acs.joc.0c02404) (Impact Factor = 4.354)
- [6] Rout, Y. **Ekbote, A.**, Misra, R. (2021) Recent development on synthesis, structures and properties of oxidized phenothiazine derivatives, *J. Mater. Chem. C.*, 9, 7508–7531 (DOI: 10.1039/D1TC00695A) (Impact Factor = 7.393)
- [7] Khan, F., **Ekbote, A.**, Misra, R. (2019) Reversible mechanochromism and aggregation induced enhanced emission in phenothiazine substituted tetraphenylethylene, *New J. Chem.*, 43, 16156–16163 (DOI:10.1039/C9NJ03290H) (Impact Factor = 3.591)

†Papers pertaining to the thesis

§Authors having equal contribution.

#### CONFERENCE PRESENTATION

▪ **International:**

- 1) **Ekbote, A.**, Mobin, S. M., Misra, R., Structure–property relationship in multi-stimuli responsive D–A–A' benzothiazole functionalized isomers, Emerging Trends in Chemistry 2019, IIT Indore, India, (12<sup>th</sup>-15<sup>th</sup> July, 2019); Poster Presented.



## TABLE OF CONTENTS

<b>1. List of Figures</b>	xxvi
<b>2. List of Schemes</b>	xxxv
<b>3. List of Tables</b>	xxxvii
<b>4. List of Charts</b>	xxxviii
<b>5. Acronyms</b>	xxxix
<b>6. Nomenclature</b>	xi

### **Chapter 1: Introduction**

1.1.	Background	1
1.2.	Aggregation-induced emission	7
1.3.	Aggregation-induced emission type luminogens	10
1.4.	Tetraphenylethylene	12
1.5.	Phenothiazine	15
1.6.	Stimuli-responsive materials	16
1.6.1.	Mechanochromic materials	17
1.7.	Organization of thesis	22
1.8.	References	24

### **Chapter 2: Materials and experimental techniques**

2.1.	Introduction	55
2.2.	Chemicals for synthesis	55
2.3.	Spectroscopic measurements	56
2.3.1.	Mass spectrometry	56
2.3.2.	NMR spectroscopy	56
2.3.3.	UV–vis spectroscopy	56
2.3.4.	Fluorescence spectroscopy	56
2.4.	Electrochemical studies	57
2.5.	Single crystal X-ray diffraction studies	57
2.6.	Powder XRD (PXRD)	58
2.7.	Computational calculations	58

2.8.	Scanning electron microscopy (SEM)	58
2.9.	Thermogravimetric analysis (TGA)	58
2.10.	Dynamic light scattering (DLS)	58
2.11.	Mechanochromism study	58
2.12.	References	59
<b>Chapter 3:</b>	<b>T-shaped donor-acceptor-donor symmetrical quinoxaline derivatives: aggregation-induced emission and mechanochromism</b>	
3.1.	Introduction	61
3.2.	Results and discussions	63
3.3.	Photophysical properties	64
3.4.	Theoretical Calculations	66
3.5.	Solvatochromism	68
3.6.	Aggregation-induced emission (AIE) studies	72
3.7.	Mechanochromism	75
3.8.	Powder X-ray diffraction studies	77
3.9.	Experimental section	78
3.10.	Conclusion	81
3.11.	References	82
<b>Chapter 4:</b>	<b>Effect of different donors on mechanochromism of AIE active unsymmetrical D-A-D' type quinoxaline derivatives</b>	
4.1.	Introduction	93
4.2.	Results and discussion	96
4.3.	Photophysical properties	98
4.4.	Theoretical studies	101
4.5.	Solvatochromism	103
4.6.	Aggregation-induced emission studies	107
4.7.	Mechanochromism	110

4.8.	Powder X-ray diffraction studies	113
4.9.	Experimental section	115
4.10.	Conclusion	120
4.11.	References	121

**Chapter 5: Stimuli responsive AIE active positional isomers of phenanthroimidazole**

5.1.	Introduction	135
5.2.	Results and discussion	137
5.3.	Thermal analysis	139
5.4.	Photophysical properties	140
5.5.	Solvatochromism	141
5.6.	Aggregation-induced emission	142
5.7.	Mechanochromism	145
5.8.	Powder X-ray diffraction studies	148
5.9.	Single crystal X-ray analysis	148
5.10.	Theoretical calculations	152
5.11.	Electrochemical studies	153
5.12.	Experimental details	154
5.13.	Conclusion	157
5.14.	References	158

**Chapter 6: Stimuli-responsive phenothiazine-based donor-acceptor isomers: AIE, mechanochromism and polymorphism**

6.1.	Introduction	171
6.2.	Results and discussion	173
6.3.	Photophysical Properties	175
6.4.	Solvatochromism	176
6.5.	Aggregation-induced emission	180
6.6.	Single crystal X-ray analysis	182
6.7.	Mechanochromism	190
6.8.	Powder X-ray diffraction studies	193

6.9.	Acidochromism	195
6.10.	Density functional theory calculations	196
6.11.	Experimental details	197
6.12.	Conclusion	200
6.13.	References	201

**Chapter 7: Structure-property relationship in multi-stimuli responsive D-A-A' benzothiazole functionalized isomers**

7.1.	Introduction	217
7.2.	Results and discussions	219
7.3.	Thermogravimetric analysis	221
7.4.	Photophysical properties	222
7.5.	Density functional theory calculations	223
7.6.	Electrochemical properties	225
7.7.	Solvatochromism	226
7.8.	Aggregation-induced emission	228
7.9.	Single crystal X-ray analysis	232
7.10.	Mechanochromism	238
7.11.	Powder X-ray diffraction studies	241
7.12.	Structure-property relationship	243
7.13.	Acidochromism	244
7.14.	Experimental details	246
7.15.	Conclusion	249
7.16.	References	251

**Chapter 8: Conclusions and future scope**

8.1.	Conclusions	267
8.2.	Future scope	272
8.3.	References	272

## LIST OF FIGURES

### Chapter 1. Introduction

- Figure 1.1.** Schematic representation of frontier orbitals and intramolecular charge transfer in donor-acceptor molecules. 3
- Figure 1.2.** Schematic representation of ACQ effect in perylene molecules. 6
- Figure 1.3.** Schematic presentation of mechanism involving AIE as restricted intramolecular rotation in hexaphenylsilole (HPS) luminogen. 7
- Figure 1.4.** Fluorescence photographs of HPS in acetonitrile/water mixtures with different water fractions. 9
- Figure 1.5.** Schematic presentation of mechanism involving AIE as restricted intramolecular vibration in 10,10',11,11'-tetrahydro-5,5'-bidibenzo[a,d][7]annulenyliene (THBA) luminogens. 10
- Figure 1.6.** Structure of tetraphenylethylene. 12
- Figure 1.7.** Structure of phenothiazine. 15
- Figure 1.8.** Chemical structure of triazole-pyrimidine-phenoxazine based mechanochromic materials **1-3** and solid-state emission spectra of pristine, ground, fumed and heated forms of **1-3**. 19
- Figure 1.9.** Chemical structure of D-A TADF-mechanochromic emitters **4-6**. PL spectra of pristine and ground form of (a) **4**, (b) **5** and (c) **6** and PL decay measurements of pristine and ground forms of (d) **4**, (e) **5** and (f) **6**. 21

**Chapter 3: T-shaped donor-acceptor-donor type symmetrical quinoxaline derivatives: aggregation-induced emission and mechanochromism**

**Figure 3.1.** (A) Electronic absorption spectra and (B) normalized fluorescence spectra of **PTZ-PQ-PTZ**, **PTZ-AQ-PTZ**, **TPE-PQ-TPE** and **TPE-AQ-TPE** recorded in THF (concentration =  $2 \times 10^{-5}$  M).

65

**Figure 3.2.** Correlation diagram showing the HOMO, and LUMO wave functions and energies of symmetrical quinoxaline derivatives as determined at the B3LYP/6-31G(d,p) level.

67

**Figure 3.3.** (A) Fluorescence spectra of (A) **PTZ-PQ-PTZ**, (B) **PTZ-AQ-PTZ**, (C) **TPE-PQ-TPE** and (D) **TPE-AQ-TPE** in different solvents of varying polarities. ( $\lambda_{\text{exc}} = 370$  nm-**TPE-PQ-TPE**, **TPE-AQ-TPE**,  $\lambda_{\text{exc}} = 420$  nm-**PTZ-PQ-PTZ**, **PTZ-AQ-PTZ**).

69

**Figure 3.4.** Electronic absorption spectra of ((A) **PTZ-PQ-PTZ**, (B) **PTZ-AQ-PTZ**, (C) **TPE-PQ-TPE** and (D) **TPE-AQ-TPE** in solvents of different polarity.

70

**Figure 3.5.** Photographs of **PTZ-PQ-PTZ**, **PTZ-AQ-PTZ**, **TPE-PQ-TPE** and **TPE-AQ-TPE** in solvents of different polarity taken under 365nm UV illumination. (Toluene, THF, Chloroform, DCM).

71

**Figure 3.6.** Emission spectra of (A) **PTZ-PQ-PTZ**, (B) **PTZ-AQ-PTZ**, (C) **TPE-PQ-TPE** and (D) **TPE-AQ-TPE** in THF-water mixtures with increasing water fractions. (conc.  $2 \times 10^{-5}$  M).

72

**Figure 3.7.** Electronic absorption spectra of (A) **PTZ-PQ-PTZ**, (B) **PTZ-AQ-PTZ**, (C) **TPE-PQ-TPE** and (D) **TPE-AQ-TPE** in different THF-water mixtures with increasing water percentage. (conc.  $2 \times 10^{-5}$  M).

74

**Figure 3.8.** Photographs of **PTZ-PQ-PTZ**, **PTZ-AQ-PTZ**, **TPE-PQ-TPE** and **TPE-AQ-TPE** in different THF-water mixtures taken under 365nm UV illumination.

74

**Figure 3.9.** Emission spectra of (A) **PTZ-PQ-PTZ**, (B) **PTZ-AQ-PTZ**, (C) **TPE-PQ-TPE** and (D) **TPE-AQ-TPE** as pristine, ground, and fumed solids and photograph taken under 365 nm UV illuminations.

76

**Figure 3.10.** PXRD curves of (A) **PTZ-PQ-PTZ**, (B) **PTZ-AQ-PTZ**, (C) **TPE-PQ-TPE** and (D) **TPE-AQ-TPE** in pristine, ground, and fumed forms.

78

**Chapter 4: Effect of different donors on mechanochromism of AIE active unsymmetrical D-A-D' type quinoxaline derivatives**

**Figure 4.1.** Electronic absorption spectra (A) and normalized emission spectra (B) of unsymmetrical quinoxaline derivatives **PQ1**, **PQ2**, **AQ1** and **AQ2** measured in THF ( $2 \times 10^{-5}$  M).

99

- Figure 4.2.** Energy level diagram illustrating the HOMO and LUMO energy levels of **PQ1**, **PQ2**, **AQ1** and **AQ2** determined at the B3LYP/6-31G+(d,p) level. 101
- Figure 4.3.** Emission spectra of (A) **PQ1**, (B) **PQ2**, (C) **AQ1** and (D) **AQ2** in solvents of different polarity. ( $\lambda_{exc} = 420\text{nm}$ ). 104
- Figure 4.4.** Electronic absorption spectra of (A) **PQ1**, (B) **PQ2**, (C) **AQ1** and (D) **AQ2** in solvents of different polarity. 106
- Figure 4.5.** Photographs of **PQ1**, **PQ2**, **AQ1** and **AQ2** in solvents of different polarity taken under 365nm UV illumination. (Toluene, THF, Chloroform, DCM). 107
- Figure 4.6.** Emission spectra of (A) **PQ1**, (B) **PQ2**, (C) **AQ1** and (D) **AQ2** in THF-water mixtures with increasing water fractions. (conc.  $2 \times 10^{-5}$  M). 108
- Figure 4.7.** Electronic absorption spectra of (A) **PQ1**, (B) **PQ2**, (C) **AQ1** and (D) **AQ2** in different THF-water mixtures with increasing water percentage. 109
- Figure 4.8.** Photographs of **PQ1**, **PQ2**, **AQ1** and **AQ2** in different THF-water mixtures taken under 365nm UV illumination. 110
- Figure 4.9.** Solid-state emission spectra of the pristine, grinded and fumed forms of (A) **PQ1** and (B) **AQ1**. ( $\lambda_{exc}=420$  nm). 111
- Figure 4.10.** Solid-state emission spectra of pristine and grinded forms of (A) **PQ2** and (B) **AQ2**. ( $\lambda_{exc}=420$  nm). 111
- Figure 4.11.** Solid-state absorption spectra of (A) **PQ2** and (B) **AQ2** in its pristine, grinded and fumed forms. 112
- Figure 4.12.** PXRD patterns of pristine, grinded and fumed solids of (A) **PQ1**, (B) **PQ2**, (C) **AQ1** and (D) **AQ2**. 114

**Chapter 5: Stimuli responsive AIE active positional isomers of phenanthroimidazole**

- Figure 5.1.** Chemical structure of phenanthroimidazole. 136
- Figure 5.2.** Thermogravimetric analysis (A) and differential scanning calorimetry (B) curves of luminophores **1** and **2**. 139
- Figure 5.3.** Electronic absorption spectra of **1** and **2** (A) and normalized fluorescence spectra of **1** and **2** (B) recorded in THF (concentration =  $2 \times 10^{-5}$  M). 140
- Figure 5.4.** (A) Fluorescence spectra of **1** (A) and **2** (B) in different solvents of varying polarities. (excitation wavelength or  $\lambda_{\text{ex}}$  = 340 nm). 141
- Figure 5.5.** UV-vis absorption spectra of **1** (A) and **2** (B) in different solvents of varying polarities. 141
- Figure 5.6.** Fluorescence spectra of **1** (A) and **2** (B) in THF–water mixtures with different water fractions (10  $\mu\text{M}$ ). (C) Plot of intensity vs % of water fraction ( $f_w$ ). Luminogen concentration: 10  $\mu\text{M}$ ; intensity calculated at  $\lambda_{\text{max}}$ . 143
- Figure 5.7.** Emission spectra of **1** and **2** at 90% THF-water mixture. 144
- Figure 5.8.** UV-vis absorption spectra of **1** (A) and **2** (B) in THF–water mixtures with different water fractions. 145
- Figure 5.9.** Photograph of **1** (A) and **2** (B) in THF–water mixtures with different water fractions (10  $\mu\text{M}$ ) under 365 nm UV illumination (0% to 90% water fraction from left to right). 145
- Figure 5.10.** Emission spectra of **1** (A) and **2** (B) as pristine, ground, and annealed solids. 146
- Figure 5.11.** Photograph of **1** (A) and **2** (B) as pristine, ground, and annealed solids taken under 365 nm UV illumination. 147
- Figure 5.12.** Powder X-ray diffraction curves of **1** (A) and **2** (B) in pristine, grinded and annealed forms. 148

- Figure 5.13.** (A) Crystal structure of phenanthroimidazole **1**. (B) Packing diagram of phenanthroimidazole **1**. (C) Crystal structure of intermediate **3**. (D) Crystal structure of intermediate **4**. 149
- Figure 5.14.** Correlation diagram showing the optimized structures, HOMO and LUMO wave functions and energies of **1** (left) and **2** (right), as determined at the B3LYP/6-31G(d,p) level. 152
- Figure 5.15.** Cyclic voltammetry (CV) plots of **1**(A) and **2**(B). 154
- Chapter 6: Stimuli-responsive phenothiazine-based donor-acceptor isomers: AIE, mechanochromism and polymorphism**
- Figure 6.1.** Electronic absorption spectra (A) and normalized emission spectra (B) of isomers *p*-PTZ, *m*-PTZ and *o*-PTZ measured in chloroform ( $2 \times 10^{-5}$  M). 175
- Figure 6.2.** Emission spectra of (A) *p*-PTZ, (B) *m*-PTZ and (C) *o*-PTZ in solvents of varying polarity. ( $\lambda_{exc} = 370\text{nm}$ ) (Photographs taken under 365 nm UV illumination). 177
- Figure 6.3.** Electronic absorption spectra of (A) *p*-PTZ, (B) *m*-PTZ and (C) *o*-PTZ in solvents of various polarity. 179
- Figure 6.4.** Emission spectra of (A) *p*-PTZ, (B) *m*-PTZ and (C) *o*-PTZ in DMSO-water mixtures with different water fractions. (Luminogen conc.  $2 \times 10^{-5}$  M) (D) Plot of intensity vs water fraction; intensity calculated at  $\lambda_{max}$  ( $\lambda_{max}$  with highest intensity considered for calculation). 181
- Figure 6.5.** Photographs of *p*-PTZ, *m*-PTZ and *o*-PTZ in THF–water mixtures with different water fractions (10  $\mu\text{M}$ ) under 365 nm UV illumination. 182
- Figure 6.6.** (A) Crystal structures of polymorphs *p*-PTZ GC and *p*-PTZ YC in its different confirmations, Crystal packing diagram and the intermolecular interactions of (B) *p*-PTZ

GC and (C) *p*-PTZ YC. 183

**Figure 6.7.** Crystal packing diagram of (A) *p*-PTZ GC and (B) *p*-PTZ YC. 184

**Figure 6.8.** (A) Crystal structure of *m*-PTZ and (B) crystal packing diagram of *m*-PTZ depicting the intermolecular interactions. 185

**Figure 6.9.** (A) Crystal structure of *o*-PTZ and (B) crystal packing diagram of *o*-PTZ depicting the intermolecular interactions. 186

**Figure 6.10.** Crystal packing diagram of (A) *m*-PTZ and (B) *o*-PTZ. 187

**Figure 6.11.** SEM images of the polymorphs (A) *p*-PTZ GC and (B) *p*-PTZ YC. 188

**Figure 6.12.** Solid-state emission spectra of (A) *p*-PTZ and its polymorphs (*p*-PTZ GC and *p*-PTZ YC), (B) *p*-PTZ, (C) *m*-PTZ and (D) *o*-PTZ as their pristine, grinded, fumed and self-reversible solids and photographs taken under 365 nm UV illumination. 190

**Figure 6.13.** Repeated switching of the solid-state fluorescence of (A) *p*-PTZ in its intermediate and strongly grinded state and (B) *p*-PTZ, (C) *m*-PTZ and (D) *o*-PTZ by repeated grinding and fuming cycles. 192

**Figure 6.14.** PXRD patterns of (A) *p*-PTZ pristine and its polymorphs *p*-PTZ GC and *p*-PTZ YC and (B) *p*-PTZ, (C) *m*-PTZ and (D) *o*-PTZ in its pristine, grinded and fumed forms. 194

**Figure 6.15.** Emission spectra of (A) *p*-PTZ, (B) *m*-PTZ and (C) *o*-PTZ in CHCl<sub>3</sub> on titration with known amounts of TFA (10 μL-

100 $\mu$ L), (Conc.  $2 \times 10^{-5}$  M). (D) Emission photographs of *p*-PTZ, *m*-PTZ and *o*-PTZ in response to TFA.

195

**Figure 6.16.** Energy level diagram showing the HOMO and LUMO energy levels of *p*-PTZ, *m*-PTZ and *o*-PTZ as determined at the B3LYP/6-31G +(d,p) level and their optimized structures.

196

### **Chapter 7: Structure-property relationship in multi-stimuli responsive D-A-A' benzothiazole functionalized isomers**

**Figure 7.1.** TGA curves of *p*-BT, *m*-BT and *o*-BT at a heating rate of 10° C min<sup>-1</sup> under a nitrogen atmosphere.

222

**Figure 7.2.** (A) UV-vis absorption spectra and (B) normalized emission spectra of *p*-BT, *m*-BT and *o*-BT in THF ( $2 \times 10^{-5}$  M).

222

**Figure 7.3.** Energy level diagram showing the HOMO and LUMO energy levels of *p*-BT, *m*-BT and *o*-BT as determined at the B3LYP/6-31G(d,p) level.

224

**Figure 7.4.** Cyclic voltammetry (CV) plots of (A) *p*-BT, (B) *m*-BT and (C) *o*-BT.

225

**Figure 7.5.** Emission spectra of the isomers (A) *p*-BT, (B) *m*-BT and (C) *o*-BT (excitation wavelength or  $\lambda_{\text{ex}}=370$  nm) in solvents of different polarities. (Photographs taken under 365 nm illumination.)

226

**Figure 7.6.** Electronic absorption spectra of the isomers (A) *p*-BT, (B) *m*-BT and (C) *o*-BT (excitation wavelength or  $\lambda_{\text{ex}}=370$  nm) in solvents of different polarities.

227

**Figure 7.7.** Emission spectra of (A) *p*-BT, (B) *m*-BT and (C) *o*-BT in DMF-water mixtures (0%–90% water), (D) Plot of

fluorescence intensity vs. % of water fraction ( $f_w$ ).  
Luminogen concentration: 10  $\mu\text{M}$ ; intensity calculated at  
 $\lambda_{\text{max}}$ . 230

**Figure 7.8.** Electronic absorption spectra of (A) *p*-BT, (B) *m*-BT and  
(C) *o*-BT in DMF-water mixtures (0% to 90% water),  
Luminogen concentration: 10  $\mu\text{M}$ ; intensity calculated at  
 $\lambda_{\text{max}}$ . 231

**Figure 7.9.** Photograph of (A) *p*-BT, (B) *m*-BT and (C) *o*-BT in THF–  
water mixtures with different water fractions (10  $\mu\text{M}$ ) (0%  
water to 90% water from left to right) under 365 nm UV  
illumination. 231

**Figure 7.10.** Crystal structure of *p*-BT 1 and *p*-BT 2; (A) Intermolecular  
interactions in (C-H $\cdots\pi$  depicted by red centroid, N $\cdots\pi$  and  
S $\cdots\pi$  depicted by yellow centroid) in the crystal packing  
diagram of *p*-BT 1 (1-D ladder), (B) Intermolecular  
interactions (C-H $\cdots\pi$  depicted by red and yellow centroid,  
N $\cdots\pi$  and S $\cdots\pi$  depicted by blue centroid, C-H $\cdots$ N weak  
hydrogen bonding interactions depicted by purple lines) in  
the crystal packing diagram of *p*-BT 2 (2-D framework). 232

**Figure 7.11.** (A) Crystal structure of *o*-BT. (B) Crystal packing diagram  
of *o*-BT (anti-parallel arrangement and 3-D framework) (C)  
Intermolecular interactions (C-H $\cdots\pi$  depicted by red  
centroid and green line, C-H $\cdots$ N weak hydrogen bonding  
interactions depicted by purple lines) in the crystal packing  
diagram of *o*-BT. 233

**Figure 7.12.** Unit cell diagrams for the crystal of (A) *p*-BT 1, (B) *p*-BT 2  
and (C) *o*-BT. 234

**Figure 7.13.** Crystal packing diagram of *p*-BT 1 (A) side view and (B)  
top view. 235

- Figure 7.14.** Crystal packing diagram of *p*-BT 2 (A) side view and (B) top view. 236
- Figure 7.15.** Crystal packing diagram of *o*-BT (A) top view and (B) side view. 236
- Figure 7.16.** Solid-state emission spectra of pristine, grinded and fumed solids of (A) *p*-BT 1 and *p*-BT 2, (B) *m*-BT and (C) *o*-BT (D) writing and erasing on a filter paper coated with *p*-BT, illustrating ink free rewritable system. (Photographs taken under 365 nm UV light) (Inset: Pristine crystals *p*-BT 1 and *p*-BT 2). 239
- Figure 7.17.** Repeated switching of the solid-state fluorescence of *p*-BT by repeated grinding and fuming cycles. 240
- Figure 7.18.** PXRD patterns of pristine, grinded and fumed solids of ((A) *p*-BT 1 and *p*-BT 2, (B) *m*-BT and (C) *o*-BT, (E) Fumed patterns of *p*-BT 1 and *p*-BT 2. 241
- Figure 7.19.** Schematic diagram for measurement of dihedral angles. 243
- Figure 7.20.** Emission spectra of (A) *p*-BT, (B) *m*-BT and (C) *o*-BT in response to known amounts of TFA in CHCl<sub>3</sub>. (Conc. 2×10<sup>-5</sup> M in CHCl<sub>3</sub>). 244
- Figure 7.21.** Emission spectra of the pristine and TFA fumed solids of (A) *p*-BT, (B) *m*-BT and (C) *o*-BT. 246

## LIST OF SCHEMES

### Chapter 1: Introduction

- Scheme 1.1.** Synthesis of TPE by using Knoevenagel like condensation reaction. 13
- Scheme 1.2.** Synthesis of TPE by using McMurry like condensation reaction. 13
- Scheme 1.3.** Synthesis of TPE by using selenobenzophenones with diphenyldiazomethane. 14

<b>Scheme 1.4.</b>	Synthesis of TPE from diphenyldichloromethane.	14
<b>Scheme 1.5.</b>	Synthesis of 10-propyl-10H-phenothiazine.	16
<b>Scheme 1.6.</b>	Synthesis of 3-bromo-10-propyl-10H-phenothiazine.	16

**Chapter 3: T-shaped donor-acceptor-donor type symmetrical quinoxaline derivatives: aggregation-induced emission and mechanochromism**

<b>Scheme 3.1.</b>	Synthesis of symmetrical PTZ and TPE substituted PQ and AQ derivatives.	63
--------------------	---	----

**Chapter 4: Effect of different donors on mechanochromism of AIE active unsymmetrical D-A-D' type quinoxaline derivatives**

<b>Scheme 4.1.</b>	Synthesis of unsymmetrical phenanthrene-quinoxaline (PQ) and acenaphthene-quinoxaline (AQ) derivatives.	96
<b>Scheme 4.2.</b>	Synthetic scheme for intermediates <b>PTZ-Bpin</b> , <b>TPE-Bpin</b> , <b>1</b> and <b>2</b> .	97

**Chapter 5: Stimuli responsive AIE active positional isomers of phenanthroimidazole**

<b>Scheme 5.1.</b>	Synthetic route for the phenanthroimidazoles <b>1</b> and <b>2</b> .	138
<b>Scheme 5.2.</b>	Synthetic scheme for intermediates <b>3</b> and <b>4</b> .	138

**Chapter 6: Stimuli-responsive phenothiazine-based donor-acceptor isomers: AIE, mechanochromism and polymorphism**

<b>Scheme 6.1.</b>	Synthesis of isomers <i>p</i> -PTZ, <i>m</i> -PTZ and <i>o</i> -PTZ.	174
<b>Scheme 6.2.</b>	Synthetic routes to intermediates.	174

**Chapter 7: Structure-property relationship in multi-stimuli responsive D-A-A' benzothiazole functionalized isomers**

<b>Scheme 7.1.</b>	Synthetic routes for <i>p</i> -BT and <i>m</i> -BT.	219
--------------------	---	-----

<b>Scheme 7.2.</b>	Synthetic route for <i>o</i> -BT.	220
<b>Scheme 7.3.</b>	Synthetic route to BTD-TPE.	220

## LIST OF TABLES

### **Chapter 3: T-shaped donor-acceptor-donor type symmetrical quinoxaline derivatives: aggregation-induced emission and mechanochromism**

<b>Table 3.1.</b>	Photophysical and thermal properties of <b>1</b> and <b>2</b> .	66
<b>Table 3.2.</b>	Theoretical calculations of symmetrical quinoxaline derivatives.	68
<b>Table 3.3.</b>	Peak emission wavelengths ( $\lambda$ , in nm) of <b>1</b> and <b>2</b> under various external stimuli.	77

### **Chapter 4: Effect of different donors on mechanochromism of AIE active unsymmetrical D-A-D' type quinoxaline derivatives**

<b>Table 4.1.</b>	Photophysical properties of PQ1, PQ2, AQ1, and AQ2.	100
<b>Table 4.2.</b>	DFT calculations of unsymmetrical PQ and AQ derivatives.	102

### **Chapter 5: Stimuli responsive AIE active positional isomers of phenanthroimidazole**

<b>Table 5.1.</b>	Photophysical and thermal properties of <b>1</b> and <b>2</b> .	140
<b>Table 5.2.</b>	Solvatochromic properties of luminophores <b>1</b> and <b>2</b> .	142
<b>Table 5.3.</b>	Peak emission wavelengths ( $\lambda$ , in nm) of <b>1</b> and <b>2</b> as pristine, grinded and annealed solids.	146
<b>Table 5.4.</b>	Crystal data and structure refinement for <b>1</b> , <b>3</b> and <b>4</b> .	150
<b>Table 5.5.</b>	Electrochemical and theoretical properties of <b>1</b> and <b>2</b>	154

**Chapter 6: Stimuli-responsive phenothiazine-based donor-acceptor isomers: AIE, mechanochromism and polymorphism**

**Table 6.1.** Photophysical properties of isomers *p*-PTZ, *m*-PTZ and *o*-PTZ. 176

**Table 6.2.** Quantum yield *p*-PTZ, *m*-PTZ and *o*-PTZ in various solvents. 180

**Table 6.3.** Crystal data and structure refinement for *p*-PTZ GC, *p*-PTZ YC, *m*-PTZ and *o*-PTZ. 188

**Table 6.4.** Peak emission wavelengths ( $\lambda$ , in nm) of *p*-PTZ, *m*-PTZ and *o*-PTZ as pristine, grinded and fumed solids. 193

**Table 6.5.** DFT calculations of *p*-PTZ, *m*-PTZ and *o*-PTZ. 197

**Chapter 7: Structure-property relationship in multi-stimuli responsive D-A-A' benzothiazole functionalized isomers**

**Table 7.1.** Photophysical and thermal properties of *p*-BT, *m*-BT and *o*-BT. 223

**Table 7.2.** Electrochemical properties and DFT calculations of *p*-BT, *m*-BT and *o*-BT. 224

**Table 7.3.** Crystal data and structure refinement for *p*-BT1, *p*-BT2 and *o*-BT. 237

**Table 7.4.** Peak emission wavelengths ( $\lambda$ , in nm) of *p*-BT, *m*-BT and *o*-BT as pristine, grinded and fumed solids. 240

**LIST OF CHARTS**

**Chapter 1: Introduction**

**Chart 1.1.** Examples of donor and acceptor moieties. 4

**Chart 1.2.** Examples of different aggregation-induced emission (AIE) type luminogens. 11

## ACRONYMS

D-A	Donor-acceptor
SCXRD	Single Crystal X-ray diffraction
NMR	Nuclear Magnetic Resonance
DMF	Dimethylformamide
DCM	Dichloromethane
THF	Tetrahydrofuran
UV-Vis	UV-Visible Spectroscopy
Calcd.	Calculated
CDCl <sub>3</sub>	Chloroform-d
ESI-MS	Electrospray Ionization- Mass Spectrometry
EtOH	Ethanol
MeOH	Methanol
TLC	Thin Layer Chromatography
AIE	Aggregation-induced emission
TPE	Tetraphenylethylene
TPA	Triphenylamine
PTZ	Phenothiazine
PI	Phenanthroimidazole
BT	Benzothiazole
BTD	Benzothiadiazole
QY	Quantum yield
PXRD	Powder X-ray diffraction
MFC	Mechanfluorochromic

## NOMENCLATURE

$\lambda$	Wavelength
$\varepsilon$	Extinction coefficient
$\alpha$	Alfa
$\beta$	Beta
$\gamma$	Gamma
$\pi$	Pi
$\phi_f$	Fluorescence quantum yield
$\sigma$	Sigma
$\text{\AA}$	Angstrom
nm	Nanometer
cm	Centimeter
$^{\circ}$	Degree
$^{\circ}\text{C}$	Degree Centigrade
mmol	Millimol
mL	Milliliter
$\mu\text{L}$	Microliter
a. u.	Arbitrary Unit





# Chapter 1

## Introduction

---

---

### 1.1 Background

Luminescent materials have received significant interest of the scientific community, with the advent of new-age technologies such as optoelectronic devices,<sup>[1]</sup> stimuli-responsive materials,<sup>[2]</sup> bioimaging,<sup>[3]</sup> fluorescent probes,<sup>[4]</sup> sensors,<sup>[5]</sup> data storage,<sup>[6]</sup> solid-state lasers,<sup>[7]</sup> biomedical applications<sup>[8]</sup> and material devices<sup>[9]</sup>. Researchers have been constantly intrigued by the various luminescence phenomena and have made efforts in deciphering the processes involved in obtaining effective luminescence which can be further applied for developing multifunctional materials.<sup>[10]</sup> Luminescence in general is the process of spontaneous emission of light not occurring because of heat.<sup>[11]</sup> Photoluminescence is a process involving emission of light caused by relaxation of electronically excited states formed by absorption of photons from a given light source by a chromophoric molecule.<sup>[12]</sup> Emission of light is often generated by radiative relaxation of the excited state primarily by two processes namely fluorescence and phosphorescence whereas the non-radiative relaxation of the excited state via different processes results in quenching of emission.<sup>[13]</sup> Organic luminescent materials have emerged as promising candidates for future applications and can be effectively constructed from a range of organic luminogens and chromophores which allow development of diverse structures and accurate tuning of optical properties.<sup>[14]</sup> Organic luminescent materials are preferable over their inorganic and polymeric counterparts for application in different technologies due to the following benefits like definite chemical structures, easy reproducibility, low-cost purification, design versatility and compatibility with different substrates.<sup>[15]</sup> Organic luminescent materials are usually associated with  $\pi$ -conjugated structures and precise alteration in the  $\pi$ -conjugation length or incorporation of

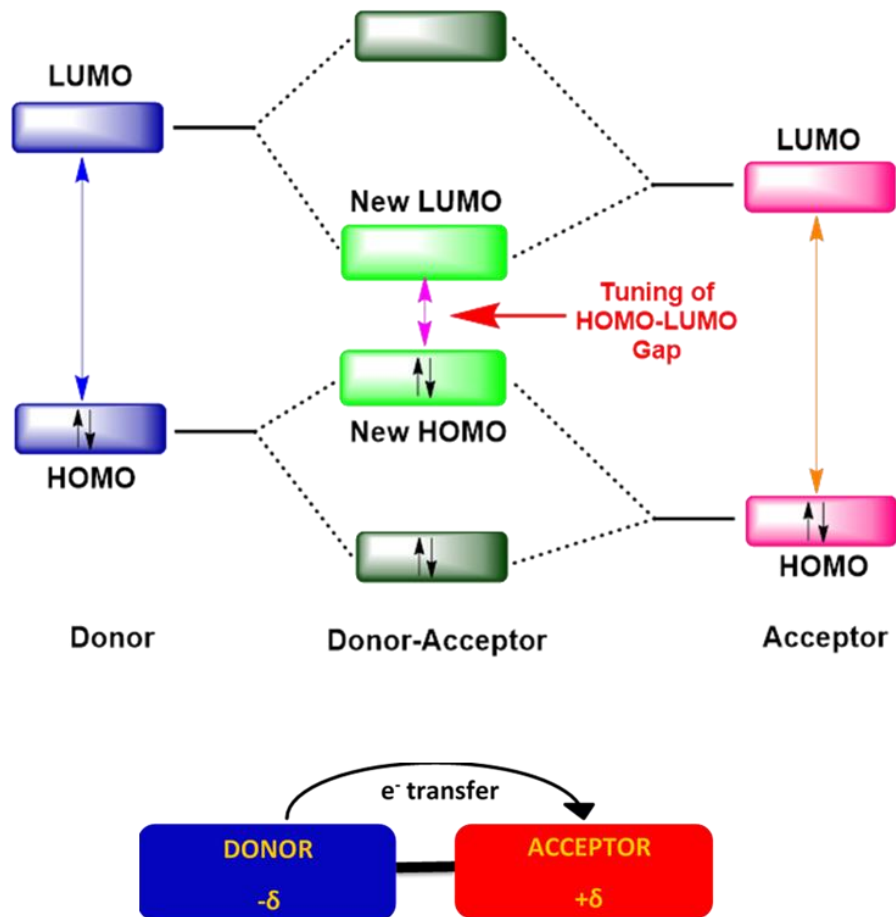
different electron donating or electron withdrawing units enable modulation of luminescence properties.<sup>[16]</sup> Emissive organic  $\pi$ -conjugated small molecules comprising of an electron donor and an electron acceptor display interesting electronic and optical features such as broad absorption spectra, higher absorption coefficients, small HOMO-LUMO gap, narrow emission peaks and formation of strong dipoles.<sup>[17]</sup> The fusion of highest occupied molecular orbital (HOMO) and lowest unoccupied molecular orbital (LUMO) of the individual donor and acceptor moieties results in formation of distinct HOMO and LUMO energy levels in the donor-acceptor functionalized organic molecules (Figure 1.1). Donor-acceptor systems possess induced dipoles on their donor and acceptor fragments which contribute to the charge transfer processes.<sup>[18]</sup> The process of electron transfer from a donor unit to an acceptor unit located in the same molecule is known as intramolecular charge transfer (ICT) and is a crucial factor in tuning the optical and electronic properties of donor-acceptor systems.<sup>[18]</sup> The ICT process imparts new absorption and emission characteristics which can be effectively controlled by integration of suitable donor and acceptor units.

The luminescent properties of donor-acceptor systems can be perturbed by (1) Utilizing donor and acceptors of varying strengths, (2) By using different heterocyclic donor and acceptor moieties having various intermolecular interactions, (3) Regulating the donor-acceptor character by using different alkyl, aryl or halogen substitutions and using  $\pi$ -linker or spacer moieties between donor and acceptor units.<sup>[19]</sup>

Organic chromophores containing electron donating or withdrawing components can be employed in various donor-acceptor structures such as D-A, D-A-D, D- $\pi$ -A, D-A-A', D-A-D' *etc.* to produce luminescent molecules useful in different applications such as

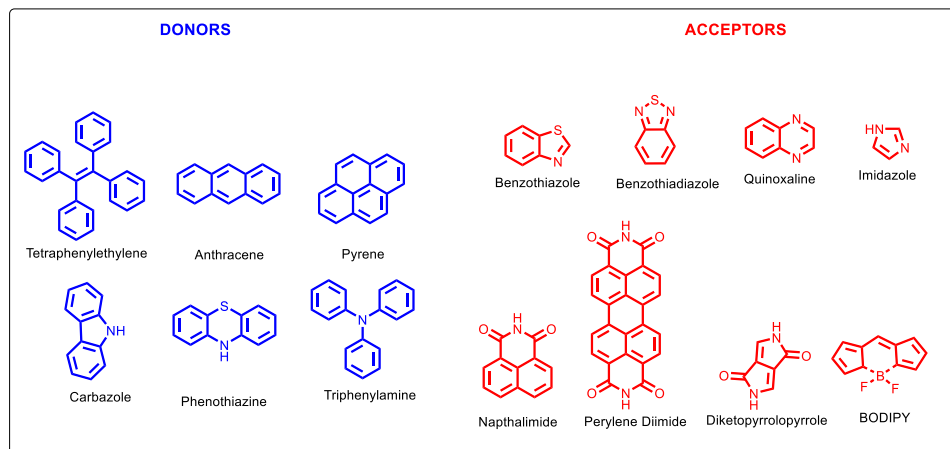
- Organic light emitting diodes (OLEDs)<sup>[20]</sup>
- Bioimaging and photodynamic therapy<sup>[21]</sup>

- Stimuli-responsive materials<sup>[22]</sup>
- Sensors<sup>[23]</sup>
- Organic field effect transistors (OFETs)<sup>[24]</sup>
- Flat panel Displays<sup>[25]</sup>
- Non-linear optics (NLOs)<sup>[26]</sup>



**Figure 1.1** Schematic representation of frontier orbitals and intramolecular charge transfer in donor-acceptor molecules.

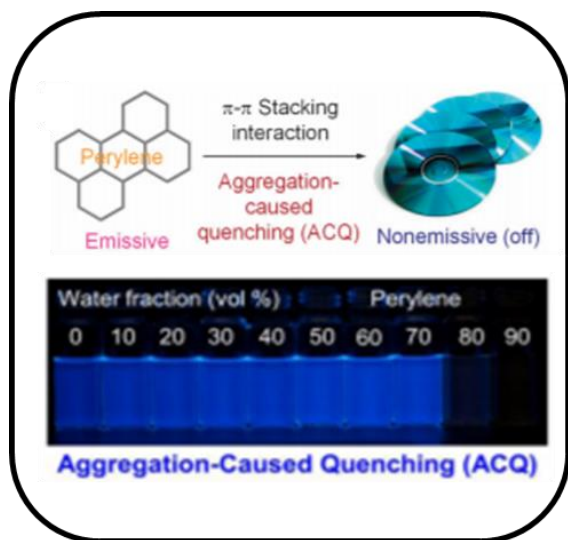
The different donor and acceptor chromophores are as shown in Chart 1.1.



**Chart 1.1** Examples of donor and acceptor moieties.

Organic luminescent molecules find place in different applications in solution as well as solid state, however most of the applications such as OLEDs, OFETs, stimuli-responsive materials *etc.* exploit the solid state of emissive molecules.<sup>[27]</sup> For instance, the fabrication of OLEDs or OFETs is done by preparation of vacuum deposition of emissive substances over solid films. Furthermore, the biological or sensing applications are mostly performed in aqueous media in which most of the organic luminophores are partially soluble leading to formation of nanoaggregates, which are invisible in naked eye. Over the past few years, a wide variety of photoluminescent organic molecules have been developed and the mechanisms related to the photoluminescence processes of these molecules have been extensively studied.<sup>[28]</sup> In the earlier stage, the photoluminescent processes for organic dyes were mostly studied in dilute solutions where the dyes exist as an isolated species not affected by any interactions with other dye molecules. It was observed that most of the organic dyes were highly luminescent in their dilute solution but on increasing the concentration the luminescence drastically decreased owing to the “concentration-quenching” effect. Jean Perrin in 1923 investigated the concentration effect on photoluminescence of uranine and discovered that the increase in concentration of uranine

initially leads to increase in photoluminescence intensity owing to higher number of dye molecules but at higher concentrations the photoluminescence intensity decreases significantly.<sup>[29]</sup> In 1955 Theodor Förster found that the fluorescence of pyrene decreases on increasing concentration which was ascribed to the formation of excimers at higher concentration facilitated by collisional interactions between the aromatic rings. It was thus concluded that the concentration quenching of organic molecules at higher concentrations could be due to strong  $\pi$ - $\pi$  interactions or face to face interactions between the aromatic rings.<sup>[30]</sup> J.B. Birks in “*Photophysics of Aromatic Molecules*” published in 1970 has summarized that such type of concentration quenching effect is displayed by most of the well-known organic aromatic molecules.<sup>[31]</sup> The established organic luminophores in their aggregated or solid state have slightly diminished or completely quenched emissions as compared to their dilute solutions, and the phenomenon in general is referred to as “Aggregation caused quenching” (ACQ).<sup>[31]</sup> The aromatic molecules in their solutions are well-separated and do not interact with each other thereby exhibiting strong emission. However, the molecules on aggregation come in close proximity of each other and the aromatic rings of the luminophores undergo extensive  $\pi$ - $\pi$  stacking interaction (like discs or rods stacked on one another) creating non-radiative channels for relaxation of their excited states resulting in quenched emission of organic luminophores in their aggregated state. The ACQ effect is a common obstacle resulting in non-emissive aggregated states of organic molecules.<sup>[32]</sup>



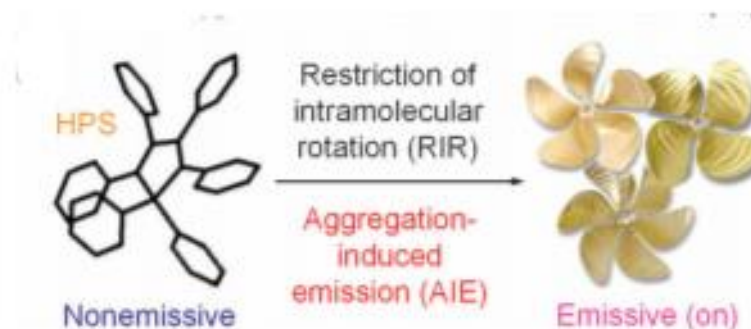
**Figure 1.2.** Schematic representation of ACQ effect in perylene molecules.

Figure 1.2 represents the ACQ effect observed in perylene dye. The solution of perylene in THF is highly emissive. Perylene is insoluble in water and hence a gradual increase of water fraction in THF results in increased concentration of perylene molecules which thereby leads to aggregation of the molecules. The perylene dye molecules shows diminished or quenched emission at 80% and 90% THF-water mixtures of due to  $\pi$ - $\pi$  stacking between the planar rings on aggregate formation.

Several chemical strategies have been executed by researchers to reduce the ACQ effect such as addition of polar groups, bulky substituents or branched alkyl chains on aromatic cores which could reduce the hydrophobicity of aromatic rings thereby decreasing the possibility of aggregation in aqueous media.<sup>[33]</sup> Also, physical processing methods such as mixing of transparent polymers and organic luminophores could avoid the molecules from coming together on aggregation thereby decreasing ACQ effect.<sup>[34][38]</sup> However, all these strategies have failed to lessen the ACQ effect making the organic molecules difficult to be used in practical applications. Hence, researchers have made efforts to come up with an approach which rather than obstructing the spontaneously occurring aggregation process could utilize it constructively to enhance the emission of organic molecules in the solid state.<sup>[35][39]</sup>

## 1.2. Aggregation-induced emission

In 2001, Tang and coworkers discovered “Aggregation-induced emission” (AIE) which takes the advantage of the aggregation process to produce effective emission.<sup>[36]</sup> AIE is an anti-ACQ effect which was first detected in hexaphenylsilole (HPS) and its derivatives.<sup>[37]</sup> The HPS molecule has a unique propeller type confirmation with the central silole ring acting as stator for the six-phenyl ring which act as rotors (Figure 1.3).



**Figure 1.3.** Schematic presentation of mechanism involving AIE as restricted intramolecular rotation in hexaphenylsilole (HPS) luminogen.

In solution, the phenyl rings undergo continuous intramolecular rotations around the single bond attached with the stator silole ring generating non-radiative decay channels for its excited state resulting in quenching of emission. In contrast to the quenched emission of HPS in solution, it displays excellent emission in the aggregated state due to restriction of intramolecular rotation (RIR).<sup>[37]</sup> In the aggregated state, the HPS molecules retain their non-planar framework which interrupts the stacking process observed in planar disc type molecules and are also unable to rotate freely as they lie close to each other which allows the molecules to relax their excited state radiatively making their aggregated state highly emissive. The non-planar frameworks of the luminogens with AIE or AIE gens works in a positive way to generate emission in aggregated state via RIR contrary to the planar structures of the ACQ molecules.

The AIE effect have been explored in detail using fluorescence and absorption spectroscopy. The HPS molecules were dissolved in acetonitrile and HPS being insoluble in water, the aggregates were produced by slowly increasing the water amount from 0-90% in acetonitrile solution of HPS. In pure acetonitrile solution, the HPS molecules have reduced emission with a quantum yield ( $\Phi_F$ ) 0.22%. The emission of HPS remains constant even at 50% water fraction but increases significantly at 80-90% water fraction with quantum yield ( $\Phi_F$ ) reaching to 56%. The absorption spectra of HPS molecules on aggregation *i.e.* at 80-90% water fraction exhibit the Mie scattering effect prominently observed in nanoparticles which is confirmed for HPS molecules by the extended tail-type absorption in higher wavelength region.<sup>[38]</sup> The aggregates of size 190 nm and 130 nm are formed at 80% and 90% water fractions respectively, which confirms the generation of nanoparticles on aggregation in HPS molecules. Figure 1.4 shows pictorial representation of AIE effect in acetonitrile-water mixture of HPS molecules. The AIEgens emit efficiently on aggregation by RIR and this hypothesis has also been validated by activating the RIR process externally *i.e.* by controlling the intramolecular interactions using experiments such as decreasing the temperature of system, increasing the viscosity of a solution system and applying pressure.<sup>[39]</sup> All these physical changes affect the intramolecular interactions and improve the emission by triggering the RIR process in AIEgens. Thus, effective emission in solid state could be obtained by exploring different non-planar propeller type structures which can emit via RIR.<sup>[40]</sup>

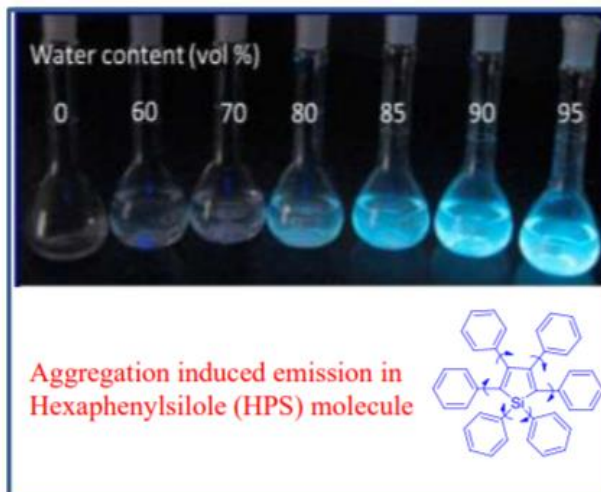


**Figure 1.4.** Fluorescence photographs of HPS in acetonitrile/water mixtures with different water fractions.

Several non-planar AIEgenes have been investigated whose AIE activity is ascribed to a different mechanism namely restriction of intramolecular vibrations (RIV) rather than RIR. The organic molecule 10,10',11,11'-tetrahydro-5,5'-bidibenzo[a,d][7]annulenyliene (THBA) is non-emissive in its solution but exhibits substantial emission as aggregates.<sup>[41]</sup> The THBA molecule has phenyl rings which are connected by an ethylene bond which brings a restraint on the rotational motions of the phenyl rings. The phenyl rings in THBA can undergo vibrational motions which can non-radiatively decay the excited state energy in solution similar to the rotational motions. (Figure 1.5).<sup>[42]</sup> However, in the aggregated state the emission is enhanced by the restriction of intramolecular vibrations (RIV). The quantum mechanics and molecular mechanics studies reveal that the single THBA in solution possesses six normal vibrational modes which can significantly utilize the excited state energy. However, in the aggregated state, THBA possesses only three normal vibrational modes which limits the consumption of excited state energy to approximately 30%, allowing THBA to display radiative emissions in aggregated state. Thus, in addition to RIR the RIV mechanism also effectively results in AIE behavior for luminogens with structures similar to THBA. In general, the restriction of any kinds of

motions (rotation, vibration, flapping, twisting, scissoring *etc.*) that result in non-radiative decay of excited state can result in AIE activity. Hence, the AIEgens can be elucidated as systems working on restriction of intramolecular motions (RIM) mechanism where (M) is any kind of motion including vibration (V) and rotation (R).<sup>[37]</sup>

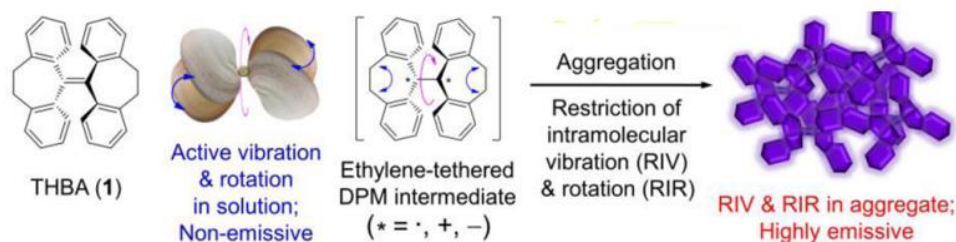


**Figure 1.5.** Schematic presentation of mechanism involving AIE as restricted intramolecular vibration in 10,10',11,11'- tetrahydro-5,5'-bidibenzo[a,d][7]annulenyliene (THBA) luminogens.

### 1.3. Aggregation-induced emission type luminogens

Organic molecules which are emissive in aggregated state are termed as aggregation-induced emission (AIE) luminogens or AIEgens and are suitable for developing solid-state emissive molecules.<sup>[43]</sup> The AIE luminogens possess unique non-planar twisted frameworks which produce intense emission in the aggregated state due to RIR or RIV process.<sup>[40]</sup> The AIEgens are usually non-emissive in solution owing to the continuous intramolecular rotations of the aromatic rings which render non-radiative decay of their excited state. A variety of AIE luminogens with the ability to generate emission via RIR, have been developed over past few years by careful structural manipulation of organic molecules.<sup>[40]</sup> The well-known AIE luminogens rely on a structure consisting of a fixed central unit (olefin or aromatic unit) acting as stator surrounded by different aromatic units which behave as rotors attached by freely rotating single bond. Chart 1.2 depicts the structures of commonly employed AIE luminogens.<sup>[44]</sup> Tetraphenylethylene (TPE) and hexaphenylsilole (HPS) are widely used

AIEgens displaying high emission on aggregation and have rotor-stator based structures.<sup>[45]</sup> Similar to the RIR mechanism, certain non-planar molecules apart from the rotor-stator type molecules that exhibit any kind of restricted intramolecular motions (RIM) in their aggregated state also have efficient emission in their aggregated states.<sup>[41]</sup> [45]

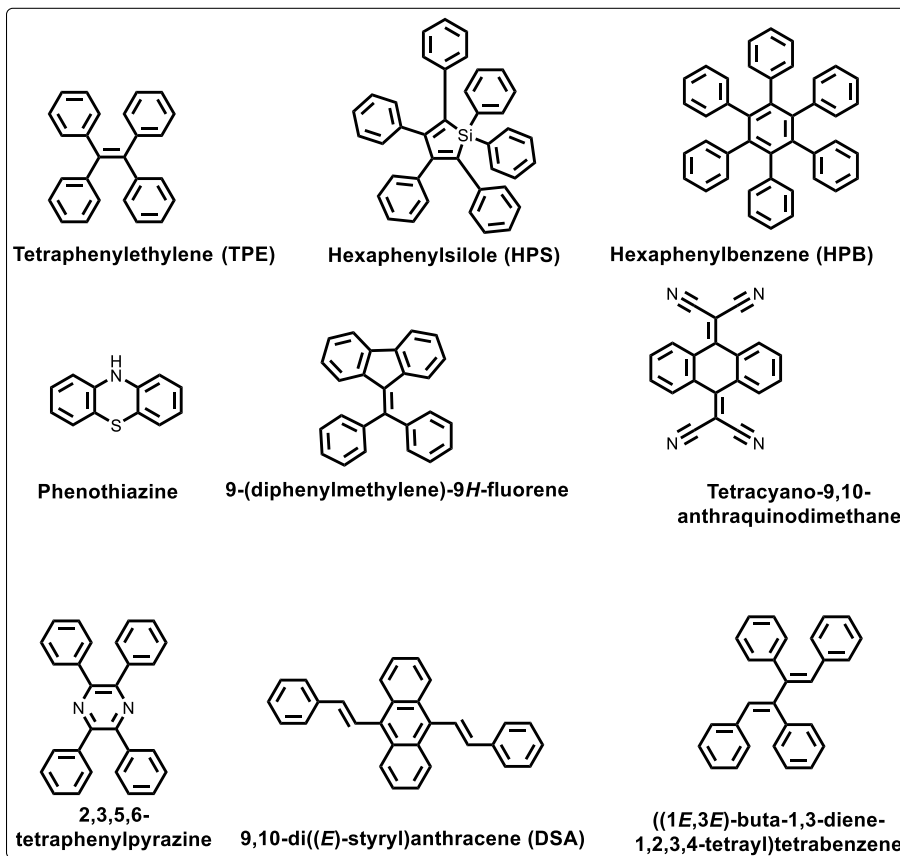


**Chart 1.2.** Examples of different aggregation-induced emission (AIE) type luminogens.

Phenothiazine (PTZ) with a bent butterfly structure manifests AIE characteristics by restriction of intramolecular vibrations (RIV).<sup>[46]</sup> Similarly, anthraquinodimethane derivatives retain bent structures and manifest AIE nature by restricting the flapping and vibrations of its aromatic cores.<sup>[47]</sup> Thus, a wide variety of AIEgens having non-planar, bent, propeller type twisted architectures that carefully restrict any kind of intramolecular motions which create non-radiative decay channels thereby emitting efficiently in aggregated state have been reported in literature. The

inclusion of AIE units in traditional ACQ chromophores is a decent approach to induce intense emission into the non-emissive aggregated states of ACQ chromophores. The integration of AIE units acting as electron donors and conventional ACQ chromophores acting as electron acceptors result in donor-acceptor systems with high solid-state emission.<sup>[48]</sup>

#### 1.4. Tetraphenylethylene

Tetraphenylethylene (TPE) is a conventional AIE luminogen and has many uses in organic light emitting diodes (OLEDs), non-linear optics (NLOs), mechanochromic materials and bioimaging.<sup>[49]</sup> Tetraphenylethylene has an exclusive non-planar architecture with an ethylene double bond in the center working as stator unit with the four phenyl rings surrounding it which act as rotor units (Figure 1.6.). The TPE moiety maintains a propeller confirmation which was confirmed by Hong *et al.* from its crystal structure analysis and has twisting angle of  $\sim 50^\circ$ .<sup>[50]</sup> The phenyl rings attached to the central olefin can freely rotate in solution via the single bond attachment and produce non-radiative decay paths for the excited state decay. However, the propeller framework of TPE renders the aggregated emissive via RIR process and absence of stacked structures.<sup>[51]</sup> TPE moiety by virtue of its rigid structure possess good thermal and chemical stability and can be easily synthesized and functionalized to its different bromo, hydroxy or other halogenated derivatives.

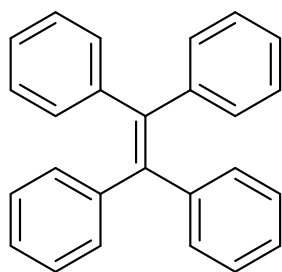
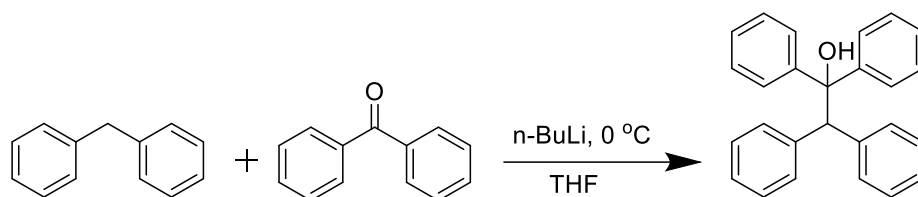


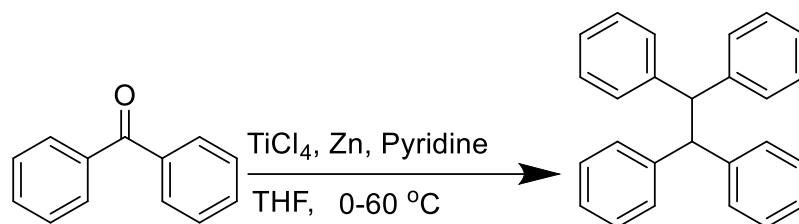
**Figure 1.6.** Structure of tetraphenylethylene.

De Boissieu synthesized TPE for the first time in 1888 *via* dry distillation of diphenylmethane in the presence of bromine.<sup>[52]</sup> Numerous synthetic methods for TPE preparation have been published in the literature

(Scheme 1.1–1.4). Some of these methods can also be used to make functionalized TPEs. TPE can be easily synthesized *via* a condensation process similar to Knoevenagel condensation. Wang *et al.* synthesized TPE *via* a Knoevenagel-like condensation process (Scheme 1.1).<sup>[53]</sup> To make tetraphenylethanol, diphenylmethane was first deprotonated with n-BuLi in THF at 0 °C, then benzophenone was progressively added. The water was removed using the Dean-Stark apparatus *via* an azeotropic combination with toluene, and the resultant tertiary alcohol was dehydrated using catalytic para-toluene sulphonic acid (PTSA). This method is also essential in the design of different functionalized TPEs, such as halogenated TPE. However, the n-BuLi approach has constraints in terms of using substituted diphenylmethane or benzophenone derivatives, such as the production of unstable anion when using electron donating substituents on the diphenylmethane unit.



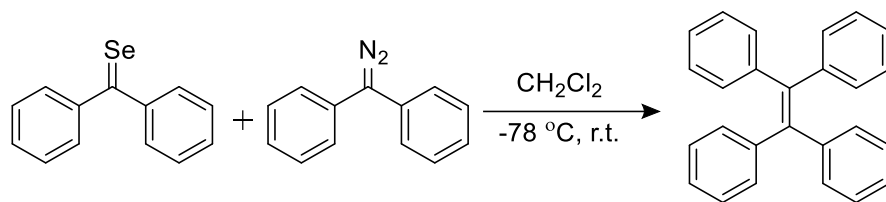
**Scheme 1.1.** Synthesis of TPE by using Knoevenagel like condensation reaction.



**Scheme 1.2.** Synthesis of TPE by using McMurry like condensation reaction.

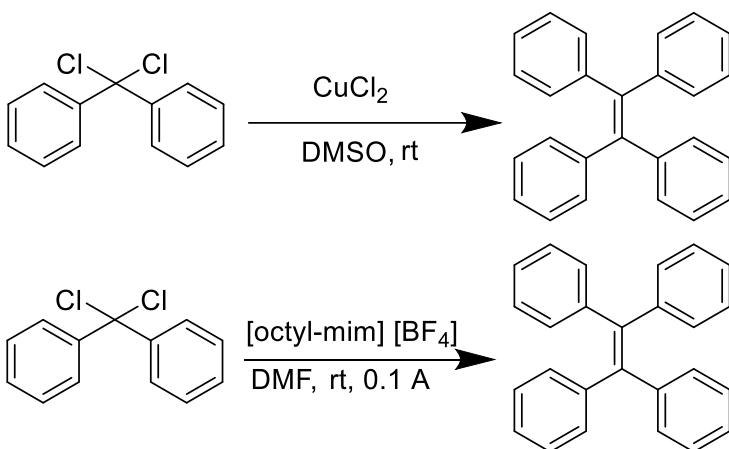
TPE can be effectively synthesized utilizing a McMurry-like condensation process (Scheme 1.2).<sup>[54]</sup> The McMurry coupling is a second significant technique for manufacturing TPE and its derivatives. The two ketones

(benzophenone) get fused to form TPE in the presence of Ti(IV) and Ti(IV) salts, as well as the reducing agent Zn (Scheme 1.2).



**Scheme 1.3.** Synthesis of TPE by using selenobenzophenones with diphenyldiazomethane.

The synthesis of TPE was achieved by reacting selenobenzophenones with diphenyldiazomethane in dichloromethane at  $-40\text{ }^\circ\text{C}$ , as shown in Scheme 1.3.<sup>[55]</sup> This reaction is initiated by a 1,3,4-selenadiazoline intermediate, followed by deselenization and nitrogen gas evolution. Unsymmetrical TPE derivatives can also be obtained using this technique.



**Scheme 1.4.** Synthesis of TPE from diphenyldichloromethane.

The synthesis of TPE from diphenyldichloromethane is shown in Scheme 1.4. In DMSO, diphenyldichloromethane undergoes an exothermic reaction with stoichiometric copper metal to produce TPE (Scheme 1.4).<sup>[56]</sup> A copper carbenoid intermediate is thought to be involved in this process. Barhadi *et al.* synthesized TPE using electrochemical coupling reactions of

diphenyldichloromethane with nickel catalyst at room temperature ionic liquids (Scheme 1.4)<sup>[56]</sup>.

### 1.5. Phenothiazine

Phenothiazine is one of the most attractive cores amongst all heterocyclic organic compounds because of its remarkable photophysical and electrochemical characteristics. Phenothiazine (PTZ) is a tricyclic heteroarene with a nonplanar butterfly shaped structure and behaves as a strong electron donor due to the presence of electron-rich sulphur and nitrogen heteroatoms in the thiazine ring.<sup>[57]</sup> Phenothiazine has multiple active positions (5 (S), 10 (N), 3 and 7-positions) which improve the photophysical and electrochemical properties by extending the  $\pi$ -conjugations (Figure 1.7).<sup>[58]</sup> Phenothiazine unit shows electrophilic substitution at 3 and 7-positions, nucleophilic substitution at *N*-position and oxidation at the S-position.<sup>[58]</sup> The phenothiazine derivatives have been mostly used as electron donor in various optoelectronic applications due to its low reversible oxidation potentials produced by sulfur atom. In recent years, phenothiazine based  $\pi$ -conjugated derivatives have been used in several applications like photovoltaic devices like dye-sensitized solar cells (DSSCs) and bulk heterojunction solar cells, organic light emitting diodes (OLEDs), as phosphorescent materials and thermally activated delayed fluorescence (TADF) materials, aggregation-induced enhanced emission (AIEE) luminogens, sensors and mechanochromic materials.<sup>[59]</sup>

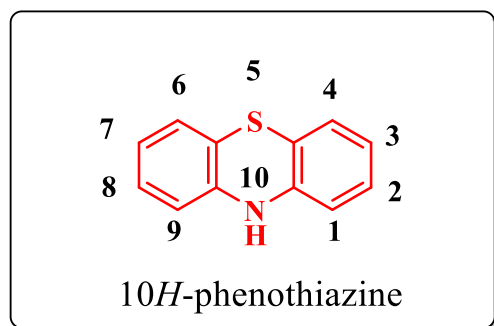
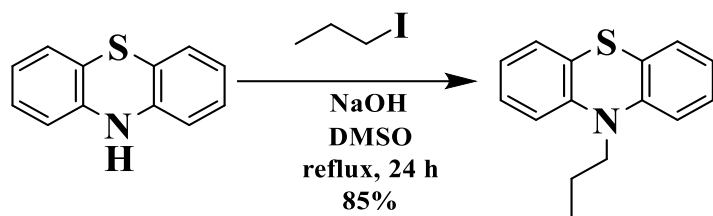


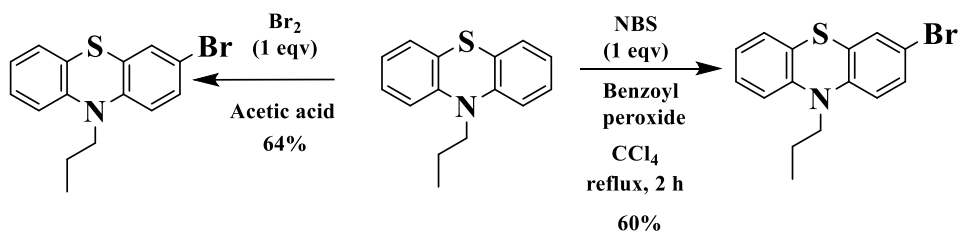
**Figure 1.7.** Structure of phenothiazine.

The N-position of the 10*H*-phenothiazine unit is readily alkylated through nucleophilic substitution. In the presence of dry DMSO, the reaction of 10*H*-phenothiazine with 1-iodopropane, and sodium hydroxide produced 10-propyl-10*H*-phenothiazine (Scheme 1.5).<sup>[60]</sup> At the 3,7-positions, phenothiazine is extremely sensitive to electrophilic substitution reactions. The most widely utilised compounds are 3,7-brominated phenothiazine derivatives.



**Scheme 1.5.** Synthesis of 10-propyl-10*H*-phenothiazine.

The reaction of 10-propyl-10*H*-phenothiazine with bromine (1 equivalent) in acetic acid or with *N*-bromosuccinimide (NBS) (1 equivalent for monobromination) in presence of catalytic amount of benzoyl peroxide in  $\text{CCl}_4$  results in mono brominated phenothiazine.<sup>[61]</sup>



**Scheme 1.6.** Synthesis of 3-bromo-10-propyl-10*H*-phenothiazine.

## 1.6. Stimuli-responsive materials

Stimuli-responsive materials termed as *smart* materials manifesting evident changes as a response to different external stimuli (mechanical force or pressure, temperature, polarity, ions, pH *etc.*) are of great importance for different optoelectronic applications.<sup>[62]</sup> Luminescent materials are suitable for designing stimuli-responsive materials as the detection of stimuli by visualizing optical changes is preferred because of its higher response speed

and sensitivity, good resolution, easy tuneability and visible in-situ changes.<sup>[63]</sup> Stimuli-responsive changes in emission can be observed in both solution state and solid state; however the application of most stimuli like pressure, vapor or electricity is possible for solid-state materials. Additionally, the luminescence in solution is prone to quenching processes and is suitable for only observing stimuli-responsive changes associated to non-radiative processes (turn on-turn off emission changes).<sup>[64]</sup> On the contrary, the solid-state emission can be easily regulated and is best suited for observing response for all kinds of external stimuli and different optoelectronic and material applications. Hence, it is essential for stimuli-responsive materials to possess efficient emission in its solid state which can be easily achieved by utilization of AIE active luminogens. Organic  $\pi$ -conjugated donor-acceptor systems fused with AIE luminogens can exhibit exceptional solid-state emission and can serve as effective functionalities for stimuli-responsive materials.<sup>[65]</sup> The luminescence of organic systems hugely depends on the choice of donor/acceptors and AIEgens, level of conjugation, molecular conformation and intermolecular interactions.<sup>[66]</sup> The response on application of different external stimuli is achieved by variations in the molecular conformation which can be attained by AIEgens which own a certain degree of flexibility owing to their non-planar frameworks.<sup>[67]</sup> Furthermore, the external stimuli also exert influence on the intermolecular interactions present between the molecules in the solid state and hence regulation of the intermolecular interactions results in tunable emission in solid state.<sup>[66]</sup> The broad class of stimuli-responsive materials can be further classified based on the external stimuli applied.

### **1.6.1. Mechanochromic materials**

The category of stimuli-responsive materials that change their emission wavelength or intensity on applying mechanical force like grinding, scratching, rubbing *etc.* are known as mechanochromic materials.<sup>[68]</sup> Mechanochromic materials have acquired immense importance amongst all the stimuli-responsive materials because of its use as pressure sensors,

rewritable inks, data storage devices and in optoelectronics.<sup>[69]</sup> The mechanical stimuli induced response is achieved either by alterations in chemical structure or in physical structure. Chemical changes induced by mechanical stimuli involve bond breaking or formation and very few reports relate to this are present in literature due to the drawbacks such as low reversibility, incomplete reaction and higher pressure required for chemical transformation. Mechanochromic materials displaying emission switching brought about by physical structural changes are reversible in nature, hence being more common.<sup>[70]</sup> The mechanochromic emission switching is therefore greatly affected by fine physical structural changes associated with changes in the molecular packing of the system, disruption of intermolecular interactions, fluctuations in conformation or dihedral angle, phase transitions (one crystalline state to another, crystalline to amorphous and vice versa), ring opening/closing and configurational changes (E/Z).<sup>[71]</sup> The initial state of mechanochromic materials available before grinding can be restored either by solvent fumigation, thermal annealing or by self-recovery. Mechanochromic behavior essentially requires emission in the solid state which can be easily attained by incorporation of AIE luminogens such as TPE or PTZ. Organic  $\pi$ -conjugated molecules are appropriate for mechanochromism as their solid-state emission can be tuned by regulating the intermolecular interactions using different donor-acceptor, different alkyl/aryl/halogen/heteroatom substituents or by positional changes.<sup>[72]</sup>

The first ever emission color switching was reported in 2000 by Weder *et al.* for oligo(p-phenylene) vinylene (OPV) dyes blended with linear low-density polyethylene (LLDPE).<sup>[73]</sup> Different emission colors were observed for the polymer-dyes blends by regulating the composition of blends, aggregation processes and temperature and the tensile deformation resulted in solid-state emission color changes. Park *et al.* in 2010 presented the first AIE based mechanochromic material which was a cyano substituted distyrylbenzene derivative and displayed mechanochromic behavior corresponding to the modification in the

molecular sheet type crystal arrangement.<sup>[74]</sup> Following these two initial discoveries, a variety of mechanochromic materials have been developed over past few years.

Yang *et al.* in 2018 designed stimuli-responsive D-A derivatives **1-3** based on [1,2,4]triazolo[1,5-a]pyrimidine (TzPm) as acceptor and phenoxazine as donor attached at 5-position, 7-position and 5,7-positions of TzPm respectively.<sup>[75]</sup> The molecules **1-3** have high PLQY 0.45-0.70 in films and can act as thermally activated delayed fluorescence (TADF) emitters owing to the favorable singlet-triplet splitting energy  $\Delta E_{ST}$  0.06-0.10 eV which allows easy reverse intersystem crossing (RISC).

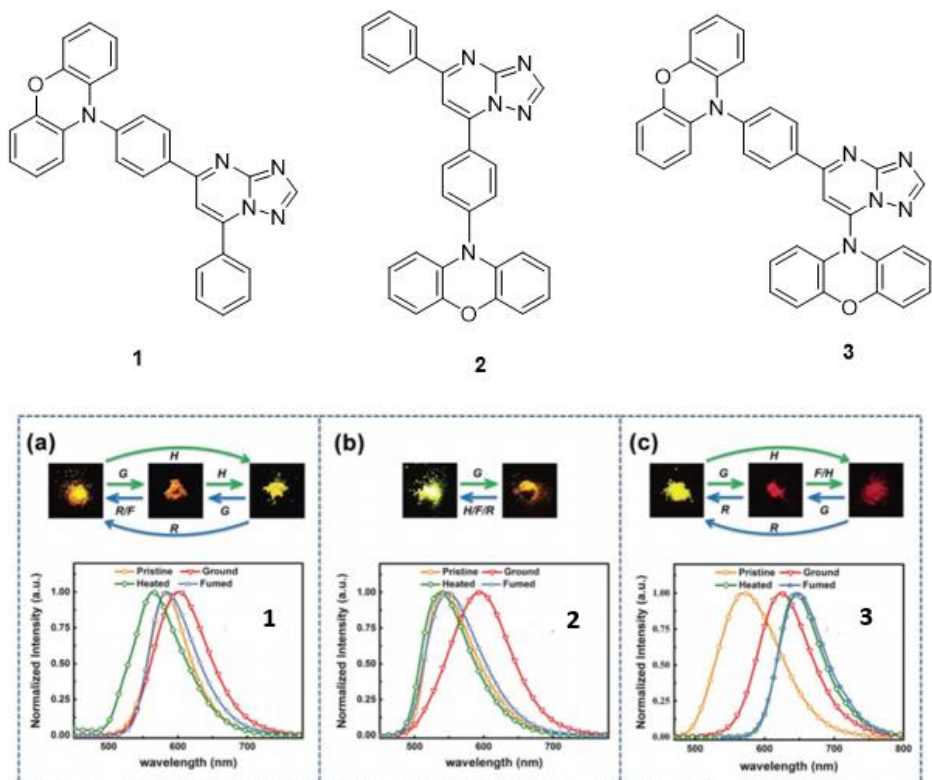


**Figure 1.8.** Chemical structure of triazole-pyrimidine-phenoxazine based mechanochromic materials **1-3** and solid-state emission spectra of pristine, ground, fumed and heated forms of **1-3**.

Molecules **1,2** and **3** in its pristine form emit at 583 nm, 541 nm and 570 nm respectively. The grinding of **1,2** and **3** red-shift the emission to 599

nm, 593 nm and 623 nm respectively. The grinded solids of **1** and **2** can return to their pristine form on fuming with dichloromethane, however the fumigation of grinded form of **3** results in additional red-shift upto 648 nm. Thermal annealing of the ground samples of **1**, **2** and **3** results in blue-shifted emission at 563 nm for **1**, retaining the pristine emission for **2** whereas red-shifted emission at 645 nm for **3**. Thus, the molecule **2** exhibited two-color mechanochromic switching while **1** and **3** display tri-color mechanochromism. The mechanochromism for **1-3** was related to phase change between different micro-crystalline to amorphous. All the three molecules were fabricated as OLEDs and reached a maximum external quantum efficiency of 14.3 % with yellow emission. Figure 1.8 shows the molecular structures of D-A derivatives **1-3** and their mechanochromic behavior.

Yasuda *et al.* have recently reported mechanochromic TADF emission change in three carbazole isophthalonitrile D-A molecules **4-6**.<sup>[76]</sup> The photoluminescence (PL) spectra for pristine powders of **4** and **5** shows peaks at 470 nm ( $\Phi_{\text{PL}}=98\%$ ) and 466 nm ( $\Phi_{\text{PL}}=98\%$ ) which on mechanical grinding with mortar and pestle is red shifted to 515 nm ( $\Phi_{\text{PL}}=80\%$ ) and 512 nm ( $\Phi_{\text{PL}}=75\%$ ) respectively. The pristine form of compound **6** emits at 525 nm ( $\Phi_{\text{PL}}=92\%$ ) whereas the grinded form emits at 557 nm ( $\Phi_{\text{PL}}=80\%$ ) with a striking color change from green to yellow. A color change from blue to green is observed in **4** and **5** with the photoluminescence quantum yield ( $\Phi_{\text{PL}}$ ) being very high in pristine and grinded forms which suggest effective reduction of ACQ processes owing to the non-planar propeller type structures. The pristine form for **4-6** were regained on exposing the grinded forms to vapors of tetrahydrofuran or chloroform confirming the reversible mechanochromic behavior. The time-resolved PL decay of the pristine and grinded forms for **4-6** reveal two-component decay (nanoseconds prompt fluorescence and microseconds delayed fluorescence) which is a character of TADF process suggesting the mechanochromic behavior is linked to TADF color changes. The unusual TADF based color

changing behavior is associated to change in dihedral angles between donor and acceptor in intramolecular charge transfer (ICT) excited states. The change from pristine form to grinded form display crystalline to amorphous morphological transformation. The amorphous state possesses almost perpendicularly oriented donor-acceptor moieties in excited states which are absent in the crystalline state due to densely packed structures which are disordered on griding. The TADF mechanochromic behavior of compounds **4-6** was exploited to develop bicolor non-doped OLEDs with simultaneous blue and green emission originating from a single emitter.

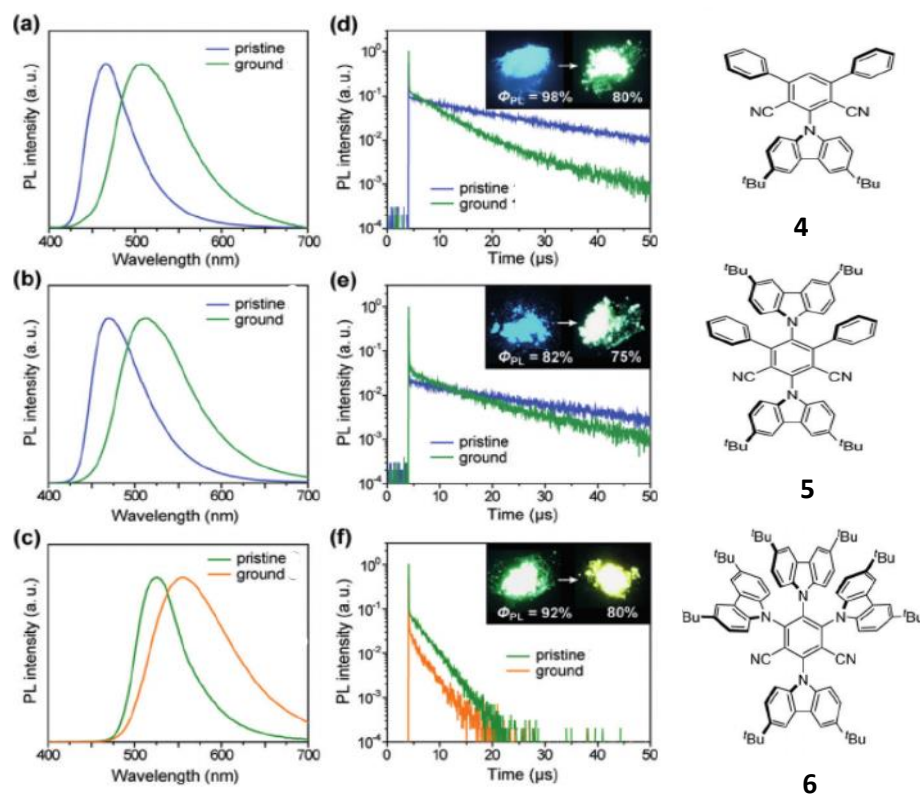


**Figure 1.9.** Chemical structure of D-A TADF-mechanochromic emitters **4-6**. PL spectra of pristine and ground form of (a) **4**, (b) **5** and (c) **6** and PL decay measurements of pristine and ground forms of (d) **4**, (e) **5** and (f) **6**.

Figure 1.9. depicts chemical structure of D-A TADF-mechanochromic emitters **4-6**, their PL spectra and their PL decay measurements in pristine and ground forms.

*The main objectives of the current work are:*

- To design and synthesize luminescent donor-acceptor systems using various architectures such as D-A-D, D-A, D- $\pi$ -A, D-A-D' or D-A-A' for developing AIE active stimuli-responsive materials.
- To design and synthesize donor-acceptor functionalized organic luminogens with effective emission in the solution state and in the solid state.
- To investigate the AIE, photophysical and stimuli-responsive properties such as solvatochromism, mechanochromism, acidochromism of the D-A luminogens using different spectroscopic techniques.
- To alter the intermolecular interactions and molecular packing in solid state by employing different donor AIEgens or different heterocyclic acceptors, positional isomerism, symmetrical and unsymmetrical substitution of donor/acceptor.
- To study the impact of the above-mentioned structural changes on the photophysical, electronic and stimuli-responsive properties.
- To explore the structural features of the donor-acceptor functionalized luminogens essential for inducing AIE nature and stimuli-responsive nature via single-crystal X-ray diffraction analysis, powder-X-ray-diffraction analysis and density functional theory (DFT) calculations.

## **1.7 Organization of thesis**

**Chapter 1** provides background about donor-acceptor functionalized stimuli-responsive materials, the underlying mechanisms responsible for the stimuli-responsive nature, their importance in different optoelectronic applications and the design strategies used to obtain AIE active stimuli-responsive materials.

**Chapter 2** summarizes the general experimental methods, characterization techniques and details of the instruments used for the characterization.

**Chapter 3** discusses the design and synthesis of T-shaped donor-acceptor-donor type symmetrical quinoxaline derivatives functionalized with tetraphenylethylene (TPE) and phenothiazine (PTZ) as donors. The effect of use of two different donors on the photophysical, AIE, solvatochromic and mechanochromic properties of the quinoxaline derivatives have been studied in detail. This work provides strategy to design stimuli-responsive molecules with distinct properties influenced by donor-acceptor interactions.

**Chapter 4** summarizes about the design and synthesis of unsymmetrical quinoxaline derivatives utilizing phenothiazine, tetraphenylethylene and N-substituted phenothiazine as different terminal donor units. The donor-acceptor character of the quinoxaline derivatives can be subtly regulated by unsymmetrical substitution and the influence of these structural changes on the photophysical, solvatochromic, AIE and mechanochromic properties have been investigated. The presented strategy can help in understanding the influence of different donor-acceptor structures on the AIE and stimuli-responsive characteristics and in further development of donor-acceptor stimuli-responsive materials.

**Chapter 5** discusses about the development of AIE active mechanochromic phenanthroimidazole (PI) derivatives which are positional isomers incorporating a triphenylamine and tetraphenylethylene unit. The influence of positional change on AIE and mechanochromism of PI derivatives were studied. The combination of phenanthroimidazole, TPA and TPE synergistically result in the high solid-state emission which can be further employed in optoelectronic applications.

**Chapter 6** contributes on the design and synthesis of donor-acceptor (D-A) isomers obtained by attaching the phenothiazine (**PTZ**) moiety at *ortho*, *meta* and *para* positions of the phenyl benzothiazole (**BT**) unit. This chapter provides in-depth comparison of the photophysical, electronic, structural, AIE and stimuli-responsive properties such as solvatochromism,

mechanochromism and acidochromism properties of the *o/m/p* positional isomers with an aim to study the outcome of the positional change.

**Chapter 7** discusses about the design and synthesis of multichromophoric D-A-A' positional isomers involving benzothiazole, benzothiadiazole and tetraphenylethylene formed by incorporating the BT-D-TPE moiety at *ortho*, *meta* and *para* positions of the phenyl BT unit. A comparative study of the photophysical, AIE and MFC properties of the isomers has been carried out to investigate the effect of positional change. The opted strategy allows modulation of fluorescence properties making them potential stimuli responsive materials with applications in mechano-sensors, security inks and optoelectronic-devices.

**Chapter 8** summarizes the salient features of the work and provides insight to develop new D-A stimuli responsive materials which can be employed for a wide range of optoelectronic applications.

## 1.8. References

- [1] ((a) Chen, X., Yang, Z., Li, W., Mao, Z., Zhao, J., Zhang, Y., Wu, Y.C., Jiao, S., Liu, Y. and Chi, Z., (2019) Nondoped red fluorophores with hybridized local and charge-transfer state for high-performance fluorescent white organic light-emitting diodes. *ACS Appl. Mater. Interfaces*, 11(42), 39026-39034. (DOI:10.1021/acsami.9b15278); (b) Cai, X. and Su, S.J., (2018). Marching toward highly efficient, pure-blue, and stable thermally activated delayed fluorescent organic light-emitting diodes. *Adv. Funct. Mater.*, 28(43), 1802558 (DOI:10.1002/adfm.201802558); (c) Miwa, T., Kubo, S., Shizu, K., Komino, T., Adachi, C. and Kaji, H., (2017). Blue organic light-emitting diodes realizing external quantum efficiency over 25% using thermally activated delayed fluorescence emitters. *Sci. Rep.*, 7(1), 1-8 (DOI: 10.1038/s41598-017-00368-5); (d) Liu, Y., Li, C., Ren, Z., Yan, S. and Bryce, M.R., (2018). All-organic thermally activated delayed fluorescence materials for organic light-emitting diodes. *Nat. Rev.*

- Mater.*, 3(4), 1-20 (DOI:10.1038/natrevmats.2018.20); (e) Hotta, S., Yamao, T., Bisri, S.Z., Takenobu, T. and Iwasa, Y., (2014). Organic single-crystal light-emitting field-effect transistors. *J. Mater. Chem. C*, 2(6), 965-980 (DOI: 10.1039/C3TC31998A); (f) Figueira-Duarte, T.M. and Mullen, K., (2011). Pyrene-based materials for organic electronics. *Chem. Rev.*, 111(11), 7260-7314 (DOI: 10.1021/cr100428a).
- [2] (a) Gong, Y., Tan, Y., Liu, J., Lu, P., Feng, C., Yuan, W.Z., Lu, Y., Sun, J.Z., He, G. and Zhang, Y., (2013). Twisted D- $\pi$ -A solid emitters: efficient emission and high contrast mechanochromism. *Chem. Commun.*, 49(38), 4009-4011 (DOI: 10.1039/C3CC39243K); (b) Ubba, E., Tao, Y., Yang, Z., Zhao, J., Wang, L. and Chi, Z., (2018). Organic Mechanoluminescence with Aggregation-Induced Emission. *Chem. Asian J.*, 13(21), 3106-3121 (DOI: 10.1039/D1QM00578B); (c) Feng, J., Tian, K., Hu, D., Wang, S., Li, S., Zeng, Y., Li, Y. and Yang, G., (2011). A Triarylboron-Based Fluorescent Thermometer: Sensitive Over a Wide Temperature Range. *Angew. Chem. Int. Ed.* 123(35), 8222-8226 (DOI: 10.1002/anie.201102390); (d) Bi, X., Shi, Y., Peng, T., Yue, S., Wang, F., Zheng, L. and Cao, Q.E., (2021). Multi-Stimuli Responsive and Multicolor Adjustable Pure Organic Room Temperature Fluorescence-Phosphorescent Dual-Emission Materials. *Adv. Fun. Mater.*, 2101312 (DOI: 10.1002/adfm.202101312); (e) Sun, Z., Ni, Y., Prakasam, T., Liu, W., Wu, H., Zhang, Z., Di, H., Baldrige, K.K., Trabolsi, A. and Olson, M.A., (2021). The Unusual Photochromic and Hydrochromic Switching Behavior of Cellulose-Embedded 1, 8-Naphthalimide-Viologen Derivatives in the Solid-State. *Chem. Eur. J.* 27(36), 9360-9371 (DOI:10.1002/chem.202100601); (f) Ma, C., Xu, B., Xie, G., He, J., Zhou, X., Peng, B., Jiang, L., Xu, B., Tian, W., Chi, Z. and Liu, S., (2014). An AIE-active luminophore with tunable and remarkable fluorescence switching based on the piezo and protonation-

- deprotonation control. *Chem. Commun.*, 50(55), 7374-7377 (DOI: 10.1039/C4CC01012D).
- [3] (a) Wu, X. and Zhu, W., (2015). Stability enhancement of fluorophores for lighting up practical application in bioimaging. *Chem. Soc. Rev.*, 44(13), 4179-4184 (DOI: 10.1039/C4CS00152D); (b) Zhu, S., Tian, R., Antaris, A.L., Chen, X. and Dai, H., (2019). Near-infrared-II molecular dyes for cancer imaging and surgery. *Adv. Mater.*, 31(24), 1900321 (DOI:10.1002/adma.201900321); (c) Jiang, R., Liu, M., Chen, T., Huang, H., Huang, Q., Tian, J., Wen, Y., Cao, Q.Y., Zhang, X. and Wei, Y., (2018). Facile construction and biological imaging of cross-linked fluorescent organic nanoparticles with aggregation-induced emission feature through a catalyst-free azide-alkyne click reaction. *Dyes and Pigments*, 148, 52-60 (DOI:10.1016/j.jcis.2018.05.043); (d) Zhang, J., Li, H., Lin, B., Luo, X., Yin, P., Yi, T., Xue, B., Zhang, X.L., Zhu, H. and Nie, Z., (2021). Development of Near-Infrared Nucleic Acid Mimics of Fluorescent Proteins for In Vivo Imaging of Viral RNA with Turn-On Fluorescence. *J. Am. Chem. Soc.*, 143(46), 19317-19329 (DOI:10.1021/jacs.1c04577).
- [4] (a) Gao, P., Pan, W., Li, N. and Tang, B., (2019). Fluorescent probes for organelle-targeted bioactive species imaging. *Chem. Sci*, 10(24), 6035-6071 (DOI: 10.1039/C9SC01652J); (b) Neto, B.A., Correa, J.R. and Spencer, J., (2021). Fluorescent Benzothiadiazole Derivatives as Fluorescence Imaging Dyes: A Decade of a New Generation Probes *Chem. Eur. J* (DOI:10.1002/chem.202103262); (c) Wu, D., Chen, L., Lee, W., Ko, G., Yin, J. and Yoon, J., (2018). Recent progress in the development of organic dye based near-infrared fluorescence probes for metal ions. *Coord. Chem. Rev.* 354, 74-97 (DOI:10.1016/j.ccr.2017.06.011).
- [5] (a) Thomas, S.W., Joly, G.D. and Swager, T.M., (2007). Chemical sensors based on amplifying fluorescent conjugated polymers. *Chem.*

- Rev.*, 107(4), 1339-1386 (DOI: 10.1021/cr0501339); (b) Li, Y.P., Zhu, X.H., Li, S.N., Jiang, Y.C., Hu, M.C. and Zhai, Q.G., (2019). Highly selective and sensitive turn-off-on fluorescent probes for sensing Al<sup>3+</sup> ions designed by regulating the excited-state intramolecular proton transfer process in metal-organic frameworks. *ACS Appl. Mater. Interfaces*, 11(12), 11338-11348 (DOI:10.1021/acsami.8b20410); (c) Steinegger, A., Wolfbeis, O.S. and Borisov, S.M., (2020). Optical sensing and imaging of pH values: spectroscopies, materials, and applications. *Chem. Rev.*, 120(22), 12357-12489 (DOI: acs.chemrev.0c00451); (d) Wu, D., Sedgwick, A.C., Gunnlaugsson, T., Akkaya, E.U., Yoon, J. and James, T.D., (2017). Fluorescent chemosensors: the past, present and future. *Chem. Soc. Rev.*, 46(23), 7105-7123 (DOI: 10.1039/C7CS00240H); (e) Roy, B., Bar, A.K., Gole, B. and Mukherjee, P.S., (2013). Fluorescent tris-imidazolium sensors for picric acid explosive. *J. Org. Chem.*, 78(3), 1306-1310 (DOI: 10.1021/jo302585a).
- [6] (a) Zhuang, Y., Wang, L., Lv, Y., Zhou, T.L. and Xie, R.J., (2018). Optical data storage and multicolor emission readout on flexible films using deep-trap persistent luminescence materials. *Adv. Fun. Mater.*, 28(8), 1705769 (DOI:10.1002/adfm.201705769); (b) Yu, J., Luo, M., Lv, Z., Huang, S., Hsu, H.H., Kuo, C.C., Han, S.T. and Zhou, Y., (2020). Recent advances in optical and optoelectronic data storage based on luminescent nanomaterials. *Nanoscale*, 12(46), 23391-23423 (DOI: f10.1039/D0NR06719A); (c) Chen, J., Zhong, W., Tang, Y., Wu, Z., Li, Y., Yi, P. and Jiang, J., (2015). Amphiphilic BODIPY-based photoswitchable fluorescent polymeric nanoparticles for rewritable patterning and dual-color cell imaging. *Macromolecules*, 48(11), 3500-3508 (DOI:10.1021/acs.macromol.5b00667).
- [7] (a) Jiang, Y., Liu, Y.Y., Liu, X., Lin, H., Gao, K., Lai, W.Y. and Huang, W., (2020). Organic solid-state lasers: a materials view and future development. *Chem. Soc. Rev.* 49(16), 5885-5944 (DOI:

- 10.1039/D0CS00037J); (b) Fang, H.H., Yang, J., Feng, J., Yamao, T., Hotta, S. and Sun, H.B., (2014). Functional organic single crystals for solid-state laser applications. *Laser Photon Rev*, 8(5), 687-715 (DOI:10.1002/lpor.201300222); (c) Gierschner, J., Varghese, S. and Park, S.Y., (2016). Organic single crystal lasers: A materials view. *Adv Optical Mater*, 4(3), 348-364 (DOI:10.1002/adom.201500531).
- [8] (a) Kobayashi, H., Ogawa, M., Alford, R., Choyke, P.L. and Urano, Y., (2010). New strategies for fluorescent probe design in medical diagnostic imaging. *Chem. Rev.* 110(5), 2620-2640 (DOI: 10.1021/cr900263j); (b) Qin, W., Ding, D., Liu, J., Yuan, W.Z., Hu, Y., Liu, B. and Tang, B.Z., (2012). Biocompatible nanoparticles with aggregation-induced emission characteristics as far-red/near-infrared fluorescent bioprobes for in vitro and in vivo imaging applications. *Adv Funct Mater*, 22(4), 771-779 (DOI:10.1002/adfm.201102191); (c) Zhou, J. and Ma, H., (2016). Design principles of spectroscopic probes for biological applications. *Chem. Sci.*, 7(10), 6309-6315 (DOI: 10.1039/C6SC02500E); (d) Wang, H. and Liu, G., (2018). Advances in luminescent materials with aggregation-induced emission (AIE) properties for biomedical applications. *J. Mater. Chem. B*, 6(24), 4029-4042 (DOI: 10.1039/C8TB00674A).
- [9] (a) Mazzio, K.A. and Luscombe, C.K., (2014). The future of organic photovoltaics. *Chem. Soc. Rev.*, 44(1), 78-90 (DOI: 10.1039/C4CS00227J); (b) Yao, H., Ye, L., Zhang, H., Li, S., Zhang, S. and Hou, J., (2016). Molecular design of benzodithiophene-based organic photovoltaic materials. *Chem. Rev.*, 116(12), 7397-7457 (DOI: 10.1021/acs.chemrev.6b00176); (c) Zhang, X., Dong, H. and Hu, W., (2018). Organic semiconductor single crystals for electronics and photonics. *Adv. Mater*, 30(44), 1801048 (DOI: 10.1002/adma.201801048); (d) Xu, S., Wu, W., Cai, X., Zhang, C.J., Yuan, Y., Liang, J., Feng, G., Manghnani, P. and Liu, B., (2017). Highly

- efficient photosensitizers with aggregation-induced emission characteristics obtained through precise molecular design *Chem. Commun.*, *53*(62), 8727-8730 (DOI: 10.1039/C7CC04864E).
- [10] (a) Stennett, E.M., Ciuba, M.A. and Levitus, M., (2014). Photophysical processes in single molecule organic fluorescent probes. *Chem. Soc. Rev.*, *43*(4), 1057-1075 (DOI: 10.1039/C3CS60211G); (b) Shimizu, M. and Hiyama, T., (2010). Organic fluorophores exhibiting highly efficient photoluminescence in the solid state. *Chem. – Asian J.*, *5*(7), 1516-1531 (DOI: 10.1002/asia.200900727); (c) Woodward, A.N., Kolesar, J.M., Hall, S.R., Saleh, N.A., Jones, D.S. and Walter, M.G., (2017). Thiazolothiazole fluorophores exhibiting strong fluorescence and viologen-like reversible electrochromism. *J. Am. Chem. Soc.*, *139*(25), 8467-8473 (DOI: 10.1021/jacs.7b01005).
- [11] Valeur, B. and Berberan-Santos, M.N., (2011). A brief history of fluorescence and phosphorescence before the emergence of quantum theory. *J. Chem. Educ.* *88*(6), 731-738 (DOI: 10.1021/ed100182h).
- [12] Valeur, B. and Berberan-Santos, M.N., 2012. *Molecular fluorescence: principles and applications*. John Wiley & Sons. (DOI:10.1002/978352765000)
- [13] Gao, R., Kodaimati, M.S. and Yan, D., (2021). Recent advances in persistent luminescence based on molecular hybrid materials. *Chem. Soc. Rev.* (DOI: 10.1039/D0CS01463J).
- [14] (a) Kim, C.H. and Joo, T., (2009). Coherent excited state intramolecular proton transfer probed by time-resolved fluorescence. *Phys. Chem. Chem. Phys.*, *11*(44), 10266-10269 (DOI: 10.1039/B915768A); (b) Tahara, H., Uranaka, K., Hirano, M., Ikeda, T., Sagara, T. and Murakami, H., (2018). Electrochromism of ferrocene-and viologen-based redox-active ionic liquids composite. *ACS Appl. Mater. Interfaces*, *11*(1), 1-6 (DOI: 10.1021/acsami.8b16410); (c) Klajn, R., (2014). Spiropyran-based dynamic materials. *Chem. Soc. Rev.*, *43*(1), 148-184 (DOI:

- 10.1039/C3CS60181A); (d) Li, Z., Dong, Y., Mi, B., Tang, Y., Häußler, M., Tong, H., Dong, Y., Lam, J.W., Ren, Y., Sung, H.H. and Wong, K.S., (2005). Structural control of the photoluminescence of silole regioisomers and their utility as sensitive regiodiscriminating chemosensors and efficient electroluminescent materials. *The J. Phys. Chem. B*, *109*(20), 10061-10066 (DOI: 10.1021/jp0503462); (e) Bullock, J.E., Carmieli, R., Mickley, S.M., Vura-Weis, J. and Wasielewski, M.R., (2009). Photoinitiated charge transport through  $\pi$ -stacked electron conduits in supramolecular ordered assemblies of donor–acceptor triads. *J. Am. Chem. Soc.*, *131*(33), 11919-11929 (DOI: 10.1021/ja903903q); (f) Chen, C.H., Ting, H.C., Li, Y.Z., Lo, Y.C., Sher, P.H., Wang, J.K., Chiu, T.L., Lin, C.F., Hsu, I.S., Lee, J.H. and Liu, S.W., (2019). New D–A–A-Configured Small-Molecule Donors for High-Efficiency Vacuum-Processed Organic Photovoltaics under Ambient Light. *ACS Appl. Mater. Interfaces*, *11*(8), 8337-8349 (DOI: 10.1021/acsami.8b20415); (g) Gautam, P., Misra, R., Siddiqui, S.A. and Sharma, G.D., (2015). Unsymmetrical donor–acceptor–acceptor– $\pi$ -donor type benzothiadiazole-based small molecule for a solution processed bulk heterojunction organic solar cell. *ACS Appl. Mater. Interfaces*, *7*(19), 10283-10292 (10.1021/acsami.5b02250).
- [15] (a) Zhang, G., Sun, J., Xue, P., Zhang, Z., Gong, P., Peng, J. and Lu, R., (2015). Phenothiazine modified triphenylacrylonitrile derivatives: AIE and mechanochromism tuned by molecular conformation. *J. Mater. Chem. C*, *3*(12), pp.2925-2932 (DOI: 10.1039/C4TC02925A); (b) Sagara, Y., Mutai, T., Yoshikawa, I. and Araki, K., (2007). Material design for piezochromic luminescence: hydrogen-bond-directed assemblies of a pyrene derivative. *J. Am. Chem. Soc.*, *129*(6), 1520-1521 (10.1021/ja0677362); (c) Sase, M., Yamaguchi, S., Sagara, Y., Yoshikawa, I., Mutai, T. and Araki, K., (2011). Piezochromic luminescence of amide and ester derivatives of tetraphenylpyrene—role of amide hydrogen bonds in sensitive piezochromic response. *J.*

- Mater. Chem.*, 21(23), 8347-8354 (DOI: 10.1039/C0JM03950K); (d) Zhang, X., Wang, J.Y., Ni, J., Zhang, L.Y. and Chen, Z.N., (2012). Vapochromic and mechanochromic phosphorescence materials based on a platinum (II) complex with 4-trifluoromethylphenylacetylide. *Inorg. Chem.*, 51(10), 5569-5579 (DOI: 10.1021/acs.cgd.9b01596); (e) Kosuge, T., Zhu, X., Lau, V.M., Aoki, D., Martinez, T.J., Moore, J.S. and Otsuka, H., (2019). Multicolor mechanochromism of a polymer/silica composite with dual distinct mechanophores. *J. Am. Chem. Soc.*, 141(5), 1898-1902 (DOI: 10.1021/jacs.8b13310).
- [16] (a) Cai, S., Shi, H., Li, J., Gu, L., Ni, Y., Cheng, Z., Wang, S., Xiong, W.W., Li, L., An, Z. and Huang, W., (2017). Visible-light-excited ultralong organic phosphorescence by manipulating intermolecular interactions. *Adv. Mater.*, 29(35), 1701244 (DOI: 10.1002/adma.201701244); (b) Yu, Y., Wang, C., Wei, Y., Fan, Y., Yang, J., Wang, J., Han, M., Li, Q. and Li, Z., (2019). Halogen-Containing TPA-Based Luminogens: Different Molecular Packing and Different Mechanoluminescence. *Adv. Opt. Mater.*, 7(18), 1900505 (DOI:10.1002/adom.201900505); (c) Li, Q. and Li, Z., (2020). Molecular packing: another key point for the performance of organic and polymeric optoelectronic materials. *Acc Chem Res*, 53(4), 962-973 (DOI: 10.1021/acs.accounts.0c00060); (d) Li, Q. and Li, Z., (2020). Miracles of molecular uniting. *Sci China Mater*, 63(2), 177-184. (doi.org/10.1007/s40843-019- 1172-2).
- [17] (a) Zöphel, L., Beckmann, D., Enkelmann, V., Chercka, D., Rieger, R. and Müllen, K., (2011). Asymmetric pyrene derivatives for organic field-effect transistors. *Chem. Commun.*, 47(24), 6960-6962 (DOI: 10.1039/C1CC11827G); (b) Lu, X., Fan, S., Wu, J., Jia, X., Wang, Z.S. and Zhou, G., (2014). Controlling the charge transfer in D–A–D chromophores based on pyrazine derivatives. *J. Org. Chem.*, 79(14), 6480-6489 (DOI: 10.1021/cm301520z); (c) Kivala, M., Boudon, C.,

- Gisselbrecht, J.P., Seiler, P., Gross, M. and Diederich, F., (2007). A novel reaction of 7, 7, 8, 8-tetracyanoquinodimethane (TCNQ): charge-transfer chromophores by [2+ 2] cycloaddition with alkynes. *Chem. Commun.*, (45), 4731-4733 (DOI: 10.1039/B713683H); (d) Beaujuge, P.M., Amb, C.M. and Reynolds, J.R., (2010). Spectral engineering in  $\pi$ -conjugated polymers with intramolecular donor–acceptor interactions. *Acc. Chem. Res.*, 43(11), 1396-1407 (DOI: 10.1021/ar100043u).
- [18] (a) Kurata, R., Ito, A., Gon, M., Tanaka, K., Chujo, Y. (2017). Diarylamino-and diarylboryl-substituted donor–acceptor pyrene derivatives: influence of substitution pattern on their photophysical properties. *J. Org. Chem.*, 82(10), 5111-5121. (DOI: <https://doi.org/10.1021/acs.joc.7b00315>); (b) Panja, S. K., Dwivedi, N., Saha, S. (2016). Tuning the intramolecular charge transfer (ICT) process in push–pull systems: effect of nitro groups. *RSC Adv.*, 6(107), 105786-105794. (DOI: 10.1039/C6RA17521J) (d) Sung, J., Nowak-Król, A., Schlosser, F., Fimmel, B., Kim, W., Kim, D., Würthner, F. (2016). Direct observation of excimer-mediated intramolecular electron transfer in a cofacially-stacked perylene bisimide pair. *J. Am. Chem. Soc.*, 138(29), 9029-9032. (DOI: <https://doi.org/10.1021/jacs.6b04591>)
- [19] (a) Zhang, Y., Wang, K., Zhuang, G., Xie, Z., Zhang, C., Cao, F., Pan, G., Chen, H., Zou, B., Ma, Y. (2015). Multicolored-fluorescence switching of ICT-type organic solids with clear color difference: mechanically controlled excited state. *Chem. Eur. J.*, 21(6), 2474-2479. (DOI: <https://doi.org/10.1002/chem.201405348>); (b) Kim, T. D., Lee, K. S. (2015). D- $\pi$ -A Conjugated Molecules for Optoelectronic Applications. *Macromol. Rapid Commun.*, 36(11), 943-958. (DOI: <https://doi.org/10.1002/marc.201400749>); (c) Bures, F., Schweizer, W. B., May, J. C., Boudon, C., Gisselbrecht, J.- P., Gross, M., Biaggio, I., Diederich, F. (2007). Property Tuning in

- Charge-Transfer Chromophores by Systematic Modulation of the Spacer between Donor and Acceptor. *Chem. Eur. J.*, 13, 5378–5387 (DOI: 10.1002/chem.200601735); (d) Wang, J.-L., Xiao, Q., Pei, J. (2010). Benzothiadiazole-Based D- $\pi$ -A- $\pi$ -D Organic Dyes with Tunable Band Gap: Synthesis and Photophysical Properties. *Org. Lett.*, 12, 4164–4167 (DOI: 10.1021/ol101754q).
- [20] (a) Park, S., Seo, J., Kim, S. H., Park, S. Y. (2008). Tetraphenylimidazole-Based Excited-State Intramolecular Proton-Transfer Molecules for Highly Efficient Blue Electroluminescence. *Adv. Funct. Mater.*, 18(5), 726-731. (DOI: <https://doi.org/10.1002/adfm.200700827>); (b) Liu, T., Zhu, L., Zhong, C., Xie, G., Gong, S., Fang, J., Ma, D., Yang, C. (2017). Naphthothiadiazole-Based Near-Infrared Emitter with a Photoluminescence Quantum Yield of 60% in Neat Film and External Quantum Efficiencies of up to 3.9% in Nondoped OLEDs. *Adv. Funct. Mater.*, 27(12), 1606384. (DOI: <https://doi.org/10.1002/adfm.201606384>); (c) Sharma, C. P.; Gupta, N. M.; Singh, J.; Yadav, R. A. K.; Dubey, D. K.; Rawat, K. S.; Jha, A. K.; Jou, J.-H.; Goel, A. Synthesis of Solution-Processable Donor–Acceptor Pyranone Dyads for White Organic Light-Emitting Devices. *J. Org. Chem.* 2019, 84, 7674–7684, (DOI: <https://doi.org/10.1021/acs.joc.9b00293>); (d) Tang, X., Liu, H., Xu, L., Xu, X., He, X., Liu, F., Chen, J., Peng, Q. (2021). Achieving High Efficiency at High Luminance in Fluorescent Organic Light-Emitting Diodes through Triplet–Triplet Fusion Based on Phenanthroimidazole-Benzothiadiazole Derivatives. *Chem. Eur. J.*, 27(55), 13828-13839. (DOI: <https://doi.org/10.1002/chem.202102136>)
- [21] (a) Crossley, D. L., Urbano, L., Neumann, R., Bourke, S., Jones, J., Dailey, L. A., Green, M., Humphries, M. J., King, S. M., Turner, M. L., Ingleson, M. J. (2017), Post-polymerization C–H Borylation of Donor–

- Acceptor Materials Gives Highly Efficient Solid State Near-Infrared Emitters for Near-IR-OLEDs and Effective Biological Imaging, *ACS Appl. Mater. Interfaces*, 9, 34, 28243-28249 (DOI: 10.1021/acsami.7b08473); (b) Liao, Y., Wang, R., Wang, S., Xie, Y., Chen, H., Huang, R., Shao, L., Zhu, Q., Liu, Y., *ACS Appl. Mater. Interfaces* (2021), 13(46), 54783-54793 (DOI: <https://doi.org/10.1021/acsami.1c17476>); (c) Zhao, Y., Zhang, Z., Lu, Z., Wang, H., Tang, Y. (2019), Enhanced Energy Transfer in a Donor–Acceptor Photosensitizer Triggers Efficient Photodynamic Therapy, *ACS Appl. Mater. Interfaces*, 11, 42, 38467- 38474 (DOI: 10.1021/acsami.9b12375); (d) Jung, H. S.; Verwilst, P.; Sharma, A.; Shin, J.; Sessler, J. L.; Kim, J. S. Organic molecule-based photothermal agents: an expanding photothermal therapy universe. *Chem. Soc. Rev.* 2018, 47, 2280–2297. (DOI: 10.1039/C7CS00522A)
- [22] (a) Chen, J., Vachon, J., Feringa, B. L. (2018). Design, synthesis, and isomerization studies of light-driven molecular motors for single molecular imaging. *J. Org. Chem.*, 83(11), 6025-6034. (DOI: <https://doi.org/10.1021/acs.joc.8b00654>); (b) Zhao, B., Li, N., Wang, X., Chang, Z., Bu, X. H. (2017). Host–Guest Engineering of Coordination Polymers for Highly Tunable Luminophores Based on Charge Transfer Emissions. *ACS Appl. Mater. Interfaces*, 9(3), 2662-2668. (DOI: <https://doi.org/10.1021/acsami.6b14554>); (c) Jadhav, T., Dhokale, B., Patil, Y., Mobin, S. M., Misra, R. (2016). Multi-stimuli responsive donor–acceptor tetraphenylethylene substituted benzothiadiazoles. *J. Phys. Chem. C*, 120(42), 24030-24040. (DOI: <https://doi.org/10.1021/acs.jpcc.6b09015>); (d) Zhu, H., Chen, P., Kong, L., Tian, Y., Yang, J. (2018). Twisted donor– $\pi$ –acceptor carbazole luminophores with substituent-dependent properties of aggregated behavior (Aggregation-Caused quenching to aggregation-enhanced emission) and mechanoresponsive luminescence. *J. Phys. Chem.*

*C*, 122(34), 19793-19800. (DOI: <https://doi.org/10.1021/acs.jpcc.8b05638>)

- [23] (a) Wu, D., Sedgwick, A. C., Gunnlaugsson, T., Akkaya, E. U., Yoon, J., James, T. D. (2017). Fluorescent chemosensors: the past, present and future. *Chem. Soc. Rev.*, 46(23), 7105-7123. (DOI: 10.1039/C7CS00240H); (b) Collot, M. (2020). Recent advances in dioxaborine-based fluorescent materials for bioimaging applications. *Mater. Horiz.*, 2021, 8, 501-514 (DOI: 10.1039/D0MH01186J); (c) Hu, Y., Long, S., Fu, H., She, Y., Xu, Z., Yoon, J. (2021). Revisiting imidazolium receptors for the recognition of anions: Highlighted research during 2010–2019. *Chem. Soc. Rev.*, 2021, 50, 589-618. (DOI: 10.1039/D0CS00642D); (d) Sedgwick, A. C., Wu, L., Han, H. H., Bull, S. D., He, X. P., James, T. D., Sessler, J.L., Tang, B.Z., Tian, H., Yoon, J. (2018). Excited-state intramolecular proton-transfer (ESIPT) based fluorescence sensors and imaging agents. *Chem. Soc. Rev.*, 47(23), 8842-8880. (DOI: 10.1039/C8CS00185E); (e) Cheon, H. J., Li, X., Jeong, Y. J., Sung, M. J., Li, Z., Jeon, I., Tang, X., Girma, H.G., Kong, H., Kwon, S.K., An, T.K., Kim, S. H., Kim, Y. H. (2020). A novel design of donor–acceptor polymer semiconductors for printed electronics: application to transistors and gas sensors. *J. Mater. Chem. C*, 8(25), 8410-8419. (DOI: <https://doi.org/10.1039/D0TC01341B>)
- [24] (a) Sirringhaus, H. (2014), 25th anniversary article: organic field-effect transistors: the path beyond amorphous silicon. *Adv. Mater.*, 26, 9, 1319–1335 (DOI: 10.1002/adma.201304346); (b) Shuai, Q., Black, H., Dadvand, A., Perepichka, D. (2014), Dithienonaphthothiadiazole semiconductors: synthesis, properties, and application to ambipolar field effect transistors. *J. Mater. Chem. C*, 2, 3972–3979 (DOI: 10.1039/C4TC00094C); (c) Chen, R., Lu, R.-Q., Shi, K., Wu, F., Fang, H.-X., Niu, Z.-X., Yan, X.-Y., Luo, M., Wang, X.-C., Yang, C.-Y., et al. (2015), Corannulene derivatives with low LUMO levels and

- dense convex-concave packing for n-channel organic field-effect transistors. *Chem. Commun.* 51, 13768–13771 (DOI: 10.1039/C5CC03550C); (d) Guo, X., Ortiz, R. P., Zheng, Y., Hu, Y., Noh, Y.-Y., Baeg, K.-J., Facchetti, A., Marks, T. J. (2011), Bithiophene-Imide-Based Polymeric Semiconductors for Field-Effect Transistors: Synthesis, Structure-Property Correlations, Charge Carrier Polarity, and Device Stability. *J. Am. Chem. Soc.* 133, 1405–1418 (DOI: 10.1021/ja107678m).
- [25] (a) Ran, H., Zhao, Z., Duan, X., Xie, F., Han, R., Sun, H., Hu, J. Y. (2021). Blue-emitting butterfly-shaped donor–acceptor-type 1, 3, 5, 9-tetraarylpyrenes: easily available, low-cost conventional fluorophores for high-performance near ultraviolet electroluminescence with CIE  $y < 0.05$ . *J. Mater. Chem. C*, 9(1), 260-269. (DOI: 10.1039/D0TC03612A); (b) Lee, K. H., Kim, Y. K., Yoon, S. S. (2011). Donor-Acceptor-Donor Type Red Fluorescent Emitters Containing Adamandane-substituted Julolidines for OLEDs. *Bull Korean Chem Soc B*, 32(8), 2787-2790. (DOI: <https://doi.org/10.5012/bkcs.2011.32.8.2787>)
- [26] (a) Huo, F., Zhang, H., Chen, Z., Qiu, L., Liu, J., Bo, S., Kityk, I. V. (2019), Novel nonlinear optical push–pull fluorene dyes chromophore as promising materials for telecommunications, *J Mater Sci: Mater Electron*, 30, 12180–12185 (DOI: 10.1007/s10854-019-01576-7), ); (b) Zheng, Z., Li, D., Liu, Z., Peng, H., Sung, H. H. Y., Kwok, R. T. K., Williams, I. D., Lam, J. W. Y., Qian, J., Tang, B. Z. (2019), Aggregation-Induced Nonlinear Optical Effects of AIE gen Nanocrystals for Ultradeep In Vivo Bioimaging. *Adv. Mater.*, 31, issue 44 (DOI: 10.1002/adma.201904799); (c) Dini, D., Calvete, M. J., Hanack, M. (2016), Nonlinear Optical Materials for the Smart Filtering of Optical Radiation. *Chem. Rev.*, 116, 22 13043-13233 (DOI: 10.1021/acs.chemrev.6b00033).

- [27] (a) Belletete M., Bouchard J., Leclerc M., Durocher G., (2005), Photophysics and solvent-induced aggregation of 2,7-carbazole-based conjugated polymers, *Macromolecules*, 38, 880–887 (DOI: 10.1021/MA048202T); (b) Samuel W. Thomas III., Guy D. J., Swager T. M. (2007), Chemical sensors based on amplifying fluorescent conjugated polymers, *Chem. Rev.*, 2007, 107, 1339–1386 (DOI: 10.1021/CR0501339); (c) Chen C-T. (2004), Evolution of red organic light-emitting diodes: *Materials and devices*, (DOI: 10.1021/CM049679M); (d) Jakubiak R., Collison C. J., Wan W. C., Rothberg L. J., Hsieh B. R. (1999), Aggregation quenching of luminescence in electroluminescent conjugated polymers, *J. Phys. Chem. A*, 103, 2394–2398 (DOI: 10.1021/JP9839450).
- [28] Arney, K., Fluorescein has been discovered with strong green emission when it was dissolved in alcohol or water and put under an ultraviolet light, <https://www.chemistryworld.com/podcasts/fluorescein/9574.article>.
- [29] Perrin, J. B. (1923), *C. R. Acad. Sci.*, 177.
- [30] Förster, S. (1954). Th., u. K. Kasper: *Z. physik. Chem., NF*, 1, 275.
- [31] Birks, J. B. (1970). Photophysical processes. Photophysics of Aromatic Molecules. JB Birks, editor. *Wiley-Interscience, London*, 29-43.
- [32] (a) Tang, C. W., VanSlyke, S. A. (1987). Organic electroluminescent diodes. *Appl. Phys. Lett.*, 51(12), 913-915. (DOI: <https://doi.org/10.1063/1.98799>); (b) Geddes, C. D., Aslan, K., Gryczynski, I., Malicka, J., Matveeva, E. (2005). In CD Geddes and JR Lakowicz. *Topics in Fluorescence in Fluorescence Spectroscopy*, 401-448.; (c) Jares-Erijman, E. A., Jovin, T. M. (2003). FRET imaging. *Nat. Biotechnol.*, 21(11), 1387-1395. (DOI: <https://doi.org/10.1038/nbt896>); (d) Saigusa, H., Lim, E. C. (1995). Excited-state dynamics of aromatic clusters: correlation between exciton interactions and excimer formation dynamics. *J. Phys.*

- Chem.*, 99(43), 15738-15747. (DOI: <https://doi.org/10.1021/j100043a010>)
- [33] (a) Wang, J., Zhao, Y., Dou, C., Sun, H., Xu, P., Ye, K., Zhang, J., Jiang, S., Li, F., Wang, Y. (2007). Alkyl and dendron substituted quinacridones: synthesis, structures, and luminescent properties. *J. Phys. Chem. B*, 111(19), 5082-5089. (DOI: <https://doi.org/10.1021/jp068646m>); (b) Hecht, S., Fréchet, J. M. (2001). Dendritic encapsulation of function: applying nature's site isolation principle from biomimetics to materials science. *Angew. Chem. Int. Ed.*, 40(1), 74-91. (DOI: [https://doi.org/10.1002/1521-3773\(20010105\)40:1<74::AID-ANIE74>3.0.CO;2-C](https://doi.org/10.1002/1521-3773(20010105)40:1<74::AID-ANIE74>3.0.CO;2-C)).
- [34] (a) Nguyen, B. T., Gautrot, J. E., Ji, C., Brunner, P. L., Nguyen, M. T., Zhu, X. X. (2006). Enhancing the photoluminescence intensity of conjugated polycationic polymers by using quantum dots as antiaggregation reagents. *Langmuir*, 22(10), 4799-4803. (DOI: <https://doi.org/10.1021/la053399j>); (b) Chen, L., Xu, S., McBranch, D., Whitten, D. (2000). Tuning the properties of conjugated polyelectrolytes through surfactant complexation. *J. Am. Chem. Soc.*, 122(38), 9302-9303. (DOI: <https://doi.org/10.1021/ja001248r>); (c) Taylor, P. N., O'Connell, M. J., McNeill, L. A., Hall, M. J., Aplin, R. T., Anderson, H. L. (2000). Insulated molecular wires: synthesis of conjugated polyrotaxanes by Suzuki coupling in water. *Angewandte Chemie International Edition*, 39(19), 3456-3460. (DOI: [https://doi.org/10.1002/1521-3773\(20001002\)39:19<3456::AID-ANIE3456>3.0.CO;2-0](https://doi.org/10.1002/1521-3773(20001002)39:19<3456::AID-ANIE3456>3.0.CO;2-0)).
- [35] (a) Luo, J., Xie, Z., Lam, J. W. Y., Chen, H., Qui, C., Kwok, H. S., Zhan, X., Liu, Y., Zhu, D. Tang, B. Z. (2001). Aggregation-induced emission of 1-methyl-1, 2, 3, 4, 5-pentaphenylsilole. *Chem commu.*, (18), 1740-1741. (DOI: <https://doi.org/10.1039/B105159H>); (b) Tang, B. Z., Zhan, X., Yu, G., Lee, P. P. S., Liu, Y., Zhu, D. (2001). Efficient blue emission from siloles. *J. Mater. Chem. C*, 11(12), 2974-2978.

- (DOI: 10.1039/B102221K); (c) Liu Y., Tao X., Wang F., Dang X., Zou D., Ren Y., Jiang M. (2008), Aggregation-induced emissions of fluorenonearylamine derivatives: a new kind of materials for nondoped red organic light-emitting diodes, *J. Phys. Chem. C*, 112, 3975–3981 (DOI: 10.1021/JP7117373); (d) Davis R., Kumar N. S. S., Abraham S., Suresh C. H., Rath N. P., Tamaoki N., Das S. (2008), Molecular packing and solid-state fluorescence of alkoxy-cyano substituted diphenylbutadienes: structure of the luminescent aggregates, *J. Phys. Chem. C*, 112, 2137–2146 (DOI: 10.1021/JP710352M); (e) Ning Z., Chen Z., Zhang Q., Yan Y., Qian S., Cao Y., Tian H. (2007), Aggregation-induced emission (AIE) active starburst triarylamine fluorophores as potential non-doped red emitters for organic light-emitting diodes and c12 gas chemodosimeter, *Adv. Funct. Mater.*, 17, 3799–3807 (DOI: 10.1002/adfm.200700649).
- [36] Tang B Z., Zhan X., Yu G., Sze Lee P P., Liu Y., Zhu D. (2001), Efficient blue emission from siloles, *J. Mater. Chem.*, 11, 2974–2978 (DOI: 10.1039/b102221k).
- [37] Ju Mei, Nelson L. C. Leung, Ryan T. K. Kwok, Jacky W. Y. Lam, Ben Zhong Tang, *Chem. Rev.* 2015, 115, 11718–11940. (DOI: 10.1021/acs.chemrev.5b00263)
- [38] (a) Tang B. Z., Geng Y., Lam J. W. Y., Li B. (1999), Processible nanostructured materials with electrical conductivity and magnetic susceptibility: preparation and properties of maghemite/polyaniline nanocomposite films, *Chem. Mater.*, 11, 1581–1589 (DOI: 10.1021/CM9900305).
- [39] (a) Chen J., Law C. C. W., Lam J. W. Y., Dong Y., Lo S. M. F., Williams I. D., Zhu Daoben., Tang B. Z. (2003), Synthesis, light emission, nanoaggregation, and restricted intramolecular rotation of 1,1-substituted 2,3,4,5-tetraphenylsiloles, *Chem. Mater.*, 15, 1535–1546 (DOI: 10.1021/CM021715Z); (b) Fan X., Sun J., Wang F., Chu

- Z., Wang P., Dong Y., Hu R., Tang B Z., Zou D. (2008), Photoluminescence and electroluminescence of hexaphenylsilole are enhanced by pressurization in the solid state, *Chem. Commun.*, 124, 2989 (DOI: 10.1039/b803539c).
- [40] (a) Tong, H., Dong, Y., Hong, Y., Häußler, M., Lam, J. W., Sung, H. H. Y., Yu, X., Sun, J., Williams, I.D., Kwok, H.S., Tang, B. Z. (2007). Aggregation-induced emission: effects of molecular structure, solid-state conformation, and morphological packing arrangement on light-emitting behaviors of diphenyldibenzofulvene derivatives. *J. Phys. Chem. C*, 111(5), 2287-2294. (DOI: <https://doi.org/10.1021/jp0630828>); (b) Dong, Y., Lam, J. W., Qin, A., Liu, J., Li, Z., Tang, B. Z., Sun, J., Kwok, H. S. (2007). Aggregation-induced emissions of tetraphenylethene derivatives and their utilities as chemical vapor sensors and in organic light-emitting diodes. *Appl. Phys. Lett.*, 91(1), 011111.(DOI: <https://doi.org/10.1063/1.2753723>).
- [41] Luo, J., Song, K., long Gu, F., and Miao, Q. (2011). Switching of non-helical overcrowded tetrabenzoheptafulvalene derivatives. *Chem. Sci.*, 2(10), 2029-2034 (DOI: 10.1039/c1sc00340b).
- [42] Leung, N. L., Xie, N., Yuan, W., Liu, Y., Wu, Q., Peng, Q., Miao, Q., Lam, J. W. Y. and Tang, B. Z. (2014). Restriction of intramolecular motions: the general mechanism behind aggregation-induced emission. *Chem. Eur. J.*, 20(47), 15349-15353 (DOI: <https://doi.org/10.1002/chem.201403811>).
- [43] (a) Xu, C., Wu, T., Duan, L., Zhou, Y., (2021). A naphthalimide-derived hypochlorite fluorescent probe from ACQ to AIE effect transformation. *Chem. Commun.*, 2021,57, 11366-11369 (DOI: <https://doi.org/10.1039/D1CC04157F>); (b) Lee, W. W., Zhao, Z., Cai, Y., Xu, Z., Yu, Y., Xiong, Y., Kwok, R. T. K., Chen, Y., Leung, N. L. C., Ma, D., Lam, J. W. Y., Qin, A., Tang, B. Z. (2018). Facile access to deep red/near-infrared emissive AIEgens for efficient non-doped

- OLEDs. *Chem. Sci.*, 9(28), 6118-6125. (DOI: 10.1039/C8SC01377B); (c) Suzuki, S., Sasaki, S., Sairi, A. S., Iwai, R., Tang, B. Z., Konishi, G. I. (2020). Principles of Aggregation-Induced Emission: Design of Deactivation Pathways for Advanced AIEgens and Applications. *Angew. Chem. Int. Ed.*, 132(25), 9940-9951. (DOI: <https://doi.org/10.1002/ange.202000940>).
- [44] (a) Yang, Z., Chi, Z., Mao, Z., Zhang, Y., Liu, S., Zhao, J., Aldred, M. P. and Chi, Z., (2018). Recent advances in mechano-responsive luminescence of tetraphenylethylene derivatives with aggregation-induced emission properties. *Mater. Chem. Front*, 2(5), 861-890 (DOI: 10.1039/c8qm00062j); (b) Zhao, Z., He, B., and Tang, B. Z., (2015). Aggregation-induced emission of siloles. *Chem. Sci.*, 6(10), 5347-5365 (DOI: 10.1039/c5sc01946j); (c) Yin, G., Li, Y., Li, S., Xu, B., Yang, Q., Zhang, Y., Zhao, J. and Cao, X. (2022). Hexaphenylbenzene based push-pull fluorophores displaying intriguing polarity-dependent fluorescence behavior, AIE(E) characteristics and mega-large Stokes shifts. *Dyes Pigm.*, 198, 110013 (DOI: 10.1016/j.dyepig.2021.110013); (d) Ekbote, A., Mobin, S. M., Misra, R. (2020). Stimuli-responsive phenothiazine-based donor-acceptor isomers: AIE, mechanochromism and polymorphism, *J. Mater. Chem. C.*, 8, 3589-3602 (DOI: 10.1039/C9TC05192A); (e) Liu, J., Meng, Q., Zhang, X., Lu, X., He, P., Jiang, L., Dong, H. and Hu, W. (2013). Aggregation-induced emission enhancement based on 11, 11, 12, 12-tetracyano-9, 10-anthraquinodimethane. *Chem. Commun.*, 49(12), 1199-1201. (DOI: 10.1039/c2cc38817k); (f) Rodrigues, A. C. B., Peixoto, M., Gomes, C., Pineiro, M. and Seixas de Melo, J. S. (2022). Aggregation-Induced Emission Leading to White Light Emission in Diphenylbenzofulvene Derivatives. *Chem. Eur. J.*, e202103768 (DOI: <https://doi.org/10.1002/chem.202103768>); (g) Gong, G., Wu, H., Zhang, T., Wang, Z., Li, X. and Xie, Y. (2021). Aggregation-

- enhanced emission in tetraphenylpyrazine-based luminogens: theoretical modulation and experimental validation. *Mater. Chem. Front*, 5(13), 5012-5023 (DOI: 10.1039/d1qm00313e); (h) Jia, X. R., Yu, H. J., Chen, J., Gao, W. J., Fang, J. K., Qin, Y. S., Hu, X. K. and Shao, G. (2018). Stimuli-Responsive Properties of Aggregation-Induced-Emission Compounds Containing a 9, 10-Distyrylanthracene Moiety. *Chem. Eur. J.*, 24(71), 19053-19059 (DOI:10.1002/chem.201804315); (i) Chen, J., Xu, B., Ouyang, X., Tang, B. Z. and Cao, Y. (2004). Aggregation-induced emission of cis-1, 2, 3, 4-tetraphenylbutadiene from restricted intramolecular rotation. *J. Phys. Chem. A*, 108(37), 7522-7526 (DOI: 10.1021/jp048475q).
- [45] (a) La, D. D., Bhosale, S. V., Jones, L. A., Bhosale, S. V. (2017). Tetraphenylethylene-based AIE-active probes for sensing applications. *ACS Appl. Mater. Interfaces*, 10(15), 12189-12216. (DOI: <https://doi.org/10.1021/acsami.7b12320>); (b) Desroches, M., Morin, J. F. (2018). Anthanthrene as a super-extended tetraphenylethylene for aggregation-induced emission. *Org. Lett.*, 20(10), 2797-2801. (DOI: <https://doi.org/10.1021/acs.orglett.8b00452>); (c) Yin, Y., Zhao, F., Chen, Z., Liu, G., Pu, S. (2018). Aggregation-induced emission enhancement (AIEE)-active mechanofluorochromic tetraphenylethylene derivative bearing a rhodamine unit. *Tetrahedron Lett*, 59(50), 4416-4419. (DOI: <https://doi.org/10.1016/j.tetlet.2018.10.073>); (d) Yu, G., Yin, S., Liu, Y., Chen, J., Xu, X., Sun, X., Ma, D., Zhan, X., Peng, Q., Shuai, Z., Tang, B., Zhu, D., Fang, W., Luo, Y. (2005). Structures, electronic states, photoluminescence, and carrier transport properties of 1, 1-disubstituted 2, 3, 4, 5-tetraphenylsiloles. *J. Am. Chem. Soc.*, 127(17), 6335-6346. (DOI: <https://doi.org/10.1021/ja044628b>)

- [46] (a) Yao, L., Zhang, S., Wang, R., Li, W., Shen, F., Yang, B., Ma, Y., (2014). Highly Efficient Near-Infrared Organic Light-Emitting Diode Based on a Butterfly-Shaped Donor–Acceptor Chromophore with Strong Solid-State Fluorescence and a Large Proportion of Radiative Excitons. *Angew. Chem., Int. Ed.* 53(8), 2119–2123. (DOI: <https://doi.org/10.1002/anie.201308486>)
- [47] (a) Liu, J., Meng, Q., Zhang, X., Lu, X., He, P., Jiang, L., Dong, H., Hu, W. (2013). Aggregation-induced emission enhancement based on 11, 11, 12, 12-tetracyano-9, 10-anthraquinodimethane. *Chem. Commun.*, 49(12), 1199-1201. (DOI: 10.1039/C2CC38817K).
- [48] (a) Liang, J., Tang, B. Z., Liu, B. (2015). Specific light-up bioprobes based on AIEgen conjugates. *Chem. Soc. Rev.*, 44(10), 2798-2811. (DOI: 10.1039/C4CS00444B); (b) Hu, R., Leung, N. L., Tang, B. Z. (2014). AIE macromolecules: syntheses, structures and functionalities. *Chem. Soc. Rev.*, 43(13), 4494-4562. (DOI: 10.1039/C4CS00044G); (c) Imoto, H., Fujii, R., Naka, K. (2018). 3, 4-Diaminomaleimide Dyes–Simple Luminophores with Efficient Orange-Red Emission in the Solid State. *Eur. J. Org. Chem.*, 2018(6), 837-843. (DOI: <https://doi.org/10.1002/ejoc.201701479>); (d) Chen, C., Li, R. H., Zhu, B. S., Wang, K. H., Yao, J. S., Yin, Y. C., Yao, M.M., Yao, H.B., Yu, S. H. (2018). Highly Luminescent Inks: Aggregation-Induced Emission of Copper–Iodine Hybrid Clusters. *Angew. Chem. Int. Ed.*, 57(24), 7106-7110. (DOI: <https://doi.org/10.1002/anie.201802932>)
- [49] (a) Feng, X., Qi, C., Feng, H. T., Zhao, Z., Sung, H. H., Williams, I. D., Kwok, R. T. K., Lam, J.W. Y., Qin, A., Tang, B. Z. (2018). Dual fluorescence of tetraphenylethylene-substituted pyrenes with aggregation-induced emission characteristics for white-light emission. *Chem. Sci*, 9(25), 5679-5687. (DOI: 10.1039/C8SC01709C); (b) Zhang, X., Ma, S., Wu, G., Liu, X., Mateen, M., Ghadari, R., Wu, Y., Ding, Y., Cai, M., Dai, S. (2020).

- Fused tetraphenylethylene–triphenylamine as an efficient hole transporting material in perovskite solar cells. *Chem. Commun.*, 56(21), 3159-3162. (DOI: 10.1039/C9CC09901H); (c) La, D. D., Bhosale, S. V., Jones, L. A., Bhosale, S. V. (2017). Tetraphenylethylene-based AIE-active probes for sensing applications. *ACS Appl. Mater. Interfaces*, 10(15), 12189-12216. (DOI: <https://doi.org/10.1021/acsami.7b12320>).
- [50] Rathore R., Lindeman S. V., Kumar A. S., Kochi J. K. (1998). Disproportionation and Structural Changes of Tetraarylethylene Donors upon Successive Oxidation to Cation Radicals and to Dications. *J. Am. Chem. Soc.*, 120, 6931–6939 (DOI: 10.1021/JA981095W)
- [51] (a) Hong Y., Lam J W Y., Tang B Z. (2009). Aggregation-induced emission: phenomenon, mechanism and applications. *Chem. Commun.*, 1, 4332 (DOI: 10.1039/b904665h); (b) Cheng K. H., Zhong Y., Xie B. Y., Dong Y. Q., Hong Y., Sun J. Z., Tang B. Z., Wong K. S. (2008). Fabrication of and ultraviolet lasing in tpe/pmma polymer nanowires. *J. Phys. Chem. C*, 112, 17507–17511 (DOI: 10.1021/jp805158b).
- [52] Anon (1888). Organic chemistry. *J. Chem. Soc. Abstr.*, 54, 928 (DOI: 10.1039/ca8885400928)
- [53] Wang W., Lin T., Wang M., Liu T-X., Ren L., Chen D., Huang S. (2010). Aggregation emission properties of oligomers based on tetraphenylethylene. *J. Phys. Chem. B*, 114, 5983–5988 (DOI: 10.1021/jp911311j).
- [54] Schreivogel A., Maurer J., Winter R., Baro A., Laschat S. (2006). Synthesis and electrochemical properties of tetrasubstituted tetraphenylethenes. *European J. Org. Chem.*, 2006, 3395–3404 (DOI: 10.1002/ejoc.200600123).
- [55] Okuma K., Kojima K., Oyama K., Kubo K., Shioji K. (2004). Selenobenzophenones and diazoalkanes: isolation of

- tetraarylethylenes 28 by the reaction of benzophenone hydrazones with diselenium dibromide. *European J. Org. Chem.*, 2004, 820–825 (DOI: 10.1002/ejoc.200300510).
- [56] (a) Minato M., Yamamoto K., Tsuji J. (1990). Osmium tetroxide catalyzed vicinal hydroxylation of higher olefins by using hexacyanoferrate(III) ion as a cooxidant, *J. Org. Chem.*, 55, 766–768 (DOI: 10.1021/jo00289a066); (b) Barhdadi R., Courtinard C., Nédélec J. Y., Troupel M. (2003). Roomtemperature ionic liquids as new solvents for organic electrosynthesis. The first examples of direct or nickel-catalysed electroreductive coupling involving organic halides. *Chem. Commun.*, 1434–1435 (DOI: 10.1039/B302944A).
- [57] (a) Hauck, M., Stolte, M., Schönhaber, J., Kuball, H.-G., Müller, T. J. J. (2011) Synthesis, Electronic, and Electro-Optical Properties of Emissive Solvatochromic Phenothiazinyl Merocyanine. *Dyes. Chem. Eur. J.*, 17, 9984–9998 (DOI: 10.1002/chem.201100592); (b) Bejan, A., Shova, S., Damaceanu, M.-D., Simionescu, B. C., Marin L. (2016). Structure-Directed Functional Properties of Phenothiazine Brominated Dyes: Morphology and Photophysical and Electrochemical Properties. *Cryst. Growth Des.*, 16, 3716–3730 (DOI: 10.1021/acs.cgd.6b00212).
- [58] (a) Konidena, R. K., Thomas, K. R. J., Kumar, S., Wang, Y.-C., Li, C.-J., Jou, J.-H. (2015). Phenothiazine Decorated Carbazoles: Effect of Substitution Pattern on the Optical and Electroluminescent Characteristics. *J. Org. Chem.*, 80, 5812–5823 (DOI: 10.1021/acs.joc.5b00787); (b) Hauck, M., Schönhaber, J., Zuccherro, A. J., Hardcastle, K. I., Müller, T. J. J., Bunz, U. H. F. (2007). Phenothiazine Cruciforms: Synthesis and Metallochromic Properties. *J. Org. Chem.*, 72, 6714–6725 (DOI: 10.1021/jo0709221); (c) Wang, W., Li, X., Lan, J., Wu, D., Wang, R., You, J. (2018). Construction of 3,7-Dithienyl Phenothiazine-Based Organic Dyes via Multistep Direct C–H Arylation Reactions. *J. Org. Chem.*, 83, 8114–8126

- (DOI: 10.1021/acs.joc.8b00915); (d) Rechmann, J., Sarfraz, A., Götzinger, A. C., Dirksen, E., Müller, T. J. J., Erbe A. (2015). Surface Functionalization of Oxide-Covered Zinc and Iron with Phosphonated Phenylethynyl Phenothiazine. *Langmuir*, 31, 7306–7316 (DOI: 10.1021/acs.langmuir.5b01370); (e) Rajakumar P., Kanagalatha, R. (2007). Synthesis and optoelectrochemical properties of novel phenothiazinophanes. *Tetrahedron Lett*, 48, 8496–8500 (DOI: 10.1016/j.tetlet.2007.09.161).
- [59] (a) Duvva, N., Eom, Y. K., Reddy, G., Schanze, K. S., Giribabu, L. (2020). Bulky Phenanthroimidazole–Phenothiazine D– $\pi$ -A Based Organic Sensitizers for Application in Efficient Dye-Sensitized Solar Cells. *ACS Appl. Energy Mater.* 3(7), 6758-6767. (DOI: <https://doi.org/10.1021/acsaem.0c00892>); (b) Tang, G., Sukhanov, A. A., Zhao, J., Yang, W., Wang, Z., Liu, Q., Voronkova, V.K., Di Donato, M., Escudero, D., Jacquemin, D. (2019). Red thermally activated delayed fluorescence and the intersystem crossing mechanisms in compact naphthalimide–phenothiazine electron donor/acceptor dyads. *J. Phys. Chem. C*, 123(50), 30171-30186. (DOI: <https://doi.org/10.1021/acs.jpcc.9b09335>); (c) Takeda, Y., Data, P., Minakata, S. (2020). Alchemy of donor–acceptor–donor multi-photofunctional organic materials: from construction of electron-deficient azaaromatics to exploration of functions. *Chem. Commun.*, 56(63), 8884-8894. (DOI: 10.1039/D0CC03322G)
- [60] Kim, S. H., Sakong, C., Chang, J. B., Kim, B., Ko, M. J., Kim, D. H., Hong, K. S., Kim, J. P. (2013), The effect of N-substitution and ethylthio substitution on the performance of phenothiazine donors in dye-sensitized solar cells, *Dyes Pigm*, 97, 262-271 (DOI: 10.1016/j.dyepig.2012.12.007).
- [61] Sailer, M., Franz, A. W., Müller, T. J. (2008). Synthesis and electronic properties of monodisperse oligophenothiazines. *Chem. Eur.*

*J.*, 14(8), 2602-2614. (DOI: <https://doi.org/10.1002/chem.200701341>).

- [62] (a) Beharry, A. A., Woolley, G. A. (2011). Azobenzene photoswitches for biomolecules. *Chem. Soc. Rev.*, 40(8), 4422-4437. (DOI: 10.1039/C1CS15023E); (b) Cui, J., Kwon, J. E., Kim, H. J., Whang, D. R., Park, S. Y. (2017). Smart fluorescent nanoparticles in water showing temperature-dependent ratiometric fluorescence color change. *ACS Appl. Mater. Interfaces*, 9(3), 2883-2890. (DOI: <https://doi.org/10.1021/acsami.6b13818>); (c) Vyšniauskas, A., Qurashi, M., Gallop, N., Balaz, M., Anderson, H. L., Kuimova, M. K. (2015). Unravelling the effect of temperature on viscosity-sensitive fluorescent molecular rotors. *Chem. Sci*, 6(10), 5773-5778. (DOI: 10.1039/C5SC02248G); (d) Sagara, Y., Yamane, S., Mitani, M., Weder, C., Kato, T. (2016). Mechanoresponsive luminescent molecular assemblies: an emerging class of materials. *Adv. Mater.*, 28(6), 1073-1095 (DOI: 10.1002/adma.201502589).
- [63] (a) McDonagh, C., Burke, C. S., MacCraith, B. D. (2008). Optical chemical sensors. *Chem. Rev.*, 108(2), 400-422. (DOI: <https://doi.org/10.1021/cr068102g>); (b) R. Weissleder, M. J. Pittet, *Nature* 2008, 452, 580 (c) Hou, X., Ke, C., Bruns, C. J., McGonigal, P. R., Pettman, R. B., Stoddart, J. F. (2015). Tunable solid-state fluorescent materials for supramolecular encryption. *Nat. Commun.*, 6(1), 1-9. (DOI: <https://doi.org/10.1038/ncomms7884>).
- [64] (a) Mutoh, K., Miyashita, N., Arai, K., Abe, J. (2019). Turn-on mode fluorescence switch by using negative photochromic imidazole dimer. *J. Am. Chem. Soc.*, 141(14), 5650-5654. (DOI: <https://doi.org/10.1021/jacs.9b01870>).
- [65] (a) Roy, B., Reddy, M. C., Hazra, P. (2018). Developing the structure–property relationship to design solid state multi-stimuli responsive materials and their potential applications in different fields. *Chem sci*, 9(14), 3592-3606. (DOI: 10.1039/C8SC00143J); (b) Li, S., Yan,

- D. (2018). Two-Component Aggregation-Induced Emission Materials: Tunable One/Two-Photon Luminescence and Stimuli-Responsive Switches by Co-Crystal Formation. *Adv. Opt. Mater.*, 6(19), 1800445. (DOI: <https://doi.org/10.1002/adom.201800445>); (c) Wu, X., Guo, J., Cao, Y., Zhao, J., Jia, W., Chen, Y., Jia, D. (2018). Mechanically triggered reversible stepwise tricolor switching and thermochromism of anthracene-o-carborane dyad. *Chem sci*, 9(23), 5270-5277. (DOI: [10.1039/C8SC00833G](https://doi.org/10.1039/C8SC00833G)); (d) Chai, J., Wu, Y., Yang, B., Liu, B. (2018). The photochromism, light harvesting and self-assembly activity of a multi-function Schiff-base compound based on the AIE effect. *J. Mater. Chem. C*, 6(15), 4057-4064. (DOI: <https://doi.org/10.1039/C8TC00509E>)
- [66] (a) Li, Q., Li, Z. (2017). The strong light-emission materials in the aggregated state: what happens from a single molecule to the collective group. *Adv. Sci.*, 4(7), 1600484. (DOI: <https://doi.org/10.1002/advs.201600484>); (b) Wang, C., Li, Z. (2017). Molecular conformation and packing: their critical roles in the emission performance of mechanochromic fluorescence materials. *Mater. Chem. Front.*, 1(11), 2174-2194. (DOI: [10.1039/C7QM00201G](https://doi.org/10.1039/C7QM00201G)); (c) Xue, S., Qiu, X., Sun, Q., Yang, W. (2016). Alkyl length effects on solid-state fluorescence and mechanochromic behavior of small organic luminophores. *J. Mater. Chem. C*, 4(8), 1568-1578. (DOI: [10.1039/C5TC04358A](https://doi.org/10.1039/C5TC04358A)); (d) Zhang, Y., Chen, Z., Song, J., He, J., Wang, X., Wu, J., Chen, S., Qu, J., Wong, W. Y. (2019). Rational design of high efficiency green to deep red/near-infrared emitting materials based on isomeric donor-acceptor chromophores. *J. Mater. Chem. C*, 7(7), 1880-1887. (DOI: [10.1039/C8TC05383A](https://doi.org/10.1039/C8TC05383A)).
- [67] (a) Desroches, M., Morin, J. F. (2018). Anthanthrene as a super-extended tetraphenylethylene for aggregation-induced emission. *Org.*

- lett.*, 20(10), 2797-2801. (DOI: <https://doi.org/10.1021/acs.orglett.8b00452>); (b) Martínez-Abadía, M., Giménez, R., Ros, M. B. (2018), Self-Assembled  $\alpha$ -Cyanostilbenes for Advanced Functional Materials, *Adv. Mater.*, 30(5), 1704161 (DOI: <https://doi.org/10.1002/adma.201704161>); (c) Kwon, M. S., Gierschner, J., Yoon, S. J., Park, S. Y. (2012). Unique piezochromic fluorescence behavior of dicyanodistyrylbenzene based donor–acceptor–donor triad: mechanically controlled photo-induced electron transfer (eT) in molecular assemblies. *Adv. Mater.*, 24(40), 5487-5492 (DOI: 10.1002/adma.201202409); (d) Revoju, S., Matuhina, A., Canil, L., Salonen, H., Hiltunen, A., Abate, A., Vivo, P. (2020). Structure-induced optoelectronic properties of phenothiazine-based materials. *J. Mater. Chem. C*, 8(44), 15486-15506.(DOI: 10.1039/D0TC03421E); (e) Huang, M., Lu, H., Wang, M., Liu, B., Ma, Z., Wang, Z., Yang, J. (2021). Phenothiazine-Based Luminophores with AIE, Solvatochromism, and Mechanochromic Characteristics. *J. Phys. Chem. B*, 125(41), 11548-11556. (DOI: <https://doi.org/10.1021/acs.jpcc.1c07304>).
- [68] (a) Ciardelli, F., Ruggeri, G., Pucci, A. (2013). Dye-containing polymers: methods for preparation of mechanochromic materials. *Chem. Soc. Rev.*, 42(3), 857-870 (DOI: 10.1039/C2CS35414D); (b) Chi, Z., Zhang, X., Xu, B., Zhou, X., Ma, C., Zhang, Y., Liu, S., Xu, J. (2012). Recent advances in organic mechanofluorochromic materials. *Chem. Soc. Rev.*, 41(10), 3878-3896. (DOI: 10.1039/C2CS35016E); (c) Crenshaw, B. R., Burnworth, M., Khariwala, D., Hiltner, A., Mather, P. T., Simha, R., Weder, C. (2007). Deformation-induced color changes in mechanochromic polyethylene blends. *Macromolecules*, 40(7), 2400-2408 (DOI: 10.1021/ma062936j); (d) Wu, X., Guo, J., Cao, Y., Zhao, J., Jia, W., Chen, Y., Jia, D. (2018). Mechanically triggered reversible stepwise

- tricolor switching and thermochromism of anthracene-o-carborane dyad. *Chem sci*, 9(23), 5270-5277. (DOI: 10.1039/C8SC00833G); (f) Kishimura, A., Yamashita, T., Yamaguchi, K., Aida, T. (2005). Rewritable phosphorescent paper by the control of competing kinetic and thermodynamic self-assembling events. *Adv. Funct. Mater.*, 4(7), 546-549 (DOI: 10.1038/nmat1401).
- [69] (a) Yagai, S., Okamura, S., Nakano, Y., Yamauchi, M., Kishikawa, K., Karatsu, T., Kitamura, A., Ueno, A., Kuzuhara, D., Yamada, H., Seki, T., Ito, H. (2014), Design amphiphilic dipolar  $\pi$ -systems for stimuli-responsive luminescent materials using metastable states, *Nat. Commun.*, 5(1), 1-10 (DOI: <https://doi.org/10.1038/ncomms5013>); (b) Ito, H., Muromoto, M., Kurenuma, S., Ishizaka, S., Kitamura, N., Sato, H., Seki, T. (2013). Mechanical stimulation and solid seeding trigger single-crystal-to-single-crystal molecular domino transformations. *Nat comm.*, 4(1), 1-5. (DOI: <https://doi.org/10.1038/ncomms3009>); (c) Davis, D. A., Hamilton, A., Yang, J., Cremer, L. D., Van Gough, D., Potisek, S. L., Ong, M. T., Braun, P. V., Martinez, T. J., White, S. R., Moore, J. S., Sottos, N. R. (2009). Force-induced activation of covalent bonds in mechanoresponsive polymeric materials. *Nature*, 459(7243), 68-72 (DOI: 10.1038/nature07970); (d) Zhang, G., Lu, J., Sabat, M., & Fraser, C. L. (2010). Polymorphism and reversible mechanochromic luminescence for solid-state difluoroboron avobenzene. *J. Am. Chem. Soc.*, 132(7), 2160-2162. (DOI: <https://doi.org/10.1021/ja9097719>); (e) Balch, A. L. (2009). Dynamic Crystals: Visually Detected Mechanochemical Changes in the Luminescence of Gold and Other Transition-Metal Complexes. *Angew. Chem. Int. Ed.*, 48(15), 2641-2644 (DOI: 10.1002/anie.200805602); (f) Lavrenova, A., Balkenende, D. W., Sagara, Y., Schrettl, S., Simon, Y. C., Weder, C. (2017). Mechano- and thermoresponsive photoluminescent

- supramolecular polymer. *J. Am. Chem. Soc.*, 139(12), 4302-4305. (DOI: <https://doi.org/10.1021/jacs.7b00342>).
- [70] (a) Ikeya, M., Katada, G., Ito, S., (2019). Tunable mechanochromic luminescence of 2-alkyl-4-(pyren-1-yl)thiophenes: controlling the selfrecovering properties and the range of chromism. *Chem. Commun.* 55(82), 12296–12299. (DOI: <https://doi.org/10.1039/C9CC06406K>); (b) Matsuo, Y., Wang, Y., Ueno, H., Nakagawa, T., Okada, H. (2019). Mechanochromism, Twisted/Folded Structure Determination, and Derivatization of (N-Phenylfluorenylidene) acridane. *Angew. Chem. Int. Ed.*, 131(26), 8854-8859. (DOI: <https://doi.org/10.1002/anie.201902636>).
- [71] (a) Sasaki, S., Suzuki, S., Sameera, W. M. C., Igawa, K., Morokuma, K., Konishi, G. I. (2016). Highly twisted N, N-dialkylamines as a design strategy to tune simple aromatic hydrocarbons as steric environment-sensitive fluorophores. *J. Am. Chem. Soc.*, 138(26), 8194-8206 (DOI: 10.1021/jacs.6b03749); (b) Sekiguchi, S., Kondo, K., Sei, Y., Akita, M., Yoshizawa, M. (2016). Engineering Stacks of V-Shaped Polyaromatic Compounds with Alkyl Chains for Enhanced Emission in the Solid State. *Angewandte Chemie*, 128(24), 7020-7024 (DOI: 10.1002/ange.201602502); (c) Meng, X., Qi, G., Zhang, C., Wang, K., Zou, B., Ma, Y. (2015). Visible mechanochromic responses of spiropyrans in crystals via pressure-induced isomerization. *Chem. Commun.*, 51(45), 9320-9323. (DOI: 10.1039/C5CC01064K); (d) Dong, Y., Xu, B., Zhang, J., Tan, X., Wang, L., Chen, J., Lv, H., Wen, S., Li, B., Ye, L., Zou, B., Tian, W. (2012). Piezochromic luminescence based on the molecular aggregation of 9, 10-Bis ((E)-2-(pyrid-2-yl) vinyl) anthracene. *Angew. Chem. Int. Ed.*, 51(43), 10782-10785. (DOI: <https://doi.org/10.1002/anie.201204660>); (e) Nguyen, N. D., Zhang, G., Lu, J., Sherman, A. E., Fraser, C. L. (2011). Alkyl chain length effects on solid-state difluoroboron  $\beta$ -diketonate mechanochromic luminescence. *J. Mater. Chem.*, 21(23), 8409-8415

- (DOI: 10.1039/C1JM00067E); (f) Yoshii, R., Hirose, A., Tanaka, K., Chujo, Y. (2014). Functionalization of boron diiminates with unique optical properties: multicolor tuning of crystallization-induced emission and introduction into the main chain of conjugated polymers. *J. Am. Chem. Soc.*, *136*(52), 18131-18139 (DOI: 10.1021/ja510985v); (g) Zhang, Y., Mao, H., Kong, L., Tian, Y., Tian, Z., Zeng, X., Zhi, J., Shi, J., Tong, B., Dong, Y. (2016). Effect of E/Z isomerization on the aggregation-induced emission features and mechanochromic performance of dialdehyde-substituted hexaphenyl-1, 3-butadiene. *Dyes Pigm.*, *133*, 354-362. (DOI: <https://doi.org/10.1016/j.dyepig.2016.06.016>).
- [72] (a) Huang, X., Qian, L., Zhou, Y., Liu, M., Cheng, Y., Wu, H. (2018). Effective structural modification of traditional fluorophores to obtain organic mechanofluorochromic molecules. *J. Mater. Chem. C*, *6*(19), 5075-5096. (DOI: <https://doi.org/10.1039/C8TC00043C>); (b) Xue, S., Qiu, X., Sun, Q., Yang, W. (2016). Alkyl length effects on solid-state fluorescence and mechanochromic behavior of small organic luminophores. *J. Mater. Chem. C*, *4*(8), 1568-1578. (DOI: <https://doi.org/10.1039/C5TC04358A>); (c) Jadhav, T., Choi, J. M., Dhokale, B., Mobin, S. M., Lee, J. Y., Misra, R. (2016). Effect of end groups on mechanochromism and electroluminescence in tetraphenylethylene substituted phenanthroimidazoles. *J. Phys. Chem. C*, *120*(33), 18487-18495 (DOI: 10.1021/acs.jpcc.6b06277).
- [73] Löwe, C., Weder, C. (2002). Oligo (p-phenylene vinylene) excimers as molecular probes: deformation-induced color changes in photoluminescent polymer blends. *Advanced Materials*, *14*(22), 1625-1629. (DOI: [https://doi.org/10.1002/1521-4095\(20021118\)14:22<1625::AID-ADMA1625>3.0.CO;2-Q](https://doi.org/10.1002/1521-4095(20021118)14:22<1625::AID-ADMA1625>3.0.CO;2-Q)).
- [74] Yoon, S. J., Chung, J. W., Gierschner, J., Kim, K. S., Choi, M. G., Kim, D., Park, S. Y. (2010). Multistimuli two-color luminescence switching via different slip-stacking of highly fluorescent molecular

- sheets. *J. Am. Chem. Soc.*, 132(39), 13675-13683 (DOI: 10.1021/ja1044665).
- [75] Zeng, X., Zhou, T., Liu, J., Wu, K., Li, S., Xiao, X., Zhang, Y., Gong, S., Xie, G. and Yang, C. (2018). Incorporating Thermally Activated Delayed Fluorescence into Mechanochromic Luminescent Emitters: High-Performance Solution-Processed Yellow Organic Light Emitting Diodes. *Adv. Optical Mater.*, 6(24), 1801071 (DOI: 10.1002/adom.201801071)
- [76] Yang, M., Park, I. S., Miyashita, Y., Tanaka, K., Yasuda, T. (2020). Mechanochromic Delayed Fluorescence Switching in Propeller-Shaped Carbazole–Isophthalonitrile Luminogens with Stimuli-Responsive Intramolecular Charge-Transfer Excited States. *Angew. Chem. Int. Ed.*, 59(33), 13955-13961. (DOI: <https://doi.org/10.1002/anie.202005584>).



## Chapter 2

### Materials and experimental techniques

---

---

#### 2.1. Introduction

This chapter describes the materials, general synthetic procedures, characterization techniques and the instrumentation employed in this thesis.

#### 2.2. Chemicals for synthesis

The common solvents used for syntheses were purified according to established procedures.<sup>[1]</sup> The solvents and reagents were used as received unless otherwise indicated. Photophysical and electrochemical studies were performed with spectroscopic grade solvents.

2,1,3-Benzothiadiazole, 9,10-phenanthroquinone, acenaphthaquinone, n-BuLi, 4-bromobenzophenone, diphenylmethane, Pd(PPh<sub>3</sub>)<sub>4</sub>, Pd(dppf)Cl<sub>2</sub>, Pd(OAc)<sub>2</sub>, Ph(*t*-Bu)<sub>3</sub>, sodium tert-butoxide, 4-iodoaniline, 4-(diphenylamino)benzaldehyde, 4-bromobenzaldehyde, 3-bromobenzaldehyde, 2-bromobenzaldehyde, 2-aminothiophenol, tributyltin chloride, potassium carbonate, potassium acetate, sodium carbanote, Bis(pinacolato) diboron, phenothiazine, iodopropane, bromine, glacial acetic acid, hydrobromic acid, p-Toluenesulfonic acid, sodium borohydride, Rhodamine-6G, 9,10-diphenylanthracene, quinine sulphate, tetrabutylammonium hexafluorophosphate (TBAF<sub>6</sub>) and were procured from Aldrich chemicals USA.

Silica gel (100–200 mesh and 230–400 mesh) were purchased from Rankem chemicals, India. TLC pre-coated silica gel plates (Kieselgel 60F254, Merck) were purchased from Merck, India and Spectrochem, India.

Dry solvents dichloromethane, 1,2-dichloroethane, chloroform, tetrahydrofuran (THF), 1,2-dichlorobenzene, 1,4-dioxane, ethanol, N,N-dimethylformamide and methanol were obtained from Spectrochem India and S. D. Fine chem. Ltd. All the oxygen or moisture sensitive reactions

were performed under nitrogen/argon atmosphere using standard schlenk method.

## **2.3. Spectroscopic measurements**

### **2.3.1. Mass spectrometry**

High resolution mass spectra (HRMS) were recorded on Bruker-Daltonics, micrOTOF-Q II mass spectrometer using positive and negative mode electrospray ionizations.

### **2.3.2. NMR spectroscopy**

$^1\text{H}$  NMR (400 MHz),  $^1\text{H}$  NMR (500 MHz), and  $^{13}\text{C}$  NMR (100 MHz) spectra were recorded on the Bruker Avance (III) 400 MHz, using  $\text{CDCl}_3$  and acetone- $d_6$  as solvent. Chemical shifts in  $^1\text{H}$ , and  $^{13}\text{C}$  NMR spectra were reported in parts per million (ppm). In  $^1\text{H}$  NMR chemical shifts are reported relative to the residual solvent peak ( $\text{CDCl}_3$ , 7.26 ppm). Multiplicities are given as: s (singlet), d (doublet), t (triplet), q (quartet), dd (doublet of doublets), m (multiplet), and the coupling constants  $J$ , are given in Hz.  $^{13}\text{C}$  NMR chemical shifts are reported relative to the solvent residual peak ( $\text{CDCl}_3$ , 77.16 ppm).

### **2.3.3. UV-Vis spectroscopy**

UV-Vis absorption spectra were recorded using a Varian Cary100 Bio UV-Vis and Perkin Elmer LAMBDA 35 UV/Vis spectrophotometer.

### **2.3.4. Fluorescence spectroscopy**

Fluorescence emission spectra were recorded upon specific excitation wavelength on a Horiba Scientific Fluoromax-4 spectrophotometer. The measurements were performed at 25 °C and path length of 1 cm quartz cuvette. The 2.0 mL volume of luminogen solutions were used for study. The solid state fluorescence measurements were performed on glass slide and front face sample holder accessory were used in fluorimeter. The quantum yields in the solid state were measured using a K-sphere integrating sphere. The excitation and emission slits were 2/2 nm for the emission measurements and 3/3 for solid quantum yield measurements.

### ***The fluorescence quantum yields ( $\phi_F$ )***

The fluorescence quantum yields ( $\phi_F$ ) of compounds were calculated by the steady-state comparative method using following equation,

$$\phi_F = \phi_{st} \times S_u/S_{st} \times A_{st} / A_u \times \eta_u^2/\eta_{st}^2 \dots\dots\dots (Eq. 1)$$

Where  $\phi_F$  is the emission quantum yield of the sample,  $\phi_{st}$  is the emission quantum yield of the standard,  $A_{st}$  and  $A_u$  represent the absorbance of the standard and sample at the excitation wavelength, respectively, while  $S_{st}$  and  $S_u$  are the integrated emission band areas of the standard and sample, respectively, and  $\eta_{st}$  and  $\eta_u$  the solvent refractive index of the standard and sample, u and st refer to the unknown and standard, respectively.

### **2.4. Electrochemical studies**

Cyclic voltamograms (CVs) were recorded on CHI620D electrochemical analyzer using Glassy carbon as working electrode, Pt wire as the counter electrode, and Saturated Calomel Electrode (SCE) as the reference electrode. The scan rate was 100 mVs<sup>-1</sup>. A solution of tetrabutylammonium hexafluorophosphate (TBAPF<sub>6</sub>) in CH<sub>2</sub>Cl<sub>2</sub> (0.1 M) was employed as the supporting electrolyte.

### **2.5. Single crystal X-ray diffraction studies**

Single crystal X-ray diffraction studies were performed on SUPER NOVA diffractometer, BRUKER KAPPA APEX II CCD Duo with graphite monochromatic Mo Ka radiation (0.71073 Å), on Xcalibur, Eos, Gemini diffractometer and on Bruker D8 VENTURE diffractometer equipped with a CMOS Photon 100 detector and MoKa (λ = 0.71073 Å) radiation was used. The strategy for the data collection was evaluated by using the CrysAlisPro CCD software. The data were collected by the standard 'phi-omega scan techniques, and were scaled and reduced using CrysAlisPro RED software. The structures were solved by direct methods using SHELXS-97, and refined by full matrix least-squares with SHELXL-97, refining on F<sup>2</sup>.1. The positions of all the atoms were obtained by direct methods. All non-hydrogen atoms were refined anisotropically. The remaining hydrogen atoms were placed in geometrically constrained positions, and refined with

isotropic temperature factors, generally  $1.2U_{eq}$  of their parent atoms. The CCDC numbers contain the respective supplementary crystallographic data. These data can be obtained free of charge via [www.ccdc.cam.ac.uk/conts/retrieving.html](http://www.ccdc.cam.ac.uk/conts/retrieving.html) (or from the Cambridge Crystallographic 42 Data Centre, 12 union Road, Cambridge CB21 EZ, UK; Fax: (+44) 1223-336-033; or [deposit@ccdc.cam.ac.uk](mailto:deposit@ccdc.cam.ac.uk)).

## **2.6. Powder XRD (PXRD)**

Powder X-ray Diffraction (PXRD) analyses were performed on the Rigaku SmartLab, Automated Multipurpose x-ray Diffractometer.

## **2.7. Computational calculations**

The density functional theory (DFT) calculation were carried out at the B3LYP/6-31G\*\* level for C, N, S, H, and Lan12DZ level for Fe in the Gaussian 09 program.<sup>[2]</sup>

## **2.8. Scanning electron microscopy (SEM)**

The SEM images were collected on Carl Zeiss supra 55 and Field emission JSM-7001F (JEOL) operated at 15 kV after sputtering with gold. The samples for SEM were prepared by drop casting AIE solution of luminogens.

## **2.9. Thermogravimetric analysis (TGA)**

Thermogravimetric analyses were performed on the Metler Toledo thermal analysis system. The measurements were done at heating rate of 10 °C/minute and heated upto 800 °C.

## **2.10. Dynamic light scattering (DLS)**

The dynamic light scattering (DLS) studies were done on a Micromeritics Nanoplus 3 instrument. The samples for DLS study was used as it is AIE solution of luminogens.

## **2.11. Mechanochromism study**

The mechanochromic properties were studied mainly by grinding, fuming and annealing. The grinded samples were prepared by taking the pristine/synthesized sample into a mortar and grinding it for approximately 10 minutes by using a pestle. Annealing was done by heating the grinded

samples in oven in open atmosphere at respective temperatures. In order to perform fumigation, the grinded samples were taken on a glass plate. The glass plate was further placed in a solvent chamber saturated with the vapors of the particular solvent

## 2.12. References

[1] (a) Vogel A. I., Tatchell A. R., Furnis B. S., Hannaford A. J., & Smith, P. W. G. (1996), *Vogel's Textbook of Practical Organic Chemistry (5<sup>th</sup> Edition)* (5th ed.). (b) Wei Ssberger A. Proskraner E. S. Riddick J. A., Toppos Jr. E. F. (1970). *Organic Solvents in Techniques of Organic Chemistry*, Vol. IV, 3rd Edition, Inc. New York.

[2] (a) Lee C., Yang W., & Parr R. G. (1988). Development of the Colle-Salvetti correlation-energy formula into a functional of the electron density. *Physical Review B*, 37(2), 785–789 (DOI: 10.1103/PhysRevB.37.785). (b) A. D. Becke (1993), A new mixing of Hartree-Fock and local densityfunctional theories, *J. Chem. Phys.* 98 (2), 1372–377 (DOI: 10.1063/1.464304). (c) Frisch M. J., Trucks G. W., Schlegel H. B., Scuseria G. E., Robb M. A., Cheeseman J. R., Scalmani G., Barone V., Mennucci B., Petersson G. A., Nakatsuji H., Caricato M., Li X., Hratchian H. P., Izmaylov A. F., Bloino J., Zheng G., Sonnenberg J. L., Hada M., Ehara M., Toyota K., Fukuda R., Hasegawa J., Ishida M. Nakajima T., Honda Y., Kitao O., Nakai H., Vreven T., Montgomery J. A. Jr., Peralta J. E., Ogliaro F., Bearpark M., Heyd J. J., Brothers E., Kudin K. N., Staroverov V. N., Kobayashi R., Normand J., Raghavachari K., Rendell A., Burant J. C., Iyengar S. S., Tomasi J., Cossi M., Rega N., Millam N. J., Klene M., Knox J. E., Cross J. B., Bakken V., Adamo C., Jaramillo J., Gomperts R., Stratmann R. E., Yazyev O., Austin A. J., Cammi R., Pomelli C.; Ochterski J. W., Martin R. L., Morokuma K., Zakrzewski V. G., Voth G. A., Salvador P., Dannenberg J. J., Dapprich S., Daniels A. D., Farkas O., Foresman J. B., Ortiz J. V., Cioslowski J., Fox D. J. (2009), *Gaussian 09, revision A.02; Gaussian, Inc.*:Wallingford, CT.



## Chapter 3

# T-shaped donor-acceptor-donor type symmetrical quinoxaline derivatives: aggregation-induced emission and mechanochromism

---

---

### 3.1. Introduction

In recent years, materials with high solid-state emission have gained significant attention due to their application in mechanofluorochromism and optoelectronic devices.<sup>[1]</sup> The mechanofluorochromic materials have a wide range of potential applications in mechanosensors, photo modulation, security inks, memory chips, luminescent switches, data storage and fluorescent probes.<sup>[2]</sup> This class of smart materials undergo reversible solid-state emission in response to external stimuli. High solid-state emission is one of the most important requirements for mechanofluorochromic materials and can be achieved by structural modifications and design strategies altering the molecular arrangement.<sup>[3]</sup> The factors governing solid state emission of organic materials are effective planarity, conjugation length, incorporation of different substituents (alkyl, aryl, halogen) and their interactions with the surrounding environment.<sup>[3,4]</sup> However, the use of traditional fluorophores is limited in mechanofluorochromic material as they are non-emissive in solid state due to aggregation caused quenching (ACQ).<sup>[5]</sup> Tang *et al* have designed a family of molecules which are emissive in solid state and have termed as aggregation-induced emission (AIE) which is contradictory to ACQ.<sup>[6]</sup> The use of AIE active fluorophores has been proved to be an effective approach to increase the solid state emission and hence the mechanochromic property. The propeller shaped structure of tetraphenylethylene (TPE) fulfils the requirement of restricted intramolecular rotations (RIR) thereby making it a well-known AIE active molecule which has been employed in various applications such as organic light emitting diodes (OLEDs), bioimaging, mechanochromic materials,

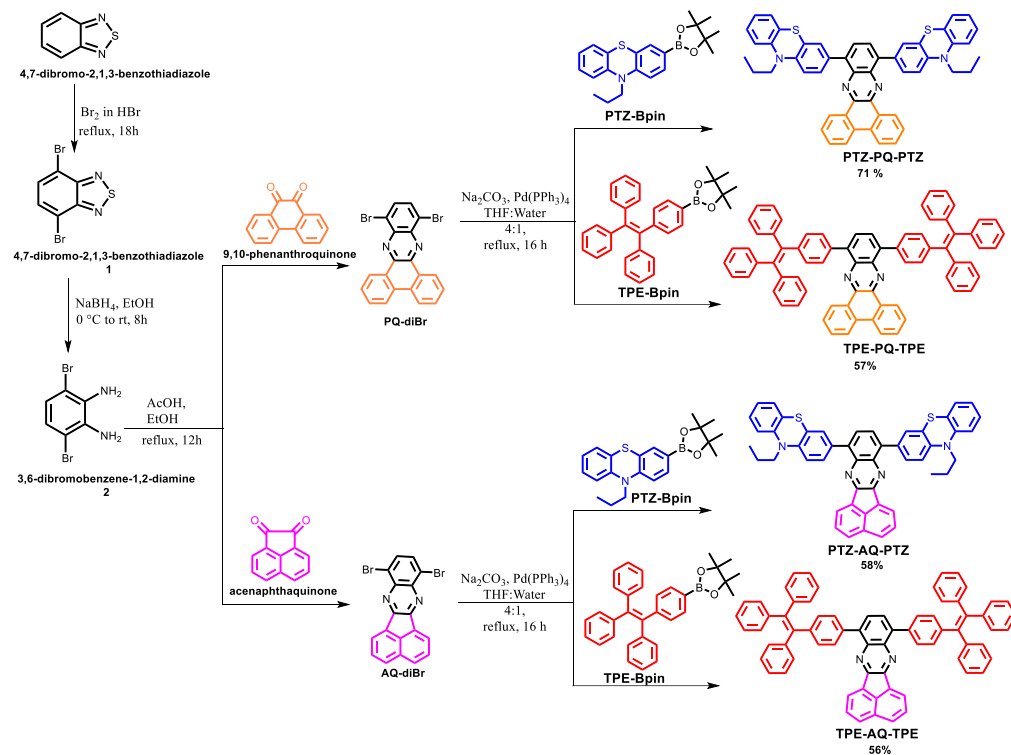
sensors and many more.<sup>[7]</sup> In recent years, heterocyclic donor phenothiazine (PTZ) has emerged as an effective AIEgen and has been utilized to develop a range of stimuli-responsive materials, TADF materials, room-temperature phosphorescent (RTP) materials and optoelectronic devices such as OLEDs, organic solar cells (OSCs) and perovskite solar cells (PSCs).<sup>[8]</sup>

The molecules having a donor (D) and acceptor (A) type (D-A-D) architecture are promising candidates for stimuli responsive materials and other optoelectronic properties.<sup>[9]</sup> The D-A-D structured luminogens enable us to attain tunable electronic states due to their intramolecular charge transfer (ICT) characteristic, which endows them with unique optoelectronic properties.<sup>[10]</sup> The use of typical AIEgens as donors in combination fusion with different acceptor units can produce efficient stimuli-responsive solid-state emissive materials. The TPE being a weak donor on combination with an electron acceptor generates a donor-acceptor type architecture which can be further utilized to develop good mechanochromic material as well as highly efficient solid-state emitters with exceptional stability. On the other hand, PTZ has a stronger electron-donating ability as compared to TPE and can result in distinct solid-state emission properties on fusion with an electron acceptor. Quinoxaline has outstanding electron accepting ability because of a strong electronegativity of two N atoms and stable quinoid structure leading to remarkable photophysical properties such as unique absorption and emission and high charge-carrier mobility.<sup>[11]</sup> Quinoxaline and its derivatives have been explored in opto-electronic devices like light-emitting diodes (LEDs), organic photovoltaics (OPVs), dye-sensitized solar cells (DSSCs), organic field-effect transistors (OFETs), nonlinear optics, and fluorescent chemosensors owing to the facile synthesis and versatility.<sup>[12]</sup> The electron acceptor nature, highly fused structure and extended conjugation length of quinoxaline motivated us to choose phenanthrene-quinoxaline and acenaphthene-quinoxaline as an acceptor. Keeping all this in view, we have synthesized T-shaped symmetrical donor-acceptor-donor type

phenanthrene-quinoxaline **PQ** (A) and acenaphthene-quinoxaline **AQ** (A') based symmetrical derivatives **TPE-PQ-TPE**, **TPE-AQ-TPE** and **PTZ-PQ-PTZ**, **PTZ-AQ-PTZ** functionalized with tetraphenylethylene (TPE) as donor (D) and phenothiazine (PTZ) as donor D' respectively and investigated their photophysical, AIE and stimuli-responsive properties. All the symmetrical quinoxaline derivatives show reversible mechanochromic behaviour and are good solid-state emitters.

### 3.2. Results and discussion

#### Synthesis



**Scheme 3.1.** Synthesis of symmetrical PTZ and TPE substituted PQ and AQ derivatives.

A straight-forward three step approach was proposed for the synthesis of the T-shaped symmetrical luminophores **PTZ-PQ-PTZ**, **PTZ-AQ-PTZ**, **TPE-PQ-TPE** and **TPE-AQ-TPE** and (Scheme 3.1.). The reduction of 4,7-dibromo-2,1,3-benzothiadiazole **1** was carried out by a reported

procedure using NaBH<sub>4</sub> in ethanol which resulted in 3,6-dibromobenzene-1,2-diamine **2**.<sup>[13]</sup> The intermediate **2** was further condensed with 9,10-phenanthroquinone and acenaphthaquinone yielding 10,13-dibromodibenzo[a,c]phenazine (**PQ-diBr**) and 8,11-dibromoacenaphtho[1,2-b]quinoxaline (**AQdi-Br**) respectively.<sup>[14]</sup> The symmetrical derivatives **PTZ-PQ-PTZ** and **PTZ-AQ-PTZ** consists of phenothiazine (PTZ) moiety as donor (D) whereas **TPE-PQ-TPE** and **TPE-AQ-TPE** utilize tetraphenylethylene (TPE) as donor (D'). The Suzuki cross-coupling reaction of **PQdi-Br** and **AQdi-Br** with PTZ-Bpin using Pd(PPh<sub>3</sub>)<sub>4</sub> as catalyst afforded symmetrical di-substituted PTZ quinoxaline derivatives **PTZ-PQ-PTZ** and **PTZ-AQ-PTZ** in 71% and 58% yields respectively. The symmetrical derivatives **TPE-PQ-TPE** and **TPE-AQ-TPE** were obtained by a Suzuki cross-coupling reaction of **PQ-diBr** and **AQdi-Br** with TPE-Bpin using Pd(PPh<sub>3</sub>)<sub>4</sub> as catalyst in argon atmosphere respectively. The **TPE-PQ-TPE** and **TPE-AQ-TPE** were obtained in 57% and 56% yields respectively. The PTZ and TPE substituted quinoxaline derivatives were purified using column chromatography. The symmetrical quinoxaline derivatives were well characterized by NMR and high-resolution mass spectrometry (HRMS) techniques.

### 3.3. Photophysical properties

The photophysical properties of the symmetrical quinoxaline luminophores **PTZ-PQ-PTZ**, **PTZ-AQ-PTZ**, **TPE-PQ-TPE** and **TPE-AQ-TPE** were studied using UV-visible and fluorescence spectroscopy. The electronic absorption and fluorescence spectra were recorded in tetrahydrofuran solution (Figure 3.1.) and the data are compiled in Table 3.1. The symmetrical quinoxaline derivatives **PTZ-PQ-PTZ**, **PTZ-AQ-PTZ**, **TPE-PQ-TPE** and **TPE-AQ-TPE** displays absorption bands in the region of 300–400 nm corresponding to  $\pi \rightarrow \pi^*$  transitions of the PTZ, TPE and the quinoxaline units.<sup>[15]</sup>

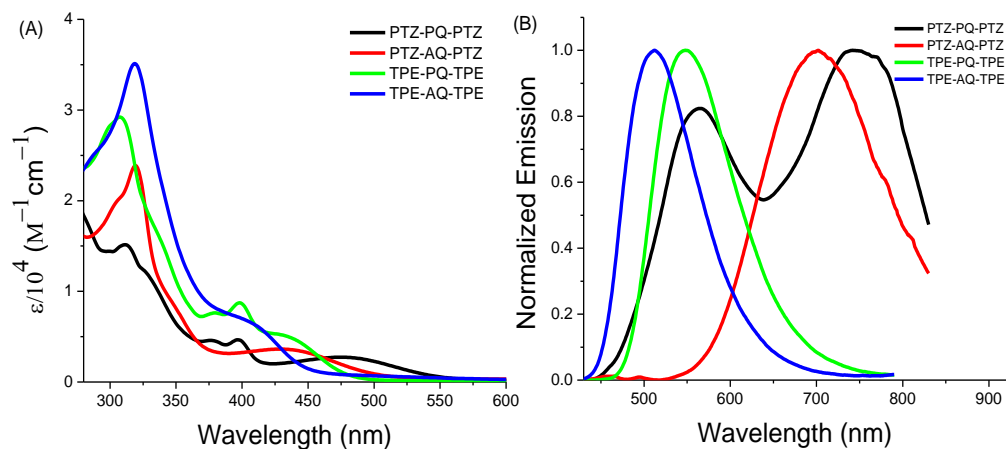


**Figure 3.1.** (A) Electronic absorption spectra and (B) normalized fluorescence spectra of **PTZ-PQ-PTZ**, **PTZ-AQ-PTZ**, **TPE-PQ-TPE** and **TPE-AQ-TPE** recorded in THF (concentration =  $2 \times 10^{-5}$  M).

The symmetrical quinoxaline luminophores **PTZ-PQ-PTZ**, **PTZ-AQ-PTZ**, **TPE-PQ-TPE** and **TPE-AQ-TPE** also display an absorption band in the higher wavelength region at 485 nm, 440 nm, 440 nm and 414 nm respectively which could be originating from the intramolecular charge transfer (ICT) transition occurring from the donor (PTZ or TPE) to the acceptor quinoxaline units (**PQ** or **AQ**).<sup>[15]</sup> The phenanthrene-quinoxaline derivatives **PTZ-PQ-PTZ** and **TPE-PQ-TPE** have multiple strong absorption bands (300–400 nm) associated to the  $\pi-\pi^*$  transitions which could be due to the highly conjugated phenanthrene ring. Further, the ICT absorption bands for PTZ substituted quinoxaline derivatives **PTZ-PQ-PTZ** and **PTZ-AQ-PTZ** derivatives are red shifted as compared to the TPE-substituted quinoxaline derivatives **TPE-PQ-TPE** and **TPE-AQ-TPE** owing to the higher electron-donating ability of PTZ as compared to TPE which could result in a stronger ICT. The emission spectra of symmetrical derivative **PTZ-PQ-PTZ** shows an emission maximum at 750 nm which could be ascribed to the ICT emission, accompanied with an emission peak at 567 nm which could be due to a localized excited (LE) emission. The molecule **PTZ-AQ-PTZ** exhibits emission maximum at 700 nm which could be corresponding to the ICT emission. The emission spectra of the

luminophores **TPE-PQ-TPE** and **TPE-AQ-TPE** show emission maxima at 548 nm and 511 nm respectively.

**Table 3.1.** Photophysical and thermal properties of **1** and **2**.

Compounds	$\lambda_{ab}[\text{nm}]$ ( $\epsilon[\text{Lmol}^{-1}\text{cm}^{-1}]$ ) <sup>a</sup>	$\lambda_{em.}$ (nm) <sup>b</sup>
<b>PTZ-PQ-PTZ</b>	312 (15138), 376 (4584), 397 (4660), 485 (2660)	567, 750
<b>PTZ-AQ-PTZ</b>	319 (23869), 440 (3516)	702
<b>TPE-PQ-TPE</b>	307 (29223), 378 (7598), 397 (8700), 440 (4690)	548
<b>TPE-AQ-TPE</b>	318 (35118), 414 (5896)	511

<sup>a,b</sup> Measured in tetrahydrofuran

### 3.4. Theoretical calculations

In order to gain an insight of the electronic structures of the symmetrical quinoxaline luminophores (**PTZ-PQ-PTZ**, **PTZ-AQ-PTZ**, **TPE-PQ-TPE** and **TPE-AQ-TPE**), the density functional theory (DFT) calculation was performed at the B3LYP/6-31G(d,p) level.<sup>[16]</sup> The calculated frontier molecular orbitals of the symmetrical quinoxaline derivatives are shown in Figure 3.2. and the values are tabulated in Table 3.2. The D-A-D symmetrical quinoxaline derivatives **PTZ-PQ-PTZ**, **PTZ-AQ-PTZ**, **TPE-PQ-TPE** and **TPE-AQ-TPE** possess non-planar architecture due to the incorporation of PTZ and TPE units at end capping positions which have a butterfly shape and a propeller structure respectively.

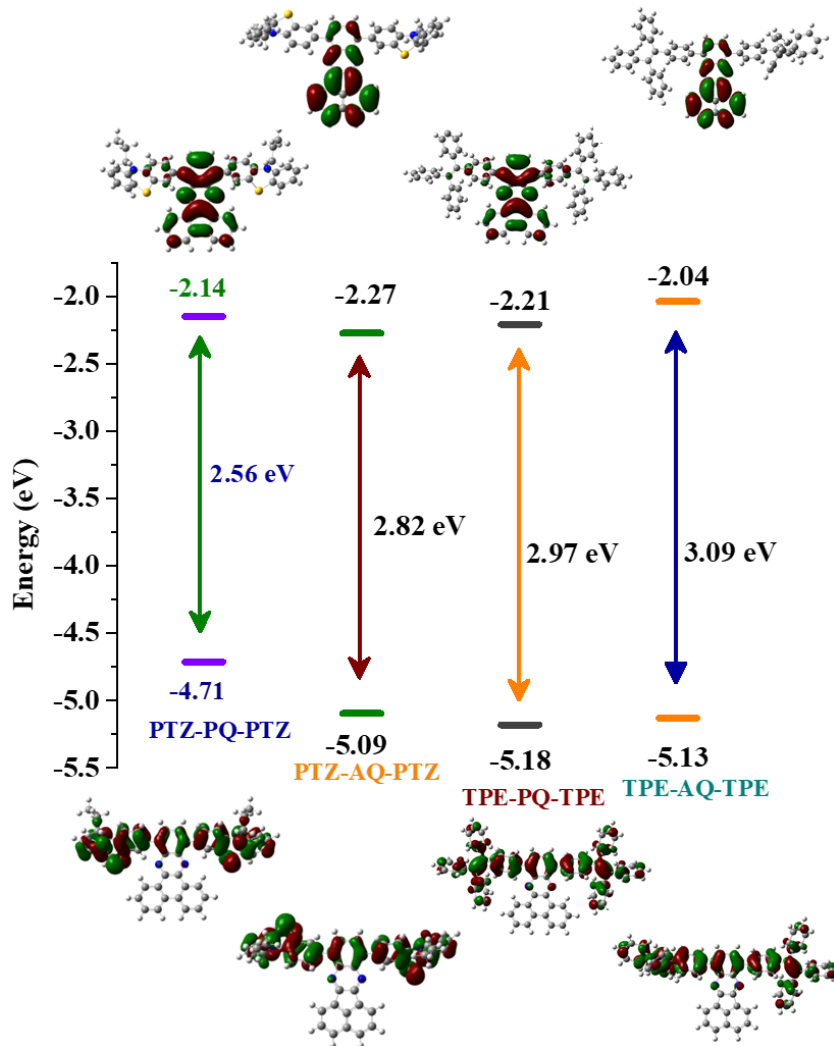


**Figure 3.2.** Correlation diagram showing the HOMO, and LUMO wave functions and energies of symmetrical quinoxaline derivatives as determined at the B3LYP/6-31G(d,p) level.

In the case of **PTZ-PQ-PTZ** and **PTZ-AQ-PTZ**, the electron density of HOMO is mainly spread over both the PTZ unit and the benzene ring of the quinoxaline unit due to the C-substitution of the PTZ unit on the quinoxaline unit. The HOMOs for luminophores **TPE-PQ-TPE** and **TPE-AQ-TPE** are localized on the TPE unit extended to the central benzene of the quinoxaline unit. Further, the LUMOs for **PTZ-PQ-PTZ**, **PTZ-AQ-PTZ**, **TPE-PQ-TPE** and **TPE-AQ-TPE** are completely localized on central quinoxaline unit **PQ** and **AQ** suggesting the electron-accepting ability of the quinoxaline

unit in the D-A-D system. It is apparent from the DFT studies that the HOMO and LUMO for both the luminophores are well separated on the two  $\pi$  conjugated arms. This leads to stronger ICT transitions between the electron donor and acceptor. The estimated HOMO-LUMO gaps for **PTZ-PQ-PTZ**, **PTZ-AQ-PTZ**, **TPE-PQ-TPE** and **TPE-AQ-TPE** are 2.56 eV, 2.82 eV, 2.97 eV and 3.09 eV respectively.

**Table 3.2.** Theoretical calculations of symmetrical quinoxaline derivatives

Compounds	HOMO <sup>a</sup> eV	LUMO <sup>a</sup> eV	HOMO-LUMO gap eV
<b>PTZ-PQ-PTZ</b>	-4.71	-2.14	2.56
<b>PTZ-AQ-PTZ</b>	-5.09	-2.27	2.82
<b>TPE-PQ-TPE</b>	-5.18	-2.21	2.97
<b>TPE-AQ-TPE</b>	-5.13	-2.04	3.09

<sup>a</sup> Calculated from CV: Reference electrode- Ag/AgCl.

### 3.5. Solvatochromism

The symmetrical quinoxaline luminophores **PTZ-PQ-PTZ**, **PTZ-AQ-PTZ**, **TPE-PQ-TPE** and **TPE-AQ-TPE** display an intramolecular charge transfer peak (ICT) owing to their D-A-D structure. The ICT transitions are highly sensitive to solvent polarity; hence the solvatochromic studies were performed on the target quinoxaline luminophores.<sup>[17]</sup> The solvatochromic effect was investigated by recording the emission (Figure 3.3) and the absorption spectra (Figure 3.4.) of **PTZ-PQ-PTZ**, **PTZ-AQ-PTZ**, **TPE-PQ-TPE** and **TPE-AQ-TPE** in solvents of varying polarities (toluene, tetrahydrofuran, chloroform and dichloromethane).

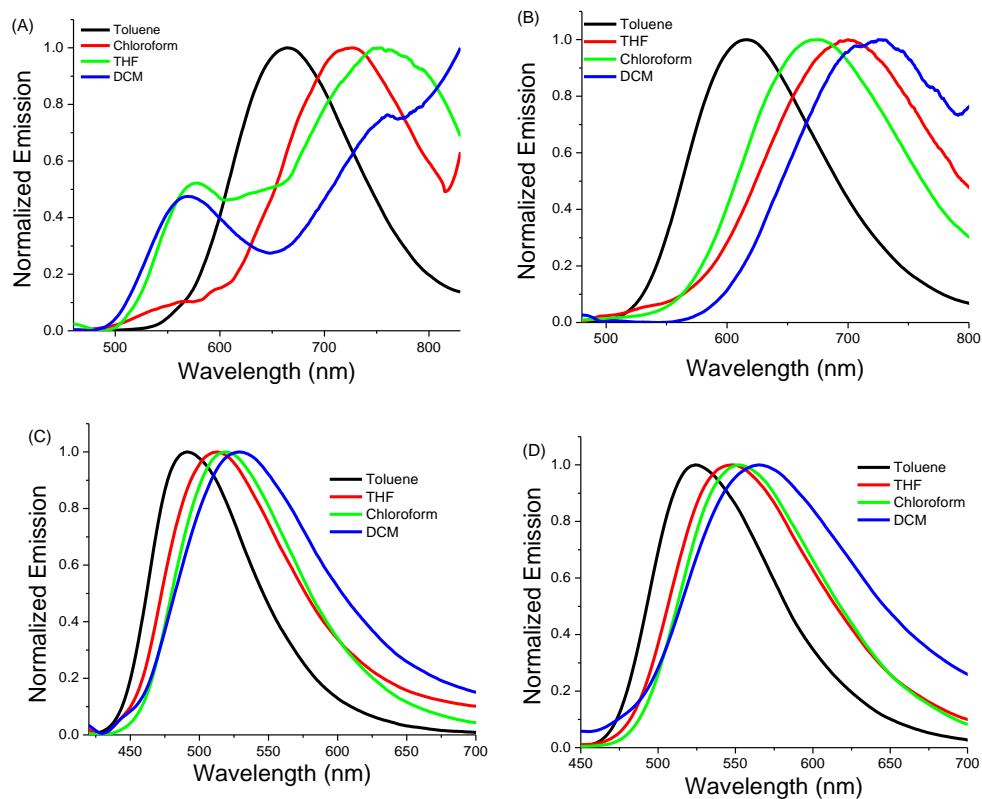


**Figure 3.3.** (A) Fluorescence spectra of (A) **PTZ-PQ-PTZ**, (B) **PTZ-AQ-PTZ**, (C) **TPE-PQ-TPE** and (D) **TPE-AQ-TPE** in different solvents of varying polarities. ( $\lambda_{exc} = 370$  nm-**TPE-PQ-TPE**, **TPE-AQ-TPE**,  $\lambda_{exc} = 420$  nm-**PTZ-PQ-PTZ**, **PTZ-AQ-PTZ**).

The absorption spectra (Figure 3.4.) of quinoxaline luminophores **PTZ-PQ-PTZ**, **PTZ-AQ-PTZ**, **TPE-PQ-TPE** and **TPE-AQ-TPE** are less sensitive to change in solvent polarity as compared to the emission spectra. The weak solvatochromism in the absorption spectra suggest that the ground state electronic structures are independent of change in solvent polarity. On the other hand, a notable solvatochromism in the emission spectra (Figure 3.3.) is attributed to the more polarized excited states. The symmetrical luminophore **PTZ-PQ-PTZ** in toluene exhibits emission maxima due to charge transfer (CT) state at 564 nm which bathochromically shifts to 728 nm in chloroform and up to 753 nm in THF. A shoulder peak arises in the region of 550-580 nm for THF and

chloroform which could be due to the LE emissions. In DCM, the luminophore **PTZ-PQ-PTZ** shows a strong LE emission at 570 nm although the CT emission becomes distorted due to decrease in intensity and appears as a shoulder around 760 nm.

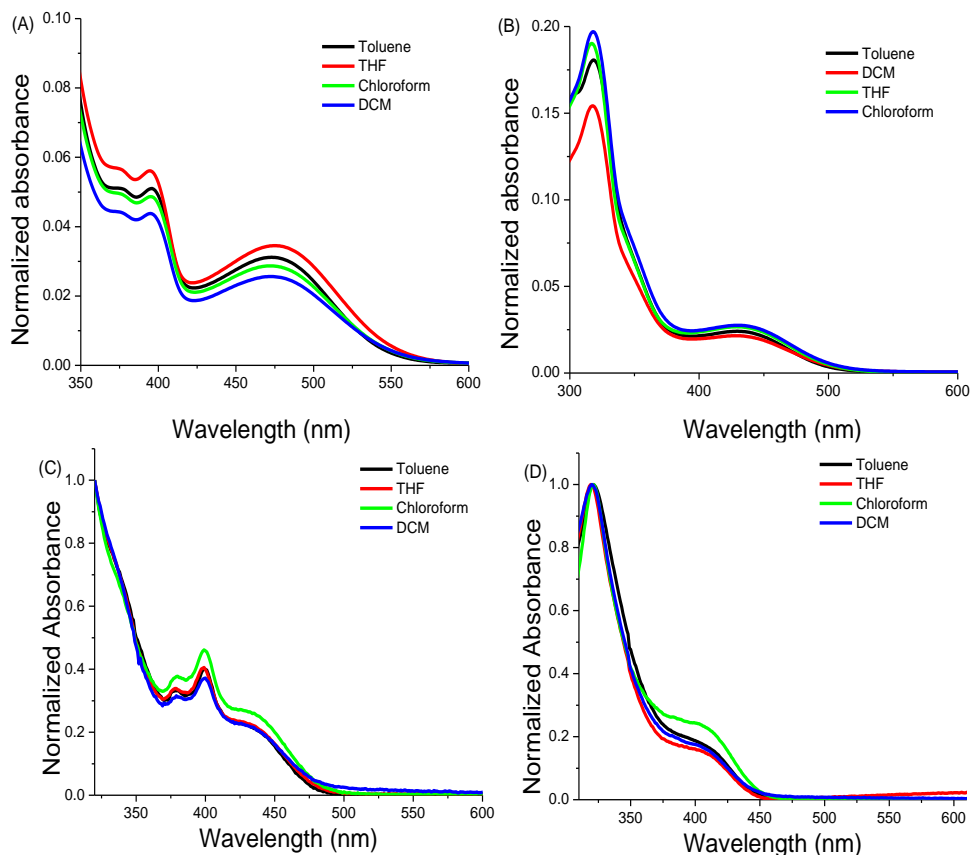


**Figure 3.4.** Electronic absorption spectra of ((A) **PTZ-PQ-PTZ**, (B) **PTZ-AQ-PTZ**, (C) **TPE-PQ-TPE** and (D) **TPE-AQ-TPE** in solvents of different polarity.

The **AQ** based symmetrical derivative **PTZ-AQ-PTZ** has an emission maximum at 616 nm in toluene which shifts bathochromically in chloroform, THF and DCM to 675 nm, 700 nm and 725 nm respectively. A bathochromic shift of almost 180 nm and 109 nm occurs for **PTZ-PQ-PTZ** and **PTZ-AQ-PTZ** respectively on moving from toluene to DCM. The emission spectra of **TPE-PQ-TPE** and **TPE-AQ-TPE** also shows a bathochromic shift on increasing the solvent polarity. The symmetrical **PQ**

based luminophore **TPE-PQ-TPE** in toluene emitted green fluorescence at 524 nm and yellow fluorescence in dichloromethane at 565 nm with a red shift of 41 nm. Similarly, the luminophore **TPE-AQ-TPE** emitted sky-blue fluorescence in toluene at 490 nm and a green fluorescence in dichloromethane at 529 nm which was red shifted by 39 nm.

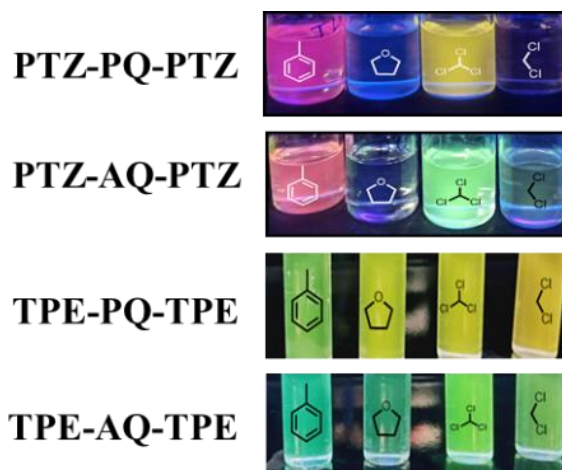


**Figure 3.5.** Photographs of **PTZ-PQ-PTZ**, **PTZ-AQ-PTZ**, **TPE-PQ-TPE** and **TPE-AQ-TPE** in solvents of different polarity taken under 365nm UV illumination. (From left to right- toluene, THF, chloroform, DCM).

The PTZ substituted symmetrical quinoxaline derivatives **PTZ-PQ-PTZ** and **PTZ-AQ-PTZ** show higher bathochromic shifts on varying the polarity as compared to the TPE substituted derivatives **TPE-PQ-TPE** and **TPE-AQ-TPE**. Hence the PTZ substituted symmetrical quinoxaline derivatives exhibit an increased charge transfer character due inclusion of strong electron donating PTZ unit as compared to the weak donor TPE. The charge transfer transition leads to larger charge separation and a higher dipole moment in the excited state. The reorientation of solvent molecules stabilizes the enhanced dipole moment of excited state by accommodating the higher dipole moment thereby decreasing the energy of the system consequently leading to a bathochromic shift. The photographs for solvatochromism of the symmetrical quinoxaline derivatives under UV illumination are shown in Figure 3.5.

### 3.6. Aggregation-induced emission (AIE) studies

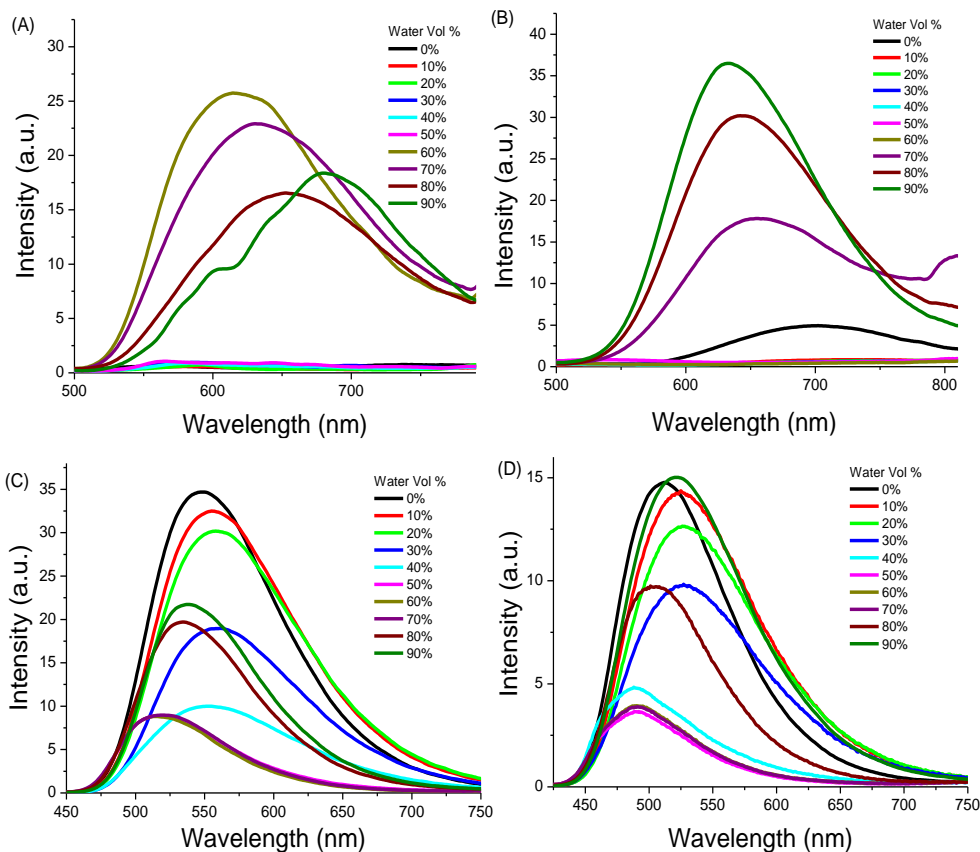


**Figure 3.6.** Emission spectra of (A) **PTZ-PQ-PTZ**, (B) **PTZ-AQ-PTZ**, (C) **TPE-PQ-TPE** and (D) **TPE-AQ-TPE** in THF-water mixtures with increasing water fractions. (conc.  $2 \times 10^{-5}$  M).

The symmetrical luminophores **PTZ-PQ-PTZ**, **PTZ-AQ-PTZ**, **TPE-PQ-TPE** and **TPE-AQ-TPE** contain PTZ and TPE unit which are AIE active and hence the AIE properties for the symmetrical luminophores were investigated using fluorescence spectroscopy (Figure 3.6.). All the symmetrical quinoxaline luminophores are highly soluble in THF but poorly soluble in water. Using this idea, we prepared nanoaggregates by increasing percentage of water in THF solution. The AIE property was examined by preparing aggregates with gradual increase of water percentage in  $10\mu\text{M}$  THF solution. The PTZ substituted symmetrical quinoxaline molecules **PTZ-PQ-PTZ** and **PTZ-AQ-PTZ** in pure THF

exhibit less intense emissions around 700-750 nm due to the polarized ICT state which are not much altered up to  $f_w$  40-50%. A high intensity emission peak for **PTZ-PQ-PTZ** is observed at 615 nm for  $f_w$  60% which is due to the formation of aggregates in the solution. The molecule **PTZ-PQ-PTZ** at higher water percentage (70-90%) shows slight reduction in emission intensity (630 nm-680 nm) due to presence of large sized aggregates. Similarly, **PTZ-AQ-PTZ** exhibits increased emission at 654 nm for  $f_w$  60% due to aggregation and the emission is enhanced twice in intensity up to  $f_w$  90% and blue shifts to 630 nm. The TPE based symmetrical luminophores **TPE-PQ-TPE** and **TPE-AQ-TPE** are highly fluorescent in solution due to the intramolecular charge transfer from the weak donor (TPE) to the acceptor moiety as compared to the PTZ based symmetrical quinoxaline luminophores which have low intensity emissions in pure THF due to higher stabilization of their ICT emission. The luminophores are highly fluorescent at high water percentage owing to formation of aggregates. The **PQ** based luminophore **TPE-PQ-TPE** emits bright yellow fluorescence at 547 nm whereas the **AQ** based luminophore **TPE-AQ-TPE** emits yellowish green fluorescence in pure THF solution at 510nm. The addition of water up to 50% ( $f_w$ ) causes decrease in fluorescence intensity for **TPE-PQ-TPE** and **TPE-AQ-TPE**. This can be attributed to ICT bands and stabilization of charge transfer on increasing solvent polarity, also known as solvatochromism.

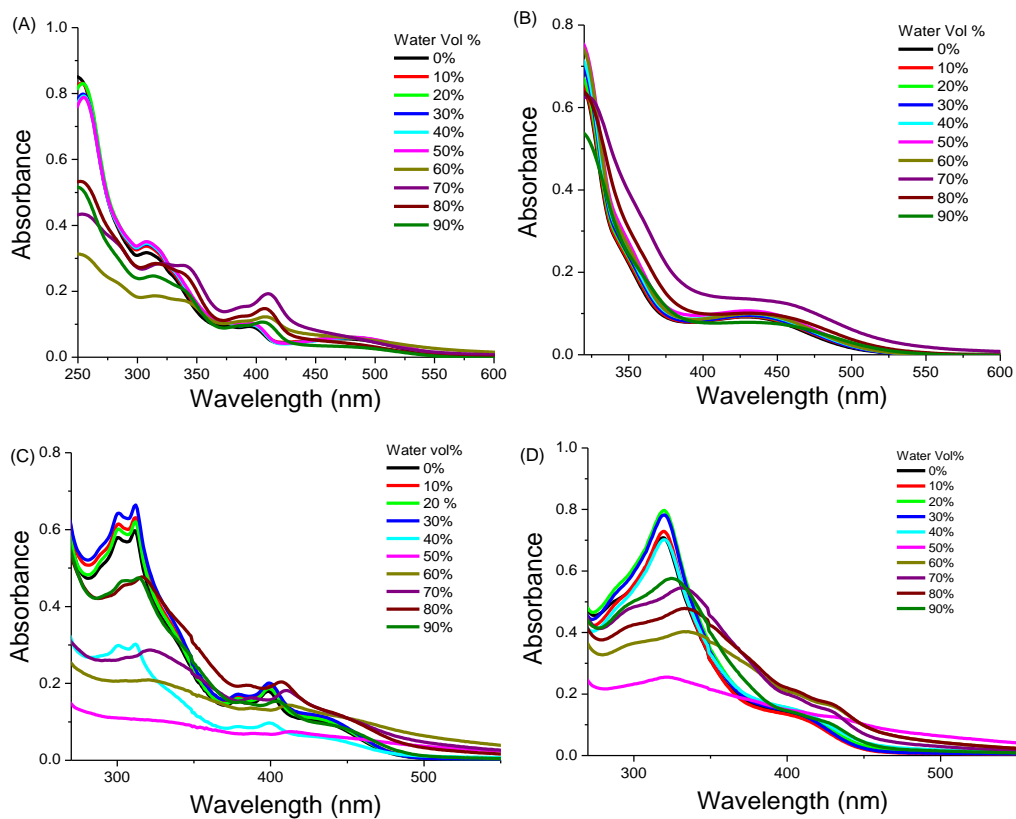


**Figure 3.7.** Electronic absorption spectra of (A) **PTZ-PQ-PTZ**, (B) **PTZ-AQ-PTZ**, (C) **TPE-PQ-TPE** and (D) **TPE-AQ-TPE** in different THF-water mixtures with increasing water percentage. (conc.  $2 \times 10^{-5}$  M).

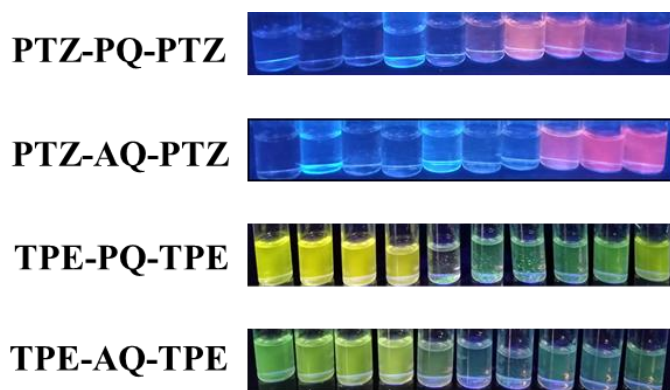


**Figure 3.8.** Photographs of **PTZ-PQ-PTZ**, **PTZ-AQ-PTZ**, **TPE-PQ-TPE** and **TPE-AQ-TPE** in different THF-water mixtures taken under 365nm UV illumination. (From left to right 0% -90% water volume fraction)

The solvatochromic effect is dominant upto 50% ( $f_w$ ) water percentage for **TPE-PQ-TPE** and **TPE-AQ-TPE**. The formation of aggregates for **TPE-PQ-TPE** and **TPE-AQ-TPE** was initiated after 50% ( $f_w$ ) which was confirmed by consequent increase in fluorescence intensity upto 90% ( $f_w$ ). It was thus concluded that the AIE effect dominates solvatochromism after 50% ( $f_w$ ) for **TPE-PQ-TPE** and **TPE-AQ-TPE**. The AIE behaviour of the symmetrical quinoxaline luminophores was further explored using absorption spectra (Figure 3.7.). The formation of nanoaggregates in the suspension leads to scattering of light for **PTZ-PQ-PTZ** and **PTZ-AQ-PTZ** above  $f_w$  60% and above  $f_w$  50% for **TPE-PQ-TPE** and **TPE-AQ-TPE** which further confirms aggregate formation. The photographs of the THF-water mixtures of the symmetrical quinoxaline derivatives (Figure 3.8.) under UV illumination further confirm the AIE behaviour.

### 3.7. Mechanochromism

The mechanochromic behaviour of the symmetrical quinoxaline luminophores **PTZ-PQ-PTZ**, **PTZ-AQ-PTZ**, **TPE-PQ-TPE** and **TPE-AQ-TPE** was studied using solid state emission spectra (Figure 3.9.) and the corresponding data are compiled in Table 3.3. The pristine solid of **PTZ-PQ-PTZ** displays light orange emission at 600 nm which on mechanical grinding is bathochromically shifted to bright red emission at 678 nm. The grinded powder of **PTZ-PQ-PTZ** on fuming with a mixture of DCM-hexane vapors returns to the pristine form with emission at 598 nm. The pristine solid of **PTZ-AQ-PTZ** has a yellow emission at 563 nm which on mechanical grinding exhibits red-shifted dark orange emission at 635 nm and reverts to its original form on fuming with an emission at 565 nm. The luminophore **TPE-PQ-TPE** in its pristine form shows green emission at 518 nm which on mechanical grinding exhibits a yellow emission at 545 nm. On the other hand, the luminophore **TPE-AQ-TPE** exhibits bluish green emission at 484 nm in its pristine form and upon mechanical grinding in a mortar pestle a green emission at 508 nm was observed. The grinded

forms of **TPE-PQ-TPE** and **TPE-AQ-TPE** revert to its original form on fuming with dichloromethane (DCM) and exhibit emission at 524 nm and 489 nm respectively. The grinding induced spectral shift for **PTZ-PQ-PTZ**, **PTZ-AQ-PTZ**, **TPE-PQ-TPE** and **TPE-AQ-TPE** was 80 nm, 72 nm, 27 nm and 24 nm respectively.

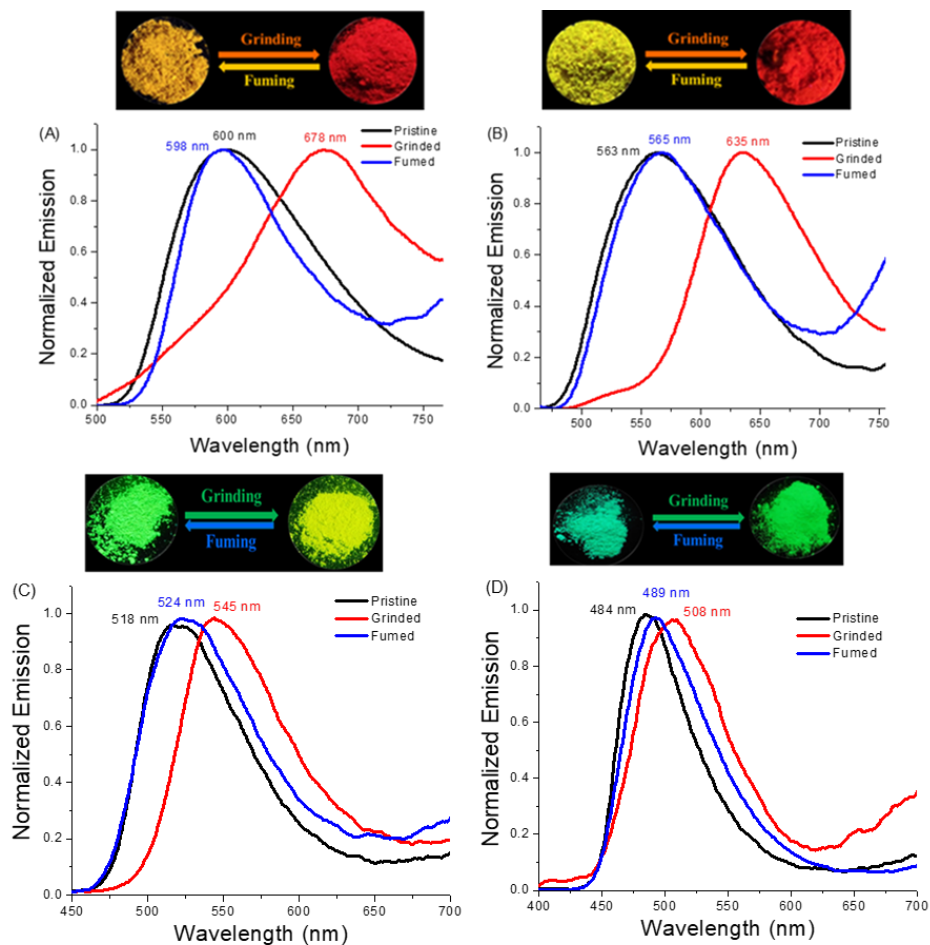


**Figure 3.9.** Emission spectra of (A) **PTZ-PQ-PTZ**, (B) **PTZ-AQ-PTZ**, (C) **TPE-PQ-TPE** and (D) **TPE-AQ-TPE** as pristine, ground, and fumed solids and photograph taken under 365 nm UV illuminations.

**Table 3.3.** Peak emission wavelengths ( $\lambda$ , in nm) of **1** and **2** under various external stimuli.

<b>Emission</b>				
<b>Compounds</b>	$\lambda_{\text{pristine}}$ (nm)	$\lambda_{\text{ground}}$ (nm)	$\lambda_{\text{fumed}}$ (nm)	$\Delta\lambda^a$ (nm)
<b>PTZ-PQ-PTZ</b>	600	678	598	80
<b>PTZ-AQ-PTZ</b>	563	635	565	72
<b>TPE-PQ-TPE</b>	518	545	524	27
<b>TPE-AQ-TPE</b>	484	508	489	24

<sup>a</sup> Grinding-induced spectral shift,  $\Delta\lambda = \lambda_{\text{ground}} - \lambda_{\text{original}}$ .

### 3.8. Powder X-ray diffraction studies

For a deeper understanding about mechanochromism, powder X-ray diffraction (PXRD) (Figure 3.10.) study was conducted for pristine, grinded and fumed samples of **PTZ-PQ-PTZ**, **PTZ-AQ-PTZ**, **TPE-PQ-TPE** and **TPE-AQ-TPE**. The symmetrical quinoxaline luminophores **PTZ-PQ-PTZ**, **PTZ-AQ-PTZ**, **TPE-PQ-TPE** and **TPE-AQ-TPE** in their pristine form displayed multiple intense sharp peaks indicating its crystalline nature. The diffraction pattern upon grinding of **PTZ-PQ-PTZ**, **PTZ-AQ-PTZ**, **TPE-PQ-TPE** and **TPE-AQ-TPE** shows broad and diffused peaks suggesting its amorphous nature. The crystalline state of the luminophores was destroyed upon grinding. The grinded samples of **PTZ-PQ-PTZ**, **PTZ-AQ-PTZ**, **TPE-PQ-TPE** and **TPE-AQ-TPE** after fuming again exhibit sharp diffraction patterns indicating conversion to crystalline state and thus proving reversible mechanochromic behaviour.

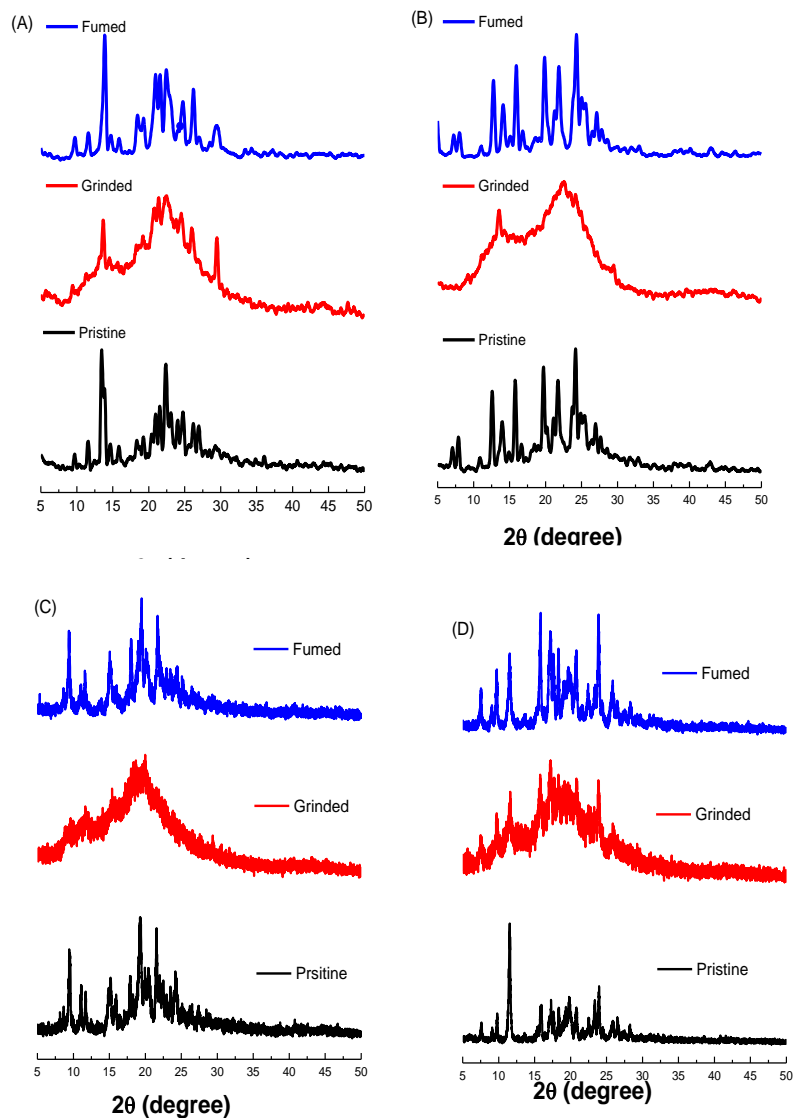


**Figure 3.10.** PXRD curves of (A) **PTZ-PQ-PTZ**, (B) **PTZ-AQ-PTZ**, (C) **TPE-PQ-TPE** and (D) **TPE-AQ-TPE** in pristine, ground, and fumed forms.

### 3.9. Experimental section

#### General methods

Chemicals were used as received unless otherwise indicated. All oxygen or moisture sensitive reactions were performed under nitrogen/argon atmosphere.  $^1\text{H}$  NMR (400 MHz) spectra were recorded on the Bruker Avance (III) 400 MHz instrument by using  $\text{CDCl}_3$ .  $^1\text{H}$  NMR chemical shifts

are reported in parts per million (ppm) relative to the solvent residual peak (CDCl<sub>3</sub>, 7.26 ppm). Multiplicities are given as: s (singlet), d (doublet), m (multiplet), and the coupling constants, *J*, are given in Hz. Thermogravimetric analyses were performed on the Metler Toledo Thermal Analysis system. UV visible absorption spectra were recorded on a Carry 100 Bio UV visible Spectrophotometer. Emission spectra were taken in a fluoromax4p fluorimeter from HoribaYovin (model: FM-100). The excitation and emission slits were 2/2 nm for the emission measurements. All of the measurements were done at 25°C. HRMS was recorded on Bruker Daltonics, micrOTOF Q II mass spectrometer. The density functional theory (DFT) calculation was carried out at the B3LYP/6 31G (d, p) level in the Gaussian 09 program.

#### **Synthesis and Characterization of PTZ-PQ-PTZ:**

A mixture of **PQ-diBr** (1.0 mmol) and 10-propyl-3-(4,4,5,5-tetramethyl-1,3,2-dioxaborolan-2-yl)-10H-phenothiazine (**PTZ-Bpin**) (2.2 mmol), was dissolved in THF/water (4/1, v/v) and then sodium carbonate (6.6 mmol) was added. After degassing the reaction mixture for 10 minutes, Pd(PPh<sub>3</sub>)<sub>4</sub> (0.1 mmol) was added and the reaction mixture was heated to reflux for 16 h under a nitrogen atmosphere. The reaction mixture was cooled to room temperature and then worked up with dichloromethane. The organic layer was dried over anhydrous sodium sulphate and solvent was evaporated. The residue was purified by silica-gel column chromatography using hexane/dichloromethane (40:60) as the eluent. An orange solid of PTZ-PQ-PTZ was obtained in 71 % yield. <sup>1</sup>H NMR (400 MHz, CDCl<sub>3</sub>, 25°C): δ 9.19 (d, *J* = 8 Hz, 2H), 8.56 (d, *J* = 8 Hz, 2H), 7.93 (s, 2H), 7.85-7.69 (m, 9H), 7.20 (t, *J* = 8 Hz, 3H), 7.10 (d, *J* = 8 Hz, 2H), 6.96 (t, *J* = 8 Hz, 4H), 3.97 (t, *J* = 6 Hz, 4H), 2.03-1.95 (m, 4H), 1.11 (t, *J* = 8 Hz, 6H). HRMS (ESI): Calcd. for [M + H]<sup>+</sup>: 759.2611. Found: 759.2168.

### Synthesis and Characterization of PTZ-AQ-PTZ:

A mixture of **AQ-diBr** (1.0 mmol) and 10-propyl-3-(4,4,5,5-tetramethyl-1,3,2-dioxaborolan-2-yl)-10H-phenothiazine (**PTZ-Bpin**) (2.2 mmol) was dissolved in THF/ water (4/1 v/v) and then Sodium carbonate (6.6 mmol) was added. After degassing the reaction mixture for 10 min, Pd(PPh<sub>3</sub>)<sub>4</sub> (0.1 mmol) was added and the reaction mixture was heated to reflux for 16 h under a nitrogen atmosphere. The reaction mixture was cooled to room temperature and worked up with dichloromethane. The organic layer was dried over anhydrous sodium sulphate and solvent was evaporated. The residue was purified by silica-gel column chromatography using hexane/dichloromethane (65:35) as the eluent. A yellow solid of PTZ-AQ-PTZ was obtained in 56% yield. ; <sup>1</sup>H NMR (500 MHz, CDCl<sub>3</sub>, 25<sup>o</sup>C): δ 8.35 (d, *J* = 5 Hz, 2H), 8.08 (d, *J* = 10 Hz, 2H), 7.82-7.79 (m, 4H), 7.71-7.69 (m, 4H), 7.20-7.17 (m, 4H), 7.05 (d, *J* = 10 Hz, 2H), 6.96-6.92 (m, 4H), 3.94 (t, *J* = 5 Hz, 4H), 1.99-1.92 (m, 4H), 1.09 (t, *J* = 7.5 Hz, 6H). HRMS (ESI): Calcd. for [M]<sup>+</sup>: 732.2376. Found: 732.2399.

### Synthesis and characterization of TPE-PQ-TPE:

Pd(PPh<sub>3</sub>)<sub>4</sub> (0.026 mmol) was added to a well degassed mixture of dibromo compound (**PQ-diBr**) (0.2 mmol), 4-(1,2,2-triphenylvinyl)phenylboronic acid pinacol ester (**TPE-Bpin**) (0.5 mmol) and sodium carbonate (1.61 mmol) in THF (40 mL) and water (10 mL). The mixture was stirred and refluxed overnight at 80 <sup>o</sup>C under nitrogen atmosphere. The completion of reaction was monitored with thin layer chromatography. The mixture was evaporated to dryness under reduced pressure and the resulting residue was purified by column chromatography (silica gel, CH<sub>2</sub>Cl<sub>2</sub>) to obtain TPE-PQ-TPE. Yield: 57%, as a yellowish green solid. <sup>1</sup>H NMR (400 MHz, CDCl<sub>3</sub>, 25 <sup>o</sup>C): δ 8.25 (d, *J* = 8.0 Hz, 2H), 8.09 (d, *J* = 8.0 Hz, 2H), 7.79–7.84 (m, 4H), 7.63 (d, *J* = 8.0 Hz, 4H), 7.08-7.23 (m, 34H). HRMS (ESI): Calcd. for [M + H]<sup>+</sup>: 915.3770. Found: 915.3734.

### Synthesis and characterization of TPE-AQ-TPE:

Pd(PPh<sub>3</sub>)<sub>4</sub> (0.026 mmol) was added to a well degassed mixture of dibromo compound (**AQ-diBr**) (0.2 mmol), 4-(1,2,2-triphenylvinyl)phenylboronic acid pinacol ester (**TPE-Bpin**) (0.5 mmol) and sodium carbonate (1.61 mmol) in THF (40 mL) and water (10 mL). The mixture was stirred and refluxed overnight at 80 °C under nitrogen atmosphere. The completion of reaction was monitored with thin layer chromatography. The mixture was evaporated to dryness under reduced pressure and the resulting residue was purified by column chromatography (silica gel, CH<sub>2</sub>Cl<sub>2</sub>) to obtain TPE-AQ-TPE. Yield: 56%, as a yellowish green solid. <sup>1</sup>H NMR (400 MHz, CDCl<sub>3</sub>, 25 °C): δ 8.94 (d, *J* = 8.0 Hz, 2H), 8.54 (d, *J* = 8.0 Hz, 2H), 7.90 (s, 4H), 7.65-7.79 (m, 8H), 7.09-7.24 (m, 34H). HRMS (ESI): Calcd. for [M + H]<sup>+</sup>: 941.3837. Found: 941.3890.

### 3.10. Conclusion

In conclusion, we have synthesized novel T-shaped donor-acceptor-donor type phenanthrene-quinoxaline (**PQ**)-A and acenaphthene-quinoxaline (**AQ**)-A' functionalized symmetrical luminophores **PTZ-PQ-PTZ**, **PTZ-AQ-PTZ** and **TPE-PQ-TPE**, **TPE-AQ-TPE** employing phenothiazine (PTZ)-D and tetraphenylethylene (TPE)-D' respectively by utilizing a Suzuki cross-coupling reaction. The D-A-D structured symmetrical quinoxaline luminophores **PTZ-PQ-PTZ**, **PTZ-AQ-PTZ**, **TPE-PQ-TPE**, **TPE-AQ-TPE** generates intramolecular charge transfer (ICT) transitions which is confirmed by solvatochromism. The PTZ based symmetrical luminophores **PTZ-PQ-PTZ** and **PTZ-AQ-PTZ** manifest higher donor-acceptor character as compared to the TPE substituted luminophores owing to the higher donor character of PTZ in comparison to TPE. All the symmetrical quinoxaline luminophores exhibit AIE characteristics due to the incorporation of AIEgens PTZ and TPE which makes them suitable solid-state emitters. The AIE properties for

luminophores **TPE-PQ-TPE** and **TPE-AQ-TPE** reveal that AIE dominates the emission at higher water percentage; whereas at low water percentage emission is dependent on solvent polarity. The symmetrical quinoxaline luminophores **PTZ-PQ-PTZ**, **PTZ-AQ-PTZ**, **TPE-PQ-TPE**, **TPE-AQ-TPE** display reversible emission changes in response to mechanical stimuli with a good color contrast. The PTZ substituted luminophores **PTZ-PQ-PTZ** and **PTZ-AQ-PTZ** shows a color change from yellow to red with higher grinding induced spectral shift upto 80 nm. The TPE substituted quinoxaline luminophores **TPE-PQ-TPE** and **TPE-AQ-TPE** shows a color change from green to yellow. The AIEgen PTZ exhibits better stimuli-responsive behavior as compared to AIEgen TPE owing to the better conformational flexibility of butterfly shaped PTZ unit. The mechanochromic behavior was further studied using powder XRD which suggests that a morphological change from crystalline to amorphous is responsible for mechanochromism. The DFT calculations reveal that HOMO and LUMO for both the luminophores are well separated on the two  $\pi$  conjugated arms which supports the strong ICT transitions. The PTZ and TPE based symmetrical quinoxaline derivatives behave as good solid-state emitters and the distinct donor acceptor interaction between the two moieties can be further exploited to employ these materials in various optoelectronic devices. The attachment of AIEgens PTZ and TPE to quinoxaline adds to the wide applications of quinoxaline and provides a novel approach to synthesis of mechanochromic materials.

### 3.11. References

- [1] (a) Weder, C. (2011). Mechanoresponsive materials. *J. Mater. Chem.*, 21(23), 8235-8236 (DOI: 10.1039/C1JM90068D); (b) Kishimura, A., Yamashita, T., Yamaguchi, K., Aida, T. (2005). Rewritable phosphorescent paper by the control of competing kinetic and thermodynamic self-assembling events. *Nat. Mater.*, 4(7), 546-549 (DOI: 10.1038/nmat1401); (c) Ciardelli, F., Ruggeri, G., Pucci, A.

- (2013). Dye-containing polymers: methods for preparation of mechanochromic materials. *Chem. Soc. Rev.*, *42*(3), 857-870 (DOI: 10.1039/C2CS35414D); (d) Farinola, G. M., Ragni, R. (2011). Electroluminescent materials for white organic light emitting diodes. *Chem. Soc. Rev.*, *40*(7), 3467-3482 (DOI: 10.1039/C0CS00204F).
- [2] (a) Chi, Z., Zhang, X., Xu, B., Zhou, X., Ma, C., Zhang, Y., Liu, S., Xu, J. (2012). Recent advances in organic mechanofluorochromic materials. *Chem. Soc. Rev.*, *41*(10), 3878-3896 (DOI: 10.1039/C2CS35016E); (b) Sagara, Y., Kato, T. (2009). Mechanically induced luminescence changes in molecular assemblies. *Nat. Chem.*, *1*(8), 605-610 (DOI: 10.1038/nchem.411); (c) Davis, D. A., Hamilton, A., Yang, J., Cremar, L. D., Van Gough, D., Potisek, S. L., Ong, M.T., Braun, P.V., Martínez, T.J., White, S.R., Sottos, N. R. (2009). Force-induced activation of covalent bonds in mechanoresponsive polymeric materials. *Nature*, *459*(7243), 68-72 (DOI: 10.1038/nature07970); (d) Dong, Y., Xu, B., Zhang, J., Tan, X., Wang, L., Chen, J., Lv, H., Wen, S., Li, B., Ye, L., Tian, W. (2012). Piezochromic luminescence based on the molecular aggregation of 9, 10-Bis ((E)-2-(pyrid-2-yl) vinyl) anthracene. *Angew. Chem., Int. Ed.*, *51*(43), 10782-10785 (DOI: 10.1002/anie.201204660); (e) Luo, X., Li, J., Li, C., Heng, L., Dong, Y. Q., Liu, Z., Bo, Z., Tang, B. Z. (2011). Reversible switching of the emission of diphenyldibenzofulvenes by thermal and mechanical stimuli. *Adv. Mater.*, *23*(29), 3261-3265 (DOI: 10.1002/adma.201101059); (f) Ning, Z., Chen, Z., Zhang, Q., Yan, Y., Qian, S., Cao, Y., Tian, H. (2007). Aggregation-induced emission (AIE)-active starburst triarylamine fluorophores as potential non-doped red emitters for organic light-emitting diodes and Cl<sub>2</sub> gas chemodosimeter. *Adv. Funct. Mater.*, *17*(18), 3799-3807 (DOI: 10.1002/adfm.200700649); (g) Sagara, Y., Yamane, S., Mutai, T., Araki, K., Kato, T. (2009). A stimuli-responsive, photoluminescent,

- anthracene-based liquid crystal: emission color determined by thermal and mechanical processes. *Adv. Funct. Mater.*, 19(12), 1869-1875 (DOI: 10.1002/adfm.200801726); (h) Toal, S. J., Jones, K. A., Magde, D., Trogler, W. C. (2005). Luminescent silole nanoparticles as chemoselective sensors for Cr (VI). *J. Am. Chem. Soc.*, 127(33), 11661-11665 (DOI: 10.1021/ja052582w); (i) Zhao, N., Yang, Z., Lam, J. W., Sung, H. H., Xie, N., Chen, S., Su, H., Gao, M., Williams, I.D., Wong, K.S., Tang, B. Z. (2012). Benzothiazolium-functionalized tetraphenylethene: an AIE luminogen with tunable solid-state emission. *Chem. Commun.*, 48(69), 8637-8639 (DOI: 10.1039/C2CC33780K); (j) Hirata, S., Watanabe, T. (2006). Reversible thermoresponsive recording of fluorescent images (TRF). *Adv. Mater.*, 18(20), 2725-2729 (DOI: 10.1002/adma.200600209); (k) Sun, H., Liu, S., Lin, W., Zhang, K. Y., Lv, W., Huang, X., Huo, F., Yang, H., Jenkins, G., Zhao, Q., Huang, W. (2014). Smart responsive phosphorescent materials for data recording and security protection. *Nat. Commun.*, 5(1), 1-9 (DOI: 10.1038/ncomms4601); (l) Samuel, I. D. W., Turnbull, G. A. (2007). Organic semiconductor lasers. *Chem. Rev.*, 107(4), 1272-1295 (DOI: 10.1021/cr050152i).
- [3] (a) Mutai, T., Satou, H., Araki, K. (2005). Reproducible on-off switching of solid-state luminescence by controlling molecular packing through heat-mode interconversion. *Nat. Mater.*, 4(9), 685-687 (DOI: 10.1038/nmat1454); (b) Yuan, W. Z., Tan, Y., Gong, Y., Lu, P., Lam, J. W., Shen, X. Y., Feng, C., Sung, H.H.Y., Lu, Y., Williams, I.D., Tang, B. Z. (2013). Synergy between twisted conformation and effective intermolecular interactions: strategy for efficient mechanochromic luminogens with high contrast. *Adv. Mater.*, 25(20), 2837-2843 (DOI: 10.1002/adma.201205043); (c) Xu, B., Xie, M., He, J., Xu, B., Chi, Z., Tian, W., Jiang, L., Zhao, F., Liu, S., Zhang, Y., Xu, J. (2013). An aggregation-induced emission luminophore with multi-stimuli single- and two-photon fluorescence switching and large two-photon

- absorption cross section. *Chem. Commun.*, 49(3), 273-275 (DOI: 10.1039/C2CC36806D); (d) Kwon, M. S., Gierschner, J., Yoon, S. J., Park, S. Y. (2012). Unique piezochromic fluorescence behavior of dicyanodistyrylbenzene based donor–acceptor–donor triad: mechanically controlled photo-induced electron transfer (eT) in molecular assemblies. *Adv. Mater.*, 24(40), 5487-5492 (DOI: 10.1002/adma.201202409); (e) Zhang, X., Chi, Z., Xu, B., Jiang, L., Zhou, X., Zhang, Y., Liu, S., Xu, J. (2012). Multifunctional organic fluorescent materials derived from 9, 10-distyrylanthracene with alkoxy endgroups of various lengths. *Chem. Commun.*, 48(88), 10895-10897 (DOI: 10.1039/C2CC36263E); (f) Xue, S., Liu, W., Qiu, X., Gao, Y., Yang, W. (2014). Remarkable isomeric effects on optical and optoelectronic properties of N-phenylcarbazole-capped 9, 10-divinylanthracenes. *J. Phys. Chem. C.*, 118(32), 18668-18675 (DOI: 10.1021/jp505527f); (g) Seki, T., Takamatsu, Y., Ito, H. (2016). A screening approach for the discovery of mechanochromic gold (I) isocyanide complexes with crystal-to-crystal phase transitions. *J. Am. Chem. Soc.*, 138(19), 6252-6260 (DOI: 10.1021/jacs.6b02409); (h) Jadhav, T., Dhokale, B., Patil, Y., Mobin, S. M., Misra, R. (2016). Multi-stimuli responsive donor–acceptor tetraphenylethylene substituted benzothiadiazoles. *J. Phys. Chem. C.*, 120(42), 24030-24040 (DOI: 10.1021/acs.jpcc.6b09015).
- [4] Jadhav, T., Dhokale, B., Mobin, S. M., Misra, R. (2015). Aggregation induced emission and mechanochromism in pyrenoimidazoles. *J. Mater. Chem. C*, 3(38), 9981-9988 (DOI: 10.1039/C5TC02181B); (b) Jadhav, T., Choi, J. M., Dhokale, B., Mobin, S. M., Lee, J. Y., Misra, R. (2016). Effect of end groups on mechanochromism and electroluminescence in tetraphenylethylene substituted phenanthroimidazoles. *J. Phys. Chem. C.*, 120(33), 18487-18495 (DOI: 10.1021/acs.jpcc.6b06277).

- [5] (a) Birks, J. B., *Photophysics of Aromatic Molecules*. Wiley-Interscience, London 1970. 704 Seiten. Preis: 210s (DOI: 10.1002/bbpc.19700741223); (b) Jayanty, S., Radhakrishnan, T. P. (2004). Enhanced fluorescence of remote functionalized diaminodicyanoquinodimethanes in the solid state and fluorescence switching in a doped polymer by solvent vapors. *Chem. – Eur. J.*, *10*(3), 791-797 (DOI: 10.1002/chem.200305123); (c) Tracy, H. J., Mullin, J. L., Klooster, W. T., Martin, J. A., Haug, J., Wallace, S., Rudloe, I., Watts, K. (2005). Enhanced photoluminescence from group 14 metalloles in aggregated and solid solutions. *Inorg. Chem.*, *44*(6), 2003-2011 (DOI: 10.1021/ic049034o); (d) Th. Forster, K. Z. Kasper, *Phys. Chem.*, (Munich) 1954, **1**, 275-282.
- [6] (a) Kwok, H. S., Zhan, X., Liu, Y., Zhuc, D., Tang, B. Z. (2001). Jingdong Luo, Zhiliang Xie, Jacky WY Lam, Lin Cheng, Haiying Chen, b Chengfeng Qiu, b. *Chem. Commun*, *1740*, 1741 (DOI: 10.1039/B105159H); (b) Li, Y., Liu, T., Liu, H., Tian, M. Z., Li, Y. (2014). Self-assembly of intramolecular charge-transfer compounds into functional molecular systems. *Acc. Chem. Res.*, *47*(4), 1186-1198 (DOI: 10.1021/ar400264e); (c) Liu, H., Xu, J., Li, Y., Li, Y. (2010). Aggregate nanostructures of organic molecular materials. *Acc. Chem. Res.*, *43*(12), 1496-1508 (DOI: 10.1021/ar100084y); (d) Hong, Y., Lam, J. W., Tang, B. Z. (2011). Aggregation-induced emission. *Chem. Soc. Rev.*, *40*(11), 5361-5388, (DOI: 10.1039/C1CS15113D).
- [7] (a) Dong, Y., Lam, J. W., Qin, A., Liu, J., Li, Z., Tang, B. Z., Sun, J., Kwok, H. S. (2007). Aggregation-induced emissions of tetraphenylethene derivatives and their utilities as chemical vapor sensors and in organic light-emitting diodes. *Appl. Phys. Lett.*, *91*(1), 011111 (DOI: 10.1063/1.2753723); (b) Huang, J., Yang, X., Wang, J., Zhong, C., Wang, L., Qin, J., Li, Z. (2012). New tetraphenylethene-based efficient blue luminophors: aggregation induced emission and partially controllable emitting color. *J. Mater. Chem.*, *22*(6), 2478-2484

- (DOI: 10.1039/C1JM14054J); (c) Wang, J., Mei, J., Hu, R., Sun, J. Z., Qin, A., Tang, B. Z. (2012). Click synthesis, aggregation-induced emission, E/Z isomerization, self-organization, and multiple chromisms of pure stereoisomers of a tetraphenylethene-cored luminogen. *J. Am. Chem. Soc.*, 134(24), 9956-9966 (DOI: 10.1021/ja208883h); (d) Wang, S., Oldham, W. J., Hudack, R. A., Bazan, G. C. (2000). Synthesis, morphology, and optical properties of tetrahedral oligo (phenylenevinylene) materials. *J. Am. Chem. Soc.*, 122(24), 5695-5709. (DOI: <https://doi.org/10.1021/ja992924w>); (e) Yuan, W. Z., Gong, Y., Chen, S., Shen, X. Y., Lam, J. W., Lu, P., Lu, Y., Wang, Z., Hu, R., Xie, N., Tang, B. Z. (2012). Efficient solid emitters with aggregation-induced emission and intramolecular charge transfer characteristics: molecular design, synthesis, photophysical behaviors, and OLED application. *Chem. Mater.*, 24(8), 1518-1528 (DOI: 10.1021/cm300416y); (f) Gong, Y., Tan, Y., Liu, J., Lu, P., Feng, C., Yuan, W. Z., Lu, Y., Sun, J.Z., He, G., Zhang, Y. (2013). Twisted D- $\pi$ -A solid emitters: efficient emission and high contrast mechanochromism. *Chem. Commun.*, 49(38), 4009-4011 (DOI: 10.1039/C3CC39243K); (g) Yuan, H., Wang, K., Yang, K., Liu, B., Zou, B. (2014). Luminescence properties of compressed tetraphenylethene: the role of intermolecular interactions. *J. Phys. Chem. Lett.*, 5(17), 2968-2973 (DOI: 10.1021/jz501371k); (h) Misra, R., Jadhav, T., Dhokale, B., Mobin, S. M. (2014). Reversible mechanochromism and enhanced AIE in tetraphenylethene substituted phenanthroimidazoles, *Chem. Commun.*, 50(65), 9076-9078 (DOI: 10.1039/C4CC02824D); (i) Jadhav, T., Dhokale, B., Mobin, S. M., Misra, R. (2015). Aggregation induced emission and mechanochromism in pyrenoidimidazoles. *J. Mater. Chem., C*, 3(38), 9981-9988 (DOI: 10.1039/C5TC02181B).
- [8] (a) Xue, P., Ding, J., Chen, P., Wang, P., Yao, B., Sun, J., Sun, J., Lu, R. (2016). Mechanical force-induced luminescence enhancement and

chromism of a nonplanar D–A phenothiazine derivative. *J. Mater. Chem. C*, 4(23), 5275-5280 (DOI: 10.1039/C6TC01193D); (b) Zhang, G., Sun, Y., Data, P., Pander, P., Higginbotham, H., Monkman, A. P., Minakata, S. (2017). Thermally activated delayed fluorescent phenothiazine–dibenzo [a, j] phenazine–phenothiazine triads exhibiting tricolor-changing mechanochromic luminescence. *Chem. Sci*, 8(4), 2677-2686 (DOI: 10.1039/C6SC04863C); (c) Tian, H., Yang, X., Chen, R., Pan, Y., Li, L., Hagfeldt, A., Sun, L. (2007). Phenothiazine derivatives for efficient organic dye-sensitized solar cells. *Chem. Commun.*, (36), 3741-3743 (DOI: 10.1039/B707485A); (d) Ramachandran, E., Dhamodharan, R. (2015). Rational design of phenothiazine (PTz) and ethylenedioxythiophene (EDOT) based donor–acceptor compounds with a molecular aggregation breaker for solid state emission in red and NIR regions. *J. Mater. Chem. C*, 3(33), 8642-8648 (DOI: 10.1039/C5TC01423A)

- [9] (a) Chang, Z. F., Jing, L. M., Chen, B., Zhang, M., Cai, X., Liu, J. J., Ye, Y.C., Lou, X., Zhao, Z., Liu, B., Tang, B. Z. (2016). Rational design of asymmetric red fluorescent probes for live cell imaging with high AIE effects and large two-photon absorption cross sections using tunable terminal groups. *Chem. Sci.*, 7(7), 4527-4536 (DOI: 10.1039/C5SC04920B); (b) Chang, Z. F., Jing, L. M., Wei, C., Dong, Y. P., Ye, Y. C., Zhao, Y. S., Wang, J. L. (2015). Hexaphenylbenzene-Based,  $\pi$ -Conjugated Snowflake-Shaped Luminophores: Tunable Aggregation-Induced Emission Effect and Piezofluorochromism. *Chem. Eur. J.*, 21(23), 8504-8510 (DOI: 10.1039/C7TC03535G); (c) Guo, Z. H., Jin, Z. X., Wang, J. Y., Pei, J. (2014). A donor–acceptor–donor conjugated molecule: twist intramolecular charge transfer and piezochromic luminescent properties. *Chem. Commun.*, 50(46), 6088-6090 (DOI: 10.1039/C3CC48980A); (d) Sun, J., Dai, Y., Ouyang, M., Zhang, Y., Zhan, L., Zhang, C. (2015). Unique torsional cruciform  $\pi$ -architectures

- composed of donor and acceptor axes exhibiting mechanochromic and electrochromic properties. *J. Mater. Chem., C*, 3(14), 3356-3363 (DOI: 10.1039/C4TC02046D); (e) Grabowski, Z. R., Rotkiewicz, K., Rettig, W. (2003). Structural changes accompanying intramolecular electron transfer: focus on twisted intramolecular charge-transfer states and structures. *Chem. Rev.*, 103(10), 3899-4032 (DOI: 10.1021/cr9407451); (f) Jadhav, T., Dhokale, B., Misra, R. (2015). Effect of the cyano group on solid state photophysical behavior of tetraphenylethene substituted benzothiadiazoles. *J. Mater. Chem., C*, 3(35), 9063-9068 (DOI: 10.1039/C5TC01871D).
- [10] (a) Sun, X., Liu, Y., Xu, X., Yang, C., Yu, G., Chen, S., Zhao, Z., Qiu, W., Li, Y., Zhu, D. (2005). Novel electroactive and photoactive molecular materials based on conjugated donor– acceptor structures for optoelectronic device applications. *J. Phys. Chem. B.*, 109(21), 10786-10792 (DOI: 10.1021/jp0509515); (b) Shirota, Y. (2005). Photo-and electroactive amorphous molecular materials—molecular design, syntheses, reactions, properties, and applications. *J. Mater. Chem.*, 15(1), 75-93 (DOI: 10.1039/B413819H); (c) Shen, X. Y., Yuan, W. Z., Liu, Y., Zhao, Q., Lu, P., Ma, Y., Williams, I.D., Qin, A., Sun, J.Z., Tang, B. Z. (2012). Fumaronitrile-based fluorogen: red to near-infrared fluorescence, aggregation-induced emission, solvatochromism, and twisted intramolecular charge transfer. *J. Phys. Chem. C*, 116(19), 10541-10547 (DOI: 10.1021/jp303100a); (d) Kim, F. S., Guo, X., Watson, M. D., Jenekhe, S. A. (2010). High-mobility Ambipolar Transistors and High-gain Inverters from a Donor– Acceptor Copolymer Semiconductor. *Adv. Mater.*, 22(4), 478-482 (DOI: 10.1002/adma.200901819).
- [11] Zhang, Y., Zou, J., Yip, H. L., Chen, K. S., Zeigler, D. F., Sun, Y., Jen, A. K. Y. (2011). Indacenodithiophene and quinoxaline-based conjugated polymers for highly efficient polymer solar cells. *Chem. Mater.*, 23(9), 2289-2291 (DOI: 10.1021/cm200316s).

- [12](a) Biegger, P., Stolz, S., Intorp, S. N., Zhang, Y., Engelhart, J. U., Rominger, F., Hardcastle, K.I., Lemmer, U., Qian, X., Hamburger, M., Bunz, U. H. F. (2015). Soluble Diazaiptycenes: Materials for Solution-Processed Organic Electronics. *J. Org. Chem.*, *80*(1), 582-589 (DOI: 10.1021/jo502564w); (b) Song, H. J., Kim, D. H., Lee, E. J., Moon, D. K. (2013). Conjugated polymers consisting of quinacridone and quinoxaline as donor materials for organic photovoltaics: orientation and charge transfer properties of polymers formed by phenyl structures with a quinoxaline derivative. *J. Mater. Chem. A*, *1*(19), 6010-6020 (DOI: 10.1039/C3TA10512A); (c) Li, C. T., Li, S. R., Chang, L. Y., Lee, C. P., Chen, P. Y., Sun, S. S., Lin, J.J., Vittal, R., Ho, K. C. (2015). Efficient titanium nitride/titanium oxide composite photoanodes for dye-sensitized solar cells and water splitting. *J. Mater. Chem. A*, *3*(8), 4695-4705 (DOI: 10.1039/C4TA05606J); (d) Yang, J., Ganesan, P., Teuscher, J., Moehl, T., Kim, Y. J., Yi, C., Comte, P., Pei, K., Holcombe, T.W., Nazeeruddin, M.K. and Hua, J., Grätzel, M. (2014). Influence of the donor size in D- $\pi$ -A organic dyes for dye-sensitized solar cells. *J. Am. Chem. Soc.*, *136*(15), 5722-5730. (e) T. Lan, X. Lu, L. Zhang, Y. Chen, G. Zhou and Z.-S. Wang, *J. Mater. Chem. A*, 2015, **3**, 9869–9881 (DOI: 10.1021/ja500280r); (e) Wang, C., Zhang, J., Long, G., Aratani, N., Yamada, H., Zhao, Y., Zhang, Q. (2015). Synthesis, structure, and air-stable n-type field-effect transistor behaviors of functionalized octaazanonacene-8, 19-dione. *Angew. Chem., Int. Ed.*, *127*(21), 6390-6394 (DOI: 10.1002/anie.201500972); (f) Wang, C., Zhang, J., Long, G., Aratani, N., Yamada, H., Zhao, Y., Zhang, Q. (2015). Synthesis, structure, and air-stable n-type field-effect transistor behaviors of functionalized octaazanonacene-8, 19-dione. *Angew. Chem. Int. Ed.*, *127*(21), 6390-6394. (DOI: <https://doi.org/10.1002/ange.201500972>); (g) Lin, T. C., Chien, W., Liu, C. Y., Tsai, M. Y., Huang, Y. J. (2013). Synthesis and Two-Photon Absorption Properties of Symmetrical Chromophores Derived from 2,

- 3, 5-Trisubstituted Quinoxaline Units. *Eur. J. Org. Chem.*, 2013(20), 4262-4269 (DOI: 10.1002/ejoc.201300345); (h) de Torres, M., Semin, S., Razdolski, I., Xu, J., Elemans, J. A., Rasing, T., T., Rowan, A.E., Nolte, R. J. (2015). Extended  $\pi$ -conjugated ruthenium zinc-porphyrin complexes with enhanced nonlinear-optical properties. *Chem. Commun.*, 51(14), 2855-2858 (DOI: 10.1039/C4CC09592H); (i) Nagata, Y., Nishikawa, T., Suginome, M. (2015). Exerting control over the helical chirality in the main chain of sergeants-and-soldiers-type poly (quinoxaline-2, 3-diyl) s by changing from random to block copolymerization protocols. *J. Am. Chem. Soc.*, 137(12), 4070-4073 (DOI: 10.1021/jacs.5b01422).
- [13] Hu, J., Liu, R., Cai, X., Shu, M., Zhu, H. (2015). Highly efficient and selective probes based on polycyclic aromatic hydrocarbons with trimethylsilylethynyl groups for fluoride anion detection. *Tetrahedron*, 71(23), 3838-3843 (DOI: 10.1016/j.tet.2015.04.016).
- [14] Guo, Z. H., Lei, T., Jin, Z. X., Wang, J. Y., & Pei, J. (2013). T-Shaped donor-acceptor molecules for low-loss red-emission optical waveguide. *Organic letters*, 15(14), 3530-3533. (DOI: <https://doi.org/10.1021/ol4012025>).
- [15] Lu, X., Fan, S., Wu, J., Jia, X., Wang, Z. S., Zhou, G. (2014). Controlling the charge transfer in D-A-D chromophores based on pyrazine derivatives. *J. Org. Chem.*, 79(14), 6480-6489 (DOI: 10.1021/cm301520z).
- [16] (a) M. J. Frisch, G. W. Trucks, G. W. Schlegel, G. E. Scuseria, M. A. Robb, J. R. Cheeseman, G. Scalmani, V. Barone, B. Mennucci, G. A. Petersson, et al., Gaussian 09, revision A.02; Gaussian, Inc.: Wallingford, CT: 2009; (b) Lee, C., Yang, W., Parr, R. G. (1988). Development of the Colle-Salvetti correlation-energy formula into a functional of the electron density. *Phys. Rev. B*, 37(2), 785 (DOI:

10.1103/PhysRevB.37.785); (c) A. D. Becke, *J. Chem. Phys.*, 1993, 98, 1372–1377.

- [17] Misra, R., Jadhav, T., Dhokale, B., Gautam, P., Sharma, R., Maragani, R., Mobin, S. M. (2014). Carbazole-BODIPY conjugates: design, synthesis, structure and properties. *Dalton Trans.*, 43(34), 13076-13086 (DOI: 10.1039/c4dt00983e).
- [18] (a) Sun, Q., Lam, J. W., Xu, K., Xu, H., Cha, J. A., Wong, P. C., Wen G., Zhang, X., Jing, X., Wang, F., Tang, B. Z. (2000). Nanocluster containing mesoporous magnetoceramics from hyperbranched organometallic polymer precursors. *Chem. Mater.*, 12(9), 2617-2624 (DOI: <https://doi.org/10.1021/cm000094b>); (b) Tang, B. Z., Xu, H., Lam, J. W., Lee, P. P., Xu, K., Sun, Q., Cheuk, K. K. (2000). C60 containing poly (1-phenyl-1-alkynes): synthesis, light emission, and optical limiting. *Chem. Mater.*, 12(5), 1446-1455 (DOI: 10.1002/9783527629787).

## Chapter 4

### Effect of different donors on mechanochromism of AIE active unsymmetrical D-A-D' type quinoxaline derivatives

---

---

#### 4.1. Introduction

Solid-state emissive organic small molecules have acquired noteworthy importance of the scientific community due to their promising applications in optoelectronic devices, solid-state lasers, stimuli-responsive materials, bioimaging, sensors and many more.<sup>[1]</sup> In particular, stimuli-responsive solid-state organic emitters that display variation in their emission as a response to various external stimuli (mechanical pressure, pH, temperature, light) have gained considerable interest of researchers in recent times.<sup>[2]</sup> Mechanochromic materials which show reversible changes in emission on application of mechanical stimuli (rubbing, crushing, grinding, scratching) are termed as *smart* stimuli-responsive materials,<sup>[3]</sup> owing to their potential usage in optoelectronic devices, pressure sensors, anticounterfeiting applications, security inks and optical storage devices.<sup>[4]</sup> The changes in emission of organic molecules stimulated by mechanical pressure are attainable only in their solid state, hence adequate emission in solid state is vital for organic molecules to be employed as mechanochromic materials.<sup>[5]</sup> However, most of the typical organic chromophores are highly emissive in their solution although experience quenching of emission in their aggregated or solid state due to the phenomenon of aggregation caused quenching (ACQ).<sup>[6]</sup> This drawback of organic chromophores has been successfully controlled after the introduction of aggregation-induced emission (AIE) by Tang *et al.* in 2001 which alternatively takes advantage of aggregation to result in increased emission. The idea of AIE is to construct non-planar luminogens which show enhanced emission on aggregation or in the solid state by eliminating the  $\pi$ - $\pi$  stacking interactions as an outcome of restriction of intramolecular rotations (RIR).<sup>[7]</sup>

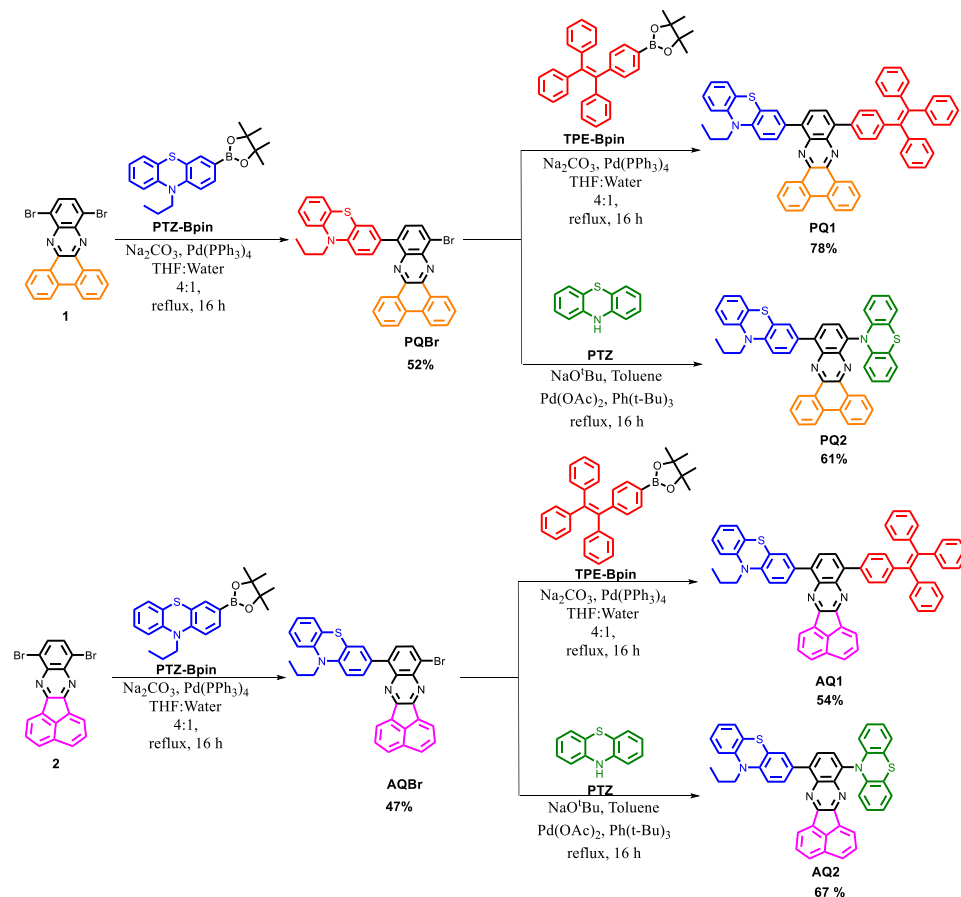
Tetraphenylethylene (TPE) is an ideal and most widely employed AIEgen owing to its distinct propeller type structure which endows the core with high solid-state emission.<sup>[8]</sup> Over the past few years, TPE and its derivatives have been widely used in developing efficient organic solid-state emitters which find numerous applications in mechanochromic materials, OLEDs, bioimaging, fluorescent probes and sensors.<sup>[9]</sup> Recently, phenothiazine (PTZ) has been exploited as a heterocyclic AIEgen by many researchers due to its butterfly shaped non-planar structure which empowers the moiety with improved solid-state emission. Furthermore, PTZ based emitters have been used in OLEDs, organic solar cells (OSCs), room-temperature phosphorescent (RTP) materials, thermally activated delayed fluorescence (TADF) materials, stimuli-responsive materials, perovskite solar cells and many more.<sup>[10]</sup>

Mechanochromic emission switching is usually achieved through modifications in the physical structure or through phase transitions, hence it heavily depends on the molecular packing modes and various intermolecular interactions occurring in the solid state.<sup>[11]</sup> Accordingly, the solid-state emission can be modulated by minor structural alterations such as inclusion of heteroatoms, incorporation of alkyl or aryl substituents, use of different halogen or heavy atoms, changes in the conjugation length and torsional angles, regio-isomerism *etc.*<sup>[12]</sup> Organic molecules comprising of various electron donor and electron acceptor units in different manners such as D-A, D-A-D, D-A-A', D- $\pi$ -A allow modulating the solid-state emission properties and hence are a good choice for developing highly emissive mechanochromic materials.<sup>[13]</sup> The utilization of heterocyclic acceptor units and AIE active donor units will not only alter the intermolecular interactions and molecular packing in the solid state but also help in generating favorable emission switching properties.<sup>[14]</sup> Quinoxaline has been widely explored in optoelectronic devices and various biological and material applications owing to its electron accepting nature induced by presence of two N atoms, outstanding chemical and thermal stability due to its largely

fused structure and favorable photophysical and electronic properties.<sup>[15]</sup> Inspired by this, we have utilized quinoxaline as acceptor in designing donor-acceptor-donor target molecules to attain tunable solid-state emission. We have developed phenanthrene-quinoxaline (PQ) and acenaphthene-quinoxaline (AQ) derivatives with unsymmetrical substitution of AIE active donors PTZ (D), TPE (D') and have exploited different attaching position of PTZ (N-position) and used N-PTZ as one of the donors (D''). In the Chapter 3, we have explored D-A-D phenanthrene-quinoxaline PQ (A) and acenaphthene-quinoxaline AQ (A') derivatives with symmetrically substituted TPE and PTZ (**PTZ-PQ-PTZ**, **PTZ-AQ-PTZ**, **TPE-PQ-TPE** and **TPE-AQ-TPE**) which exhibit admirable AIE and mechanochromic properties.<sup>[16]</sup> In this work, we have designed and synthesized D-A-D'/D-A'-D'' structured unsymmetrical phenanthrene-quinoxaline (PQ)-A and acenaphthene-quinoxaline (AQ)-A' derivatives where phenothiazine (PTZ) unit is utilized as donor (D) in combination with tetraphenylethylene (TPE) as donor (D') (**PQ1** and **AQ1**) and N-substituted phenothiazine (N-PTZ) moiety as donor (D'') (**PQ2** and **AQ2**) respectively. The unsymmetrical substitution of strong donor PTZ in combination with donors TPE and N-PTZ can perturb the donor-acceptor character and thereby exert effect on the photophysical, solvatochromic, AIE and mechanochromic properties have been investigated. The unsymmetrical derivatives show contrasting solvatochromic behaviors with highly emissive intramolecular charge transfer (ICT) state in **PQ1** and **AQ1** and quenched twisted intramolecular charge transfer (TICT) state in **PQ2** and **AQ2** respectively. The unsymmetrical derivatives **PQ1** and **AQ1** containing TPE and PTZ units exhibit AIE and mechanochromic characteristics whereas **PQ2** and **AQ2** are non-emissive in the solid state although mechanochromic in nature. The following work in-depth contributes to understanding the impact of different donor-acceptor structures on the AIE and mechanochromic characteristics.

## 4.2. Results and discussion

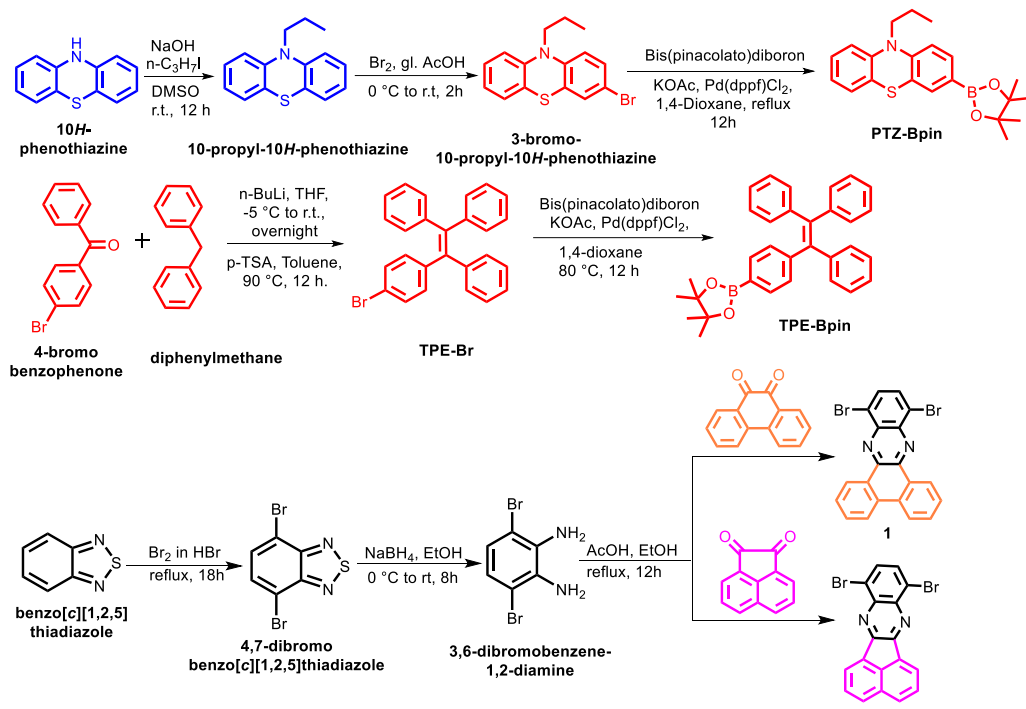
### Synthesis



**Scheme 4.1.** Synthesis of unsymmetrical phenanthrene-quinoxaline (**PQ**) and acenaphthene-quinoxaline (**AQ**) derivatives.

The unsymmetrical donor-acceptor-donor structured quinoxaline derivatives (**PQ1**, **PQ2**, **AQ1** and **AQ2**) using phenanthrene-quinoxaline (**PQ**) and acenaphthene-quinoxaline (**AQ**) as central acceptor units A and A' respectively were synthesized as shown in Scheme 4.1. Phenothiazine (PTZ) moiety was fixed as one of the terminal donors (D) unit in all the unsymmetrical quinoxaline derivatives owing to its favorable solid-state emission switching properties whereas the remaining bromo substitution of the quinoxaline unit was exploited with donors of different strengths and geometries. The unsymmetrical D-A-D'/D-A'-D' derivatives **PQ1** and **AQ1**

utilize tetraphenylethylene (TPE) as donor (D'), in addition to phenothiazine (PTZ) as donor (D). Similarly, the other set of unsymmetrical D-A-D'' and D-A'-D'' derivatives **PQ2** and **AQ2** use the N-substituted phenothiazine (N-PTZ) moiety as donor (D'') along with (PTZ) as donor (D).



**Scheme 4.2.** Synthetic scheme for intermediates **PTZ-Bpin**, **TPE-Bpin**, **1** and **2**.

The intermediates **TPE-Bpin** and **PTZ-Bpin** were synthesized using reported procedure by Miyaura Borylation reaction<sup>[17]</sup> The dibromo phenanthrene-quinoxaline **1** and acenaphthene-quinoxaline **2** were obtained from the reported condensation reaction of 3,6-dibromobenzene-1,2-diamine with 9,10-phenanthroquinone and acenaphthoquinone respectively.<sup>[18]</sup> The detailed synthesis of the intermediates is compiled in Scheme 4.2. The Suzuki cross-coupling reaction of **1** and **2** with 0.8 equivalent and 0.5 equivalent of PTZ-Bpin in THF:water as solvent and Pd(PPh<sub>3</sub>)<sub>4</sub> as catalyst results in mono-substituted PTZ bromo intermediates **PQBr** and **AQBr** in 52% and 47% yields respectively. Further, the

unsymmetrical quinoxaline derivatives **PQ1** and **AQ1** were synthesized by the Suzuki cross-coupling reaction of **PQBr** and **AQBr** with **TPEBpin** using  $\text{Pd}(\text{PPh}_3)_4$  as catalyst in 78% and 54% yield respectively. The unsymmetrical quinoxaline derivatives **PQ1** and **AQ1** were obtained by the Suzuki cross coupling with **PTZ** on one side and **TPE** on the other side. The intermediates **PQBr** and **AQBr** were further subjected to the Pd-catalyzed Buchwald-Hartwig coupling reaction with **PTZ** to form unsymmetrical quinoxaline derivatives **PQ2** and **AQ2** in 61% and 67% yields respectively. The unsymmetrical substitution in **PQ2** and **AQ2** was achieved by the Pd-catalyzed C-C cross coupling of **PTZ** on one side and the Pd-catalyzed C-N coupling reaction of **PTZ** on other side of the central quinoxaline acceptor unit. All the quinoxaline derivatives are readily soluble in tetrahydrofuran (THF), dichloromethane (DCM), chloroform, toluene, ethyl-acetate and the structures of quinoxaline derivatives (**PQ1**, **PQ2**, **AQ1** and **AQ2**) were confirmed by  $^1\text{H}$  NMR,  $^{13}\text{C}$  NMR and HMRS techniques.

### 4.3. Photophysical Properties

The photophysical properties of the quinoxaline derivatives were evaluated by recording the electronic absorption spectra and the emission spectra of the derivatives in ( $2 \times 10^{-5}$  M) THF solution as shown in Figure 4.1. and the related data are listed in Table 4.1. The phenanthrene-quinoxaline derivatives **PQ1** and **PQ2** display multiple strong absorption bands between 300–400 nm associated to the various  $\pi-\pi^*$  transitions originating either from the donor moieties or from the phenanthrene ring.

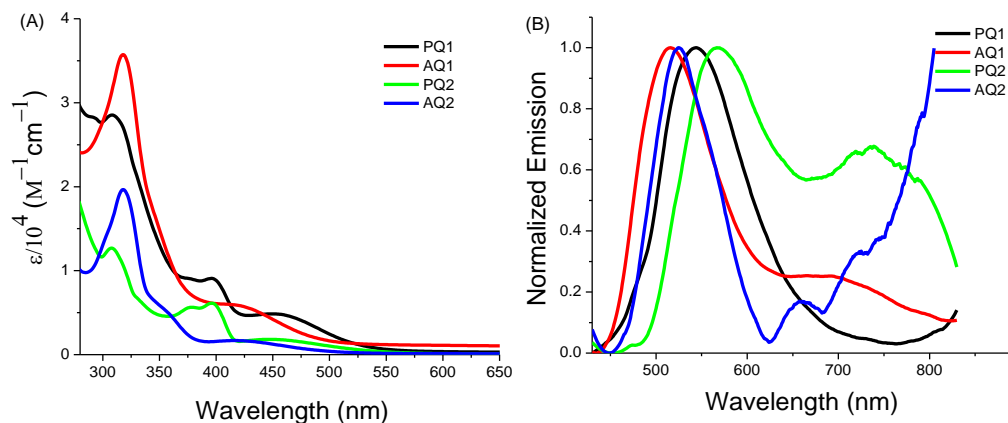


**Figure 4.1.** Electronic absorption spectra (A) and normalized emission spectra (B) of unsymmetrical quinoxaline derivatives **PQ1**, **PQ2**, **AQ1** and **AQ2** measured in THF ( $2 \times 10^{-5}$  M).

Alternatively, the acenaphthene-quinoxaline derivatives **AQ1** and **AQ2** possess only one absorption band in this region (300–400 nm) at 319 nm and 318 nm respectively owing to the  $\pi-\pi^*$  transitions. The presence of multiple  $\pi-\pi^*$  bands in **PQ** derivatives could be due to the highly conjugated phenanthrene ring. The quinoxaline derivatives **PQ1**, **PQ2**, **AQ1**, and **AQ2** also possess an absorption band in the higher wavelength region at 458 nm, 428 nm, 456 nm and 431 nm, respectively which may have originated from the intramolecular charge transfer (ICT) transition occurring from the donor to acceptor quinoxaline units which was further validated using solvatochromism studies. The absorption bands associated to the ICT transition for **PQ** derivatives were red shifted as compared the **AQ** derivatives. Furthermore, the phenanthrene-quinoxaline **PQ** and acenaphthene-quinoxaline **AQ** derivatives having symmetrical substitution of PTZ on both sides (**PTZ-PQ-PTZ** and **PTZ-AQ-PTZ**, Chapter 3, Figure 3.2.) exhibit bathochromically shifted ICT absorption band as compared to the unsymmetrical quinoxaline **PQ1**, **PQ2**, **AQ1** and **AQ2** derivatives which either possess only one PTZ donor or a weak donor TPE. The bathochromic shift in the ICT absorption band for the symmetrical quinoxaline **PQ** and **AQ** derivatives as compared to the unsymmetrical

derivatives could be ascribed to the higher electron-donating ability of PTZ and the presence of two PTZ donors which could result in a stronger D-A character. The emission spectra for **PQ1** shows emission maximum at 544nm which was similar to the emission of symmetrical TPE substituted **PQ** derivative (**TPE-PQ-TPE**) (Figure 3.2. Chapter 3). Similarly, the unsymmetrical derivative **AQ1** shows an emission maximum at 516 nm comparable to the emission of the symmetrical TPE substituted **AQ** derivative (**TPE-AQ-TPE**) accompanied with a shoulder emission at 694 nm. The molecule **PQ2** has an emission maximum at 567 nm along with a low intensity emission peak at 738 nm. The emission peak at 567 nm in **PQ2** could be due to the localized excited (LE) emission whereas the emission peak in the range of 700–800 nm could be ascribed to the ICT emission. The molecule **AQ2** shows an emission maximum at 525 nm which could be due to the LE emission along with a shoulder peak at 660 nm which could be due to the ICT emission. The quinoxaline **PQ** and **AQ** derivatives with symmetrical substitution of PTZ (**PTZ-PQ-PTZ** and **PTZ-AQ-PTZ**, Chapter 3, Figure 3.2.) have red-shifted emissions as compared to the unsymmetrical derivatives due to the presence of two PTZ donor units in conjugation with the quinoxaline moiety.

**Table 4.1.** Photophysical properties of **PQ1**, **PQ2**, **AQ1**, and **AQ2**.

<b>Compounds</b>	$\lambda_{ab}[\text{nm}] (\epsilon[\text{Lmol}^{-1}\text{cm}^{-1}])^a$	$\lambda_{em} .(\text{nm})^b$	$\Phi_f^c$
<b>PQ1</b>	288 (28356), 309 (28520), 396 (9077), 458 (4776)	544	0.05
<b>PQ2</b>	307 (12669), 378 (5643) 398 (6065), 456 (1787)	567, 738	0.01
<b>AQ1</b>	318 (35737), 425 (5701)	516, 694	0.06
<b>AQ2</b>	318 (19667), 431 (1581)	525, 660	0.02

<sup>a,b</sup> Measured in tetrahydrofuran, <sup>c</sup> The fluorescence quantum yields were recorded using Rhodamine 6G as a standard in ethanol solution

#### 4.4. Theoretical studies

The density functional theory (DFT) calculations for the unsymmetrical quinoxaline derivatives **PQ1**, **PQ2**, **AQ1** and **AQ2** were carried out to analyze the electronic structures and the distribution of frontier molecular orbitals (FMO) on the molecules by using B3LYP/631-G+(d,p) basis set.<sup>[19]</sup> The calculated frontier molecular orbitals for **PQ1**, **PQ2**, **AQ1** and **AQ2** are depicted in Figure 4.2. and the values are tabulated in Table 4.2.

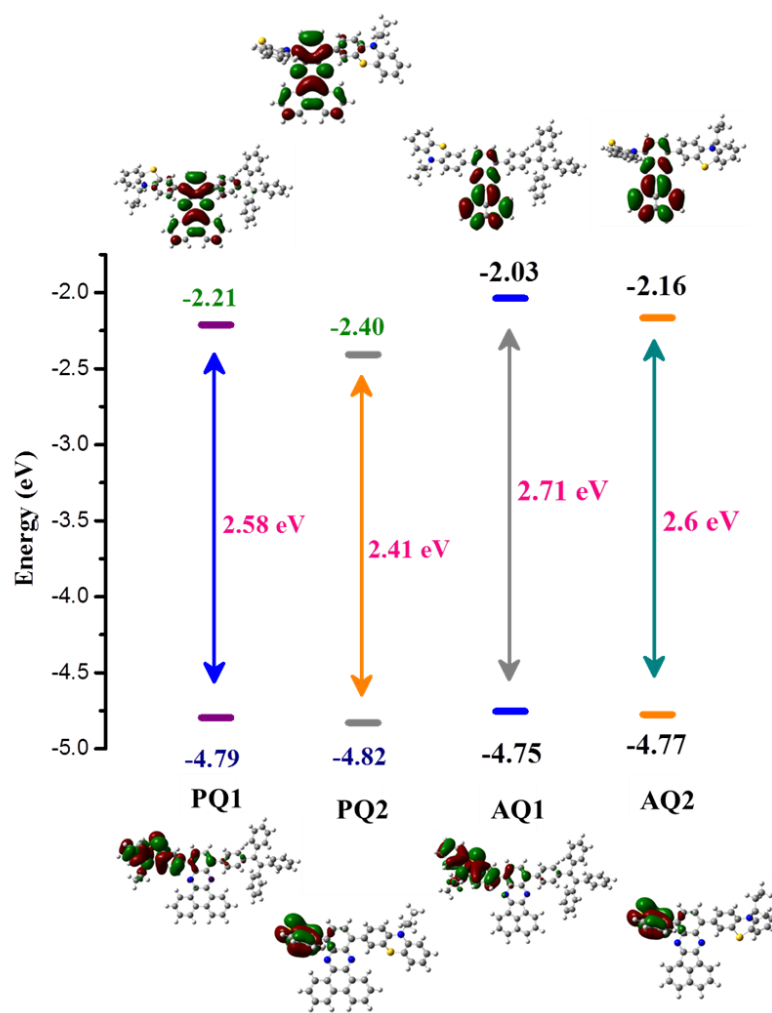


**Figure 4.2.** Energy level diagram illustrating the HOMO and LUMO energy levels of **PQ1**, **PQ2**, **AQ1** and **AQ2** determined at the B3LYP/6-31G+(d,p) level.

The unsymmetrical quinoxaline derivatives **PQ1**, **PQ2**, **AQ1** and **AQ2** exhibit non-planar structure due to the presence of PTZ and TPE units at the end capping positions which have a butterfly type structure and a propeller type structure respectively. In the case of **PQ1** and **AQ1**, the HOMO energy levels were mainly localized on the PTZ unit, due to the presence of TPE unit which acts as a weak electron donating unit. However, the HOMO energy levels of **PQ2** and **AQ2** are mainly concentrated over the N-substituted PTZ unit rather than the C-substituted PTZ unit due to its extremely twisted structure upon substitution of PTZ through -N position on the quinoxaline unit.<sup>[20]</sup> The LUMO energy level was mainly concentrated on the phenanthrene-quinoxaline unit and the acenaphthene-quinoxaline respectively in the quinoxaline derivatives **PQ1**, **PQ2**, **AQ1** and **AQ2**, indicating that the quinoxaline unit is a strong acceptor unit in the donor-acceptor-donor system. The computed HOMO-LUMO gaps for **PQ1**, **PQ2**, **AQ1**, and **AQ2** are 2.58 eV, 2.41 eV, 2.71 eV and 2.60 eV respectively.

**Table 4.2.** DFT calculations of unsymmetrical PQ and AQ derivatives.

<b>Compounds</b>	<b>HOMO<sup>a</sup> eV</b>	<b>LUMO<sup>a</sup> eV</b>	<b>HOMO-LUMO gap eV</b>
<b>PQ1</b>	-4.79	-2.21	2.58
<b>PQ2</b>	-4.82	-2.40	2.41
<b>AQ1</b>	-4.75	-2.03	2.71
<b>AQ2</b>	-4.77	-2.16	2.60

<sup>a</sup>Theoretical values calculated at B3LYP/631-G+(d,p)

#### 4.5. Solvatochromism

The donor-acceptor-donor based quinoxaline molecules are presumed of demonstrating intramolecular charge transfer (ICT) transition from the donor unit to the acceptor unit which can be easily affected by changes in the solvent polarity. Hence, the variations in the ICT transition with the use of different solvents from non-polar to polar (Toluene, THF, DCM and chloroform) were studied by emission (Figure 4.3.) and absorption spectroscopy (Figure 4.4.). The unsymmetrical PTZ-TPE based **PQ** derivative, **PQ1** in toluene has an emission maximum at 666 nm along with a shoulder peak around 526 nm. The shoulder peak in toluene (526 nm) lies at the same position as the emission maximum of TPE-based symmetrical **PQ** derivative (**TPE-PQ-TPE**) reported in Chapter 3 (Figure 3.3.). It can be concluded that the emission maximum at 666 nm in **PQ1** could be arising due to the ICT from PTZ donor to **PQ** acceptor and the shoulder at 526 nm could be the ICT emission from TPE donor to **PQ** acceptor.<sup>[16]</sup>

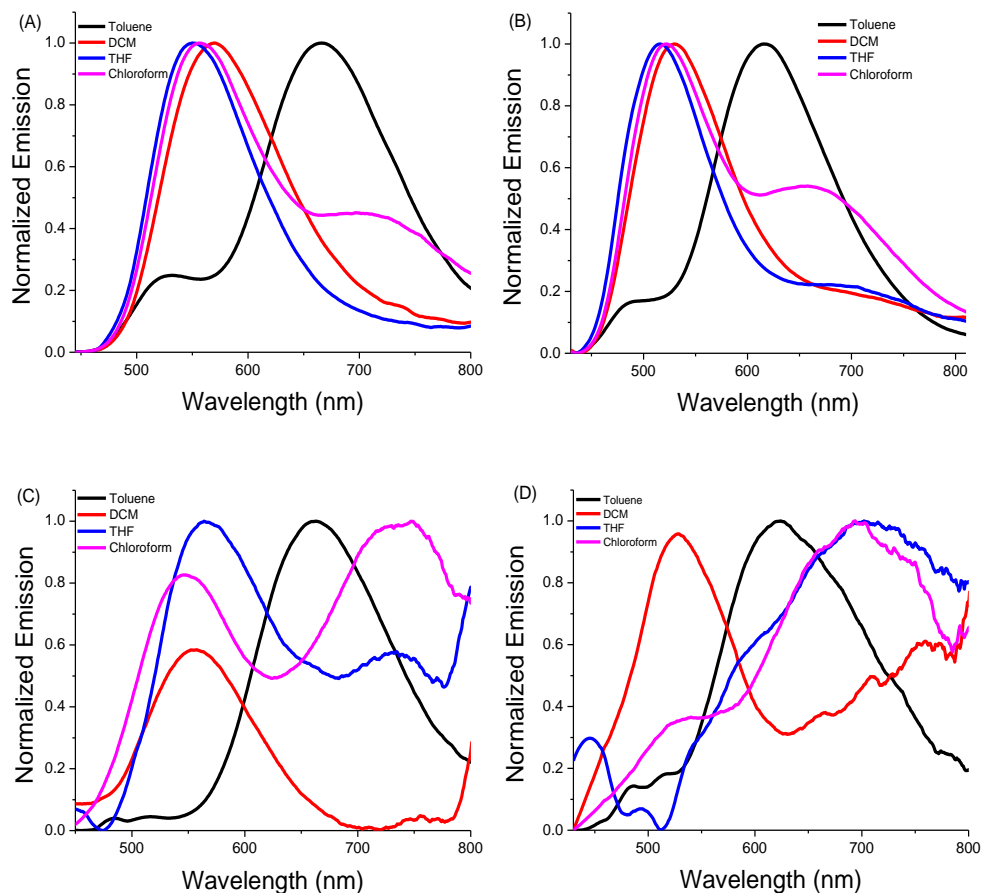


**Figure 4.3.** Emission spectra of (A) **PQ1**, (B) **AQ1**, (C) **PQ2** and (D) **AQ2** in solvents of different polarity. ( $\lambda_{exc} = 420\text{nm}$ ).

The molecule **PQ1** exhibits emission maxima at 550 nm, 556 nm and 568 nm in THF, chloroform and DCM respectively similar to the TPE based symmetrical **PQ** derivative (**TPE-PQ-TPE**) (Figure 3.3, Chapter 3). In THF and DCM, single emission peaks without shoulder emissions were observed for **PQ1** although **PQ1** in chloroform displays a shoulder peak at 721 nm which could be due to the ICT from PTZ to **PQ**. Similarly, the TPE substituted unsymmetrical derivative **AQ1** in toluene has an emission maximum at 616 nm along with shoulder peak at 486 nm. The emission of **AQ1** in toluene at 486 nm was similar to the emission of symmetrical TPE-substituted AQ molecule (**TPE-AQ-TPE**) reported in (Chapter 3, Figure 3.3) and hence the emission at 616 nm could be assigned to the ICT from PTZ to AQ. In THF, chloroform and DCM; **AQ1** shows emission maxima

at 516 nm, 522 nm and 530 nm respectively which could be ascribed to the ICT from TPE to **AQ**.<sup>[16]</sup> The molecule **AQ1** also displays shoulder peaks in THF, chloroform and DCM at 705 nm, 672 nm and 710 nm respectively which could be due to the ICT from PTZ to **AQ**. Both the unsymmetrical derivatives **PQ1** and **AQ1** display dual ICT emission occurring from the two respective donor TPE and PTZ. The ICT emission corresponding to PTZ donor has reduced intensity in polar solvents as compared to the TPE corresponding ICT emission as PTZ acts as a strong donor compared to TPE which is a weak donor. The unsymmetrical molecule **PQ2** in toluene has a charge transfer (CT) based emission maximum at 663 nm which in chloroform was red shifted to 747 nm accompanied by a LE based emission at 547 nm. In THF, the emission due to CT state appearing at 734 nm has reduced intensity whereas in DCM the CT based emission was almost quenched and appears as a small hump around 747 nm. Emission in the region of 540-560 nm associated to LE state was observed in THF and DCM for the molecule **PQ2**. A total redshift of 89 nm occurs for **PQ2** on moving from non-polar to polar solvents. The unsymmetrical molecule **AQ2** emits at 624 nm in toluene with shoulder peaks in the region of 450–530 nm ascribed to LE emissions. The emission for **AQ2** was bathochromically shifted to 696 nm and 705 nm in chloroform and THF respectively with shoulder peaks related to LE state in the region of 520–590 nm. In DCM, **AQ2** has a strong LE emission at 524 nm and the CT emission appears as a broad shoulder with reduced intensity. The unsymmetrical quinoxaline derivatives **PQ2** and **AQ2** possess N-PTZ substitution which is assumed to be almost perpendicular to the acceptor moiety which could result in formation of a twisted intramolecular charge transfer (TICT) state resulting in reduced or quenched CT emissions in polar solvents.<sup>[21]</sup> Thus, the N-PTZ unit can act as strong donor and enhance the D-A character but also results in quenched emissions in polar solvents as compared to the C-substituted PTZ unit.

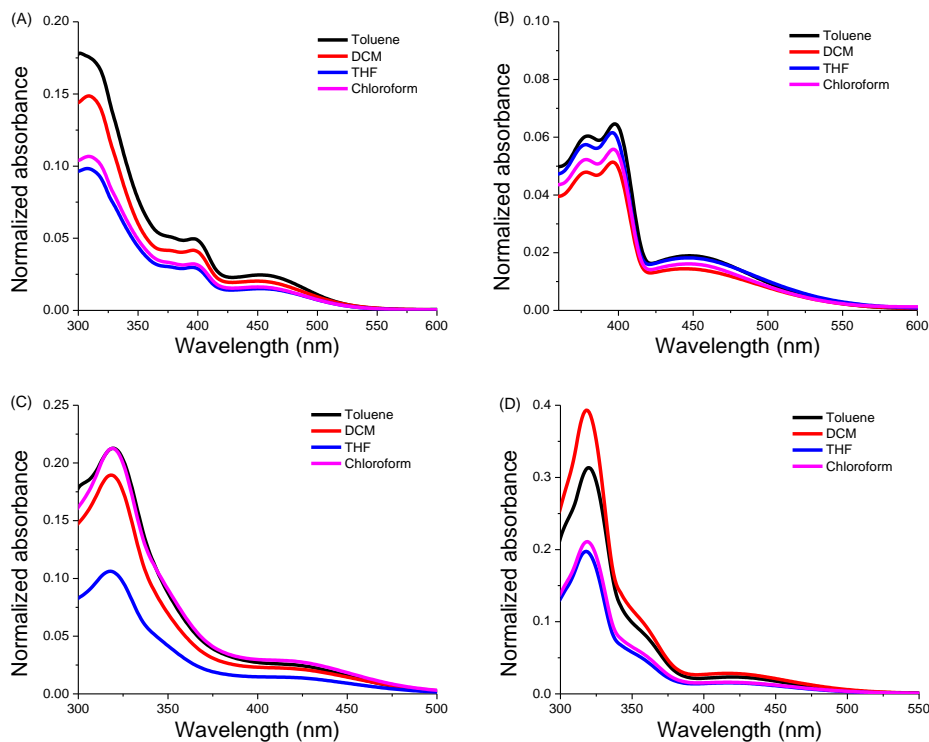


**Figure 4.4.** Electronic absorption spectra of (A) **PQ1**, (B) **PQ2**, (C) **AQ1**, (D) **AQ2** in solvents of different polarity.

The symmetrical quinoxaline derivatives using PTZ donor **PTZ-PQ-PTZ** and **PTZ-AQ-PTZ** reported in (Chapter 3, Figure 3.3) exhibit an increased charge transfer character due inclusion of strong electron donating PTZ unit on both sides as compared to the unsymmetrical quinoxaline derivatives. A polarized excited state is created on charge transfer from donor to acceptor and the reorganization of the solvent dipoles around the polarized excited state results in stabilization of the excited state which lowers the energy of the excited state thereby resulting in a bathochromic shift on increasing the polarity.<sup>[22]</sup> The solvatochromism of the unsymmetrical quinoxaline derivatives was also explored by absorption spectroscopy (Figure 4.4.) which shows negligible changes on varying the solvent polarity concluding that the ground states are less polarized compared to the excited states.<sup>[22]</sup>

The pictures of quinoxaline derivatives in different solvents are given in Figure 4.5.

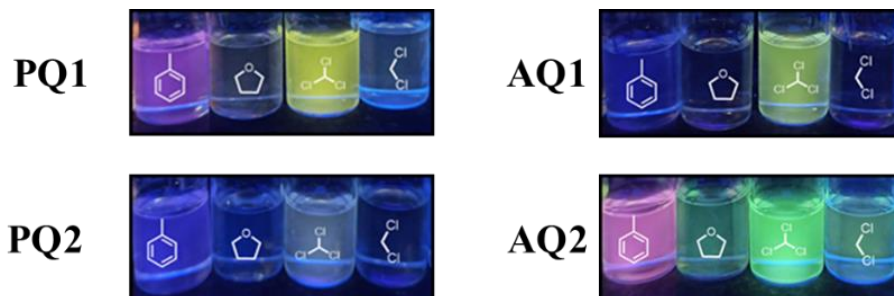


**Figure 4.5.** Photographs of **PQ1**, **PQ2**, **AQ1** and **AQ2** in solvents of different polarity taken under 365nm UV illumination. (From left to right-toluene, THF, chloroform, DCM).

#### 4.6. Aggregation-induced emission studies

The unsymmetrical quinoxaline derivatives incorporate non-planar PTZ and TPE moieties which could endow the D-A-D molecules with twisted geometries resulting in improved emission in the aggregated state. Considering the above aspects, the aggregation-induced emission (AIE) properties of the unsymmetrical quinoxaline derivatives were explored using emission (Figure 4.6.) and absorption spectroscopy (Figure 4.7.). The nanoaggregates were generated by gradual increment of water fraction ( $f_w=0-90\%$ ) in ( $2 \times 10^{-5}$  M) THF solution of the quinoxaline molecules. The addition of water in THF produces nano-aggregates as the quinoxaline molecules are readily soluble in THF but are insoluble in water.

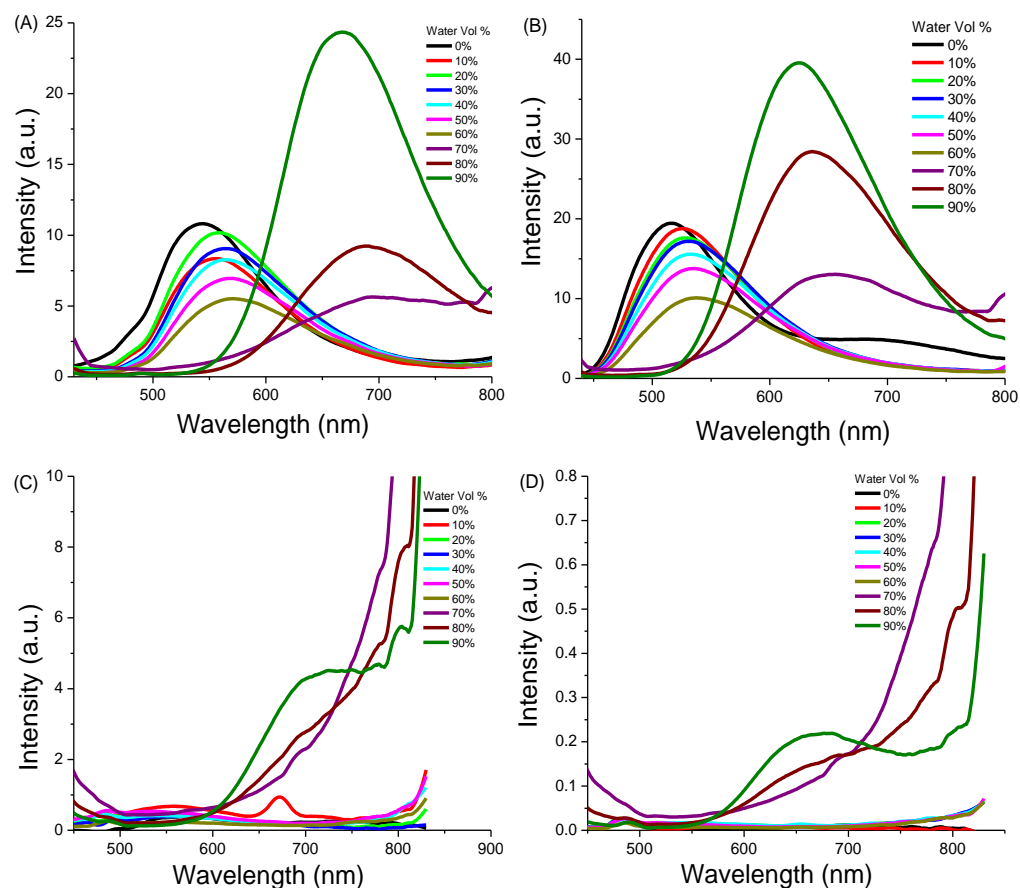


**Figure 4.6.** Emission spectra of (A) **PQ1**, (B), **AQ1**, (C) **PQ2** and (D) **AQ2** in THF-water mixtures with increasing water fractions. (conc.  $2 \times 10^{-5}$  M).

In contrast to the usual AIE behavior, the unsymmetrical TPE based quinoxaline derivatives show emission both in solution and in aggregated state. The molecules **PQ1** and **AQ1** show ICT emission in THF at 543 nm and 514 nm respectively which was red shifted with a drop in intensity on increasing the water percentage upto  $f_w$  60% attributed to the stabilization of the polarized ICT state due to increase in polarity with increasing  $f_w$ . A distinct emission peak was generated at 697 nm and 653 nm for **PQ1** and **AQ1** respectively at  $f_w$  70% owing to the nano-aggregation formation. The emission intensity increases three-fold for **PQ1** and **AQ1** due to aggregation on increasing the water fraction to 90% and the emission maximum was observed at 669 nm and 621 nm respectively. The TPE based unsymmetrical derivatives **PQ1** and **AQ1** exhibit ICT dependent emission

at lower  $f_w$  (0-60%) and at higher  $f_w$  (70-90%) the emission was influenced by the generation of nanoaggregates.<sup>[23]</sup>

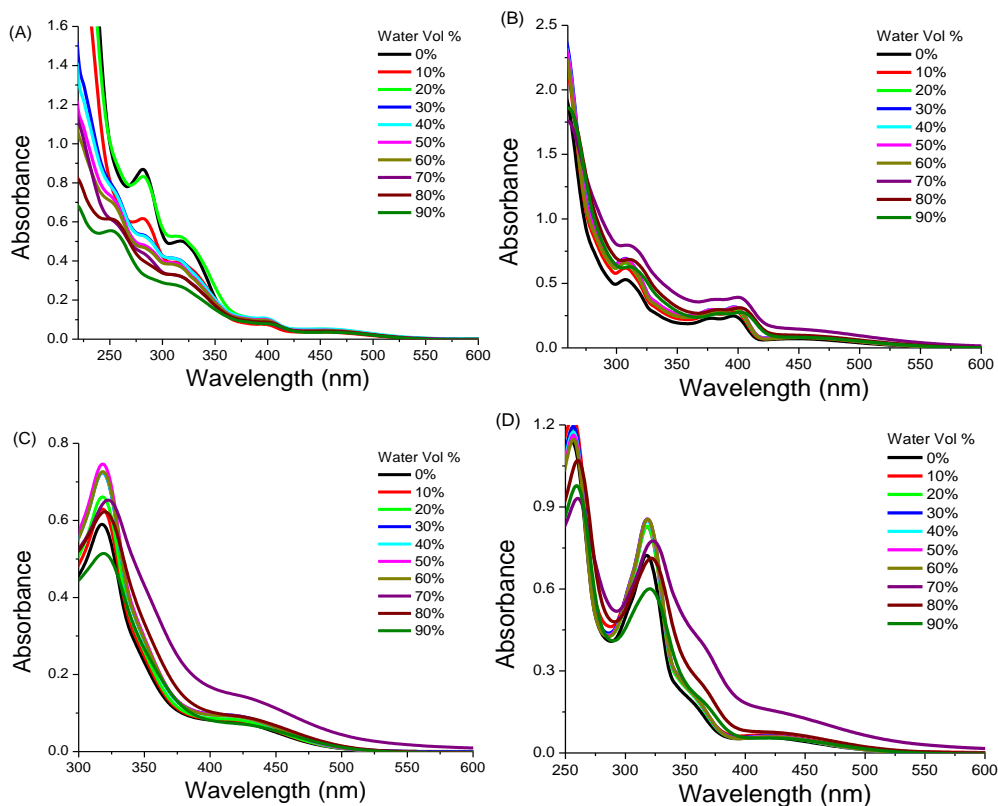


**Figure 4.7.** Electronic absorption spectra of (A) **PQ1**, (B) **PQ2**, (C) **AQ1**, and (D) **AQ2** in different THF-water mixtures with increasing water percentage.

The unsymmetrical molecules **PQ2** and **AQ2** containing N-PTZ are AIE inactive and show no significant emission on aggregation possibly due to the N-substituted PTZ which stays perpendicular to the quinoxaline moiety and could engage in intermolecular  $\pi$ - $\pi$  stacking interactions with other N-PTZ unit in their aggregated state which could result in non-radiative emission. The PTZ donor attached by C-C coupling has lower torsional angle with the quinoxaline unit as compared to N-PTZ and retains its non-

planar butterfly framework which interrupts the  $\pi$ - $\pi$  stacking in the solid state which could allow the molecule to be emissive on aggregation. Hence, the unsymmetrical quinoxaline derivatives **PQ1** and **AQ1** which have the C-substituted PTZ moiety and TPE as donor show significant AIE character compared to **PQ2** and **AQ2** which are AIE inactive due to the dominant effect of N-PTZ donor. The absorption spectra of the quinoxaline derivatives display Mie scattering effect due to aggregates present in the solution above  $f_w$  60%.<sup>[23]</sup> The pictures of the THF-water mixtures of the quinoxaline molecules are given in Figure 4.8.

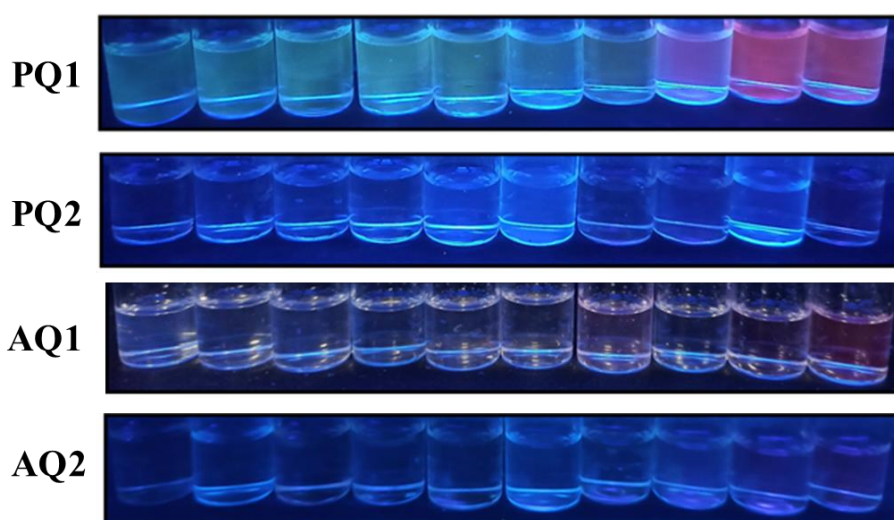


**Figure 4.8.** Photographs of **PQ1**, **PQ2**, **AQ1**, and **AQ2** in different THF-water mixtures taken under 365nm UV illumination. (From left to right-0%-90% water volume fraction.)

#### 4.7. Mechanochromism

The D-A-D **PQ** and **AQ** quinoxaline molecules exploit typical AIEgens PTZ and TPE as donors and possess twisted structures which enables these molecules with efficient solid-state emission which is sensitive to mechanical stimuli. Taking into consideration the following aspects, the mechanochromic properties of **PQ** and **AQ** quinoxaline derivatives were investigated by grinding the powders of the synthesized molecules in a

mortar-pestle and the response was recorded using emission spectroscopy (Figure 4.9.–Figure 4.11.).

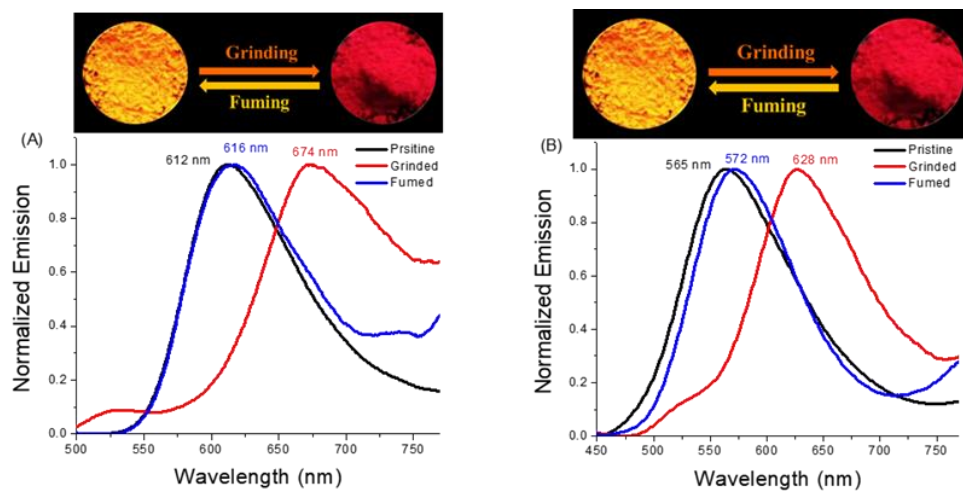


**Figure 4.9.** Solid-state emission spectra of the pristine, grinded and fumed forms of (A) **PQ1** and (B) **AQ1**. ( $\lambda_{exc}=420$  nm).

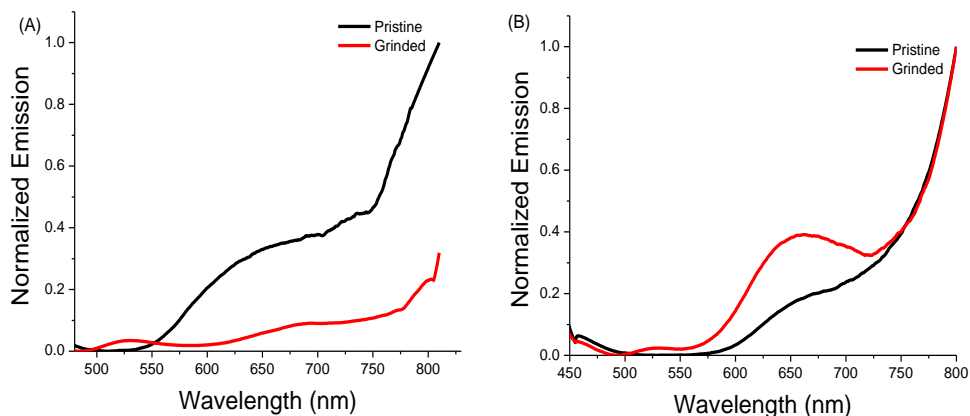


**Figure 4.10.** Solid-state emission spectra of pristine and grinded forms of (A) **PQ2** and (B) **AQ2**. ( $\lambda_{exc}=420$  nm).

The TPE based unsymmetrical derivative **PQ1** in its pristine state has a bright orange emission at 612 nm which on grinding bathochromically shifts to 674 nm and appears as a red powder. The fumigation of grinded solid of **PQ1** with DCM-Hexane (1:1) (3 minutes) allows it to return to its

pristine state emitting at 616 nm. The pristine solid of TPE based unsymmetrical derivate **AQ1** exhibits yellow emission at 565 nm which on grinding displays orange emission at 628 nm. The grinded solid of **AQ1** requires longer fuming time up to 15 minutes and reverts to its original state with an emission at 572 nm having a difference of 8 nm as compared to the pristine form. The molecule **AQ1** does not completely revert to its pristine form on fuming and hence has a lower reversibility on fuming as compared to the other quinoxaline molecules. The spectral shifted induced by grinding in **PQ1** and **AQ1** is 62 nm and 63 nm respectively which is high in comparison to other reported mechanochromic materials. The emission of **PQ** derivatives is red shifted than **AQ** derivatives suggesting higher degree of conjugation in phenanthrene ring as compared to acenaphthene ring.

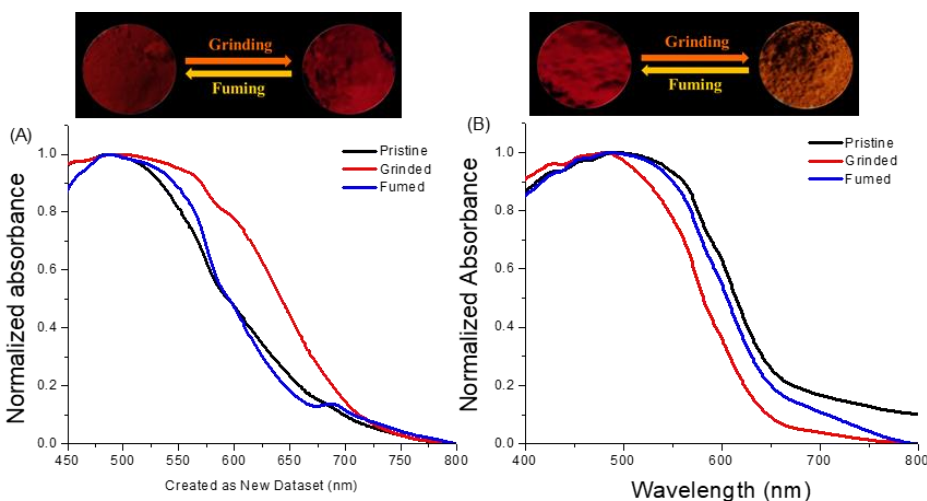


**Figure 4.11.** Solid-state absorption spectra of (A) **PQ2** and (B) **AQ2** in its pristine, grinded and fumed forms.

In contrast to the PTZ-TPE substituted unsymmetrical quinoxaline derivatives, the N-PTZ substituted quinoxaline derivatives **PQ2** and **AQ2** have quenched emissions in the solid state due to the perpendicular lying N-PTZ unit (Figure 4.10.) which was also confirmed by their AIE studies. The molecules **PQ2** and **AQ2** are completely non-emissive in their pristine form; although the grinding of pristine powders shows visual color change that can be easily observed with naked eye and returns to its original color

on fuming. The solid-state absorption spectra of the pristine, grinded and fumed solids were recorded to further confirm the mechanochromic behavior of the non-emissive **PQ2** and **AQ2** molecules (Figure 4.11.). The orange pristine powder of **PQ2** exhibits an absorption band around 520 nm which on grinding displays a red shift in the absorption band around to 560 nm and possesses a deep red color. The fumed solid of **PQ2** shows absorption around 518 nm similar to the pristine powder. Surprisingly, the orange color pristine powder of **AQ2** with absorption band around 545 nm on grinding gets converted to a yellow powder and shows a hypsochromically shifted absorption band at 488 nm. On fuming, the grinded solid of **AQ2** shows absorption band around 539 nm which was close to the absorption of the pristine powder. The emissions of molecules **PQ2** and **AQ2** were quenched in the solid state possibly be due to the planarity of N-PTZ unit which could result in  $\pi$ - $\pi$  stacking increasing the possibility of non-radiative decay of the excited state. However, the molecules **PQ2** and **AQ2** also possess C-substituted PTZ as donor on one side which has a unique non-planar butterfly architecture which could change its confirmation on grinding thereby displaying reversible color change.

#### **4.8. Powder X-ray diffraction studies.**

The mechanochromic behavior in the quinoxaline derivatives was expected to be arising from physical structure alterations which was examined by powder X-ray diffraction (PXRD) technique (Figure 4.12.). Sharp peaks depicting crystalline nature are detected for the pristine powders of **PQ1** and **AQ1**. The sharp peaks are diminished to a certain extent on grinding the powders of **PQ1** and **AQ1** and a broad diffused pattern was observed for the grinded solids which proves their amorphous nature. The crystalline peaks are completely regained for **PQ1** and **AQ1** on fumigation validating the reversible nature of the stimuli-responsive molecules. The crystalline peaks for **AQ1** were somewhat recovered on fuming similar to its emission

profile which was not fully reversed on fumigation. This shows that **AQ1** has lower reversibility from grinded to pristine form on fuming as compared to the other molecules.

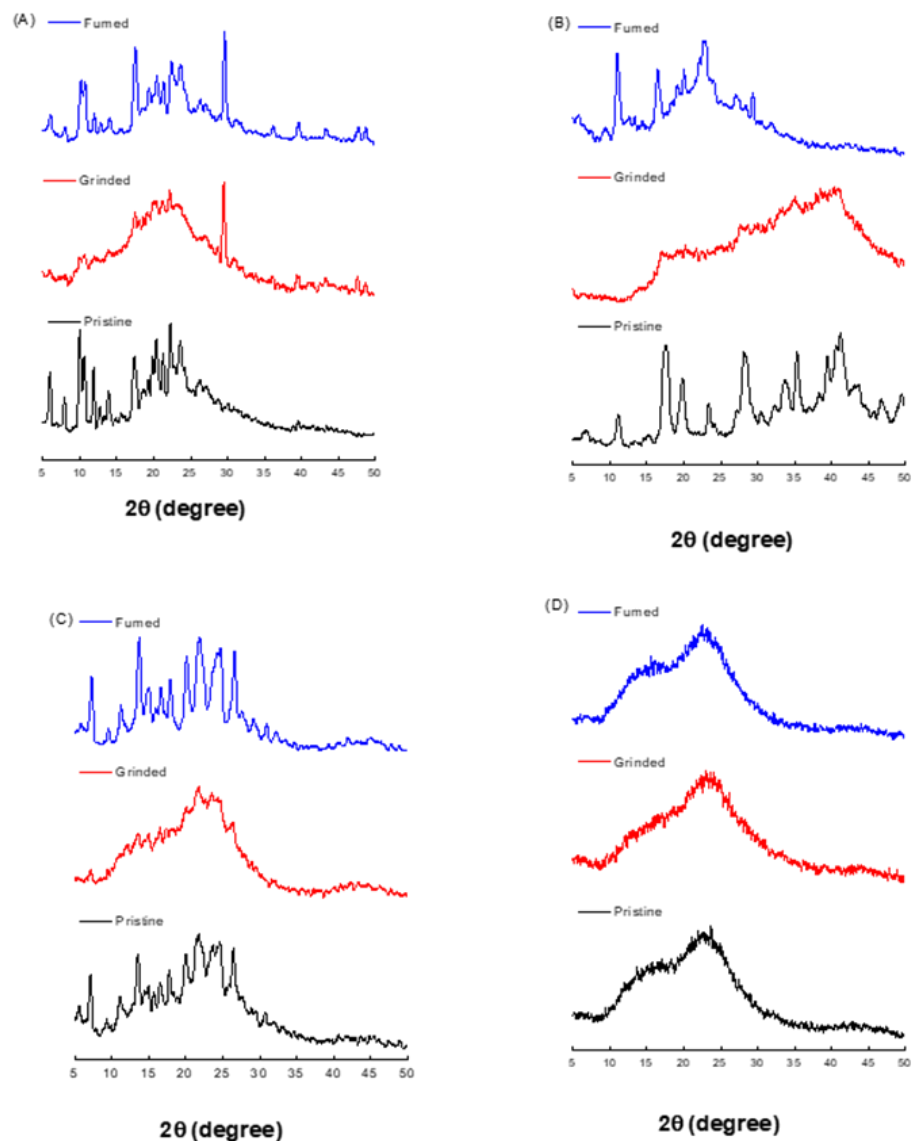


**Figure 4.12.** PXRD patterns of pristine, grinded and fumed solids of (A) **PQ1**, (B) **PQ2**, (C) **AQ1** and (D) **AQ2**.

The quinoxaline derivative **AQ2** exhibits amorphous nature with broad diffused bands in all the three forms pristine, grinded and fumed. It can be

thus concluded that the color change on grinding is associated with a morphological transformation from crystalline to amorphous state.

## 4.9. Experimental section

### General methods

Chemicals were used as received unless otherwise indicated. All oxygen or moisture sensitive reactions were performed under a nitrogen/argon atmosphere.  $^1\text{H}$  NMR (400 MHz) and  $^{13}\text{C}$  NMR (100 MHz) spectra were recorded on a Bruker Avance III instrument by using  $\text{CDCl}_3$ .  $^1\text{H}$  NMR chemical shifts are reported in parts per million (ppm) relative to the solvent residual peak ( $\text{CDCl}_3$ , 7.26 ppm). Multiplicities are given as s (singlet), d (doublet), t (triplet) and m (multiplet), and the coupling constants,  $J$ , are given in hertz.  $^{13}\text{C}$  NMR chemical shifts are reported relative to the solvent residual peak ( $\text{CDCl}_3$ , 77.0 ppm). UV-visible absorption spectra were recorded on a PerkinElmer Lambda 35 UV-visible spectrophotometer. Emission spectra were recorded using a Fluoromax-4C, S/n.1579D-1417-FM fluorescence software Ver 3.8.0.60. The relative quantum yields in solution were calculated using Rhodamine 6G in ethanol solution as a standard. The excitation and emission slits were 2/2 nm for the emission measurements. All the measurements were done at 25 °C. HRMS were recorded on a Bruker-Daltonics micrOTOF-Q II mass spectrometer. The PXRD studies were done using powdered samples on a Rigaku SmartLab automated multipurpose X-ray diffractometer, equipped with a high-accuracy theta-theta goniometer featuring a horizontal sample mount.

### Synthesis and Characterization of PQBr

A mixture of **1** (1.0 mmol) and 10-propyl-3-(4,4,5,5-tetramethyl-1,3,2-dioxaborolan-2-yl)-10H-phenothiazine (**PTZ-Bpin**) was dissolved in THF/water (4/1 v/v) and then Sodium carbonate (3.3 mmol) was added. After degassing the reaction mixture for 10 min,  $\text{Pd}(\text{PPh}_3)_4$  (0.1 mmol) was added and the reaction mixture was heated to reflux for 16 h under a nitrogen

atmosphere. The reaction mixture was cooled to room temperature and then worked up with dichloromethane. The organic layer was dried over anhydrous sodium sulphate and solvent was evaporated. The residue was purified by silica-gel column chromatography using hexane/dichloromethane (60:40) as the eluent. An orange solid of PQBr was obtained in 52% yield. ;  $^1\text{H}$  NMR( 400 MHz,  $\text{CDCl}_3$ ,  $25^\circ\text{C}$ ):  $\delta$  9.53 (d,  $J = 8$  Hz, 1H), 9.14 (d,  $J = 8$  Hz, 1H), 8.57 (d,  $J = 8$  Hz, 2H), 8.21 (d,  $J = 8$  Hz, 1H), 7.85-7.78 (m, 4H), 7.75-7.69 (m, 3H), 7.21-7.19 (m, 2H), 7.08 (d,  $J = 8$  Hz, 1H), 7.00-6.94 (m, 2H), 3.96 (t,  $J = 16$  Hz, 2H), 2.01-1.92 (m, 2H), 1.10 (t,  $J = 8$  Hz, 3H);  $^{13}\text{C}$  NMR (100 MHz,  $\text{CDCl}_3$ ,  $25^\circ\text{C}$ ):  $\delta$  147.6, 145.0, 135.4, 132.8, 132.3, 132.2, 131.9, 130.8, 130.7, 130.5, 130.0, 130.0, 129.9, 129.8, 128.9, 128.2, 128.1, 127.6, 127.6, 127.5, 127.2, 126.9, 126.8, 123.0, 122.8, 122.5, 115.4, 114.8, 49.3, 30.2, 20.2, 11.4. HRMS (ESI): Calcd. for  $[\text{M}]^+$ : 597.0869. Found: 597.0862.

### Synthesis and Characterization of AQBr

A mixture of **2** (1.0 mmol) and 10-propyl-3-(4,4,5,5-tetramethyl-1,3,2-dioxaborolan-2-yl)-10H-phenothiazine (**PTZ-Bpin**) (1 mmol) was dissolved in THF/ water (4/1 v/v) and Sodium carbonate (3.3 mmol) was added. After degassing the reaction mixture for 10min,  $\text{Pd}(\text{PPh}_3)_4$  ( 0.1 mmol) was added and the reaction mixture was heated to reflux for 16 h under a nitrogen atmosphere. The reaction mixture was cooled to room temperature and worked up with dichloromethane. The organic layer was dried over anhydrous sodium sulphate and solvent was evaporated. The residue was purified by silica-gel column chromatography using hexane/dichloromethane (75:25) as the eluent. An orange solid of AQBr was obtained in 47% yield;  $^1\text{H}$  NMR (500 MHz,  $\text{CDCl}_3$ ,  $25^\circ\text{C}$ ):  $\delta$  8.58-8.55 (m, 1H), 8.36-8.33 (m, 1H), 8.19-8.08 (m, 3H), 7.93-7.86 (m, 1H), 7.84-7.80 (m, 1H), 7.63-7.61 (m, 3H), 7.19 (d,  $J = 5$  Hz, 2H), 7.04 (d,  $J = 5$  Hz, 1H), 6.93 (d,  $J = 5$  Hz, 2H), 3.95-3.91 (m, 2H), 1.98-1.91 (m, 2H), 1.09 (t,  $J = 7.5$  Hz, 3H);  $^{13}\text{C}$  NMR (100 MHz,  $\text{CDCl}_3$ ,  $25^\circ\text{C}$ ):  $\delta$  145.0, 140.0,

139.2, 136.9, 136.6, 132.5, 131.5, 131.5, 130.2, 130.1, 130.0, 129.9, 129.8, 129.6, 129.4, 128.7, 128.6, 128.5, 127.5, 127.2, 124.4, 123.5, 123.3, 122.8, 122.6, 122.4, 115.4, 114.7, 49.2, 20.2, 11.4. HRMS (ESI): Calcd. for [M + H]<sup>+</sup>: 573.0696. Found: 573.0738.

### Synthesis and Characterization of PQ1

A mixture of **PQBr** (1.0 mmol) and 4,4,5,5-tetramethyl-2-(4-(1,2,2-triphenylvinyl)phenyl)-1,3,2-dioxaborolane (**TPE-Bpin**) (1.1 mmol) was dissolved in THF/ water (4/1 v/v) and then Sodium carbonate (3.3 mmol) was added. After degassing the reaction mixture for 10 min, Pd(PPh<sub>3</sub>)<sub>4</sub> (0.1 mmol) was added and the reaction mixture was heated to reflux for 16 h under a nitrogen atmosphere. The reaction mixture was cooled to room temperature and worked up with dichloromethane. The organic layer was dried over anhydrous sodium sulphate and solvent was evaporated. The residue was purified by silica-gel column chromatography using hexane/dichloromethane (60:40) as the eluent. An orange solid of PQ1 was obtained in 76% yield. ; <sup>1</sup>H NMR (500 MHz, CDCl<sub>3</sub>, 25<sup>o</sup>C): δ 9.18 (d, *J* = 5 Hz, 1H), 8.97 (d, *J* = 10 Hz, 1H), 8.56 (d, *J* = 5 Hz, 2H), 7.93 (s, 2H), 7.85 (s, 1H), 7.81-7.68 (m, 8H), 7.28 (s, 1H), 7.23-7.13 (m, 19H), 6.95 (s, 1H), 4.00- 3.96 (m, 2H), 2.02-1.91 (m, 2H), 1.11 (t, *J* = 7.5 Hz, 3H); <sup>13</sup>C NMR (100 MHz, CDCl<sub>3</sub>, 25<sup>o</sup> C) : δ 145.1, 144.7, 143.9, 143.8, 142.9, 141.2, 141.1, 140.1, 139.9, 139.2, 138.4, 136.6, 132.7, 132.2, 132.1, 131.6, 131.5, 131.4, 131.0, 130.6, 130.5, 130.4, 130.1, 130.1, 129.6, 128.0, 127.7, 127.6, 127.2, 126.7, 126.5, 126.5, 126.4, 124.7, 124.2, 122.8, 122.4, 115.4, 114.8, 49.3, 20.2, 11.4. HRMS (ESI): Calcd. for [M + K]<sup>+</sup>: 888.2809. Found: 888.2836.

### Synthesis and Characterization of AQ1

A mixture of **AQBr** (1.0 mmol) and 4,4,5,5-tetramethyl-2-(4-(1,2,2-triphenylvinyl)phenyl)-1,3,2-dioxaborolane (**TPE-Bpin**) (1.1 mmol) was dissolved in THF/ water (4/1 v/v) and Sodium carbonate (3.3 mmol) was added. After degassing the reaction mixture for 10 min, Pd(PPh<sub>3</sub>)<sub>4</sub> ( 0.1 mmol) was added and reaction mixture was heated to reflux for 16 h under a nitrogen atmosphere. The reaction mixture was cooled to room temperature and worked up with dichloromethane. The organic layer was dried over anhydrous sodium sulphate and solvent was evaporated. The residue was purified by silica-gel column chromatography using hexane/dichloromethane (60:40) as the eluent. A yellow solid of AQ1 was obtained in 54 % yield ; <sup>1</sup>H NMR (500 MHz, CDCl<sub>3</sub>, 25<sup>o</sup>C): δ 8.35-8.33 (m, 1H), 8.25-8.23 (m, 1H), 8.09-8.06 ( m, 2H), 7.83-7.77 (m, 4H), 7.70 (d, *J* = 5 Hz, 2H), 7.65 (d, *J* = 10 Hz, 2H), 7.23-7.10 (m, 19H), 7.05 (d, *J* = 5 Hz, 1H), 6.96-6.92 (m, 2H), 3.94 (t, *J* = 5 Hz, 2H), 1.99-1.92 (m, 2H), 1.09 (t, *J* = 7.5 Hz, 3H) ); <sup>13</sup>C NMR (125 MHz, CDCl<sub>3</sub>, 25<sup>o</sup> C) : δ 153.0, 152.9, 145.1, 144.7, 143.9, 143.9, 143.8, 142.6, 141.1, 140.9, 139.8, 139.2, 139.1, 139.0, 136.8, 136.7, 133.0, 132.2, 132.2, 131.6, 131.5, 131.4, 130.9, 130.4, 130.1, 129.8, 129.2, 128.5, 128.4, 127.8, 127.6, 127.6, 127.5, 127.1, 126.4, 126.3, 124.8, 124.1, 122.3, 122.2, 121.9, 115.3, 114.7, 49.2, 20.2, 11.4. HRMS (ESI): Calcd. for [M ]<sup>+</sup>: 823.3016. Found: 823.3116.

### Synthesis and Characterization of PQ2

To a X mL round-bottom flask, **PQBr** (1 mmol) and **PTZ** (1 mmol) was dissolved in dry toluene(40 ml) and sodium tert-butoxide (0.1 mmol) was added. After degassing the reaction mixture for 10 min, Ph(t-Bu)<sub>3</sub> (0.05 mmol) and Pd(OAc)<sub>2</sub> (0.02 mmol) were added. The reaction mixture was heated to refluxed for 16 h under nitrogen atmosphere. After completion of the reaction, the reaction mixture was allowed to cool to room temperature and the solution was filtered to remove insoluble solids. The filtrate was concentrated in vacuum and purified by silica gel column chromatography by using hexane: dichloromethane (55:45) as eluent. A Orange solid of PQ2

was obtained in 61 % yield;  $^1\text{H}$  NMR (500 MHz,  $\text{CDCl}_3$ ,  $25^\circ\text{C}$ ):  $\delta$  9.18 (d,  $J=10$  Hz, 1H), 9.12 (d,  $J = 10$  Hz, 1H), 8.53 (d,  $J = 10$  Hz, 1H), 8.49 (d,  $J = 10$  Hz, 1H), 8.09-8.04 (m, 2H), 7.90 (d,  $J = 2$  Hz, 1H), 7.86-7.83 (m, 1H), 7.82-7.76 (m, 2H), 7.74-7.69 (m, 2H), 7.59 (t,  $J = 7.5$  Hz, 1H), 7.23-7.20 (m, 2H), 7.14-7.09 (m, 3H), 6.99-6.94 (m, 2H), 6.77 (t,  $J = 7.5$  Hz, 2H), 6.71-6.68 (m, 2H), 6.16 (d,  $J = 10$  Hz, 2H), 3.98 (t,  $J = 7.5$  Hz, 2H), (m, 2H), 1.12 (t,  $J = 7.5$  Hz, 3H);  $^{13}\text{C}$  NMR (125 MHz,  $\text{CDCl}_3$ ,  $25^\circ\text{C}$ ) :  $\delta$  145.1, 144.9, 144.7, 142.1, 142.0, 141.0, 140.5, 140.0, 137.7, , 130.0, 130.1, 130.1, 130.2, 130.2, 130.4, 130.5, 132.1, 132.2, 132.3, 132.9 , 126.7, 127.0, 127.2, 127.2, 127.5, 128.0, 128.0, 128.1, 129.0, 129.1, 129.6 , 120.5, 122.2, 122.4, 122.5, 122.2, 122.8, 122.9, 124.3, 124.6, 126.2, 126.5 : HRMS (ESI). , 11.4, 20.2, 49.3, 77.2, 114.7, 114.8, 115.4, 115.5, 116.5 . Calcd. for  $[\text{M}]^+$ : 716.2063. Found: 716.2091

### Synthesis and Characterization of AQ2

To a X mL round-bottom flask, **AQBr** (1 mmol) and **PTZ** (1 mmol) was dissolved in dry toluene and sodium tert-butoxide (5 mmol) was added. After degassing the reaction mixture for 10 min  $\text{Ph}(\text{t-Bu})_3$  (0.1 mmol) and  $\text{Pd}(\text{OAc})_2$  (0.2 mmol) were added. The reaction mixture was refluxed for 16 h under nitrogen atmosphere. After completion of the reaction, the reaction mixture was allowed to cool to room temperature and the solution was filtered to remove insoluble solids. The filtrate was concentrated in vacuum and purified by silica gel column chromatography by using hexane:dichloromethane (50:50) as eluent. A Orange solid of AQ2 was obtained in 67% yield.  $^1\text{H}$  NMR (500 MHz,  $\text{CDCl}_3$ ,  $25^\circ\text{C}$ ):  $\delta$  8.37 (d,  $J = 8$  Hz, 1H), 8.33-8.28 (m, 1H), 8.07 (t,  $J = 8$  Hz, 3H), 7.92 (s, 1H), 7.83-7.75 (m, 3H), 7.21 (d,  $J = 4$  Hz, 1H), 7.09-7.04 (m, 3H), 6.95 (s, 2H), 6.81-6.71 (m, 5H), 6.15 (d,  $J = 8$  Hz, 1H), 6.09 (d,  $J = 4$  Hz, 1H), 3.96 (t,  $J =$  Hz, 2H), 2.00-1.94 (m, 2H), 1.11 (t,  $J = 8$  Hz, 3H);  $^{13}\text{C}$  NMR (100 MHz,  $\text{CDCl}_3$ ,  $25^\circ\text{C}$ ) :  $\delta$  154.0, 153.8, 145.1, 145.0, 144.5, 144.4, 141.5, 141.2, 140.3, 140.2, 138.3, 136.9, 133.2, 132.4, 132.0, 131.8, 131.7, 130.2, 129.5, 128.5,

128.4, 127.5, 127.2, 126.7, 126.3, 124.7, 124.3, 123.0, 122.4, 122.1, 120.8, 120.2, 116.5, 115.4, 114.8, 49.3, 20.2, 11.4. HRMS (ESI): Calcd. for [M]<sup>+</sup>: 690.1906. Found: 690.1923.

#### 4.10. Conclusion

In this contribution, we have designed and synthesized a series of D-A-D'/D-A'-D' quinoxaline derivatives with two types of fused quinoxaline namely phenanthrene-quinoxaline (PQ) and acenaphthene-quinoxaline (AQ) as acceptors A and A' respectively. The D-A-D'/D-A'-D' quinoxaline derivatives were substituted with three different donors namely phenothiazine (PTZ), tetraphenylethylene (TPE) and N-substituted PTZ in an unsymmetrical fashion. The unsymmetrical derivatives **PQ1** and **AQ1** comprise of strong donor PTZ (D) in combination with weak donor TPE (D') whereas **PQ2** and **AQ2** contain C-substituted PTZ as donor (D) one side and N-substituted PTZ as donor (D'') on the other side. The PQ and AQ quinoxaline derivatives exhibit contrasting photophysical properties due to the unsymmetrical substitution of different donors which majorly affects the D-A character, structural geometries and intermolecular interactions in the solid state. The unsymmetrical derivative **PQ1** and **AQ1** having donors PTZ and TPE exhibit intense ICT emissions originating from both the TPE and PTZ donors which are highly solvent-dependent. The ICT emission corresponding to PTZ donor in **PQ1** and **AQ1** exhibit reduced intensity in polar solvents as compared to the TPE corresponding ICT emission due to the stronger donating ability of PTZ in comparison to TPE which could generate highly polarized ICT state. In contrast, the unsymmetrical quinoxaline derivatives **AQ2** and **PQ2** having N-PTZ substitution along with PTZ display reduced or quenched CT emissions in polar solvents owing to the formation of a twisted intramolecular charge transfer (TICT) state originating from the almost perpendicular positioned N-PTZ unit. The presence of AIEgens PTZ and TPE in **PQ1** and **AQ1** endow the derivatives with intense emission in the aggregated state; however the unsymmetrical

derivatives **PQ2** and **AQ2** display quenching of emission in their aggregated state. The derivative **PQ1** and **AQ1** display reversible emission switching on grinding with very high grinding induced spectral shift making them suitable stimuli-responsive materials and the mechanochromic performance is related to crystalline to amorphous phase change. The derivatives **PQ2** and **AQ2** also exhibit grinding induced color-switching which is validated using solid-state absorption spectroscopy owing to their non-fluorescent pristine solids. To summarize, the donors PTZ and TPE are favorable in developing AIE active stimuli-responsive materials as compared to N-PTZ donor. The current work gives a detailed analysis of utilizing donors with different strengths in unsymmetrical fashion with heterocyclic  $\pi$ -conjugated acceptor unit and its effect on the photophysical and electronic properties, solid-state emission and stimuli-responsive properties. This contribution provides insights on choosing suitable donor and acceptor units and their proper positioning to further produce effective donor-acceptor based AIE and mechanochromic systems.

#### 4.11. References

- [1](a) Feng, J., Tian, K., Hu, D., Wang, S., Li, S., Zeng, Y., Li, Y., Yang, G. (2011). A Triarylboron-Based Fluorescent Thermometer: Sensitive Over a Wide Temperature Range, *Angew. Chem. Int. Ed.*, 123(35), 8222-8226 (DOI: <https://doi.org/10.1002/ange.201102390>); (b) Wu, D., Sedgwick, A. C., Gunnlaugsson, T., Akkaya, E. U., Yoon, J., James, T. D. (2017), Fluorescent chemosensors: the past, present and future, *Chem. Soc. Rev.*, 46(23), 7105-7123 (DOI: 10.1039/C7CS00240H); (c) Nakanotani, H., Higuchi, T., Furukawa, T., Masui, K., Morimoto, K., Numata, M., Tanaka, H., Sagara, Y., Yasuda, T., Adachi, C. (2014). High-efficiency organic light-emitting diodes with fluorescent emitters, *Nat. Commun.*, 5(1), 1-7 (DOI: 10.1038/ncomms5016); (d) Gierschner, J., Varghese, S., Park, S. Y. (2016), Organic single crystal lasers: A materials

view, *Adv. Opt. Mater.*, 4(3), 348-364 (DOI : <https://doi.org/10.1002/adom.201500531>); (e) Kuehne, A. J., Gather, M. C, (2016), Organic lasers: recent developments on materials, device geometries, and fabrication techniques, *Chem. Rev.*, 116(21), 12823-12864 (DOI: <https://doi.org/10.1021/acs.chemrev.6b00172>); (f) Li, Z., Askim, J. R., Suslick, K. S. (2018), The optoelectronic nose: colorimetric and fluorometric sensor arrays. *Chem. Rev.*, 119(1), 231-292 (DOI: <https://doi.org/10.1021/acs.chemrev.8b00226>); (g) Wu, D., Chen, L., Lee, W., Ko, G., Yin, J., Yoon, J. (2018), Recent progress in the development of organic dye based near-infrared fluorescence probes for metal ions, *Coord. Chem. Rev.*, 354, 74-97 (DOI: <https://doi.org/10.1016/j.ccr.2017.06.011>); (h) Sun, W., Guo, S., Hu, C., Fan, J., Peng, X. (2016), Recent development of chemosensors based on cyanine platforms, *Chem. Rev.*, 116(14), 7768-7817 (DOI: <https://doi.org/10.1021/acs.chemrev.6b00001>); (i) Wu, X., Zhu, W. (2015), Stability enhancement of fluorophores for lighting up practical application in bioimaging, *Chem. Soc. Rev.*, 44(13), 4179-4184 (DOI: [10.1039/C4CS00152D](https://doi.org/10.1039/C4CS00152D)); (j) Chen, X., Yang, Z., Li, W., Mao, Z., Zhao, J., Zhang, Y., Wu, Y., -C., Jiao, S., Liu, Y., Chi, Z. (2019), Nondoped red fluorophores with hybridized local and charge-transfer state for high-performance fluorescent white organic light-emitting diodes, *ACS Appl. Mater. Interfaces*, 11(42), 39026-39034 (DOI: <https://doi.org/10.1021/acsami.9b15278>); (k) Liu, Y., Li, C., Ren, Z., Yan, S., Bryce, M. R. (2018), All-organic thermally activated delayed fluorescence materials for organic light-emitting diodes, *Nat Rev Mater*, 3(4), 1-20 (DOI: <https://doi.org/10.1038/natrevmats.2018.20>); (l) Komori, T., Nakanotani, H., Yasuda, T., Adachi, C. (2014), Light-emitting organic field-effect transistors based on highly luminescent single crystals of thiophene/phenylene co-oligomers, *J. Mater. Chem. C*, 2(25), 4918-4921 (DOI: [10.1039/C4TC00164H](https://doi.org/10.1039/C4TC00164H)).

- [2] (a) Hirata, S., Watanabe, T. (2006), Reversible thermoresponsive recording of fluorescent images (TRF), *Adv. Mater.*, 18(20), 2725-2729 (DOI: <https://doi.org/10.1002/adma.200600209>); (b) Sagara, Y., Mutai, T., Yoshikawa, I., Araki, K. (2007), Material design for piezochromic luminescence: hydrogen-bond-directed assemblies of a pyrene derivative, *J. Am. Chem. Soc.*, 129(6), 1520-1521 (DOI: <https://doi.org/10.1021/ja0677362>); (c) Woodward, A. N., Kolesar, J. M., Hall, S. R., Saleh, N. A., Jones, D. S., Walter, M. G. (2017), Thiazolothiazole fluorophores exhibiting strong fluorescence and viologen-like reversible electrochromism. *J. Am. Chem. Soc.*, 139(25), 8467-8473 (DOI: <https://doi.org/10.1021/jacs.7b01005>); (d) Tang, J. H., Sun, Y., Gong, Z. L., Li, Z. Y., Zhou, Z., Wang, H., Li, X., Saha, M. L., Zhong, Y. W., Stang, P. J. (2018), Temperature-responsive fluorescent organoplatinum (II) metallacycles, *J. Am. Chem. Soc.*, 140(24), 7723–7729 (DOI: <https://doi.org/10.1021/jacs.8b04452>); (e) Zhou, X., Wang, L., Wei, Z., Weng, G., He, J. (2019), An Adaptable Tough Elastomer with Moisture-Triggered Switchable Mechanical and Fluorescent Properties, *Adv. Funct. Mater.*, 29(34), 1903543 (DOI: <https://doi.org/10.1002/adfm.201903543>); (f) Li, Z., Liu, P., Ji, X., Gong, J., Hu, Y., Wu, W., Wang, X., Peng, H, Q., T, Ryan., Kwok, K., La, J, W, Y., Lu, J., Tang, B. Z. (2020), Bioinspired simultaneous changes in fluorescence color, brightness, and shape of hydrogels enabled by AIEgens, *Adv. Mater.*, 32(11), 1906493 (DOI: <https://doi.org/10.1002/adma.201906493>); (g) Xiong, J., Wang, K., Yao, Z., Zou, B., Xu, J., Bu, X. H. (2018), Multi-stimuli-responsive fluorescence switching from a pyridine-functionalized tetraphenylethene AIEgen, *ACS Appl. Mater. Interfaces*, 10(6), 5819-5827 (DOI: <https://doi.org/10.1021/acsami.7b18718>).
- [3] (a) Sagara, Y., Kato, T., (2009), Mechanically induced luminescence changes in molecular assemblies, *Nat. Chem*, 1, 605-610 (DOI: <https://doi.org/10.1038/nchem.411>); (b) Chi, Z., Zhang, X., Xu, B.,

Zhou, X., Ma, C., Zhang, Y., Liu, S., Xu, J. (2012), Recent advances in organic mechanofluorochromic materials, *Chem. Soc. Rev.*, *41*(10), 3878-3896 (DOI: 10.1039/C2CS35016E); (c) Crenshaw, B. R., Burnworth, M., Khariwala, D., Hiltner, A., Mather, P. T., Simha, R., Weder, C. (2007), Deformation-induced color changes in mechanochromic polyethylene blends, *Macromolecules*, *40*(7), 2400-2408 (DOI: <https://doi.org/10.1021/ma062936j>); (d) Sagara, Y., Yamane, S., Mitani, M., Weder, C., Kato, T. (2016). Mechanoresponsive luminescent molecular assemblies: an emerging class of materials, *Adv. Mater.*, *28*(6), 1073-1095 (DOI: <https://doi.org/10.1002/adma.201502589>); (e) Xue, P., Ding, J., Wang, P., Lu, R. (2016), Recent progress in the mechanochromism of phosphorescent organic molecules and metal complexes, *J. Mater. Chem. C*, *4*(28), 6688-6706 (DOI: 10.1039/C6TC01503D); (f) Ciardelli, F., Ruggeri, G., Pucci, A. (2013), Dye-containing polymers: methods for preparation of mechanochromic materials, *Chem. Soc. Rev.* *42*(3), 857-870 (DOI: 10.1039/C2CS35414D); (g) Nagura, K., Saito, S., Yusa, H., Yamawaki, H., Fujihisa, H., Sato, H., Shimoikeda, Y., Yamaguchi, S. (2013), Distinct responses to mechanical grinding and hydrostatic pressure in luminescent chromism of tetrathiazolylthiophene, *J. Am. Chem. Soc.*, *135*(28), 10322-10325 (DOI: <https://doi.org/10.1021/ja4055228>); (h) Xu, J., Chi, Z. (Eds.). (2014). Mechanochromic Fluorescent Materials: Phenomena, Materials and Applications, *Royal Society of Chemistry*; (i) Ito, H., Saito, T., Oshima, N., Kitamura, N., Ishizaka, S., Hinatsu, Y., Wakeshima, M., Kato, M., Tsuge, K., Sawamura, M. (2008), Reversible mechanochromic luminescence of [(C<sub>6</sub>F<sub>5</sub>Au)<sub>2</sub>( $\mu$ -1, 4-diisocyanobenzene)], *J. Am. Chem. Soc.*, *130*(31), 10044-10045 (DOI: <https://doi.org/10.1021/ja8019356>).

- [4] (a) Man, Z., Lv, Z., Xu, Z., Liao, Q., Liu, J., Liu, Y., Fu, L., Liu, M., Bai, S., Fu, H. (2020), Highly Sensitive and Easily Recoverable Excitonic Piezochromic Fluorescent Materials for Haptic Sensors and Anti-Counterfeiting Applications, *Adv. Funct. Mater.*, 30(17), 2000105 (DOI: <https://doi.org/10.1002/adfm.202000105>); (b) Kinami, M., Crenshaw, B. R., Weder, C. (2006). Polyesters with built-in threshold temperature and deformation sensors, *Chem. Mater.*, 18(4), 946-955 (DOI: <https://doi.org/10.1021/cm052186c>); (c) Farinola, G. M., Ragni, R. (2011), Electroluminescent materials for white organic light emitting diodes, *Chem. Soc. Rev.*, 40(7), 3467-3482 (DOI: 10.1039/C0CS00204F); (d) Sun, H., Liu, S., Lin, W., Zhang, K. Y., Lv, W., Huang, X., Huo, F., Yang, H., Jenkins, G., Zhao, Q., Huang, W. (2014), Smart responsive phosphorescent materials for data recording and security protection, *Nat. Commun.*, 5(1), 1-9 (DOI: <https://doi.org/10.1038/ncomms4601>); (e) Pucci, A., Di Cuia, F., Signori, F., Ruggeri, G. (2007), Bis (benzoxazolyl) stilbene excimers as temperature and deformation sensors for biodegradable poly (1, 4-butylene succinate) films, *J. Mater. Chem.*, 17(8), 783-790 (DOI: 10.1039/B612033D); (f) Kishimura, A., Yamashita, T., Yamaguchi, K., Aida, T. (2005), Rewritable phosphorescent paper by the control of competing kinetic and thermodynamic self-assembling events, *Nat. Mater.*, 4(7), 546-549 (DOI: <https://doi.org/10.1038/nmat1401>); (g) Samuel, I. D. W., Turnbull, G. A. (2007), Organic semiconductor lasers, *Chem. Rev.*, 107(4), 1272-1295 (DOI: <https://doi.org/10.1021/cr050152i>); (h) Prusti, B., Samanta, P. K., English, N. J., Chakravarty, M. (2021), AC 3-symmetric twisted organic salt as an efficient mechano-/thermo-responsive molecule: a reusable and sensitive fluorescent thermometer, *Chem. Commun.*, 57(92), 12321-12324 (DOI: 10.1039/D1CC05599B);

- [5] (a) Yuan, W. Z., Tan, Y., Gong, Y., Lu, P., Lam, J. W., Shen, X. Y., Feng, C., Sung, H. H-Y., Lu, Y., Williams, I. D., Sun, J. Z., Zhang, Y., Tang, B. Z. (2013), Synergy between twisted conformation and effective intermolecular interactions: strategy for efficient mechanochromic luminogens with high contrast, *Adv. Mater.*, 25(20), 2837-2843 (DOI: <https://doi.org/10.1002/adma.201205043>); (b) Walters, D. T., Aghakhanpour, R. B., Powers, X. B., Ghiassi, K. B., Olmstead, M. M., Balch, A. L. (2018), Utilization of a Nonemissive Triphosphine Ligand to Construct a Luminescent Gold (I)-Box That Undergoes Mechanochromic Collapse into a Helical Complex, *J. Am. Chem. Soc.*, 140(24), 7533-7542 (DOI: <https://doi.org/10.1021/jacs.8b01666>); (c) Misra, R., Jadhav, T., Dhokale, B., Mobin, S. M. (2014), Reversible mechanochromism and enhanced AIE in tetraphenylethene substituted phenanthroimidazoles, *Chem. Commun.*, 50(65), 9076-9078 (DOI: 10.1039/C4CC02824D); (d) Hong, Y., Lam, J. W., Tang, B. Z. (2009), Aggregation-induced emission: phenomenon, mechanism and applications, *Chem. Commun.*, (29), 4332-4353 (DOI: 10.1039/B904665H).
- [6] (a) J. B. Birks, *Photophysics of Aromatic Molecules*, Wiley, London, UK, 1970; (b) Li, Q., Li, Z. (2017), The strong light-emission materials in the aggregated state: what happens from a single molecule to the collective group, *Adv. Sci.*, 4(7), 1600484 (DOI: <https://doi.org/10.1002/advs.201600484>); (c) Hong, Y., Lam, J. W., Tang, B. Z. (2011), Aggregation-induced emission, *Chem. Soc. Rev.*, 40(11), 5361-5388 (DOI: 10.1039/C1CS15113D).
- [7] (a) Luo, J., Xie, Z., Lam, J. W., Cheng, L., Chen, H., Qiu, C., Kwok, H. S., Zhan, X., Liu, Y., Zhu, D., Tang, B. Z. (2001), Aggregation-induced emission of 1-methyl-1, 2, 3, 4, 5-pentaphenylsilole, *Chem. Commun.*, (18), 1740-1741 (DOI: 10.1039/B105159H); (b) Hong, Y., Lam, J. W., Tang, B. Z. (2009), Aggregation-induced emission:

- phenomenon, mechanism and applications, *Chem. Commun.*, (29), 4332-4353 (DOI: 10.1039/B904665H); (C) Mei, J., Leung, N. L., Kwok, R. T., Lam, J. W., Tang, B. Z. (2015), Aggregation-induced emission: together we shine, united we soar!, *Chem. Rev.*, 115(21), 11718-11940 (DOI: <https://doi.org/10.1021/acs.chemrev.5b00263>); (d) Ren, Y., Lam, J. W., Dong, Y., Tang, B. Z., Wong, K. S. (2005), Enhanced emission efficiency and excited state lifetime due to restricted intramolecular motion in silole aggregates, *J. Phys. Chem. B*, 109(3), 1135-1140. (DOI: <https://doi.org/10.1021/jp046659z>).
- [8] (a) Wang, J., Mei, J., Hu, R., Sun, J. Z., Qin, A., Tang, B. Z. (2012), Click synthesis, aggregation-induced emission, E/Z isomerization, self-organization, and multiple chromisms of pure stereoisomers of a tetraphenylethene-cored luminogen, *J. Am. Chem. Soc.*, 134(24), 9956-9966 (DOI: <https://doi.org/10.1021/ja208883h>); (b) Liu, F., Tu, J., Wang, X., Wang, J., Gong, Y., Han, M., Dang, X., Liao, Q., Peng, Q., Li, Q., Li, Z. (2018), Opposite mechanoluminescence behavior of two isomers with different linkage positions, *Chem. Commun.*, 54(44), 5598-5601 (DOI: 10.1039/C8CC03083A); (c) Xu, B., Li, W., He, J., Wu, S., Zhu, Q., Yang, Z., Wu, Y-C., Zhang, Y., Jin, C., Lu, P., Chi, Z., Liu, S., Xu, J., Bryce, M. R. (2016), Achieving very bright mechanoluminescence from purely organic luminophores with aggregation-induced emission by crystal design, *Chem. Sci*, 7(8), 5307-5312 (DOI: 10.1039/C6SC01325B).
- [9] (a) Chen, Y., Zhang, W., Cai, Y., Kwok, R. T., Hu, Y., Lam, J. W., Gu, X., He, Z., Zhao, Z., Zheng, X., Chen, B., Gui, C., Tang, B. Z. (2017), AIEgens for dark through-bond energy transfer: design, synthesis, theoretical study and application in ratiometric Hg 2+ sensing, *Chem. Sci*, 8(3), 2047-2055 (DOI: 10.1039/C6SC04206F); (b) Yang, Z., Chi, Z., Mao, Z., Zhang, Y., Liu, S., Zhao, J., Aldred, M., Chi, Z. (2018), Recent advances in mechano-responsive luminescence of tetraphenylethylene derivatives with aggregation-induced emission

- properties, *Mater. Chem. Front.*, 2(5), 861-890 (DOI: 10.1039/C8QM00062J); (c) Zheng, X., Zhu, W., Zhang, C., Zhang, Y., Zhong, C., Li, H., Xie, G., Wang, X., Yang, C. (2019), Self-assembly of a highly emissive pure organic imine-based stack for electroluminescence and cell imaging, *J. Am. Chem. Soc.*, 141(11), 4704-4710 (DOI: <https://doi.org/10.1021/jacs.8b13724>); (d) Zhang, B., Kong, Y., Liu, H., Chen, B., Zhao, B., Luo, Y., Chen, L., Zhang, Y., Han, D., Zhao, Z., Tang, B. Z., Niu, L. (2021), Aggregation-induced delayed fluorescence luminogens: the innovation of purely organic emitters for aqueous electrochemiluminescence, *Chem. Sci*, 12(40), 13283-13291 (DOI: 10.1039/D1SC02918E); (e) Chen, W., Zhang, C., Han, X., Liu, S. H., Tan, Y., Yin, J. (2019), Fluorophore-labeling tetraphenylethene dyes ranging from visible to near-infrared region: AIE behavior, performance in solid state, and bioimaging in living cells, *J. Org. Chem.*, 84(22), 14498-14507 (DOI: <https://doi.org/10.1021/acs.joc.9b01976>).
- [10](a) May, L., Müller, T. J. (2020), Frontispiece: Electron-Rich Phenothiazine Congeners and Beyond: Synthesis and Electronic Properties of Isomeric Dithieno [1, 4] thiazines, *Chem. Eur. J.*, 26(53) (DOI: <https://doi.org/10.1002/chem.202085363>); (b) Chen, D. G., Lin, T. C., Chen, Y. A., Chen, Y. H., Lin, T. C., Chen, Y. T., Chou, P. T. (2018), Revisiting Dual Intramolecular Charge-Transfer Fluorescence of Phenothiazine-Triphenyltriazine Derivatives. *J. Phys. Chem. C*, 122(23), 12215-12221 (DOI: <https://doi.org/10.1021/acs.jpcc.8b04395>); (c) Li, S., Yin, C., Wang, R., Fan, Q., Wu, W., Jiang, X. (2020), Second Near-Infrared Aggregation-Induced Emission Fluorophores with Phenothiazine Derivatives as the Donor and 6, 7-Diphenyl-[1, 2, 5] Thiadiazolo [3, 4-g] Quinoxaline as the Acceptor for In Vivo Imaging, *ACS Appl. Mater. Interfaces*, 12(18), 20281-20286 (DOI: <https://doi.org/10.1021/acsami.0c03769>); (d) Yang, J., Qin, J., Geng,

- P., Wang, J., Fang, M., Li, Z. (2018), Molecular Conformation-Dependent Mechanoluminescence: Same Mechanical Stimulus but Different Emissive Color over Time. *Angew. Chem. Int. Ed.*, 130(43), 14370-14374 (DOI: <https://doi.org/10.1002/ange.201809463>); (e) Ekbote, A., Mobin, S. M., Misra, R. (2020), Stimuli-responsive phenothiazine-based donor–acceptor isomers: AIE, mechanochromism and polymorphism. *J. Mater. Chem. C*, 8(10), 3589-3602 (DOI: 10.1039/C9TC05192A).
- [11](a) Ikeya, M., Katada, G., Ito, S. (2019), Tunable mechanochromic luminescence of 2-alkyl-4-(pyren-1-yl) thiophenes: controlling the self-recovering properties and the range of chromism, *Chem. Commun.*, 55(82), 12296-12299 (DOI: 10.1039/C9CC06406K); (b) Yagai, S., Okamura, S., Nakano, Y., Yamauchi, M., Kishikawa, K., Karatsu, T., Kitamura, A., Ueno, A., Kuzuhara, D., Yamada, H., Seki, T., Ito, H. (2014), Design amphiphilic dipolar  $\pi$ -systems for stimuli-responsive luminescent materials using metastable states, *Nat. Commun.*, 5(1), 1-10 (DOI: <https://doi.org/10.1038/ncomms5013>); (c) Gierschner, J., Park, S. Y. (2013), Luminescent distyrylbenzenes: tailoring molecular structure and crystalline morphology, *J. Mater. Chem. C*, 1(37), 5818-5832 (DOI: 10.1039/C3TC31062K); (d) Dong, Y., Xu, B., Zhang, J., Tan, X., Wang, L., Chen, J., Lv, H., Wen, S., Li, B., Ye, L., Zou, B., Tian, W. (2012), Piezochromic luminescence based on the molecular aggregation of 9, 10-Bis ((E)-2-(pyrid-2-yl) vinyl) anthracene, *Angew. Chem. Int. Ed.*, 51(43), 10782-10785 (DOI: <https://doi.org/10.1002/anie.201204660>); (e) Suzuki, T., Okada, H., Nakagawa, T., Komatsu, K., Fujimoto, C., Kagi, H., Matsuo, Y. (2018), A fluorenylidene-acridane that becomes dark in color upon grinding–ground state mechanochromism by conformational change, *Chem. Sci*, 9(2), 475-482 (DOI: 10.1039/C7SC03567E).
- [12](a) Yoshii, R., Suenaga, K., Tanaka, K., Chujo, Y. (2015), Mechanofluorochromic materials based on aggregation-induced

- emission-active boron ketoiminates: regulation of the direction of the emission color changes, *Chem. Eur. J.*, 21(19), 7231-7237 (DOI: <https://doi.org/10.1002/chem.201500033>); (b) Wu, J., Cheng, Y., Lan, J., Wu, D., Qian, S., Yan, L., He, Z., Li, X., Wang, K., Zou, B., You, J. (2016), Molecular engineering of mechanochromic materials by programmed C–H arylation: making a counterpoint in the chromism trend, *J. Am. Chem. Soc.*, 138(39), 12803-12812 (DOI: <https://doi.org/10.1021/jacs.6b03890>); (c) Dong, J., Solntsev, K. M., Tolbert, L. M. (2009), Activation and tuning of green fluorescent protein chromophore emission by alkyl substituent-mediated crystal packing, *J. Am. Chem. Soc.*, 131(2), 662-670 (DOI : <https://doi.org/10.1021/ja806962e>); (d) Goto, S., Nitta, Y., Decarli, N., Sousa, L. E. D., Stachelek, P., Tohnai, N., Minakata, S., Silva, P., Data, P., Takeda, Y. (2021) Revealing Internal Heavy Chalcogen Atom Effect on the Photophysics of Dibenzo [a, j] phenazine-Cored Donor–Acceptor–Donor Triad, *J. Mater. Chem. C* ,9, 13942-13953 (DOI: <https://doi.org/10.1039/D1TC02635F>); (e) Fan, Y., Li, Q., Li, Z. (2020), Organic Luminogens Bearing Alkyl Substituents: Design Flexibility, Adjustable Molecular Packing, and the Optimized Performance, *Mater. Chem. Front.*, 5, 1525-1540 (DOI: [10.1039/D0QM00851F](https://doi.org/10.1039/D0QM00851F)); (f) Jadhav, T., Dhokale, B., Mobin, S. M., Misra, R. (2015), Aggregation induced emission and mechanochromism in pyrenoimidazoles. *J. Mater. Chem. C*, 3(38), 9981-9988 (DOI: [10.1039/C5TC02181B](https://doi.org/10.1039/C5TC02181B))
- [13] (a) Zhang, Y., Chen, Z., Song, J., He, J., Wang, X., Wu, J., Chen, S., Qu, J., Wong, W. Y. (2019), Rational design of high efficiency green to deep red/near-infrared emitting materials based on isomeric donor–acceptor chromophores, *J. Mater. Chem. C*, 7(7), 1880-1887 (DOI: [10.1039/C8TC05383A](https://doi.org/10.1039/C8TC05383A)); (b) Tsujimoto, H., Ha, D. G., Markopoulos, G., Chae, H. S., Baldo, M. A., Swager, T. M. (2017), Thermally activated delayed fluorescence and aggregation induced emission with

- through-space charge transfer, *J. Am. Chem. Soc.*, 139(13), 4894-4900 (DOI: <https://doi.org/10.1021/jacs.7b00873>); (c) Wang, Y., Xu, D., Gao, H., Wang, Y., Liu, X., Han, A., Zhang, C., Zang, L. (2018), Twisted donor–acceptor cruciform luminophores possessing substituent-dependent properties of aggregation-induced emission and mechanofluorochromism, *The Journal of Physical Chemistry C*, 122(4), 2297-2306 (DOI: <https://doi.org/10.1021/acs.jpcc.7b11368>) ; (d) Nakae, T., Nishio, M., Usuki, T., Ikeya, M., Nishimoto, C., Ito, S., Nishihara, H., Hattori, M., Hayashi, S., Yamada, T., Yamanoi, Y. (2021), Luminescent Behavior Elucidation of a Disilane-Bridged D–A–D Triad Composed of Phenothiazine and Thienopyrazine, *Angew. Chem. Int. Ed.*, 60(42), 22871-22878 (<https://doi.org/10.1002/anie.202108089>).
- [14](a) Desroches, M., Morin, J. F. (2018), Anthanthrene as a super-extended tetraphenylethylene for aggregation-induced emission, *Org. Lett.*, 20(10), 2797-2801 (DOI: <https://doi.org/10.1021/acs.orglett.8b00452>); (b) Yin, Y., Zhao, F., Chen, Z., Liu, G., Pu, S. (2018), Aggregation-induced emission enhancement (AIEE)-active mechanofluorochromic tetraphenylethene derivative bearing a rhodamine unit, *Tetrahedron Lett.*, 59(50), 4416-4419 (DOI: <https://doi.org/10.1016/j.tetlet.2018.10.073>); (c) Martínez-Abadía, M., Giménez, R., Ros, M. B. (2018), Self-Assembled  $\alpha$ -Cyanostilbenes for Advanced Functional Materials, *Adv. Mater.*, 30(5), 1704161 (DOI: <https://doi.org/10.1002/adma.201704161>).
- [15](a) Biegger, P., Stolz, S., Intorp, S. N., Zhang, Y., Engelhart, J. U., Rominger, F., Hardcastle, K., Lemmer, U., Qian, X., Hamburger, M., Bunz, U. H. F. (2015), Soluble Diazaptycenes: Materials for Solution-Processed Organic Electronics, *J. Org. Chem.*, 80(1), 582-589 (DOI: <https://doi.org/10.1021/jo502564w>); (b) Song, H. J., Kim, D. H., Lee, E. J., Moon, D. K. (2013), Conjugated polymers consisting of

- quinacridone and quinoxaline as donor materials for organic photovoltaics: orientation and charge transfer properties of polymers formed by phenyl structures with a quinoxaline derivative, *J. Mater. Chem. A*, 1(19), 6010-6020 (DOI: 10.1039/C3TA10512A); (c) Yang, J., Ganesan, P., Teuscher, J., Moehl, T., Kim, Y. J., Yi, C., Comte, P., Pei, K., Holcombe, T. W., Nazeeruddin, M. K., Hua, J., Zakeeruddin, S. M., Tian, H., Grätzel, M. (2014), Influence of the donor size in D- $\pi$ -A organic dyes for dye-sensitized solar cells, *J. Am. Chem. Soc.*, 136(15), 5722-5730 (DOI: <https://doi.org/10.1021/ja500280r>); (d) Chen, M., Li, L., Wu, H., Pan, L., Li, S., He, B., Zhang, H., Sun, J. Z., Qin, A., Tang, B. Z. (2018), Unveiling the different emission behavior of polytriazoles constructed from pyrazine-based AIE monomers by click polymerization, *ACS Appl. Mater. Interfaces*, 10(15), 12181-12188 (DOI: <https://doi.org/10.1021/acsami.8b03178>); (e) Chen, M., Li, L., Nie, H., Tong, J., Yan, L., Xu, B., Sun, J. Z., Tian, W., Zhao, Z., Qin, A., Tang, B. Z. (2015), Tetraphenylpyrazine-based AIEgens: facile preparation and tunable light emission. *Chem. Sci*, 6(3), 1932-1937 (DOI: 10.1039/C4SC03365E).
- [16] Ekbote, A., Jadhav, T., Misra, R. (2017), T-Shaped donor-acceptor-donor type tetraphenylethylene substituted quinoxaline derivatives: aggregation-induced emission and mechanochromism, *New J. Chem.*, 41(17), 9346-9353 (DOI: 10.1039/C7NJ01531C).
- [17](a) Mao, M., Zhang, X., Cao, L., Tong, Y., Wu, G. (2015), Design of Bodipy based organic dyes for high-efficient dye-sensitized solar cells employing double electron acceptors, *Dyes Pigm*, 117, 28-36 (DOI: <https://doi.org/10.1016/j.dyepig.2015.02.001>); (b) Zhang, H., Li, H., Wang, J., Sun, J., Qin, A., Tang, B. Z. (2015), Axial chiral aggregation-induced emission luminogens with aggregation-annihilated circular dichroism effect. *J. Mater. Chem. C*, 3(20), 5162-5166, (DOI: 10.1039/C5TC00629E).

- [18](a) Hu, J., Liu, R., Cai, X., Shu, M., Zhu, H. (2015), Highly efficient and selective probes based on polycyclic aromatic hydrocarbons with trimethylsilylethynyl groups for fluoride anion detection, *Tetrahedron Lett*, 71(23), 3838-3843 (DOI: <https://doi.org/10.1016/j.tet.2015.04.016>); (b) Guo, Z. H., Lei, T., Jin, Z. X., Wang, J. Y., Pei, J. (2013), T-Shaped donor–acceptor molecules for low-loss red-emission optical waveguide, *Org. Lett.*, 15(14), 3530-3533 (DOI: <https://doi.org/10.1021/ol4012025>).
- [19](a) Frisch, M. J. E. A., Trucks, G. W., Schlegel, H. B., Scuseria, G. E., Robb, M. A., Cheeseman, J. R., Scalmani, G., Barone, B., Mennucci, B., Petersson, G. A., Fox, D. J, *et al.*, (2009). gaussian 09, Revision d. 01, Gaussian. Inc., Wallingford CT, 201. (b) Lee, C., Yang, W., Parr, R. G. (1988), Phys. Rev. B: Condens. Matter Mater. Phys. (c) Becke, A. D. (1993). A new mixing of Hartree–Fock and local density-functional theories. *J. Chem. Phys.*, 98(2), 1372-1377 (DOI: <https://doi.org/10.1063/1.464304>).
- [20] Hart, A. S., KC, C. B., Subbaiyan, N. K., Karr, P. A., D’Souza, F. (2012), Phenothiazine-sensitized organic solar cells: effect of dye anchor group positioning on the cell performance. *ACS Appl. Mater. Interfaces*, 4(11), 5813-5820, (DOI: <https://doi.org/10.1021/am3014407>);
- [21](a) Roy, B., Reddy, M. C., Hazra, P. (2018), Developing the structure–property relationship to design solid state multi-stimuli responsive materials and their potential applications in different fields, *Chem. Sci*, 9(14), 3592-3606. (DOI: 10.1039/C8SC00143J); (b) Sasaki, S., Drummen, G. P., Konishi, G. I. (2016), Recent advances in twisted intramolecular charge transfer (TICT) fluorescence and related phenomena in materials chemistry, *J. Phys. Chem. C*, 4(14), 2731-2743 (DOI: 10.1039/C5TC03933A); (c) Grabowski, Z. R., Rotkiewicz, K., Rettig, W. (2003), Structural changes accompanying intramolecular electron transfer: focus on twisted intramolecular charge-transfer states

- and structures, *Chem. Rev.*, 103(10), 3899-4032 (DOI: <https://doi.org/10.1021/cr9407451>); (d) Kundu, A., Karthikeyan, S., Sagara, Y., Moon, D., Anthony, S. P. (2019), Temperature-Controlled Locally Excited and Twisted Intramolecular Charge-Transfer State-Dependent Fluorescence Switching in Triphenylamine–Benzothiazole Derivatives, *ACS omega*, 4(3), 5147-5154 (DOI: <https://doi.org/10.1021/acsomega.8b03099>).
- [22](a) Misra, R., Jadhav, T., Dhokale, B., Gautam, P., Sharma, R., Maragani, R., Mobin, S. M. (2014), Carbazole-BODIPY conjugates: design, synthesis, structure and properties, *Dalton Trans.*, 43(34), 13076-13086 (DOI: 10.1039/C4DT00983E); (b) Lu, X., Fan, S., Wu, J., Jia, X., Wang, Z. S., Zhou, G. (2014). Controlling the charge transfer in D–A–D chromophores based on pyrazine derivatives. *J. Org. Chem.*, 79(14), 6480-6489(DOI: <https://doi.org/10.1021/jo500856k>).
- [23](a) Jadhav, T., Dhokale, B., Misra, R. (2015), Effect of the cyano group on solid state photophysical behavior of tetraphenylethene substituted benzothiadiazoles, *J. Mater. Chem. C*, 3(35), 9063-9068 (DOI: 10.1039/C5TC01871D); (b) Sun, Q., Lam, J. W., Xu, K., Xu, H., Cha, J. A., Wong, P. C., Wen, G., Zhang, X., Jing, X., Wang, F., Tang, B. Z. (2000), Nanocluster-containing mesoporous magnetoceramics from hyperbranched organometallic polymer precursors, *Chem. Mater.*, 12(9), 2617-2624 (DOI: <https://doi.org/10.1021/cm000094b>); (c) Tang, B. Z., Xu, H., Lam, J. W., Lee, P. P., Xu, K., Sun, Q., Cheuk, K. K. (2000), C60-containing poly (1-phenyl-1-alkynes): synthesis, light emission, and optical limiting, *Chem. Mater.*, 12(5), 1446-1455 (DOI: <https://doi.org/10.1021/cm990799h>).

## Chapter 5

# Stimuli responsive AIE active positional isomers of phenanthroimidazole

---

---

### 5.1. Introduction

Organic materials with tunable solid-state emission are of broad and current interest owing to their promising applications in mechanical sensors, deformation detectors, security systems, memory devices, data storage, fluorescent probes and in various optoelectronic devices.<sup>[1, 2]</sup> Mechanochromic materials are a class of *smart* materials with reversible solid-state emission that can be altered on applying external stimuli.<sup>1(a), 1(e), [3]</sup> The variable emission in mechanochromic materials have been most commonly accomplished by phase transitions and alteration of the molecular packing modes.<sup>[4]</sup> A prerequisite for reversible mechanochromism is high solid-state emission<sup>[5]</sup> which mainly depends on the molecular arrangement and various factors such as planarity, effective conjugation and interaction with the surrounding environment.<sup>[6]</sup> The molecular system exhibiting aggregation-induced emission (AIE) are highly emissive in solid state<sup>[7]</sup> unlike the common organic fluorophores which are weakly emissive or non-emissive in solid state due to aggregation caused quenching (ACQ).<sup>[8]</sup> The fusion of AIE active fluorophores with the ACQ fluorophores is an effective technique for producing luminescent molecules in solid state with a wide variety of optoelectronic applications. Tetraphenylethylene (TPE) is highly emissive in solid state due to restriction of intramolecular rotations (RIR) due to the twisted propeller shaped structure and has been utilized for the development of AIE active mechanochromic materials.<sup>[9]</sup>

Recently, the development of organic light emitting diodes (OLEDs) has gained significant attention because of its applications in full colour flat

panel displays and solid state lighting.<sup>[10]</sup> The aggregation-induced emission (AIE) active materials have been effectively used in developing high performance organic light emitting diodes OLEDs.<sup>[11]</sup> The past years have witnessed use of phenanthroimidazole as a key building block in development of efficient solid state emitters due to its potential applications in sensing, bio-imaging, electrochemical luminescent cell, mechanochromic materials and organic light emitting diodes (OLEDs).<sup>[12]</sup> Phenanthroimidazole is a rigid, planar, aromatic heterocyclic compound comprising of a phenanthrene ring fused with an imidazole ring, possessing high thermal stability, good charge carrier mobility, wide band gap and excellent fluorescence quantum yield.<sup>[13]</sup> The two nitrogen atoms of the imidazole ring result in bipolar properties and easy functional modification at the N1 and C2 positions (Figure 5.1.) make phenanthroimidazole derivatives suitable to be employed in high performance organic light emitting diodes (OLEDs) and mechanochromic materials.<sup>[13]</sup>

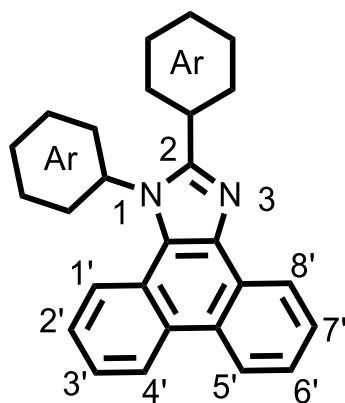


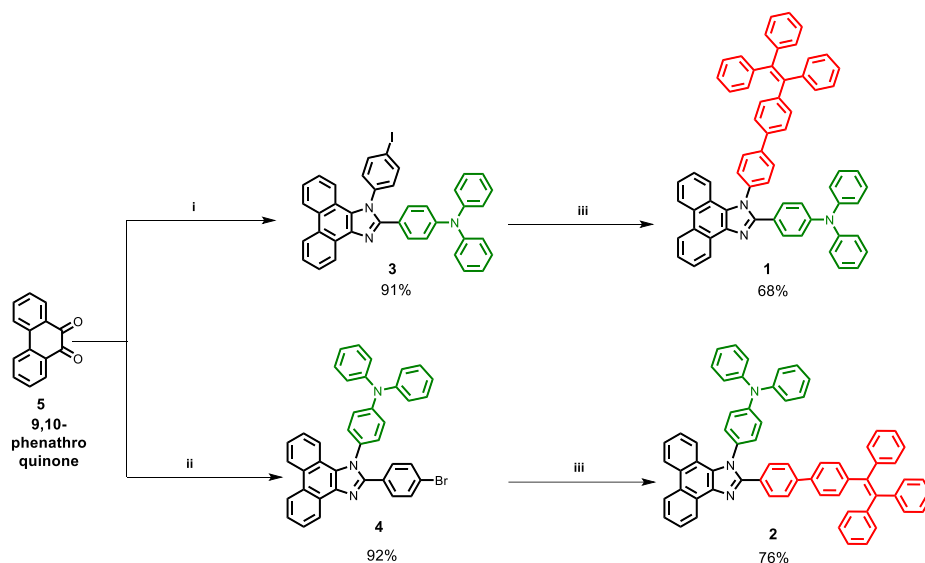
**Figure 5.1.** Chemical structure of phenanthroimidazole

The literature reveals reports on synthesis of phenanthroimidazole derivatives with reversible stimuli responsive solid state emission and efficient OLED properties.<sup>[14,15]</sup> The combination of phenanthroimidazole unit with a triphenylamine (TPA) and a tetraphenylethylene (TPE) unit simultaneously can produce materials with intriguing mechanochromic and organic light emitting diode (OLED) properties.

In this contribution we have synthesized phenanthroimidazole **1** and **2** incorporated with a triphenylamine (TPA) unit as well as a phenyl-TPE unit. The molecules are positional isomers and were synthesized with a view to study the effect of interchange of the TPA and phenyl-TPE unit on their photophysical and mechanochromic properties. Moreover, the TPA unit and the TPE unit differ in the donor strengths as well as effective conjugation which could further influence the properties. The aggregation-induced emission (AIE) and mechanochromic properties of phenanthroimidazole **1** and **2** are investigated. The phenanthroimidazoles show reversible mechanochromism between blue and green and are excellent solid-state emitters.

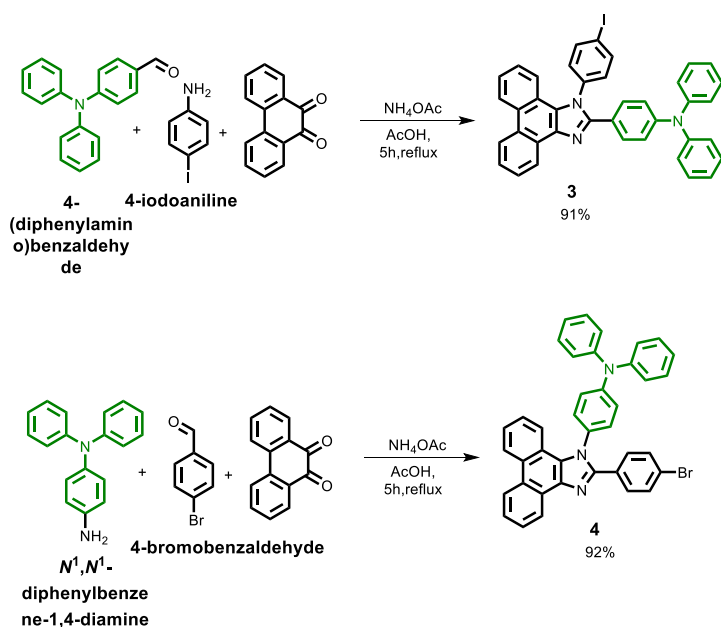
## 5.2. Results and discussions

The synthesis of phenanthroimidazoles **1** and **2** was carried out by a simple and efficient two step approach as illustrated in Scheme 5.1. The intermediates **3** and **4** were synthesized by a facile condensation reaction of 9,10-phenanthroquinone with corresponding aldehydes, amines and ammonium acetate in refluxing acetic acid. The intermediate **3** was obtained from 4-iodoaniline and 4-(diphenylamino) benzaldehyde in 91% yield, whereas the intermediate **4** was obtained from N',N'-diphenylbenzene-1,4-diamine and 4-bromobenzaldehyde in 92% yield. The aldehyde and amine intermediates of TPA were synthesized by reported procedures (Scheme 5.2.).<sup>[16]</sup> The Suzuki cross-coupling reaction of **3** and **4** with 4-(1,2,2-triphenylvinyl)phenylboronic acid pinacol ester<sup>[5(e)]</sup> in argon atmosphere using Pd(PPh<sub>3</sub>)<sub>4</sub> as catalyst furnished the target phenanthroimidazoles **1** and **2** in 68% and 76% yields respectively. All the newly synthesized molecules were well characterized by NMR and HRMS techniques. The phenanthroimidazole **1** and intermediate **3,4** and were characterized by single crystal analysis.



**Scheme 5.1.** Synthetic route for the phenanthroimidazoles **1** and **2**<sup>a</sup>

<sup>a</sup> (i) 4-iodoaniline, 4-(diphenylamino) benzaldehyde, acetic acid (AcOH) and ammonium acetate (NH<sub>4</sub>OAc), 5 hours, 120 °C (ii) N',N'-diphenylbenzene-1,4-diamine, 4-bromobenzaldehyde, acetic acid (AcOH) and ammonium acetate (NH<sub>4</sub>OAc), 5 hours, 120 °C (iii) 4-(1,2,2-triphenylvinyl)phenylboronic acid pinacol ester, K<sub>2</sub>CO<sub>3</sub>, Pd(PPh<sub>3</sub>)<sub>4</sub>, toluene:ethanol:water (10.0 mL:4.0 mL:0.5 mL), 12 hours, 110 °C.



**Scheme 5.2.** Synthetic scheme for intermediates **3** and **4**

### 5.3. Thermal analysis

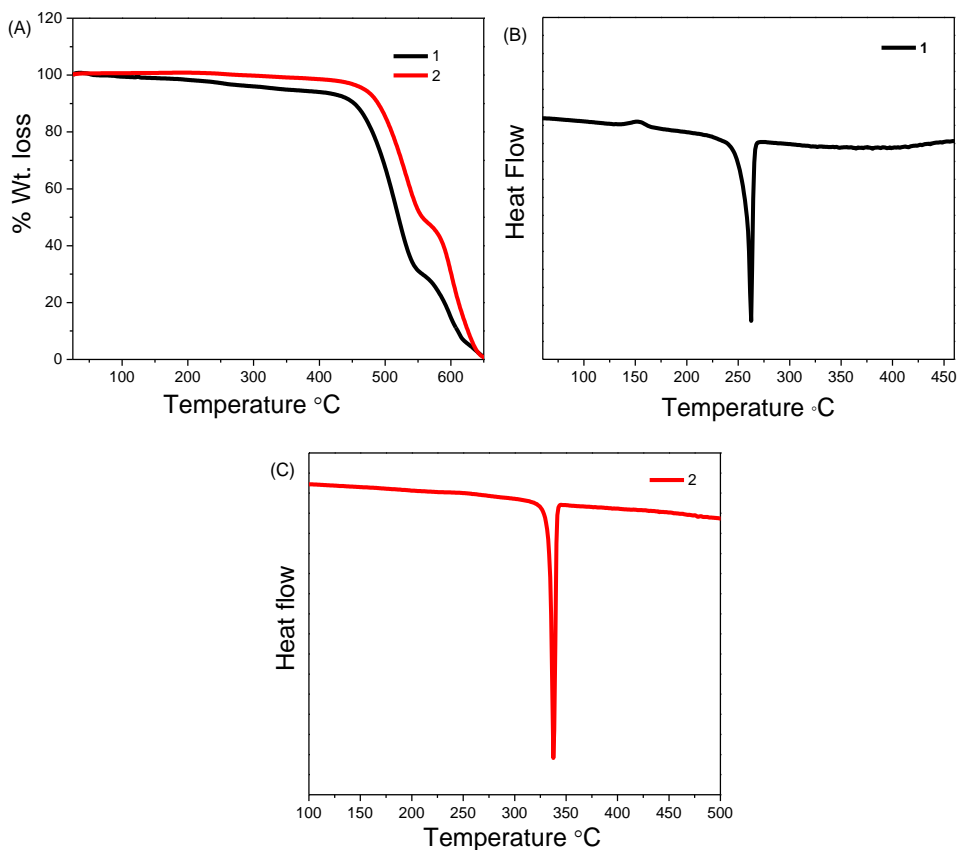


**Figure 5.2.** Thermogravimetric analysis (A) and differential scanning calorimetry curves of luminophores **1** (B) and **2** (C).

The fabrication of solid-state devices requires materials to withstand high temperatures and hence the materials should be stable at elevated temperatures. Hence, the thermal stability of phenanthroimidazoles **1** and **2** was checked by thermogravimetric analysis (TGA) and differential scanning calorimetry (DSC) (Figure 5.2.). The decomposition temperatures and melting temperatures are given in Table 5.1. The thermal decomposition temperatures ( $T_d$ ) for **1** and **2** are 422 °C and 432 °C respectively and correspond to 5% weight loss under a nitrogen atmosphere. The phenanthroimidazoles **1** and **2** are thermally stable above 400 °C and hence a suitable choice for material applications. The rigid structure of both the molecules leads to a high thermal stability, the phenanthroimidazole **2**

being more stable than **1**. The differential scanning calorimetry (DSC) curves reveal an endothermic process for **1** and **2** and a high melting temperature of 261 °C and 339 °C (Figure 5.2.).

#### 5.4. Photophysical properties

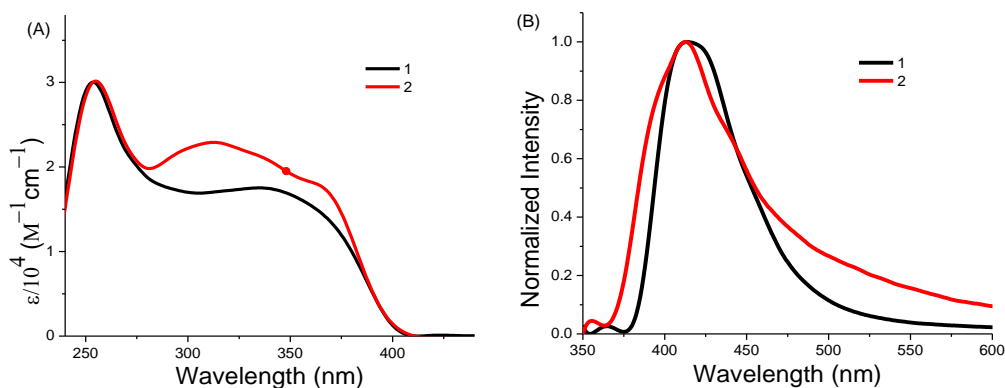


**Figure 5.3.** Electronic absorption spectra of **1** and **2** (A) and normalized fluorescence spectra of **1** and **2** (B) recorded in THF (concentration =  $2 \times 10^{-5}$  M).

**Table 5.1.** Photophysical and thermal properties of **1** and **2**.

Compounds	$\lambda_{ab}$ [nm $1\text{cm}^{-1}$ ] <sup>a</sup>	$(\epsilon[\text{Lmol}^{-1}$	$\lambda_{em.}$ (nm) <sup>b</sup>	$\Phi_f^c$	$T_d$ (°C)	$T_m$ (°C)
<b>1</b>	253(30028), 342(17487)		413	0.032	422 °C	261 °C
<b>2</b>	255(30180), 355(18532)		413	0.031	432 °C	339 °C

<sup>a,b</sup> Recorded in tetrahydrofuran, <sup>c</sup> The fluorescence quantum yields were recorded using 9,10-diphenylanthracene as a standard in ethanol solution.

The phenanthroimidazoles **1** and **2** are soluble in common organic solvents such as dichloromethane (DCM), tetrahydrofuran (THF), chloroform, and hexane but are poorly soluble in water, methanol and acetonitrile. The photophysical properties of **1** and **2** were studied in THF solution using electronic absorption and fluorescence spectroscopy (Figure 5.3.) and the data are listed in Table 5.1. The phenanthroimidazoles **1** and **2** display

absorption peaks at 250 nm and 260 nm respectively corresponding to the combined  $\pi$ - $\pi^*$  transitions of the aromatic segments. The absorption peaks between 340 to 360 nm arise from the delocalized  $\pi$ - $\pi^*$  transitions of the phenanthroimidazole unit.<sup>[17]</sup> The emission spectra reveal emission maximum at 413 nm for both the molecules.

### 5.5. Solvatochromism

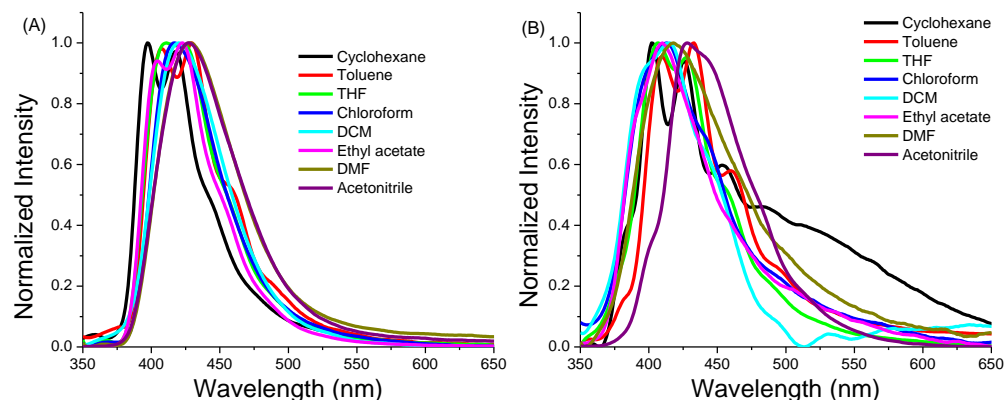


**Figure 5.4.** (A) Fluorescence spectra of **1** (A) and **2** (B) in different solvents of varying polarities. (excitation wavelength or  $\lambda_{ex}$  = 340 nm).

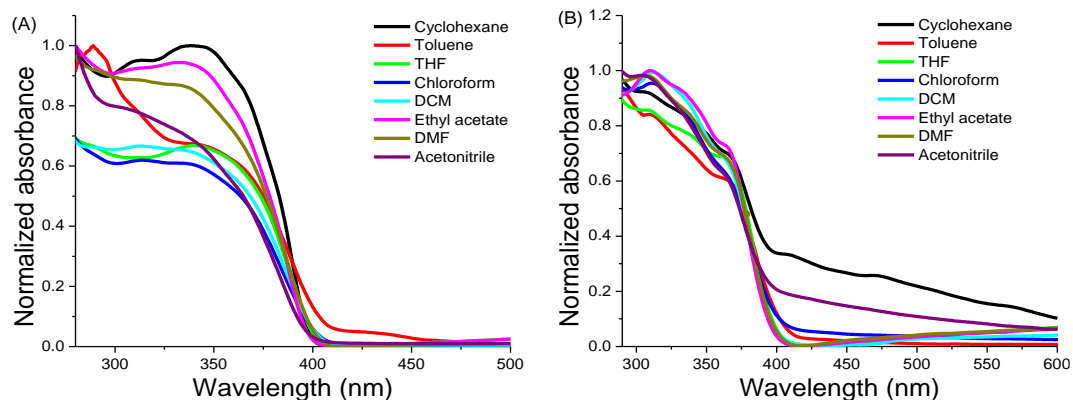


**Figure 5.5.** UV-vis absorption spectra of **1** (A) and **2** (B) in different solvents of varying polarities.

The solvatochromism was examined by recording the fluorescence (Figure 5.4.) and absorption spectra (Figure 5.5.) of phenanthroimidazoles **1** and **2** in solvents of varying polarity (cyclohexane, toluene, tetrahydrofuran

(THF), chloroform, dichloromethane (DCM), ethyl acetate, dimethylformamide (DMF) and acetonitrile).

**Table 5.2.** Solvatochromic properties of luminophores **1** and **2**.

Comp.	Solvent	$\lambda_{ab}$ (nm)	$\lambda_{em}$ (nm)	Stokes shift (cm <sup>-1</sup> )	$\Phi_f^a$
<b>1</b>	Cyclohexane	337	397	4484.67	0.0187
	Toluene	340	407	4841.74	0.0438
	Chloroform	337	417	5782.38	0.0153
	DCM	336	420	5952.38	0.0207
	Ethyl acetate	333	422	6333.35	0.0193
	DMF	334	428	6575.63	0.0208
	Acetonitrile	310	428	8893.57	0.0115
<b>2</b>	Cyclohexane	367	402	2372.34	0.0081
	Toluene	361	409	3250.95	0.0276
	Chloroform	365	411	3451.82	0.0100
	DCM	363	415	3066.36	0.0111
	Ethyl acetate	363	409	3098.33	0.0059
	DMF	364	417	3491.71	0.0118
	Acetonitrile	365	428	4026.77	0.0284

<sup>a</sup>The fluorescence quantum yields were recorded using 9,10-diphenylanthracene as a standard in ethanol solution.

The fluorescence spectra of phenanthroimidazoles **1** and **2** in the non-polar solvents display fine vibrational structure which vanishes in polar solvents; also, emission was red shifted in polar solvents. In non-polar solvent emission arises from the localised excited (LE) state whereas in polar solvents the emission is from charge transfer (CT) state. <sup>[14(b)]</sup> The solvatochromic properties have been compiled in Table 5.2.

### 5.6. Aggregation-induced emission

The TPE moiety is well established for its aggregation-induced emission (AIE) characteristics due to its inbuilt propeller shaped, following which fluorescence spectroscopy was used to study the aggregation-induced

emission (AIE) properties of phenanthroimidazoles **1** and **2** (Figure 5.6.). The phenanthroimidazoles **1** and **2** exhibit good solubility in THF and poor solubility in water. The gradual increase of water percentage in THF solution consequently initiates the formation of nanoaggregates.

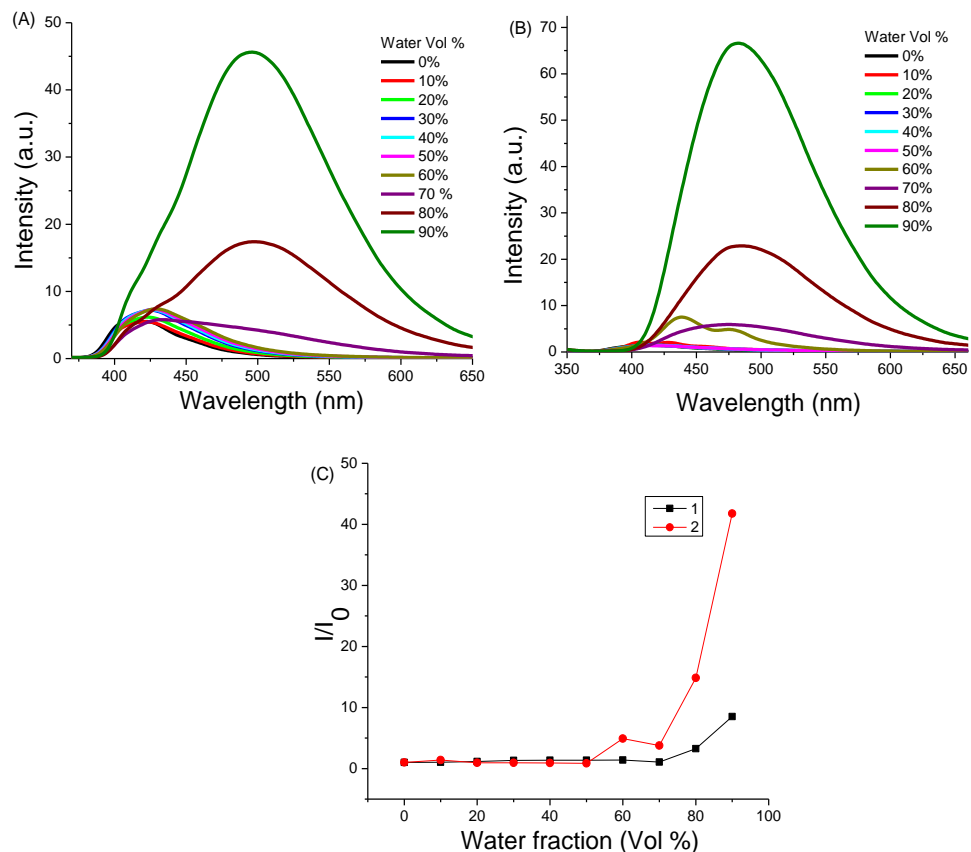


**Figure 5.6.** Fluorescence spectra of **1** (A) and **2** (B) in THF–water mixtures with different water fractions (10  $\mu$ M). (C) Plot of intensity vs % of water fraction ( $f_w$ ). Luminogen concentration: 10  $\mu$ M; intensity calculated at  $\lambda_{max}$ .

The phenanthroimidazoles **1** and **2** are weakly emissive at low water fraction. The relative PLQY at 0% water for **1** is 0.016 and for **2** is 0.005. The non-radiative energy loss of the excited state caused by the free rotation of phenyl rings of the TPE moiety in the solution state renders the solutions non-emissive. The formation of aggregates at higher water percentage restricts the free rotation of phenyl ring resulting in enhanced intensity and red shifted emission. The phenanthroimidazoles **1** and **2** exhibit increase in

the emission with a bathochromic shift above 60% water fractions respectively due to aggregate formation. There is slight decrease of  $I/I_0$  value at 70% water for both **1** and **2**. The phenanthroimidazole **2** has higher degree of enhancement in intensity as compared to phenanthroimidazole **1** which could be due to the positional effect. The superposition of the emission spectra of **1** and **2** (Figure 5.7.) at 90% water fraction gives a clear idea about the intensity enhancement. The aggregation-induced emission (AIE) behaviour was also studied using absorption spectroscopy (Figure 5.8.). The absorption spectra for phenanthroimidazoles **1** and **2** reveal similar trend of the absorption bands upto 60% water fraction, above which there is scattering of light or Mie effect observed due to formation of nanoaggregates. The aggregation-induced emission (AIE) behaviour of **1** and **2** is shown in photographs (Figure 5.9.) under UV illumination.

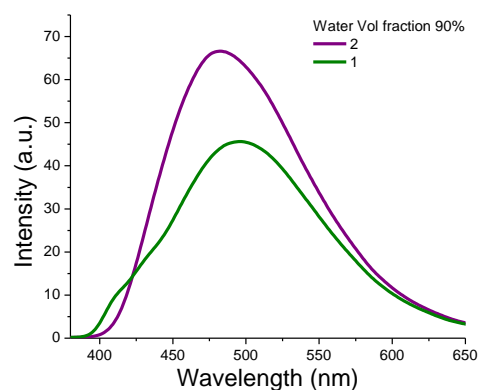


**Figure 5.7.** Emission spectra of **1** and **2** at 90% THF-water mixture.

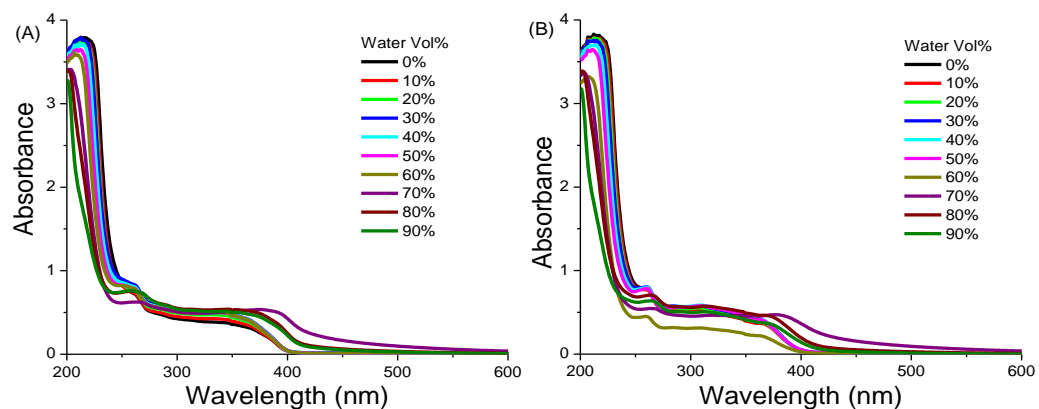


**Figure 5.8.** UV-vis absorption spectra of **1** (A) and **2** (B) in THF–water mixtures with different water fractions.

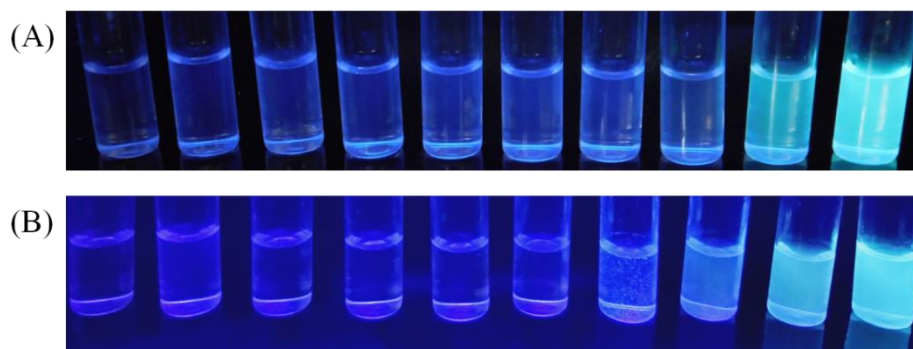


**Figure 5.9.** Photograph of **1** (A) and **2** (B) in THF–water mixtures with different water fractions (10  $\mu$ M) under 365 nm UV illumination (0% to 90% water fraction from left to right).

### 5.7. Mechanochromism

The phenanthroimidazoles **1** and **2** were presumed to display reversible mechanochromic behaviour on account of the twisted structure of the TPE moiety. The mechanochromic behaviour was studied using the fluorescence spectroscopy (Figure 5.10.) and the data are listed in Table 5.3.

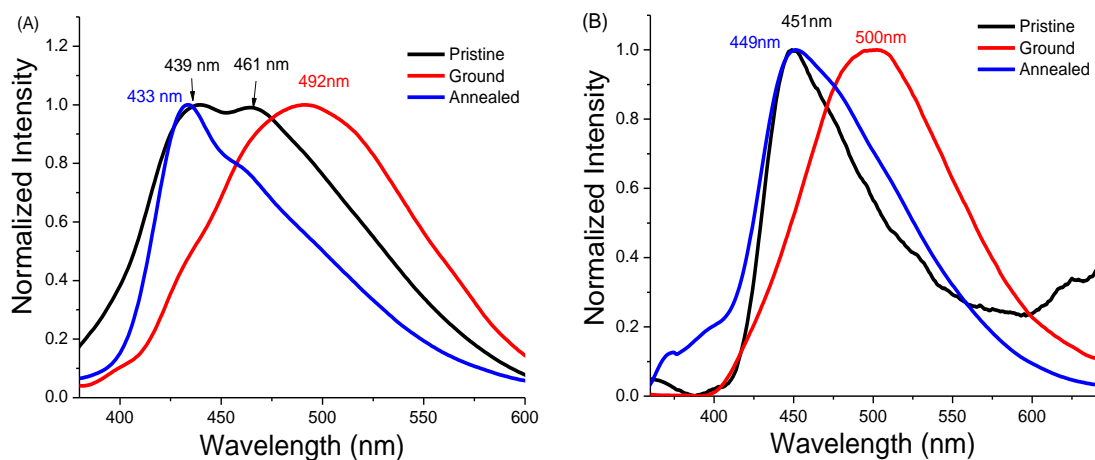


**Figure 5.10.** Emission spectra of **1** (A) and **2** (B) as pristine, ground, and annealed solids.

**Table 5.3.** Peak emission wavelengths ( $\lambda$ , in nm) of **1** and **2** as pristine, grinded and annealed solids.

Emission				
Compounds	$\lambda_{\text{pristine}}$ (nm)	$\lambda_{\text{ground}}$ (nm)	$\lambda_{\text{annealed}}$ (nm)	$\Delta\lambda^a$ (nm)
<b>1</b>	461	492	433	59
<b>2</b>	449	500	451	49

<sup>a</sup> Grinding-induced spectral shift,  $\Delta\lambda = \lambda_{\text{ground}} - \lambda_{\text{annealed}}$

The phenanthroimidazoles **1** and **2** were mechanically grinded with the aid of a mortar and pestle. The phenanthroimidazole **1** in its pristine form emits at 439 nm and a lower intensity peak at 461 nm with a bright sky-blue fluorescence, which was red shifted to 492 nm on grinding emitting a bright green fluorescence. In order to check the reversibility of the colour switching, the phenanthroimidazole **1** was annealed at 230 °C for five minutes which resulted in a same blue fluorescence as the pristine sample and with a higher blue shift in the emission wavelength upto 433 nm. The peak at 461 nm could be ascribed to intermediate species which arise from the gentle grinding of the pristine sample. However, a strong grinding results in 492 nm emission band. The results reflect a highly sensitive nature

of phenanthroimidazole **1** towards mechanical stimuli. The high sensitivity of phenanthroimidazole **1** could be due to the position of TPA and phenyl-TPE with phenyl-TPE directly attached to N atom of the imidazole ring. The phenanthroimidazole **2** similarly emitted a bright blue fluorescence at 449 nm which was red shifted on grinding to emit a bright green fluorescence at 500 nm reverting to its original form on annealing at 200 °C for five minutes. The absolute quantum yields for phenanthroimidazole **1** in their pristine, grinded and annealed forms are 34.04%, 32.85% and 51.34% respectively. The absolute quantum yields for phenanthroimidazole **2** in their pristine, grinded and annealed forms are 68.09%, 74.07% and 74.00% respectively.

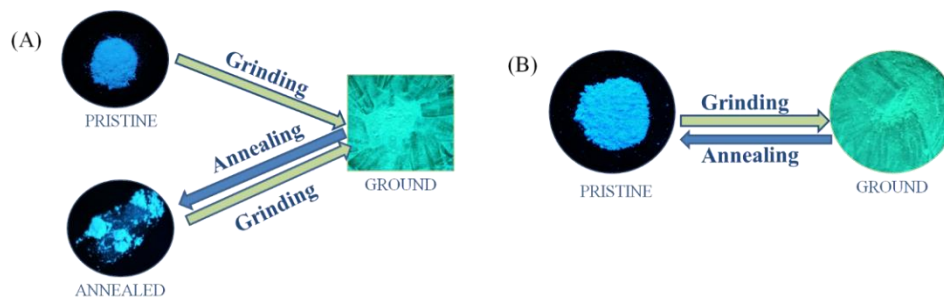


**Figure 5.11.** Photograph of **1** (A) and **2** (B) as pristine, ground, and annealed solids taken under 365 nm UV illumination.

The photographs of pristine, grinded and annealed solids taken under UV illumination are displayed in Figure 5.11. The phenanthroimidazoles **1** and **2** exhibited a grinding induced spectral shift of 59 nm and 49 nm respectively.

## 5.8. Powder X-ray diffraction studies

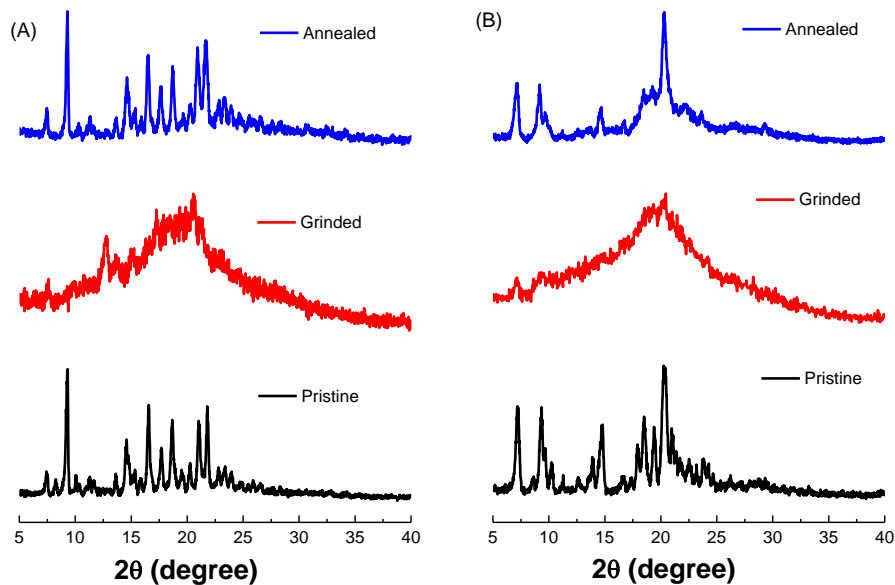


**Figure 5.12.** Powder X-ray diffraction curves of **1** (A) and **2** (B) in pristine, grinded and annealed forms.

The powder X-ray diffraction studies (PXRD) studies (Figure 5.12.) were performed to gain an insight about the morphological change which could be a possible reason associated with the reversible mechanochromic behaviour. The phenanthroimidazoles **1** and **2** in their pristine form displayed sharp and intense diffraction peaks which can be attributed to crystalline structures. The sharp diffraction peaks disappear on grinding giving a broad band indicating the morphological change from crystalline state to amorphous state caused due to grinding. The crystallinity of the phenanthroimidazoles is resumed on annealing which is clearly seen by the sharp diffraction peaks.

## 5.9. Single crystal X-ray analysis

The single crystal of **1**, **3** and **4** were obtained by slow diffusion of ethanol in DCM solution of the compounds. The single crystal of phenanthroimidazole **1** was beneficial in further understanding its mechanochromic and AIE behaviour.

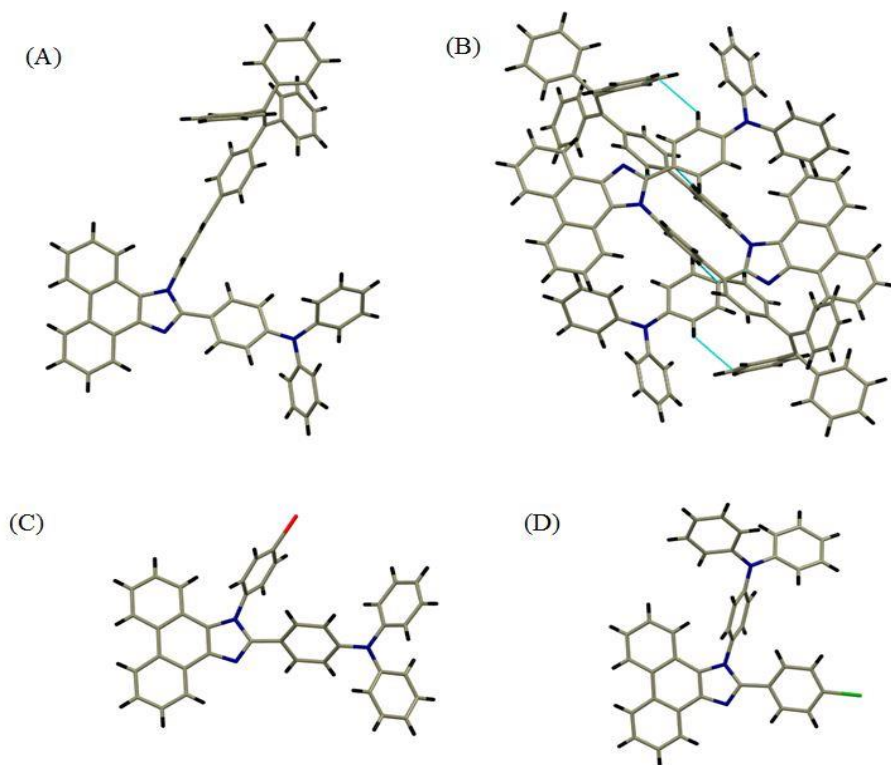


**Figure 5.13.** (A) Crystal structure of phenanthroimidazole **1**. (B) Packing diagram of phenanthroimidazole **1**. (C) Crystal structure of intermediate **3**. (D) Crystal structure of intermediate **4**.

The single crystal of **1** (Figure 5.13.(A)) shows that the TPA and phenyl-TPE unit adopt twisted conformations. In aggregated state, the twisted conformation brings a restraint on the  $\pi$ - $\pi$  stacking interaction resulting in intensified emissions. The crystal packing diagram reveals only C-H interactions and no H-bonding or  $\pi$ - $\pi$  interactions which make it loosely packed making it sensitive to grinding thereby allowing mechanochromism. The single crystal of intermediate **3** (Figure 5.13.(C)) and **4** (Figure 5.13.(D)) reveal a propeller orientation of the TPA unit. The TPA unit and the iodo-substituted phenyl ring in intermediate **3** are not in plane of the phenanthroimidazole unit and exhibit highly twisted geometry. Similarly, the TPA unit in intermediate **4** has a highly twisted geometry. However, the bromo-substituted phenyl ring is coplanar to the phenanthroimidazole unit with a slight twisting. The data for the crystals are summarized in Table 5.4.

**Table 5.4.** Crystal data and structure refinement for **1**, **3** and **4**.

Identification code		rm230	rm193
Empirical formula	C <sub>65</sub> H <sub>45</sub> N <sub>3</sub>	C <sub>39</sub> H <sub>27</sub> I N <sub>3</sub>	C <sub>39</sub> H <sub>26</sub> BrN <sub>3</sub>
Formula weight	868.04	664.53	616.54
Temperature	293(2) K	293(2) K	293(2) K
Wavelength	1.54184 Å	0.71073 Å	0.71073 Å
Crystal system, space group	Triclinic, P -1	Triclinic, P -1	Monoclinic, P21/n
a/(Å)	11.0325(4)	8.1689(12) Å	16.0838(5)
b/(Å)	13.8922(5)	11.2594(9) Å	6.9446(2)
c/(Å)	17.6967(8)	17.439(2) Å	26.8363(7)
Alpha/(°)	100.024(4)	96.245(9)	90
Beta/(°)	94.455(4)	91.993(13)	91.926(3)
Gamma/(°)	109.496(4)	101.903(10)	90
Volume	2490.68(18) Å <sup>3</sup>	1557.4(3) Å <sup>3</sup>	2995.80(15) Å <sup>3</sup>
Z, Calculated density	2, 1.157 mg/m <sup>-3</sup>	2, 1.417 mg/m <sup>-3</sup>	4, 1.367 Mg/m <sup>-3</sup>
Absorption coefficient	0.513 mm <sup>-1</sup>	1.060 mm <sup>-1</sup>	1.405 mm <sup>-1</sup>
F(000)	912	670	1264
Crystal size	0.230 x 0.180 x 0.120 mm	0.230 x 0.180 x 0.130 mm	0.260 x 0.210 x 0.180 mm
Θ range for data collection/(°)	3.454 to 71.472	3.032 to 28.846	2.911 to 32.252
Reflections collected / unique	16838 / 9463 [R(int) = 0.0683]	13182 / 7155 [R(int) = 0.0921]	37707 / 9935 [R(int) = 0.0923]
Completeness to theta	Θ = 67.684 99.8 %	Θ = 25.242 99.8 %	Θ = 25.242 99.9 %

Absorption correction	Semi-empirical from equivalents	Semi-empirical from equivalents	Semi-empirical from equivalents
Max. and min. transmission	1.00000 and 0.70721	1.00000 and 0.48753	1.00000 and 0.78417
Refinement method	Full-matrix least-squares on F <sup>2</sup>	Full-matrix least-squares on F <sup>2</sup>	Full-matrix least-squares on F <sup>2</sup>
Data / restraints / parameters	9463 / 630 / 669	7155 / 0 / 389	9935 / 0 / 389
Goodness-of-fit on F <sup>2</sup>	1.072	1.316	1.005
Final R indices [I > 2σ(I)]	R1 = 0.0780, wR2 = 0.2241	R1 = 0.1382, wR2 = 0.3736	R1 = 0.0630, wR2 = 0.1208
R indices (all data)	R1 = 0.0889, wR2 = 0.2348	R1 = 0.1809, wR2 = 0.4207	R1 = 0.1815, wR2 = 0.1661
Extinction coefficient	n/a	0.072(10)	0.0014(3)
Largest diff. peak and hole (e.Å <sup>-3</sup> )	0.348 and -0.387	1.848 and -1.929	0.351 and -0.531

## 5.10. Theoretical calculations

In order to get a clear understanding about the geometry and electronic structures of phenanthroimidazoles **1** and **2**, the density functional theory (DFT) calculations were performed at the B3LYP/6-31G(d,p) level.<sup>[18]</sup> The optimized structures, calculated highest occupied molecular orbital (HOMO) and lowest unoccupied molecular orbital (LUMO) for phenanthroimidazoles **1** and **2** are as shown in Figure 5.14. and the data are compiled in Table 5.5.

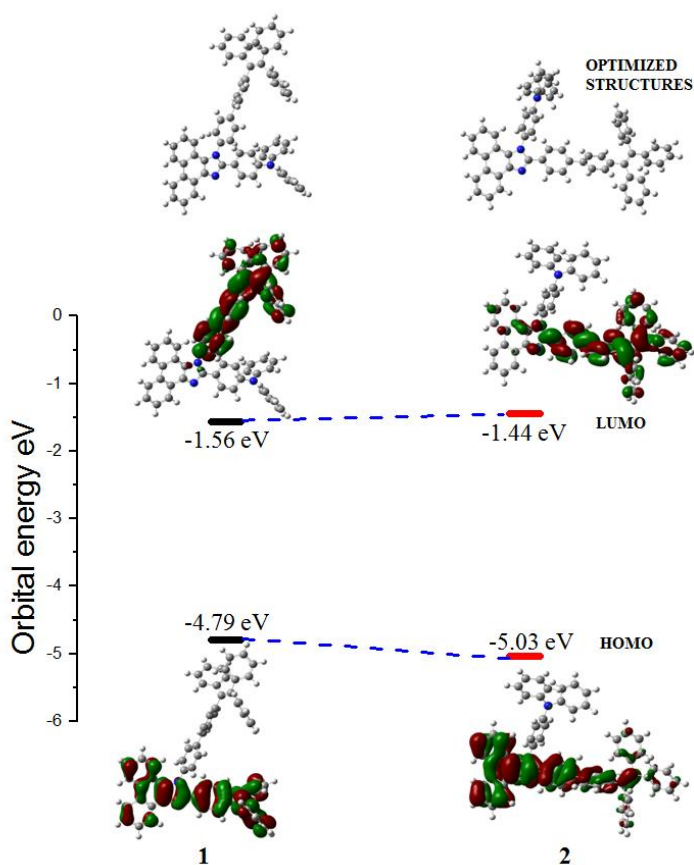


**Figure 5.14.** Correlation diagram showing the optimized structures, HOMO and LUMO wave functions and energies of **1** (left) and **2** (right), as determined at the B3LYP/6-31G(d,p) level.

The optimized structures of phenanthroimidazoles **1** and **2** reveal a twisted geometry of the TPE and TPA unit. The HOMO and LUMO are well

separated in phenanthroimidazole **1**, the HOMO mainly localized on the phenanthroimidazole and the TPA unit whereas the LUMO is localized on the TPE unit. However, in phenanthroimidazole **2** the HOMO and LUMO are not well separated and mainly localized on the TPE and imidazole unit. The attachment of the TPE unit through the N atom of the phenanthroimidazole in **1** causes a disruption in the extended conjugation resulting in a better separation of the molecular orbitals. In phenanthroimidazole **2**, the TPE unit is attached by the carbon atom of the imidazole ring producing a highly extended conjugation allowing the molecular orbitals to be delocalized on the whole molecule. The theoretical HOMO–LUMO gap of phenanthroimidazole **1** and **2** are 3.23 eV and 3.59 eV respectively.

### 5.11. Electrochemical studies

The electrochemical properties and the energy levels of the phenanthroimidazoles **1** and **2** were examined by performing the cyclic voltammetry experiment in dichloromethane (DCM) using tetrabutylammonium hexafluorophosphate (TBAPF<sub>6</sub>) as a supporting electrolyte. The cyclic voltamograms (Figure 5.15.) of phenanthroimidazole **1** and **2** reveal quasi-reversible oxidation and reduction waves. The energies for highest occupied molecular orbital (HOMO) and lowest unoccupied molecular orbital (LUMO) were calculated by applying the equation  $\text{HOMO/LUMO} = - (E_{\text{onset}} + 4.4) \text{ eV}$ , where  $E_{\text{onset}}$  is value of onset of oxidation or reduction wave<sup>[19]</sup> The energy values for HOMO of phenanthroimidazole **1** and **2** are -5.12 eV and -5.36 eV respectively, whereas the energy values for LUMO of **1** and **2** are -3.48 eV and -3.54 eV respectively.

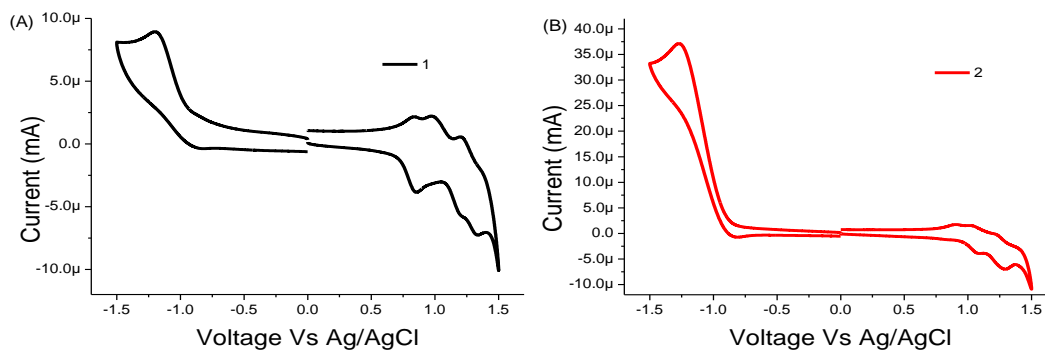


**Figure 5.15.** Cyclic voltammetry (CV) plots of **1**(A) and **2**(B).

The resulting electrochemical HOMO-LUMO gap for phenanthroimidazoles **1** and **2** are 1.64 eV and 1.82 eV respectively. The electrochemical HOMO-LUMO gap and theoretical HOMO-LUMO gap follow the same trend and are higher for the phenanthroimidazole **2**. The data of electrochemical studies are compiled in Table 5.5.

**Table 5.5.** Electrochemical and theoretical properties of **1** and **2**.

No.	Electrochemical properties		Theoretical properties			
	HOMO <sup>a</sup> eV	LUMO <sup>a</sup> eV	HOMO- LUMO gap eV	HOMO <sup>b</sup> eV	LUMO <sup>b</sup> eV	HOMO- LUMO gap Ev
<b>1</b>	-5.12	-3.48	1.64	-4.79	-1.56	3.23
<b>2</b>	-5.36	-3.54	1.82	-5.03	-1.44	3.59

<sup>a</sup> Calculated from CV: Reference electrode- Ag/AgCl <sup>b</sup> Theoretical values at B3LYP/6-31g(d,p) level.++iop v+.

## 5.12. Experimental details

### General Methods

Chemicals were used as received unless otherwise indicated. All oxygen or moisture sensitive reactions were performed under nitrogen/argon atmosphere. <sup>1</sup>H NMR (400 MHz) and <sup>13</sup>C NMR (100 MHz) spectra were

recorded on a Bruker Avance III instrument by using CDCl<sub>3</sub>. <sup>1</sup>H NMR chemical shifts are reported in parts per million (ppm) relative to the solvent residual peak (CDCl<sub>3</sub>, 7.26 ppm). Multiplicities are given as s (singlet), d (doublet), t (triplet) and m (multiplet), and the coupling constants, *J*, are given in hertz. <sup>13</sup>C NMR chemical shifts are reported relative to the solvent residual peak (CDCl<sub>3</sub>, 77.0 ppm). Thermogravimetric analyses were performed on the Mettler Toledo thermal analysis system. UV–visible absorption spectra were recorded on a Cary-100 Bio UV–visible spectrophotometer. Emission spectra were taken in a The Fluoromax-4C, S/n.1579D-1417-FM Fluorescence software Ver 3.8.0.60. The excitation and emission slits were 2/2 nm for the emission measurements. All of the measurements were done at 25 °C. HRMS were recorded on a Bruker-Daltonics micrOTOF-Q II mass spectrometer. The voltammograms were recorded on a CHI620D electrochemical analyzer in dichloromethane solvent and 0.1 M TBAF<sub>6</sub> as the supporting electrolyte. The electrodes used were glassy carbon as a working electrode, Pt wire as a counter electrode and Ag/AgCl as a reference electrode. Single-crystal X-ray structural studies of **1** and **4** were performed on a CCD equipped SUPERNOVA diffractometer from Agilent Technologies with Oxford Instruments low-temperature attachment under argon/nitrogen using standard Schlenk and vacuum-line techniques.

### **Synthesis and characterization of intermediates 3 and 4:**

**3:** A mixture of 9,10-phenanthrenequinone (2.54 mmol), 4-(diphenylamino)benzaldehyde (2.80 mmol), 4-iodoaniline (3.04 mmol) and ammonium acetate (25.4 mmol) was refluxed in glacial acetic acid (10 mL) were for 4 h under an argon atmosphere. The reaction was cooled to room temperature and was added to a methanol solution with continuous stirring. The resulting solid was filtered, washed with 30 mL water and dried to obtain intermediate **3** as a pale yellow solid. Yield: 92%. <sup>1</sup>H NMR (400 MHz, CDCl<sub>3</sub>, 25 °C): δ 8.86 (d, *J* = 8.0 Hz, 1H), 8.77 (d, *J* = 8.0 Hz, 1H),

8.70 (d,  $J = 8.0$  Hz, 1H), 7.94 (d,  $J = 8.0$  Hz, 2H), 7.73 (t,  $J = 8.0$  Hz, 1H), 7.65 (t,  $J = 8.0$  Hz, 1H), 7.52 (t,  $J = 8.0$  Hz, 1H), 7.41 (d,  $J = 8.0$  Hz, 2H), 7.26–7.34 (m, 7H), 7.19 (d,  $J = 8.0$  Hz, 1H), 7.05–7.11 (m, 6H), 6.97 (d,  $J = 8.0$  Hz, 1H).  $^{13}\text{C}$  NMR (100 MHz,  $\text{CDCl}_3$ , 25 °C):  $\delta$  150.7, 148.6, 147.1, 139.4, 138.7, 131.0, 130.1, 129.4, 129.2, 128.2, 127.7, 127.3, 127.0, 126.4, 125.7, 125.1, 124.9, 124.2, 123.6, 123.1, 122.8, 121.8, 120.6, 0.0 ppm. HRMS (ESI): Calcd. for  $[\text{M} + \text{H}]^+$ : 664.128. Found: 664.1244.

**4:** A mixture of 9,10-phenanthrenequinone (3.60 mmol), 4-bromobenzaldehyde (3.96 mmol),  $\text{N}'\text{,N}'$ -diphenylbenzene-1,4-diamine (4.32 mmol) and ammonium acetate (36.0 mmol) was refluxed in glacial acetic acid (15 mL) were for 4 h under an argon atmosphere. The reaction was cooled to room temperature and was poured in methanol solution with continuous stirring. The resulting solid was filtered, washed with 30 mL water and dried to give intermediate **4** as a grey coloured solid. Yield: 91%.  $^1\text{H}$  NMR (400 MHz,  $\text{CDCl}_3$ , 25 °C):  $\delta$  8.84 (d,  $J = 8.0$  Hz, 1H), 8.76 (d,  $J = 8.0$  Hz, 1H), 8.70 (d,  $J = 8.0$  Hz, 1H), 7.74 (t,  $J = 8.0$  Hz, 1H), 7.65 (t,  $J = 8.0$  Hz, 1H), 7.46–7.58 (m, 6H), 7.35–7.42 (m, 5H), 7.27–7.30 (m, 2H), 7.20–7.24 (m, 6H), 7.14 (t,  $J = 8.0$  Hz, 2H).  $^{13}\text{C}$  NMR (100 MHz,  $\text{CDCl}_3$ , 25 °C):  $\delta$  149.8, 149.1, 146.9, 137.2, 131.3, 131.1, 130.8, 129.6, 129.6, 129.5, 129.3, 128.4, 128.2, 127.3, 127.1, 126.2, 125.6, 125.3, 125.0, 124.2, 124.1, 123.3, 123.1, 123.0, 122.7, 122.6, 120.9, 0.0 ppm. HRMS (ESI): Calcd. for  $[\text{M} + \text{H}]^+$ : 616.1363. Found: 616.1383.

### **Synthesis and characterization of phenanthroimidazoles **1** and **2**:**

General procedure for synthesis of phenanthroimidazole **1** and **2**.  $\text{Pd}(\text{PPh}_3)_4$  (0.04 mmol) was added to a well degassed solution of intermediate **3** (0.4 mmol), 4-(1,2,2-triphenylvinyl)phenylboronic acid pinacol ester (0.52 mmol),  $\text{K}_2\text{CO}_3$  (2.0 mmol) in a mixture of toluene (24.0 mL)/ethanol (8.0 mL)/ $\text{H}_2\text{O}$  (4.0 mL). The resulting mixture was stirred at 80 °C for 24 h under an argon atmosphere. After cooling, the mixture was evaporated to dryness and the residue subjected to column chromatography on silica (Hexane–

DCM 50:50 in vol) to yield the desired product **1** as a white powder. The same procedure was employed using intermediate **4** to obtain the desired product **2** as a white powder.

**1.** Yield: 68%. <sup>1</sup>H NMR (400 MHz, CDCl<sub>3</sub>, 25 °C): δ 8.87 (d, *J* = 8.0 Hz, 1H), 8.77 (d, *J* = 8.0 Hz, 1H), 8.71 (d, *J* = 8.0 Hz, 1H), 7.80 (d, *J* = 8.0 Hz, 2H), 7.73 (t, *J* = 8.0 Hz, 1H), 7.62 (t, *J* = 8.0 Hz, 1H), 7.47–7.57 (m, 7H), 7.23–7.27 (m, 8H), 7.02–7.20 (m, 22H), 6.95 (d, *J* = 8.0 Hz, 2H). <sup>13</sup>C NMR (100 MHz, CDCl<sub>3</sub>, 25 °C): δ 147.2, 143.9, 143.6, 143.6, 141.8, 141.5, 140.2, 137.0, 132.1, 131.4, 131.3, 130.1, 129.4, 129.3, 129.1, 128.3, 127.9, 127.8, 127.7, 126.6, 126.6, 126.3, 125.0, 124.1, 123.5, 123.1, 121.9, 124.1, 120.9, 0.0 ppm. HRMS(ESI): Calcd. for [M + H]<sup>+</sup>: 868.3687. Found: 868.3686.

**2.** Yield: 76%. <sup>1</sup>H NMR (400 MHz, CDCl<sub>3</sub>, 25 °C): δ 8.87 (d, *J* = 8.0 Hz, 1H), 8.79 (d, *J* = 8.0 Hz, 1H), 8.71 (d, *J* = 8.0 Hz, 1H), 7.72–7.76 (m, 3H), 7.65 (t, *J* = 8.0 Hz, 1H), 7.53–7.57 (m, 3H), 7.48 (d, *J* = 8.0 Hz, 1H), 7.32–7.41 (m, 9H), 7.20–7.23 (m, 7H), 7.04–7.13 (m, 19H). <sup>13</sup>C NMR (100 MHz, CDCl<sub>3</sub>, 25 °C): δ 150.8, 149.0, 147.0, 143.7, 143.7, 143.2, 141.3, 140.7, 140.7, 140.4, 137.9, 137.4, 131.9, 131.6, 131.4, 131.3, 131.3, 129.7, 129.7, 129.6, 129.4, 129.3, 128.4, 128.2, 127.8, 127.7, 127.6, 127.3, 127.2, 126.5, 126.5, 126.5, 126.2, 126.1, 125.5, 125.2, 124.8, 124.1, 124.0, 123.2, 123.1, 122.8, 122.7, 0.0 ppm. HRMS(ESI): Calcd. for [M + H]<sup>+</sup>: 868.3701. Found: 868.3686.

### 5.13. Conclusion

In conclusion, we have designed and synthesized positional isomers of phenanthroimidazole comprising of a phenyl-TPE and TPA unit, using a Suzuki cross-coupling reaction. The phenanthroimidazole **1** and **2** exhibit high thermal stability making them suitable for practical applications. The single crystal of phenanthroimidazole **1** reveals a propeller orientation of the TPA unit and TPE unit which is well in accordance with the theoretically optimized structure. The phenanthroimidazole **1** and **2** display strong aggregation-induced emission (AIE) characteristics and are excellent solid-

state emitters. The phenanthroimidazole **1** and **2** display reversible emission changes in response to mechanical stimuli with a good colour contrast. The positional change results in the high sensitivity of phenanthroimidazole **1** towards mechanical stimuli as compared to **2**. The PXRD studies show that a morphological change from amorphous state to crystalline state is associated with the color change. The DFT studies reveal better separation of HOMO and LUMO in phenanthroimidazole **1** compared to phenanthroimidazole **2** which is an attribute of the positions. The inclusion of TPA and TPE on the phenanthroimidazole unit provides a new approach for the development of stimuli responsive solid-state emitters. The combination of phenanthroimidazole, TPA and TPE synergistically result in the high solid-state emission which can be further employed in optoelectronic applications.

#### 5.14. References

- [1] (a) Chi, Z., Zhang, X., Xu, B., Zhou, X., Ma, C., Zhang, Y., Xu, J. (2012). Recent advances in organic mechanofluorochromic materials. *Chem. Soc. Rev.*, *41*(10), 3878-3896 (DOI: 10.1039/C2CS35016E); (b) Sagara, Y., Kato, T. (2009). Mechanically induced luminescence changes in molecular assemblies. *Nat. Chem.*, *1*(8), 605-610 (DOI: 10.1038/nchem.411); (c) Sagara, Y., Yamane, S., Mitani, M., Weder, C., Kato, T. (2016). Mechanoresponsive luminescent molecular assemblies: an emerging class of materials. *Adv. Mater.*, *28*(6), 1073-1095 (DOI: 10.1002/adma.201502589); (d) Ito, H., Saito, T., Oshima, N., Kitamura, N., Ishizaka, S., Hinatsu, Y., Wakeshima, M., Kato, M., Tsuge, K., Sawamura, M. (2008). Reversible mechanochromic luminescence of [(C<sub>6</sub>F<sub>5</sub>Au)<sub>2</sub>( $\mu$ -1, 4-diisocyanobenzene)]. *J. Am. Chem. Soc.*, *130*(31), 10044-10045 (DOI: 10.1021/ja8019356); (e) Xu, J., Chi, Z. (Eds.). (2014). *Mechanochromic Fluorescent Materials: Phenomena, Materials and Applications*. Royal Society of Chemistry (DOI:

- 10.1039/9781782623229-00001); (f) Weder, C. (2011). Mechanoresponsive materials. *J. Mater. Chem.*, *21*(23), 8235-8236 (DOI: 10.1039/C1JM90068D); (g) Ciardelli, F., Ruggeri, G., Pucci, A. (2013). Dye-containing polymers: methods for preparation of mechanochromic materials. *Chem. Soc. Rev.*, *42*(3), 857-870 (DOI: 10.1039/C2CS35414D).
- [2] (a) Saragi, T. P., Spehr, T., Siebert, A., Fuhrmann-Lieker, T., Salbeck, J. (2007). Spiro compounds for organic optoelectronics. *Chem. Rev.*, *107*(4), 1011-1065 (DOI: 10.1021/cr0501341); (b) Liang, J., Tang, B. Z., Liu, B. (2015). Specific light-up bioprobes based on AIEgen conjugates. *Chem. Soc. Rev.*, *44*(10), 2798-2811 (DOI: 10.1039/C4CS00444B); (c) Yuan, L., Lin, W., Zheng, K., He, L., Huang, W. (2013). Far-red to near infrared analyte-responsive fluorescent probes based on organic fluorophore platforms for fluorescence imaging. *Chem. Soc. Rev.*, *42*(2), 622-661 (DOI: 10.1039/C2CS35313J); (d) Zhu, Y. X., Wei, Z. W., Pan, M., Wang, H. P., Zhang, J. Y., Su, C. Y. (2016). A new TPE-based tetrapodal ligand and its Ln (III) complexes: multi-stimuli responsive AIE (aggregation-induced emission)/ILCT (intraligand charge transfer)-bifunctional photoluminescence and NIR emission sensitization. *Dalton Trans.*, *45*(3), 943-950 (DOI: 10.1039/C5DT03640B); (e) Zheng, R., Mei, X., Lin, Z., Zhao, Y., Yao, H., Lv, W., Ling, Q. (2015). Strong CIE activity, multi-stimuli-responsive fluorescence and data storage application of new diphenyl maleimide derivatives. *J. Mater. Chem. C*, *3*(39), 10242-10248 (DOI: 10.1039/C5TC02374B); (f) Toal, S. J., Jones, K. A., Magde, D., Trogler, W. C. (2005). Luminescent silole nanoparticles as chemoselective sensors for Cr (VI). *J. Am. Chem. Soc.*, *127*(33), 11661-11665 (DOI: 10.1021/ja052582w); (g) Xu, B., Xie, M., He, J., Xu, B., Chi, Z., Tian, W., Jiang, L., Zhao, Fuli., Liu, S., Zhang, Y., Xu, Z., Xu, J. (2013). An aggregation-induced emission luminophore with multi-stimuli single-and two-photon fluorescence switching and large two-

photon absorption cross section. *Chem. Commun.*, 49(3), 273-275 (10.1039/C2CC36806D); (h) Davis, D. A., Hamilton, A., Yang, J., Cremar, L. D., Van Gough, D., Potisek, S. L., Ong, M. T., Braun, P. V., Martinez, T. J., White, S. R., Moore, J. S., Sottos, N. R. (2009). Force-induced activation of covalent bonds in mechanoresponsive polymeric materials. *Nature*, 459(7243), 68-72 (DOI: 10.1038/nature07970); (i) Ning, Z., Chen, Z., Zhang, Q., Yan, Y., Qian, S., Cao, Y., Tian, H. (2007). Aggregation-induced emission (AIE)-active starburst triarylamine fluorophores as potential non-doped red emitters for organic light-emitting diodes and Cl<sub>2</sub> gas chemodosimeter. *Adv. Funct. Mater.*, 17(18), 3799-3807 (DOI: 10.1002/adfm.200700649); (j) Kishimura, A., Yamashita, T., Yamaguchi, K., Aida, T. (2005). Rewritable phosphorescent paper by the control of competing kinetic and thermodynamic self-assembling events. *Adv. Funct. Mater.*, 4(7), 546-549 (DOI: 10.1038/nmat1401); (h) Crenshaw, B. R., Burnworth, M., Khariwala, D., Hiltner, A., Mather, P. T., Simha, R., Weder, C. (2007). Deformation-induced color changes in mechanochromic polyethylene blends. *Macromolecules*, 40(7), 2400-2408 (DOI: 10.1021/ma062936j); (k) Hirata, S., Watanabe, T. (2006). Reversible thermoresponsive recording of fluorescent images (TRF). *Adv. Mater.*, 18(20), 2725-2729 (DOI: 10.1002/adma.200600209); (l) Kwon, M. S., Gierschner, J., Yoon, S. J., Park, S. Y. (2012). Unique piezochromic fluorescence behavior of dicyanodistyrylbenzene based donor-acceptor-donor triad: mechanically controlled photo-induced electron transfer (eT) in molecular assemblies. *Adv. Mater.*, 24(40), 5487-5492 (DOI: 10.1002/adma.201202409); (m) Sun, H., Liu, S., Lin, W., Zhang, K. Y., Lv, W., Huang, X., Huo, F., Yang, H., Jenkins, G., Zhao, Q., Huang, W. (2014). Smart responsive phosphorescent materials for data recording and security protection. *Nat. Commun.*, 5(1), 1-9 (DOI: 10.1038/ncomms4601).

- [3] (a) Zhang, X., Chi, Z., Zhang, Y., Liu, S., Xu, J. (2013). Recent advances in mechanochromic luminescent metal complexes. *J. Mater. Chem. C*, *1*(21), 3376-3390 (DOI: 10.1039/C3TC30316K); (b) Luo, X., Li, J., Li, C., Heng, L., Dong, Y. Q., Liu, Z., Bo, Z., Tang, B. Z. (2011). Reversible switching of the emission of diphenyldibenzofulvenes by thermal and mechanical stimuli. *Adv. Mater.*, *23*(29), 3261-3265 (DOI: 10.1002/adma.201101059); (c) Yoon, S. J., Chung, J. W., Gierschner, J., Kim, K. S., Choi, M. G., Kim, D., Park, S. Y. (2010). Multistimuli two-color luminescence switching via different slip-stacking of highly fluorescent molecular sheets. *J. Am. Chem. Soc.*, *132*(39), 13675-13683 (DOI: 10.1021/ja1044665).
- [4] (a) Ito, H., Saito, T., Oshima, N., Kitamura, N., Ishizaka, S., Hinatsu, Y., Wakeshima, M., Kato, M., Tsuge, K., Sawamura, M. (2008). Reversible mechanochromic luminescence of [(C<sub>6</sub>F<sub>5</sub>Au)<sub>2</sub>(μ-1, 4-)]<sup>+</sup>. *J. Am. Chem. Soc.*, *130*(1), 101-105 (DOI: 10.1021/ja8019356); (b) Chandaluri, C. G., Radhakrishnan, T. P. (2012). Amorphous-to-Crystalline Transformation with Fluorescence Enhancement and Switching of Molecular Nanoparticles Fixed in a Polymer Thin Film. *Angew. Chem., Int. Ed.*, *51*(47), 11849-11852 (DOI: 10.1002/anie.201205081); (c) Zhang, G., Lu, J., Sabat, M., Fraser, C. L. (2010). Polymorphism and reversible mechanochromic luminescence for solid-state difluoroboron avobenzene. *J. Am. Chem. Soc.*, *132*(7), 2160-2162 (DOI: 10.1021/ja9097719); (d) Dong, Y., Xu, B., Zhang, J., Tan, X., Wang, L., Chen, J., Lv, H., Wen, S., Li, B., Ye, L., Zou, B., Tian, W. (2012). Piezochromic luminescence based on the molecular aggregation of 9, 10-Bis ((E)-2-(pyrid-2-yl) vinyl) anthracene. *Angew. Chem., Int. Ed.*, *51*(43), 10782-10785 (DOI: 10.1002/anie.201204660); (e) Zhang, H., Gao, F., Cao, X., Li, Y., Xu, Y., Weng, W., Boulatov, R. (2016). Mechanochromism and mechanical-force-triggered cross-linking from a single reactive moiety incorporated into polymer chains. *Angew. Chem., Int. Ed.*, *128*(9), 3092-3096 (DOI: 10.1002/anie.201510171).

- [5] (a) Mutai, T., Satou, H., Araki, K. (2005). Reproducible on–off switching of solid-state luminescence by controlling molecular packing through heat-mode interconversion. *Nat. Mater.*, 4(9), 685-687 (DOI: 10.1038/nmat1454); (b) Yuan, W. Z., Tan, Y., Gong, Y., Lu, P., Lam, J. W., Shen, X. Y., Feng, C., Sung, H.H.Y., Lu, Y., Williams, I.D., Sun, J.Z., Zhang, Z., Tang, B. Z. (2013). Synergy between twisted conformation and effective intermolecular interactions: strategy for efficient mechanochromic luminogens with high contrast. *Adv. Mater.*, 25(20), 2837-2843 (DOI: 10.1002/adma.201205043); (c) Zhang, X., Chi, Z., Xu, B., Jiang, L., Zhou, X., Zhang, Y., Liu, S., Xu, J. (2012). Multifunctional organic fluorescent materials derived from 9, 10-distyrylanthracene with alkoxy endgroups of various lengths *Chem. Commun.*, 48(88), 10895-10897 (DOI: 10.1039/C2CC36263E); (d) Xue, S., Liu, W., Qiu, X., Gao, Y., Yang, W. (2014). Remarkable isomeric effects on optical and optoelectronic properties of N-phenylcarbazole-capped 9, 10-divinylanthracenes. *J. Phys. Chem. C.*, 118(32), 18668-18675 (DOI: 10.1021/jp505527f); (e) Misra, R., Jadhav, T., Dhokale, B., Mobin, S. M. (2014). Reversible mechanochromism and enhanced AIE in tetraphenylethene substituted phenanthroimidazoles. *Chem. Commun.*, 50(65), 9076-9078 (DOI: 10.1039/C4CC02824D).
- [6] (a) Jadhav, T., Dhokale, B., Mobin, S. M., Misra, R. (2015). Mechanochromism and aggregation induced emission in benzothiazole substituted tetraphenylethylenes: a structure function correlation. *RSC Adv.*, 5(38), 29878-29884 (DOI: 10.1039/C5RA04881H); (b) Yoshii, R., Hirose, A., Tanaka, K., Chujo, Y. (2014). Functionalization of boron diimines with unique optical properties: multicolor tuning of crystallization-induced emission and introduction into the main chain of conjugated polymers. *J. Am. Chem. Soc.*, 136(52), 18131-18139 (DOI: 10.1021/ja510985v); (c) Nguyen, N. D., Zhang, G., Lu, J., Sherman, A. E., Fraser, C. L. (2011). Alkyl chain length effects on solid-state

- difluoroboron  $\beta$ -diketonate mechanochromic luminescence. *J. Mater. Chem.*, *21*(23), 8409-8415 (DOI: 10.1039/C1JM00067E); (d) Ning, Z., Chen, Z., Zhang, Q., Yan, Y., Qian, S., Cao, Y., Tian, H. (2007). Aggregation-induced emission (AIE)-active starburst triarylamine fluorophores as potential non-doped red emitters for organic light-emitting diodes and Cl<sub>2</sub> gas chemodosimeter. *Adv. Funct. Mater.*, *17*(18), 3799-3807 (DOI: 10.1002/adfm.200700649).
- [7] (a) Kwok, H. S., Zhan, X., Liu, Y., Zhuc, D., Tang, B. Z. (2001). Jingdong Luo, Zhiliang Xie, Jacky WY Lam, Lin Cheng, Haiying Chen, b Chengfeng Qiu, b. *Chem. Commun*, *1740*, 1741 (DOI: 10.1039/B105159H); (b) Li, Y., Liu, T., Liu, H., Tian, M. Z., Li, Y. (2014). Self-assembly of intramolecular charge-transfer compounds into functional molecular systems. *Acc. Chem. Res.*, *47*(4), 1186-1198 (DOI: 10.1021/ar400264e); (c) Liu, H., Xu, J., Li, Y., Li, Y. (2010). Aggregate nanostructures of organic molecular materials. *Acc. Chem. Res.*, *43*(12), 1496-1508 (DOI: 10.1021/ar100084y); (d) Hong, Y., Lam, J. W., Tang, B. Z. (2011). Aggregation-induced emission. *Chem. Soc. Rev.*, *40*(11), 5361-5388 (DOI: 10.1039/C1CS15113D).
- [8] (a) v. Büнау, G. (1970). JB Birks: Photophysics of Aromatic Molecules. Wiley-Interscience, London 1970. 704 Seiten. Preis: 210s. (DOI: 10.1002/bbpc.19700741223).
- [9] (a) Jayanty, S., Radhakrishnan, T. P. (2004). Enhanced fluorescence of remote functionalized diaminodicyanoquinodimethanes in the solid state and fluorescence switching in a doped polymer by solvent vapors. *Chem. – Eur. J.*, *10*(3), 791-797 (DOI: 10.1002/chem.200305123); (b) Tracy, H. J., Mullin, J. L., Klooster, W. T., Martin, J. A., Haug, J., Wallace, S., Rudloe, I., Watts, K. (2005). Enhanced photoluminescence from group 14 metalloles in aggregated and solid solutions. *Inorg. Chem.*, *44*(6), 2003-2011 (DOI: 10.1021/ic049034o); (c) Th. Forster, K. Z. Kasper, *Phys. Chem.*, (Munich) 1954, 1, 275-282.

- [10] (a) Dong, Y., Lam, J. W., Qin, A., Liu, J., Li, Z., Tang, B. Z., Sun, J., Kwok, H. S. (2007). Aggregation-induced emissions of tetraphenylethene derivatives and their utilities as chemical vapor sensors and in organic light-emitting diodes. *Appl. Phys. Lett.*, *91*(1), 011111 (DOI: 10.1063/1.2753723); (b) Huang, J., Yang, X., Wang, J., Zhong, C., Wang, L., Qin, J., Li, Z. (2012). New tetraphenylethene-based efficient blue luminophors: aggregation induced emission and partially controllable emitting color. *J. Mater. Chem.*, *22*(6), 2478-2484 (DOI: 10.1039/C1JM14054J); (c) Wang, S., Oldham, W. J., Hudack, R. A., Bazan, G. C. (2000). Synthesis, morphology, and optical properties of tetrahedral oligo (phenylenevinylene) materials. *J. Am. Chem. Soc.*, *122*(24), 5695-5709 (DOI: 10.1021/ja992924w); (d) Gong, Y., Tan, Y., Liu, J., Lu, P., Feng, C., Yuan, W. Z., Lu, Y., Sun, J.Z., He, G., Zhang, Y. (2013). Twisted D- $\pi$ -A solid emitters: efficient emission and high contrast mechanochromism. *Chem. Commun.*, *49*(38), 4009-4011 (DOI: 10.1039/C3CC39243K); (e) Jadhav, T., Dhokale, B., Patil, Y., Mobin, S. M., Misra, R. (2016). Multi-stimuli responsive donor-acceptor tetraphenylethylene substituted benzothiadiazoles. *J. Phys. Chem. C.*, *120*(42), 24030-24040 (DOI: 10.1021/acs.jpcc.6b09015); (f) Jadhav, T., Dhokale, B., Mobin, S. M., Misra, R. (2015). Aggregation induced emission and mechanochromism in pyrenoimidazoles. *J. Mater. Chem. C.*, *3*(38), 9981-9988 (DOI: 10.1039/C5TC02181B).
- [11] (a) Zhu, M., Yang, C. (2013). Blue fluorescent emitters: design tactics and applications in organic light-emitting diodes. *Chem. Soc. Rev.*, *42*(12), 4963-4976 (DOI: 10.1039/C3CS35440G); (b) Farinola, G. M., Ragni, R. (2011). Electroluminescent materials for white organic light emitting diodes. *Chem. Soc. Rev.*, *40*(7), 3467-3482 (DOI: 10.1039/C0CS00204F); (c) Baldo, M. A., Thompson, M. E., Forrest, S. R. (2000). High-efficiency fluorescent organic light-emitting devices using a phosphorescent sensitizer. *Nature*, *403*(6771), 750-753 (DOI: 10.1038/35001541); (d) Reineke, S., Lindner, F., Schwartz, G., Seidler,

- N., Walzer, K., Lüssem, B., Leo, K. (2009). White organic light-emitting diodes with fluorescent tube efficiency. *Nature*, 459(7244), 234-238 (DOI: 10.1038/nature08003). Reineke, S., Lindner, F., Schwartz, G., Seidler, N., Walzer, K., Lüssem, B., Leo, K. (2009). White organic light-emitting diodes with fluorescent tube efficiency. *Nature*, 459(7244), 234-238 (DOI: 10.1038/nature08003); (e) Grimsdale, A. C., Leok Chan, K., Martin, R. E., Jokisz, P. G., Holmes, A. B. (2009). Synthesis of light-emitting conjugated polymers for applications in electroluminescent devices. *Chem. Rev.*, 109(3), 897-1091 (DOI: 10.1021/cr000013v); (f) Choy, W. C., Chan, W. K., Yuan, Y. (2014). Recent advances in transition metal complexes and light-management engineering in organic optoelectronic devices. *Adv. Mater.*, 26(31), 5368-5399 (DOI: 10.1002/adma.201306133); (g) Ge, Z., Hayakawa, T., Ando, S., Ueda, M., Akiike, T., Miyamoto, H., Kajita, T., Kakimoto, M. A. (2008). Solution-processible bipolar triphenylamine-benzimidazole derivatives for highly efficient single-layer organic light-emitting diodes. *Chem. Mater.*, 20(7), 2532-2537 (DOI: 10.1039/C1JM10987A); (h) Jeong, S., Kim, M. K., Kim, S. H., Hong, J. I. (2013). Efficient deep-blue emitters based on triphenylamine-linked benzimidazole derivatives for nondoped fluorescent organic light-emitting diodes. *Org. Electron.*, 14(10), 2497-2504 (DOI: 10.1016/j.orgel.2013.06.022).
- [12] (a) Huang, J., Jiang, Y., Yang, J., Tang, R., Xie, N., Li, Q., Kwok, H.S., Tang, B.Z., Li, Z. (2014). Construction of efficient blue AIE emitters with triphenylamine and TPE moieties for non-doped OLEDs. *J. Mater. Chem. C*, 2(11), 2028-2036 (DOI: 10.1039/c3tc32207f); (b) Li, C., Wei, J., Han, J., Li, Z., Song, X., Zhang, Z. Wang, Y. (2016). Efficient deep-blue OLEDs based on phenanthro [9, 10-d] imidazole-containing emitters with AIE and bipolar transporting properties. *J. Mater. Chem. C*, 4(42), 10120-10129 (DOI: org/10.1039/C6TC03923E); (c) Yang, J., Huang, J., Li, Q., Li, Z.

- (2016). Blue AIEgens: approaches to control the intramolecular conjugation and the optimized performance of OLED devices. *J. Mater. Chem. C*, 4(14), 2663-2684 (DOI:org/10.1039/C5TC03262H).
- [13] (a) Jin, C., Liu, J., Chen, Y., Li, G., Guan, R., Zhang, P., Chao, H. (2015). Cyclometalated iridium (III) complexes with imidazo [4, 5-f][1, 10] phenanthroline derivatives for mitochondrial imaging in living cells. *Dalton Trans.*, 44(16), 7538-7547 (DOI: org/10.1039/C5DT00467E); (b) Zheng, L., Hua, R. (2014). Modular Assembly of Ring-Fused and  $\pi$ -Extended Phenanthroimidazoles via C–H Activation and Alkyne Annulation. *J. Org. Chem.*, 79(9), 3930-3936 (DOI: org/10.1021/jo500401n); (c) Zhang, Y., Wang, J. H., Zheng, J., Li, D. (2015). A Br-substituted phenanthroimidazole derivative with aggregation induced emission from intermolecular halogen–hydrogen interactions. *Chem. Commun.*, 51(29), 6350-6353 (DOI: 10.1039/C5CC00490J).; (d) Liu, B., Zhao, J., Luo, C., Lu, F., Tao, S., Tong, Q. (2016). A novel bipolar phenanthroimidazole derivative host material for highly efficient green and orange-red phosphorescent OLEDs with low efficiency roll-off at high brightness. *J. Mater. Chem. C*, 4(10), 2003-2010 (DOI: org/10.1039/C5TC04393J); (e) Chen, W. C., Lee, C. S., Tong, Q. X. (2015). Blue-emitting organic electrofluorescence materials: progress and prospective. *J. Mater. Chem. C*, 3(42), 10957-10963 (DOI: 10.1039/C5TC02420J); (f) Tang, X., Bai, Q., Peng, Q., Gao, Y., Li, J., Liu, Y., Yao, L., Lu, P., Yang, B., Ma, Y. (2015). Efficient deep blue electroluminescence with an external quantum efficiency of 6.8% and CIE  $y < 0.08$  based on a phenanthroimidazole–sulfone hybrid donor–acceptor molecule. *Chem. Mater.*, 27(20), 7050-7057 (DOI: 10.1021/acs.chemmater.5b02685); (g) Zhuang, S., Shangguan, R., Jin, J., Tu, G., Wang, L., Chen, J., Ma, D., Zhu, X. (2012). Efficient nondoped blue organic light-emitting diodes based on phenanthroimidazole-substituted anthracene

derivatives. *Org. Electron.*, 13(12), 3050-3059 (DOI: 10.1016/j.orgel.2012.08.032).

- [14] (a) Yuan, Y., Chen, J. X., Lu, F., Tong, Q. X., Yang, Q. D., Mo, H. W., Ng, T.W., Wong, F.L., Guo, Z.Q., Ye, J., Chen, Z., Zhang, X-H., Lee, C. S. (2013). Bipolar phenanthroimidazole derivatives containing bulky polyaromatic hydrocarbons for nondoped blue electroluminescence devices with high efficiency and low efficiency roll-off. *Chem. Mater*, 25(24), 4957-4965 (DOI: 10.1021/cm4030414); (b) Chen, W. C., Yuan, Y., Wu, G. F., Wei, H. X., Tang, L., Tong, Q. X., Wong, F.L., Lee, C. S. (2014). Staggered Face-to-Face Molecular Stacking as a Strategy for Designing Deep-Blue Electroluminescent Materials with High Carrier Mobility. *Adv. Opt. Mater.* 2(7), 626-631 (DOI: 10.1002/adom.201400078); (c) Wang, K., Wang, S., Wei, J., Miao, Y., Liu, Y., Wang, Y. (2014). Novel diarylborane-phenanthroimidazole hybrid bipolar host materials for high-performance red, yellow and green electrophosphorescent devices. *Org. Electron.*, 15(11), 3211-3220 (DOI: 10.1016/j.orgel.2014.08.062).
- [15] (a) Huang, J., Jiang, Y., Yang, J., Tang, R., Xie, N., Li, Q., Li, Z. (2014). Construction of efficient blue AIE emitters with triphenylamine and TPE moieties for non-doped OLEDs. *J. Mater. Chem. C*, 2(11), 2028-2036 (DOI: 10.1039/c3tc32207f).; (b) Zhang, Y., Lai, S. L., Tong, Q. X., Lo, M. F., Ng, T. W., Chan, M. Y., Lee, C. S. (2012). High efficiency nondoped deep-blue organic light emitting devices based on imidazole- $\pi$ -triphenylamine derivatives. *Chemistry of Materials*, 24(1), 61-70 (DOI: /10.1021/cm201789u); (c) Zhang, S., Yao, L., Peng, Q., Li, W., Pan, Y., Xiao, R., Ma, Y. (2015). Achieving a significantly increased efficiency in nondoped pure blue fluorescent OLED: a quasi-equivalent hybridized excited state. *Advanced Functional Materials*, 25(11), 1755-1762(DOI: 10.1002/adfm.201404260); (d) Li, W., Pan, Y., Yao, L., Liu, H., Zhang, S., Wang, C., Shen, F., Lu, P., Yang, B., Ma, Y. (2014). A hybridized local and charge-transfer excited state for

- highly efficient fluorescent oleds: Molecular design, spectral character, and full exciton utilization. *Adv. Opt. Mater.* 2(9), 892-901(DOI: 10.1002/adom.201400154); (e) Li, W., Liu, D., Shen, F., Ma, D., Wang, Z., Feng, T., Ma, Y. (2012). A twisting donor-acceptor molecule with an intercrossed excited state for highly efficient, deep-blue electroluminescence. *Advanced Functional Materials*, 22(13), 2797-2803 (DOI: 10.1002/adfm.201200116). (f) Gao, Y., Zhang, S., Pan, Y., Yao, L., Liu, H., Guo, Y., Ma, Y. (2016). Hybridization and de-hybridization between the locally-excited (LE) state and the charge-transfer (CT) state: a combined experimental and theoretical study. *Physical Chemistry Chemical Physics*, 18(35), 24176-24184 (DOI: 10.1039/C6CP02778D) (g) Li, G., Zhao, J., Zhang, D., Shi, Z., Zhu, Z., Song, H., Tong, Q. (2016). Mechanochromic asymmetric sulfone derivatives for use in efficient blue organic light-emitting diodes. *J. Mater. Chem. C*, 4(37), 8787-8794 (DOI: 10.1039/C6TC02917E).
- [16] Jadhav, T., Choi, J. M., Dhokale, B., Mobin, S. M., Lee, J. Y., Misra, R. (2016). Effect of end groups on mechanochromism and electroluminescence in tetraphenylethylene substituted phenanthroimidazoles. *The Journal of Physical Chemistry C*, 120(33), 18487-18495 (DOI: 10.1021/acs.jpcc.6b06277); (b) Jadhav, T., Choi, J. M., Shinde, J., Lee, J. Y., Misra, R. (2017). Mechanochromism and electroluminescence in positional isomers of tetraphenylethylene substituted phenanthroimidazoles. *Journal of Materials Chemistry C*, 5(24), 6014-6020 (DOI: 10.1039/C7TC00950J).
- [17] (a) Mallegol, T., Gmouh, S., Meziane, M. A. A., Blanchard-Desce, M., Mongin, O. (2005). Practical and efficient synthesis of tris (4-formylphenyl) amine, a key building block in materials chemistry. *Synthesis*, 2005(11), 1771-1774 (DOI: 10.1055/s-2005-865336); (b) Li, C., Yang, W., Zhou, W., Zhang, M., Xue, R., Li, M., Cheng, Z. (2016). Branching effect for aggregation-induced emission in fluorophores

- containing imine and triphenylamine structures. *New J. Chem.*, 40(10), 8837-8845 (DOI: 10.1039/C6NJ01558A); (c) Su, C., Ye, Y., Xu, L., Zhang, C. (2012). Synthesis and charge–discharge properties of a ferrocene-containing polytriphenylamine derivative as the cathode of a lithium ion battery. *J. Mater. Chem.*, 22(42), 22658-22662 (DOI: 10.1039/C2JM34752K).
- [18] (a) Yuan, Y., Li, D., Zhang, X., Zhao, X., Liu, Y., Zhang, J., Wang, Y. (2011). Phenanthroimidazole-derivative semiconductors as functional layer in high performance OLEDs. *New J. Chem.*, 35(7), 1534-1540 (DOI: 10.1039/C1NJ20072K); (b) Zhang, Y., Lai, S. L., Tong, Q. X., Chan, M. Y., Ng, T. W., Wen, Z. C., Zhang, G.Q., Lee, S.T., Kwong, H.L., Lee, C. S. (2011). Synthesis and characterization of phenanthroimidazole derivatives for applications in organic electroluminescent devices. *J. Mater. Chem.*, 21(22), 8206-8214 (DOI: 10.1039/C1JM10326A); (c) Liu, B., Zhao, J., Luo, C., Lu, F., Tao, S., Tong, Q. (2016). A novel bipolar phenanthroimidazole derivative host material for highly efficient green and orange-red phosphorescent OLEDs with low efficiency roll-off at high brightness. *J. Mater. Chem. C*, 2016, 4, 2003-2010 (DOI: 10.1039/C5TC04393J).
- [19] (a) Frisch, M. J., Trucks, G. W., Schlegel, G. W., Scuseria, G. E., Robb, M. A., Cheeseman, J. R., Scalmani, G., Barone, V., Mennucci, B., Petersson, G. A. *et al.*, *Gaussian 09, revision A.02*; Gaussian, Inc.: Wallingford, CT: 2009; (b) Lee, C., Yang, W., Parr, R. G. *Phys. Rev. B: Condens. Matter Mater. Phys.*, 1988, 37, 785–789 (DOI: 10.1103/PhysRevB.37.785); (c) Becke, A. D. (1993). A new mixing of Hartree–Fock and local density-functional theories. *J. Chem. Phys.*, 98(2), 1372-1377 (DOI: 10.1063/1.464304).
- [20] Janietz, S., Bradley, D. D. C., Grell, M., Giebeler, C., Inbasekaran, M., Woo, E. P. (1998). Electrochemical determination of the ionization potential and electron affinity of poly (9, 9-dioctylfluorene). *Appl. Phys. Lett.*, 73(17), 2453-2455 (DOI: 10.1063/1.122479).



## Chapter 6

### Stimuli-responsive phenothiazine-based donor-acceptor isomers:

#### AIE, mechanochromism and polymorphism

---

---

##### 6.1. Introduction

The development of emissive organic molecules responsive to external stimuli (pressure, temperature, heat, acid *etc.*)<sup>[1]</sup> has advanced the production of organic light emitting diodes (OLEDs), memory and data storage devices, sensors, security inks, fluorescent probes and switches, pressure sensors and other optoelectronic devices.<sup>[2]</sup> Mechanofluorochromic (MFC) have emerged as *smart* stimuli-responsive materials, which have their solid-state emission profiles reversibly responsive to mechanical grinding.<sup>[3]</sup> Considerable emission in solid state is essential for construction of MFC materials.<sup>[4]</sup> Typical organic fluorophores like pyrene, anthracene have substantial amount of  $\pi$ - $\pi$  stacking in their aggregated state owing to which they dissipate their excited state energy non-radiatively which is well known as aggregation caused quenching (ACQ).<sup>[5]</sup> This drawback has been successfully addressed by Tang *et al.* by establishing the idea of aggregation-induced emission (AIE). The non-planar framework of AIEgens minimize the  $\pi$ - $\pi$  stacking and as a consequence of restriction of intramolecular rotation (RIR) result in enhancement of emission in aggregated state.<sup>[6]</sup> The mechanically induced switchable emission leads to phase transformation and can be regulated easily by a variety of factors.<sup>[7]</sup> The MFC behaviour can be tuned by subtle changes in the molecular packing which are dependent on twisting or planarity in the structures, steric hindrance, inclusion of alkyl chains or heavy atoms, intermolecular interactions due to heteroatom or halogen effect, positional isomerization *etc.*<sup>[8]</sup> Polymorphism is a phenomenon in which organic molecules that can adopt different conformations exist in

more than one crystalline form for the same molecular skeleton.<sup>[9]</sup> The generation of polymorphs can result in distinct molecular packing modes which is also an effective strategy for realizing MFC behaviour in solid state.<sup>[10]</sup>

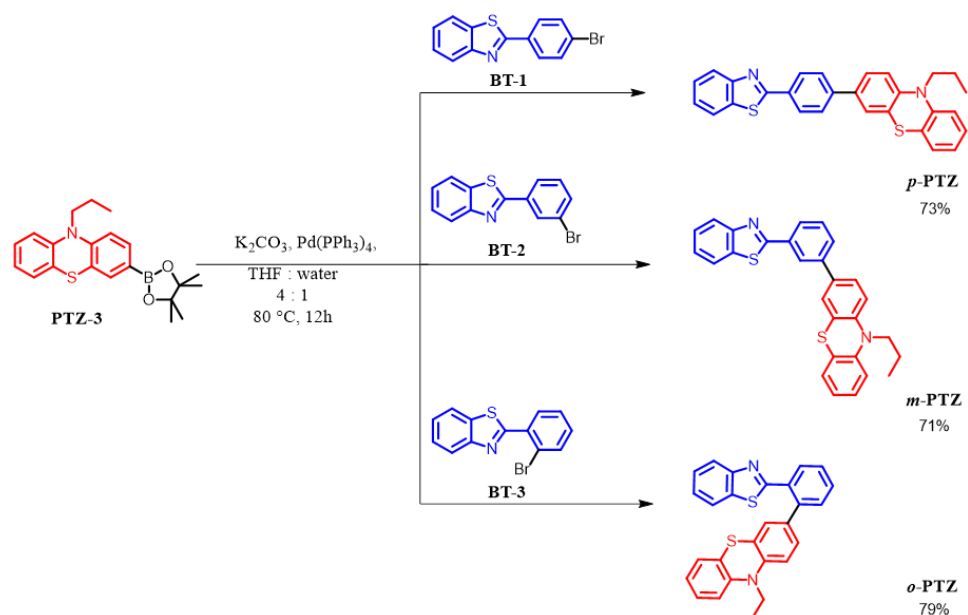
The D-A, D-A-D or D- $\pi$ -A organic frameworks have been utilized to create emissive solid-state materials displaying MFC behaviour.<sup>[11]</sup> The incorporation of non-planar twisted AIEgens like tetraphenylethylene (TPE), hexaphenylsilole (HPS), cyanostilbene *etc.* in organic donor-acceptor architectures assist in achieving high emission in aggregated state by reducing stacking and can easily get converted in different metastable states by forming more planar structures.<sup>[12]</sup> Phenothiazine (PTZ) is a familiar core with good utility in devices like OLEDs, solar cells, chemosensors and thermally activated delayed fluorescence (TADF) materials. The PTZ moiety has also surfaced as a desirable component for MFC materials following its strong electron donating nature due to “S” and “N” atoms and an unusual butterfly shape of the central heterocyclic ring.<sup>[13]</sup> Benzothiazole (BT) is a popular electron acceptor which has many pharmacological as well as material applications with easy functionalization and facile synthesis.<sup>[14]</sup> The integration of BT moiety with PTZ moiety may give rise to interesting emissive properties in solid state. In our previous work, we have coupled the BT core with TPE and investigated its AIE and MFC properties.<sup>[15]</sup> In the present contribution, we have coupled the PTZ moiety to the phenyl ring of the BT moiety at its *para*, *meta* and *ortho* position to yield D-A positional isomers ***p*-PTZ**, ***m*-PTZ** and ***o*-PTZ** respectively. The combination of BT and PTZ could produce highly emissive solid-state materials with fascinating AIE and MFC properties. The free heteroatoms in the two moieties have the ability to display supramolecular interactions and weak hydrogen bonding that can easily affect the solid-state properties. The functionalization of the donor PTZ at *para*, *meta* and *ortho* positions of acceptor phenyl **BT** was exploited to modulate the donor-acceptor character and molecular packing in the

isomers. The N-atom of PTZ moiety was alkylated using propyl chain for increasing its solubility. The twisting induced by positional isomerization results in enhancement in intensity in aggregated state with reversible MFC and effectively sense trifluoroacetic acid (TFA). Additionally, the conformational flexibility of N-alkylated PTZ moiety gives rise to self-reversible colour switching and polymorphism. The isomers display contrast charge transfer characteristics due to formation of twisted intramolecular charge transfer (TICT) state. The present study shows a detailed comparison of the AIE, mechanochromic, solvatochromic and photophysical of the D-A positional isomers *p*-PTZ, *m*-PTZ and *o*-PTZ.

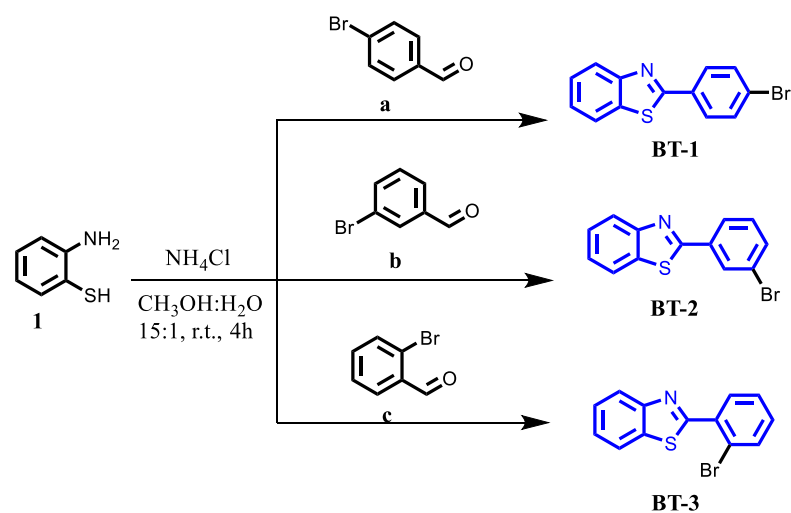
## 6.2. Results and Discussions

### Synthesis

The isomers *p*-PTZ, *m*-PTZ and *o*-PTZ involving a positional change of the phenothiazine (PTZ) moiety at the *para*, *meta* and *ortho* positions of the phenyl benzothiazole BT ring were synthesized as discussed in Scheme 6.1. The condensation reaction of 2-aminobenzenethiol **1** with 4-bromobenzaldehyde **a**, 3-bromobenzaldehyde **b** and 2-bromobenzaldehyde **c** using ammonium chloride in methanol/water produced the respective benzothiazole intermediates **BT-1**, **BT-2** and **BT-3** (Scheme 6.2).<sup>[16a]</sup> The **PTZ** moiety was converted into N-propyl phenothiazine boronate **PTZ-3** ester by a three-step approach (Scheme 6.2).<sup>[16b]</sup>



**Scheme 6.1.** Synthesis of isomers *p*-PTZ, *m*-PTZ and *o*-PTZ.



**Scheme 6.2.** Synthetic routes to intermediates.

The alkylation of **PTZ** using N-propyl iodide resulted in 10-propyl-10*H*-phenothiazine **PTZ-1** which on selective bromination with bromine in acetic acid yielded 3-bromo-10-propyl-10*H*-phenothiazine **PTZ-2**. The  $Pd(dppf)Cl_2$  catalysed borylation reaction of **PTZ-2** and bis-pinnacolatodiboron in 1,4-dioxane afforded N-propyl phenothiazine boronate ester **PTZ-3**. The **PTZ-3** was coupled in presence of  $Pd(PPh_3)_4$

with **BT-1**, **BT-2** and **BT-3** via Suzuki-cross coupling reaction to successfully form the desired isomers *p*-PTZ, *m*-PTZ and *o*-PTZ in 73%, 71% and 79% yields, respectively. All the isomers have good solubility in common organic solvents such as tetrahydrofuran (THF), dichloromethane (DCM), chloroform, toluene *etc.* and were completely characterized by  $^1\text{H}$  NMR,  $^{13}\text{C}$  NMR, HRMS and single crystal X-ray analysis.

### 6.3. Photophysical Properties

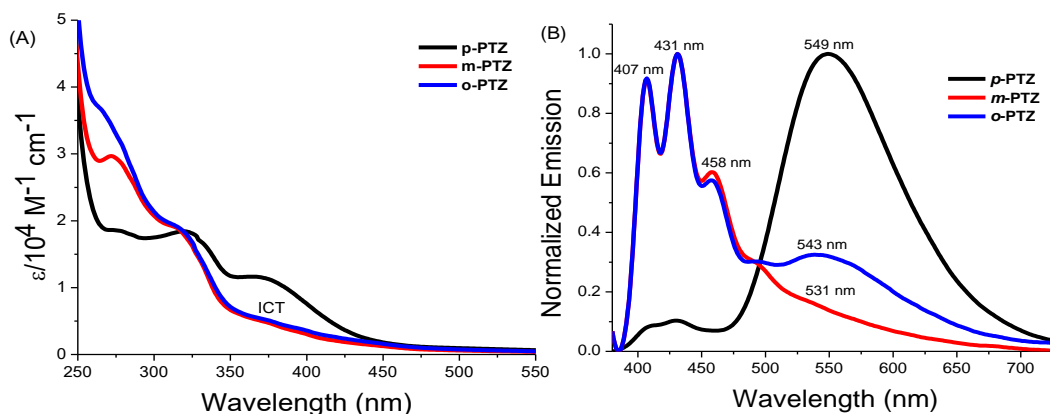


**Figure 6.1.** Electronic absorption spectra (A) and normalized emission spectra (B) of isomers *p*-PTZ, *m*-PTZ and *o*-PTZ measured in chloroform ( $2 \times 10^{-5}$  M).

The photophysical properties of the isomers *p*-PTZ, *m*-PTZ and *o*-PTZ were examined in chloroform solution by electronic absorption and emission spectroscopy (Figure 6.1.). The absorption spectra (Figure 6.1. (A)) of the isomers show bands at shorter wavelength region (250–330 nm) which could be assigned to the  $\pi\text{-}\pi^*$  transitions. The *p*-PTZ isomer shows a very strong absorption band at 375 nm possibly due to the intramolecular charge transfer (ICT) occurring from the donor PTZ to the acceptor BT moiety. A significant change was observed in the optical properties on positional change. The charge transfer band at 372 nm in *m*-PTZ and *o*-PTZ are weakened as compared to *p*-PTZ. This could possibly be explained by the formation of a twisted intramolecular charge transfer state due to the higher amount of twisting in *meta* and *ortho* isomers as compared to *para*.

The emission spectra of the isomers also confirm the different optical properties of *p*-PTZ (Figure 6.1. (B)). All the isomers show emission between 400–500 nm which could be ascribed to the localized excited (**LE**) states in the molecules. Other than the LE emission, the *p*-PTZ exhibits a strong emission at 549 nm which could be ascribed to ICT transition. On the other hand, the *m*-PTZ and *o*-PTZ have significant LE emissions and low intensity ICT emissions at longer wavelength (above 500 nm). The photophysical data are summarized in Table 6.1. and the effect of positional change on the ICT transition have been explored in detail using solvatochromic studies.

**Table 6.1.** Photophysical properties of isomers *p*-PTZ, *m*-PTZ and *o*-PTZ.

Compounds	$\lambda_{ab}[\text{nm}] (\epsilon[\text{Lmol}^{-1}\text{cm}^{-1}])^a$	$\lambda_{em} (\text{nm})^a$	$\phi^b$
<i>p</i> -PTZ	272(18620), 324(18200), 375(11280)	407,431,549	0.63
<i>m</i> -PTZ	272(29675), 316(18760), 372(4920)	407,431,458,531	0.11
<i>o</i> -PTZ	265(36730), 314(19265), 372(5280)	407,431,458,543	0.16

<sup>a</sup> Measured in chloroform ( $2 \times 10^{-5}$  M), <sup>b</sup> Fluorescence quantum yields recorded using quinine sulphate as a standard in 0.5 M H<sub>2</sub>SO<sub>4</sub> solution ( $\lambda_{exc} = 370\text{nm}$ ).

#### 6.4. Solvatochromism

The ICT transition arising in D-A molecules is easily affected by changes in solvent polarity and could be further influenced by the positional change in *p*-PTZ, *m*-PTZ and *o*-PTZ.<sup>[17a]</sup> The isomers were dissolved in solvents of different polarity from non-polar to polar (cyclohexane, toluene, THF, chloroform, DCM, 1,4-dioxane, dimethylformamide (DMF), dimethylsulphoxide (DMSO)) and the effect of solvent polarity and

positional change on ICT transition was explored in detail by emission (Figure 6.2.) and absorption spectroscopy (Figure 6.3.).

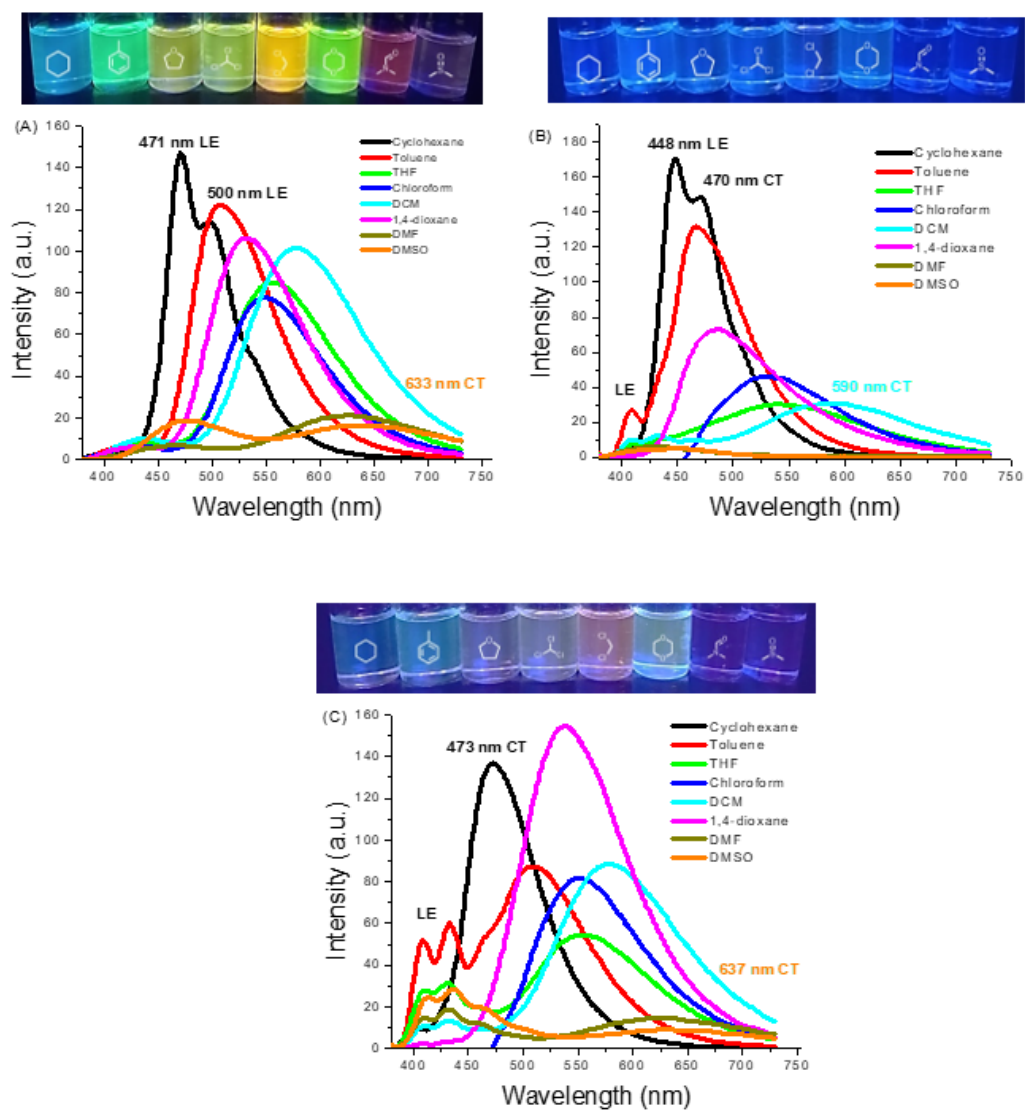


**Figure 6.2.** Emission spectra of (A) *p*-PTZ, (B) *m*-PTZ and (C) *o*-PTZ in solvents of varying polarity. ( $\lambda_{exc} = 370\text{nm}$ ) (Photographs taken under 365 nm UV illumination, from left to right cyclohexane, toluene, THF, chloroform, DCM, 1,4-dioxane, DMF and DMSO)

The *p*-PTZ isomer emits at 471 nm due to the localized-excited (LE) state with a shoulder at 500 nm corresponding to the ICT transition cyclohexane. The emission intensity of the ICT increases in toluene while the LE

emission appears as a low intensity peak. The ICT peak is further stabilized and red shifted on increasing the polarity and emits at 637 nm in DMSO. The ICT transition creates a polarized excited state stabilized by reorganization of solvent molecules around it thereby lowering its energy resulting in a red shifted weakened emission in polar solvents <sup>[17a]</sup> In cyclohexane, the *m*-PTZ isomer similarly exhibits LE emission at 448 nm and emission at 470 nm as a shoulder due to charge transfer (CT) state. On increasing the polarity from toluene to DCM, the CT emission is significant, whereas the LE emission appears as a low intensity peak. The CT emission is stabilized in moderately polar solvent like DCM with red shifted emission at 590 nm. The close vicinity of the LE and CT states rationalizes the dual emission in solvents of various polarity.<sup>[18a]</sup> Although, the intensity of CT emission substantially decreases in highly polar solvents such as DMF and DMSO with the LE emission remaining intact. The drastic reduction in emission intensity in highly polar solvents could be associated to TICT state.<sup>[18b]</sup> The free rotation around the single bond in the *meta* isomer makes it twisted which is accompanied with an instantaneous charge transfer from donor to acceptor forming a relaxed perpendicular TICT state. In non-polar solvents, a high intensity LE emission was observed at lower wavelength due to D-A coplanar conformation stabilized by mesomeric interactions, whereas in highly polar solvents the D-A relaxed perpendicular TICT state creates a non-radiative channel resulting in little or no emission.<sup>[18c,d]</sup> The *o*-PTZ isomer emits strongly at 473 nm in cyclohexane from CT state along with LE emissions below 450 nm. The increase in polarity results in stabilization of the CT emission accompanied by bathochromic shift. In DMSO, the isomer exhibits dual emission at lower wavelength due to LE states and higher wavelength due to CT state. The *ortho* isomer shows significant LE emission in highly polar solvents and the emission from CT state is slightly quenched owing to the TICT state. The *ortho* isomer has higher twisting as compared to *meta* isomer, however the electronic communication at the *ortho* position is more pronounced as compared to

*meta* position. The synergistic effect of the TICT state and the electronic communication at *ortho* position results in intermediate solvatochromic behaviour as compared to the *para* and *meta* isomer.

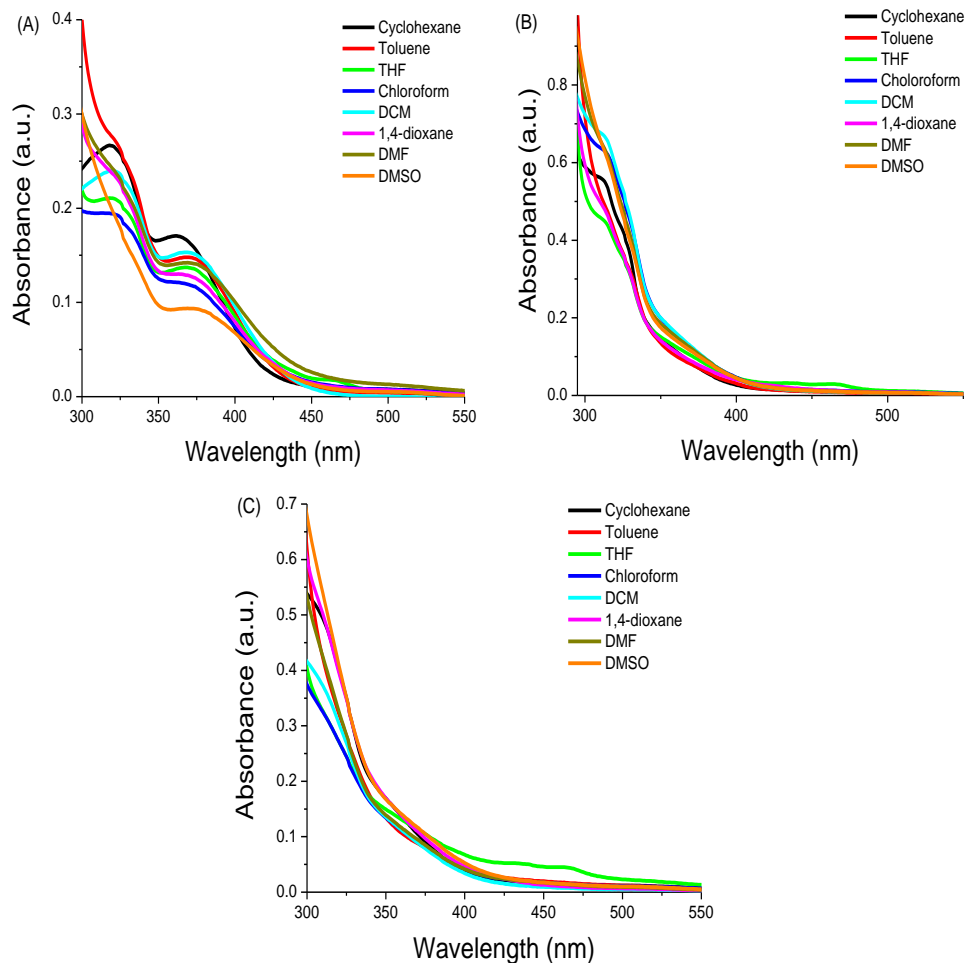


**Figure 6.3.** Electronic absorption spectra of (A) *p*-PTZ, (B) *m*-PTZ and (C) *o*-PTZ in solvents of various polarity.

The absorption spectra (Figure 6.3.) of the isomers are not much affected by changing the solvent polarity which establishes existence of more polarized excited state in contrast to ground electronic state.<sup>[17b]</sup> The quantum yield for the isomers in different solvents has been given in Table 6.2.

**Table 6.2.** Quantum yield of *p*-PTZ, *m*-PTZ and *o*-PTZ in various solvents.

Solvents	$\phi_f^a$		
	<i>p</i> -PTZ	<i>m</i> -PTZ	<i>o</i> -PTZ
Cyclohexane	0.36	0.11	0.09
Toluene	0.50	0.13	0.12
THF	0.43	0.04	0.06
Chloroform	0.68	0.05	0.12
DCM	0.51	0.03	0.12
1,4-dioxane	0.53	0.08	0.14
DMF	0.14	0.004	0.03
DMSO	0.26	0.004	0.02

<sup>a</sup> Fluorescence quantum yields recorded using quinine sulphate as a standard in 0.5 M H<sub>2</sub>SO<sub>4</sub> solution ( $\lambda_{exc} = 370\text{nm}$ ).

### 6.5. Aggregation-induced emission

The butterfly type structure of PTZ and the twisting in the isomers provided non-planar molecules with aggregation-induced emission characteristics which were investigated using emission spectroscopy (Figure 6.4.). The isomers *p*-PTZ, *m*-PTZ and *o*-PTZ are readily soluble in DMSO but insoluble in water; hence consistent increase of water in DMSO initiated the nano-aggregate formation. The *p*-PTZ has an emission maximum at 639 nm in pure DMSO contrast to the standard AIEgens as a result of the exclusive ICT transition present in the isomer. The emission intensity of ICT peak decreases on increasing the water fraction upto 30% and shifts bathochromically to 658 nm, which shows the stabilization of intramolecular charge transfer peak in polar medium. At 40% water fraction, the aggregation occurs which enhances the intensity accompanied by blue shifted emission at 485 nm. The aggregation causes intensity enhancement upto 50% water fraction, although a slight drop in intensity

was observed at 60% water fraction which could be caused by the larger sized aggregates which are less exposed to radiation. The 70% DMSO-water fraction experiences a substantial enhancement in emission intensity with appearance of new peak at 511 nm. This could be attributed to the formation of two different types of aggregates at 40% and 70% water fraction.<sup>[19a]</sup> The higher water percentage (*i.e.* 80% and above) again experience minor drop in intensity due to formation of larger sized aggregates.<sup>[19b,c]</sup> Thus, the emission at low water fractions in *p*-PTZ isomer is mainly due to the ICT which later at higher water fractions is majorly governed by aggregation.<sup>[19d]</sup>

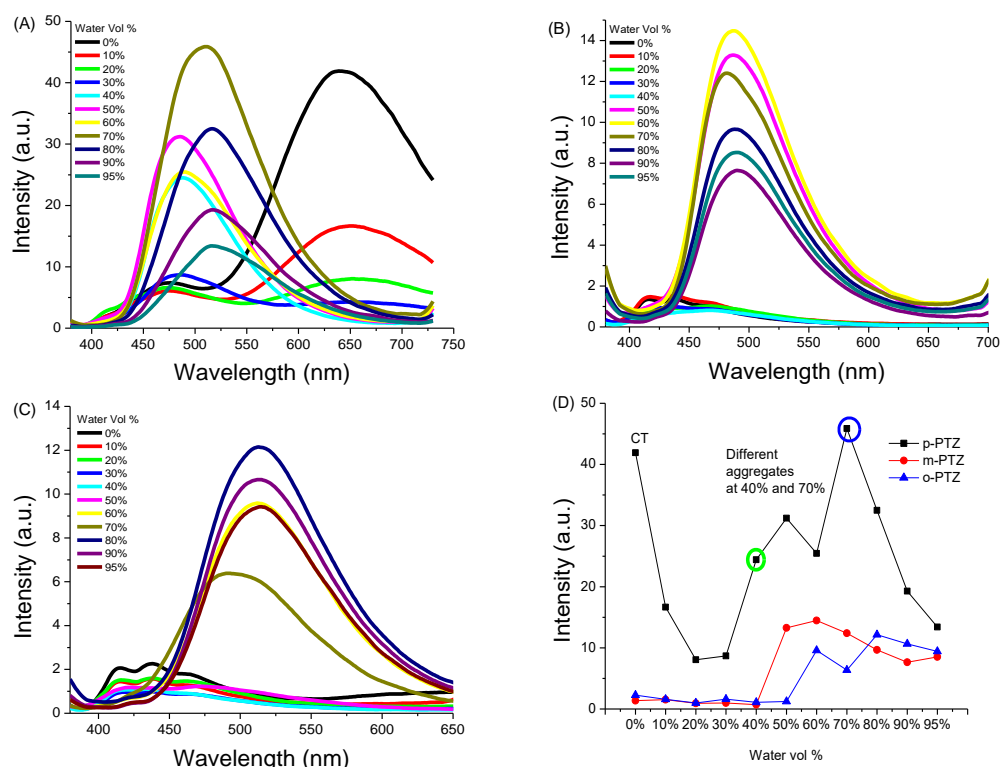


**Figure 6.4.** Emission spectra of (A) *p*-PTZ, (B) *m*-PTZ and (C) *o*-PTZ in DMSO-water mixtures with different water fractions. (Luminogen conc.  $2 \times 10^{-5}$  M) (D) Plot of intensity vs water fraction; intensity calculated at  $\lambda_{\max}$  ( $\lambda_{\max}$  with highest intensity considered for calculation).

In *p*-PTZ isomer, the AIE behaviour was observed at different wavelengths for two water fraction 40% and 70%, which may be due to formation of two different aggregates. The *m*-PTZ and *o*-PTZ isomers display contrast AIE behaviour as a consequence of the TICT state. Both the isomers have weakened emissions in pure DMSO solutions. The emission intensifies at 50% DMSO-water and 60% DMSO-water for *m*-PTZ and *o*-PTZ respectively owing to aggregate formation. The emission reduces at higher water percentage similar to *p*-PTZ. The *meta* and *ortho* isomer behave as typical AIEgens unlike the *para* isomer. The unique AIE properties in the isomers are an outcome of the TICT state formed due to positional change. The pictures of AIE behaviour are given in Figure 6.5.

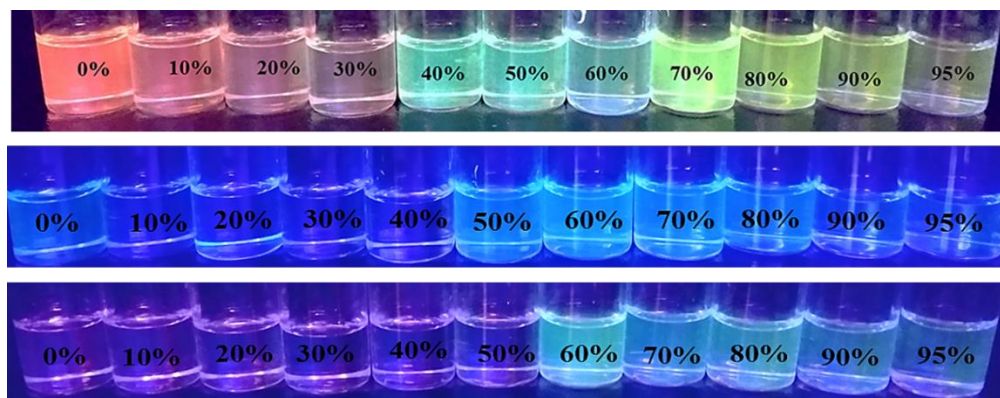


**Figure 6.5.** Photographs of *p*-PTZ, *m*-PTZ and *o*-PTZ in DMSO–water mixtures with different water fractions (10  $\mu$ M) under 365 nm UV illumination.

### 6.6. Single crystal X-ray analysis

The single crystal X-ray analysis is useful for structure elucidation and inference of properties in aggregated state. The slow evaporation of *p*-PTZ isomer in DCM serendipitously resulted in two different types of crystals. The polymorphs were denoted as *p*-PTZ GC ( $P2_1$  monoclinic system) and *p*-PTZ YC ( $Pna2_1$  orthorhombic system) according to their physical appearances; *p*-PTZ GC being green coloured rod shaped and *p*-PTZ YC being yellow plate shaped crystal (Figure 6.6 (A)).

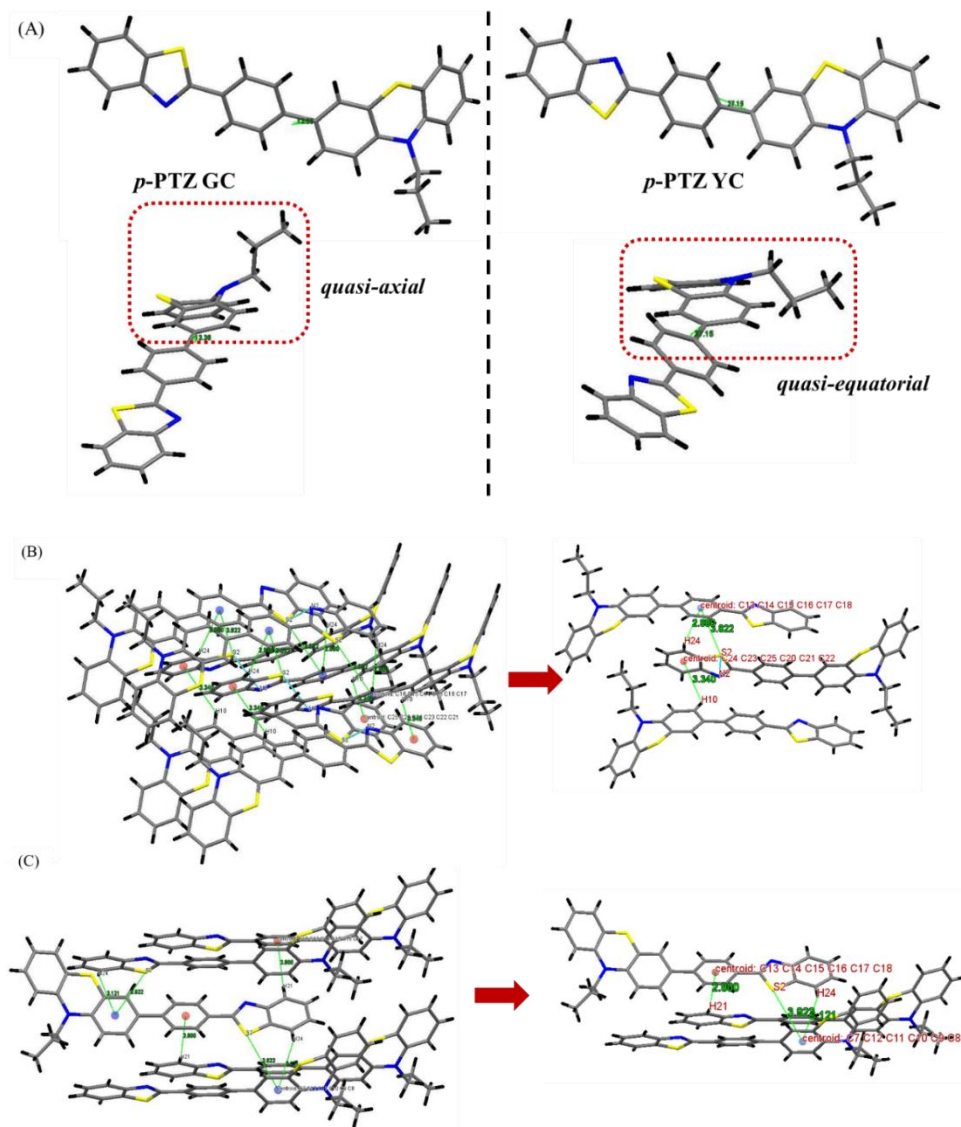


**Figure 6.6.** (A) Crystal structures of polymorphs *p*-PTZ GC and *p*-PTZ YC in its different confirmations, Crystal packing diagram and the intermolecular interactions of (B) *p*-PTZ GC and (C) *p*-PTZ YC.

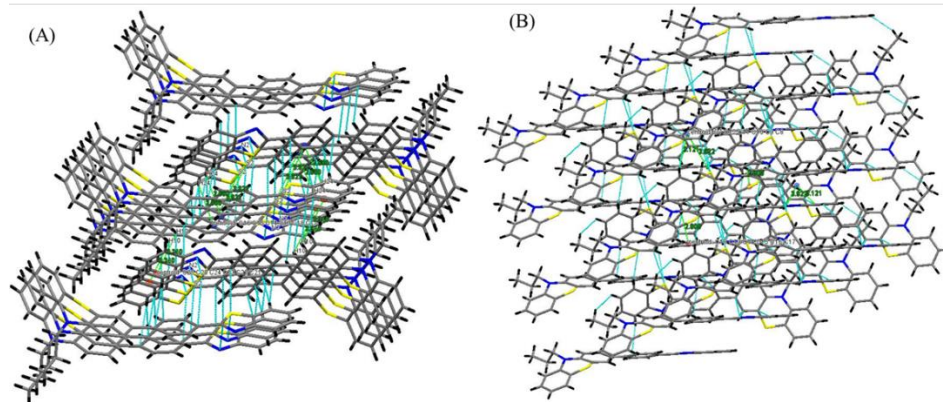


**Figure 6.7** Crystal packing diagram of (A) *p*-PTZ GC and (B) *p*-PTZ YC.

In *p*-PTZ GC, the PTZ moiety attaches at para position with a dihedral angle of  $13.36^\circ$  in a way that the N and S of PTZ are on the same side as compared to N and S of BT moiety (Figure 6.6 (A)). In *p*-PTZ YC, the dihedral angle between BT and PTZ moiety is  $27.15^\circ$  which is higher compared to *p*-PTZ GC and the N and S of PTZ moiety are anti to the N and S of BT moiety (Figure (6.6. (B))). The major difference in the polymorphs can be visualized in the terms of orientation of the propyl chain attached to the N atom of PTZ. The central six membered ring of PTZ moiety prefers a boat confirmation due to the butterfly shape of PTZ moiety. In *p*-PTZ GC, the propyl chain is quasi axial whereas in *p*-PTZ YC it is quasi equatorial (Figure 6.6. (A)) in context to the boat confirmation of PTZ moiety.<sup>[20]</sup> In *p*-PTZ GC, two molecules lie perpendicular in a head to tail arrangement and each molecule stacks parallelly in respective direction forming a tightly packed 2D stacked structure (Figure 6.7. (A)). In the aggregated state two molecules of *p*-PTZ GC exhibit two C–H..... $\pi$  interactions C(20)–H(10)..... $\pi$ (red centroid C20 C21 C22 C23 C24 C25, 3.340 Å), C(13)–H(24)..... $\pi$ (blue centroid C13 C14 C15 C16 C17 C18, 2.880 Å) and one lone pair..... $\pi$  interaction *i.e.* S(2)..... $\pi$ (blue centroid C13 C14 C15 C16 C17 C18, 3.822Å) (Figure 6.6. (B)). In *p*-PTZ YC, each molecule is surrounded by one head to head stack molecule and another molecule remaining in an antiparallel arrangement which forms 2D stacked

ladder type structure (Figure 6.7. (B)). The interactions observed in ***p*-PTZ YC** are two C–H..... $\pi$  interactions C(7)–H(24)..... $\pi$ (blue centroid C7 C8 C9 C10 C11 C12, 3.121 Å), C(18)–H(21)..... $\pi$ (red centroid C13 C14 C15 C16 C17 C18, 2.880 Å) and one lone pair..... $\pi$  interaction *i.e.* S(2)..... $\pi$  (blue centroid C7 C8 C9 C10 C11 C12, 3.922Å) (Figure 6.6. (C)).

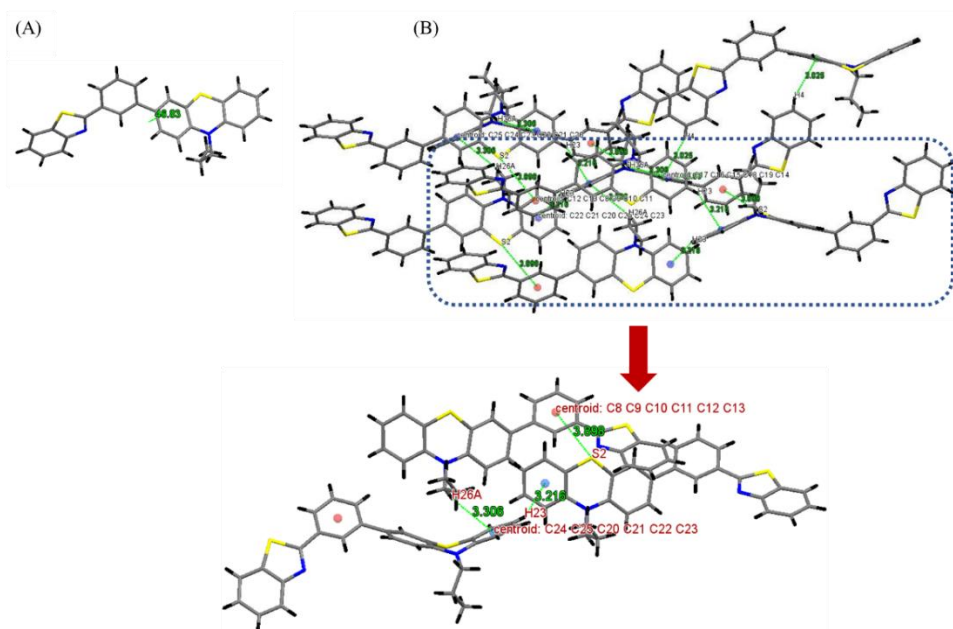


**Figure 6.8.** (A) Crystal structure of ***m*-PTZ** and (B) crystal packing diagram of ***m*-PTZ** depicting the intermolecular interactions.

The ***m*-PTZ** isomer crystallizes as  $P2_1/c$  monoclinic system by slow evaporation of compound in hexane. The crystals for ***o*-PTZ** isomer were generated by evaporation of ethyl-acetate/hexane mixture as  $P2_1/c$  monoclinic system. The dihedral angle between the donor (**PTZ**) and acceptor (**BT**) in ***m*-PTZ** is  $46.83^\circ$  (Figure 6.8. (A)) and in ***o*-PTZ** is  $70.90^\circ$  (Figure 6.9. (A)). There is a clear increment in the dihedral angle between the donor benzothiazole moiety and the acceptor phenothiazine in the following order ***o*-PTZ**>***m*-PTZ**>***p*-PTZ**, thereby altering the degree of twisting in the isomers, which could affect its solid-state emission properties. In the solid state of ***m*-PTZ** isomer, each molecule interacts with four other molecules by three C–H..... $\pi$  interactions *i.e.* C(14)–

H(4)..... $\pi$ (centroid C14 C15 C16 C17 C18 C19, 3.025 Å), C(20)–H(26A)..... $\pi$ (blue centroid C20 C21 C22 C23 C24 C25, 3.306 Å), C(25)–H(23)..... $\pi$ (blue centroid C20 C21 C22 C23 C24 C25, 3.216 Å) and one lone pair..... $\pi$  interaction *i.e.* S(2)..... $\pi$ (red centroid C8 C9 C10 C11 C12 C13, 3.898Å) (Figure 6.8. (B)). The multiple interactions give rise to a tight 2D sheet type packing in meta isomer (Figure 6.10 (A)).

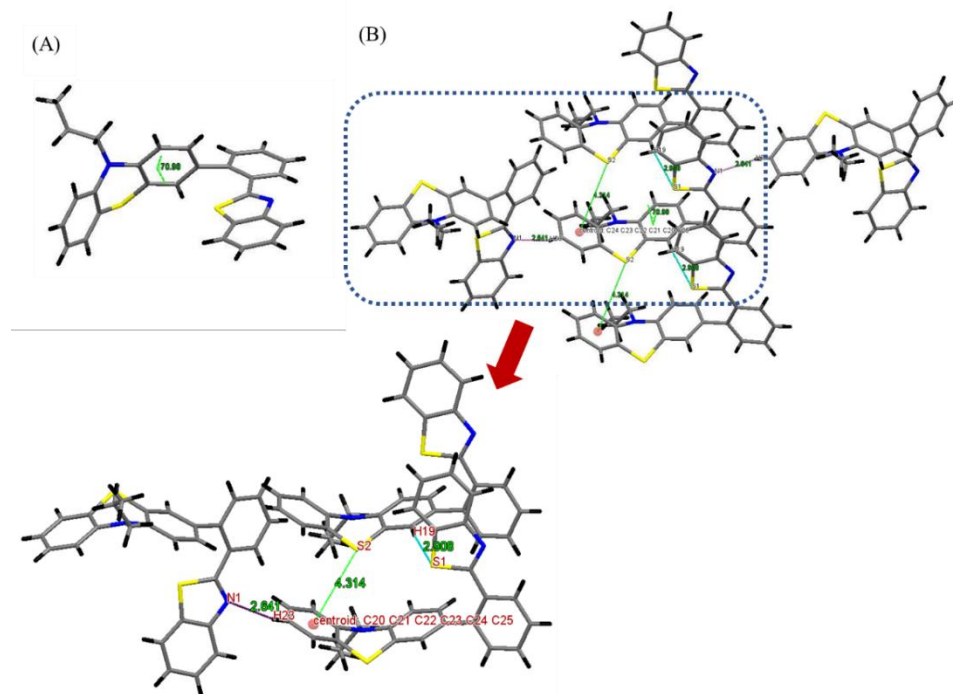


**Figure 6.9.** (A) Crystal structure of *o*-PTZ and (B) crystal packing diagram of *o*-PTZ depicting the intermolecular interactions.

On the other hand, the *o*-PTZ isomer has no C–H..... $\pi$  interactions, however exhibits one lone pair..... $\pi$  interaction S(2)..... $\pi$ (red centroid C20 C21 C22 C23 C24 C25, 4.314 Å) and two different kind of weak hydrogen bonding interactions from N and S of BT moiety *i.e.* C–H(23).....N(1) (2.641 Å) and C–H(19).....S(1) (2.908 Å) (Figure 6.9. (B)). The absence of multiple interactions in *o*-PTZ isomer results in a loosely packed zig-zag 2D arrangement (Figure 6.10. (B)).

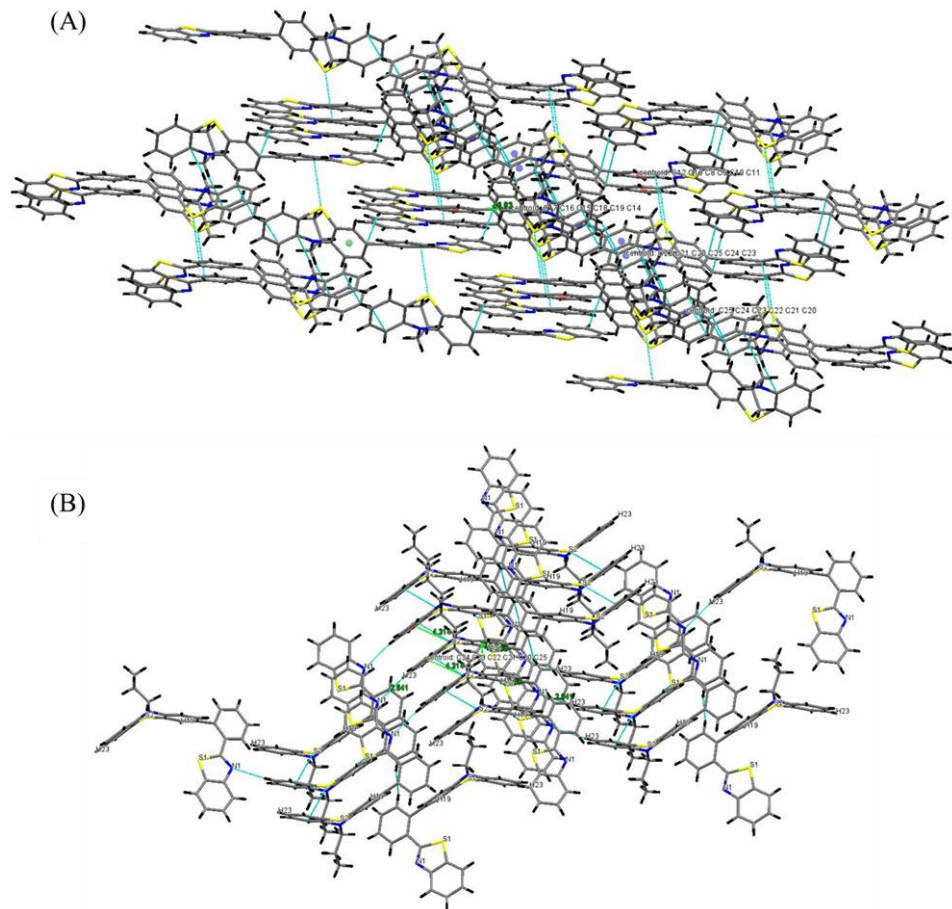


**Figure 6.10.** Crystal packing diagram of (A) *m*-PTZ and (B) *o*-PTZ.

The variable packing and twisting in the isomers could initiate intriguing properties in solid state. The **p**-PTZ GC exhibits sheet like morphology, whereas the morphology of **p**-PTZ YC has small aggregates. The crystal information for the isomers is compiled in Table 6.3. The polymorphs of **p**-PTZ isomer were also studied using scanning electron microscopy (SEM) as shown in Figure 6.11.

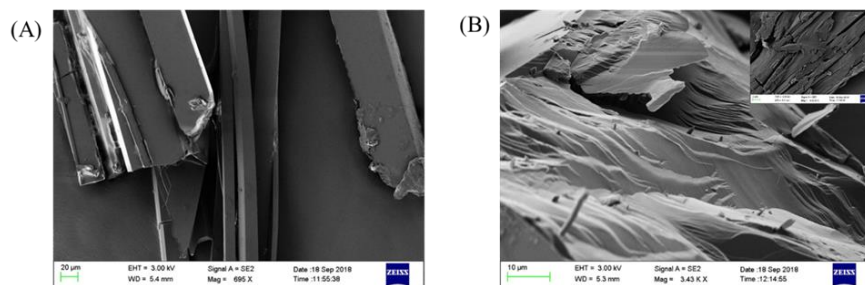


**Figure 6.11.** SEM images of the polymorphs (A) *p*-PTZ GC and (B) *p*-PTZ YC.

**Table 6.3.** Crystal data and structure refinement for *p*-PTZ GC, *p*-PTZ YC, *m*-PTZ and *o*-PTZ.

Identification code	rm259	rm257	shelx	Shelx
Empirical formula	C <sub>28</sub> H <sub>22</sub> N <sub>2</sub> S <sub>2</sub>	C <sub>28</sub> H <sub>22</sub> N <sub>2</sub> S <sub>2</sub>	C <sub>28</sub> H <sub>22</sub> N <sub>2</sub> S <sub>2</sub>	C <sub>28</sub> H <sub>22</sub> N <sub>2</sub> S <sub>2</sub>
Formula weight	450.59	450.59	450.59	450.59
Temperature	293(2) K	293(2) K	293(2) K	296(2) K
Wavelength	0.71073 Å	0.71073 Å	0.71073 Å	0.71073 Å
Crystal system, space group	Monoclinic, P 2 <sub>1</sub>	Orthorhombic, P n a 2 <sub>1</sub>	Monoclinic, P 2 <sub>1</sub> /c	Monoclinic, P 2 <sub>1</sub> /c
a/(Å)	8.5948(5)	39.769(3)	9.5843(3)	5.7861(2)
b/(Å)	5.5944(3)	7.1785(5)	8.1855(4)	23.6600(7)
c/(Å)	23.1405(11)	7.7524(8)	28.7754(13)	16.4878(5)
Alpha/(°)	90	90	90	90
Beta/(°)	95.751(5)	90	92.432(4)	92.684(2)
Gamma/(°)	90	90	90	90
Volume	1107.06(10) Å <sup>3</sup>	2213.2(3) Å <sup>3</sup>	2255.46(17) Å <sup>3</sup>	2254.69(12) Å <sup>3</sup>
Z, Calculated density	2, 1.352 mg/m <sup>-3</sup>	4, 1.352 mg/m <sup>-3</sup>	4, 1.327 mg/m <sup>-3</sup>	4, 1.327 mg/m <sup>-3</sup>
Absorption coefficient	0.260 mm <sup>-1</sup>	0.260 mm <sup>-1</sup>	0.255 mm <sup>-1</sup>	0.255 mm <sup>-1</sup>
F(000)	472	944	944	944

Crystal size	0.230 x 0.180 x 0.130 mm	0.260 x 0.230 x 0.180 mm	0.250 x 0.100 x 0.060 mm	0.300 x 0.103 x 0.030 mm
$\Theta$ range for data collection/(°)	3.384 to 29.083	2.820 to 30.551	3.273 to 29.132	1.506 to 28.433
Reflections collected / unique	9102 / 4635 [R(int) = 0.0708]	23519 / 5412 [R(int) = 0.0968]	25562 / 5521 [R(int) = 0.0674]	24538 / 5645 [R(int) = 0.0691]
Completeness to theta	$\Theta = 25.242$ 99.6 %	$\Theta = 25.242$ 99.9 %	$\Theta = 25.242$ 99.8 %	$\Theta = 25.242$ 99.7 %
Refinement method	Full-matrix least- squares on $F^2$	Full-matrix least-squares on $F^2$	Full-matrix least- squares on $F^2$	Full-matrix least- squares on $F^2$
Data / restraints / parameters	4635 / 3 / 290	5412 / 1 / 289	5521 / 0 / 289	5645 / 2 / 299
Goodness-of-fit on $F^2$	1.105	1.066	1.029	0.918
Final R indices [I > 2 $\sigma$ (I)]	R1 = 0.1287, wR2 = 0.3277	R1 = 0.0762, wR2 = 0.2056	R1 = 0.0612, wR2 = 0.1138	R1 = 0.0537, wR2 = 0.1199
R indices (all data)	R1 = 0.2379, wR2 = 0.4181	R1 = 0.1058, wR2 = 0.2487	R1 = 0.1204, wR2 = 0.1353	R1 = 0.1379, wR2 = 0.1538
Extinction coefficient	0.050(18)	n/a	n/a	n/a
Largest diff. peak and hole (e. $\text{\AA}^{-3}$ )	0.972 and - 0.606	0.658 and - 0.623	0.413 and - 0.278	0.383 and - 0.280

## 6.7. Mechanochromism

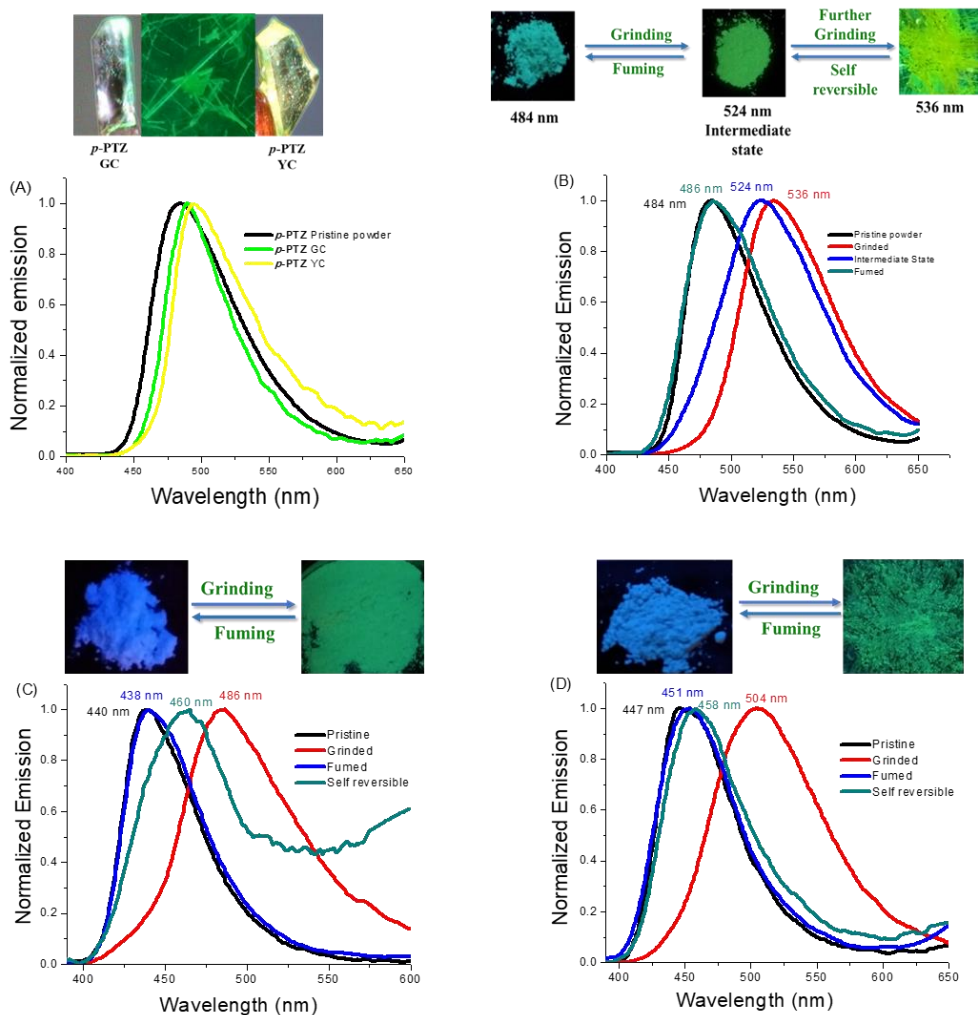


**Figure 6.12.** Solid-state emission spectra of (A) *p*-PTZ and its polymorphs (*p*-PTZ GC and *p*-PTZ YC), (B) *p*-PTZ, (C) *m*-PTZ and (D) *o*-PTZ as their pristine, grinded, fumed and self-reversible solids and photographs taken under 365 nm UV illumination.

The non-planarity and twisting in the isomers lead to significant emission in the solid state which is responsive to mechanical force. Additionally, the inclusion of PTZ moiety resulted in polymorphs for the *para* isomer owing to the formation of different conformers due to flexibility of the butterfly confirmation. Taking in consideration the above structural features, the mechanochromic behaviour of the isomers and polymorphism of *p*-PTZ

was investigated in detail using solid-state emission spectroscopy (Figure 6.12.). The ***p*-PTZ** pristine powder exhibits green emission at 484 nm, whereas its polymorphs ***p*-PTZ GC** and ***p*-PTZ YC** emit at 490 nm and 494 nm respectively. The grinding of ***p*-PTZ** pristine powder in mortar pestle resulted in bathochromically shifted bright green emission at 524 nm. The green emission red shifted to a yellow emission at 536 nm on further strong grinding, which dynamically reversed to an intermediate emission at 524 nm in about one minute. The self-reversible change from yellow emission (536 nm) to green emission (524 nm) was studied upto 7 cycles (Figure 6.13. (A)). The intermediate green emission at 524 nm was stable although restored to the pristine state with bluish green emission at 486 nm on fuming with dichloromethane for 4–5 minutes. The ***p*-PTZ** isomer exhibited a three-fold mechanochromic behaviour from bluish green to yellow via green emission with a spectral shift of 52 nm. The three-fold stepwise colour switching in ***p*-PTZ** could be ascribed to the flexible conversion of different conformers of **PTZ** moiety. The ***m*-PTZ** and ***o*-PTZ** isomers display a blue emission in its pristine state at 440 nm and 447 nm respectively. A bright green emission is generated on grinding at 486 nm and 504 nm for ***m*-PTZ** and ***o*-PTZ** respectively. The grinded solids of ***m*-PTZ** and ***o*-PTZ** restored their original blue emission at 438 nm and 451 nm respectively on fumigation with hexane for 5–7 minutes. The grinding induced spectral shift for ***m*-PTZ** and ***o*-PTZ** is 47 nm and 58 nm respectively. The grinded solid of ***m*-PTZ** when left at room temperature for over a week displayed self-reversible switching of its emission upto 460 nm whereas the grinded solid of ***o*-PTZ** switched its emission merely in 2-3 days self reversibly upto 458 nm which is close to its pristine state. The self-reversible switching of emission observed in all the isomers could be due to the flexible interconversion between different conformers of the **PTZ** moiety.<sup>[21]</sup> The isomer ***o*-PTZ** is highly twisted and is less susceptible to achieve planar confirmation on grinding and reaches to a metastable state on grinding which can easily revert to the original state. Thus, the self-recovering

mechanochromic behaviour is highest in ortho isomer which shows that self-reversible switching somewhat also depends on the flexibility of the donor and acceptor moieties.

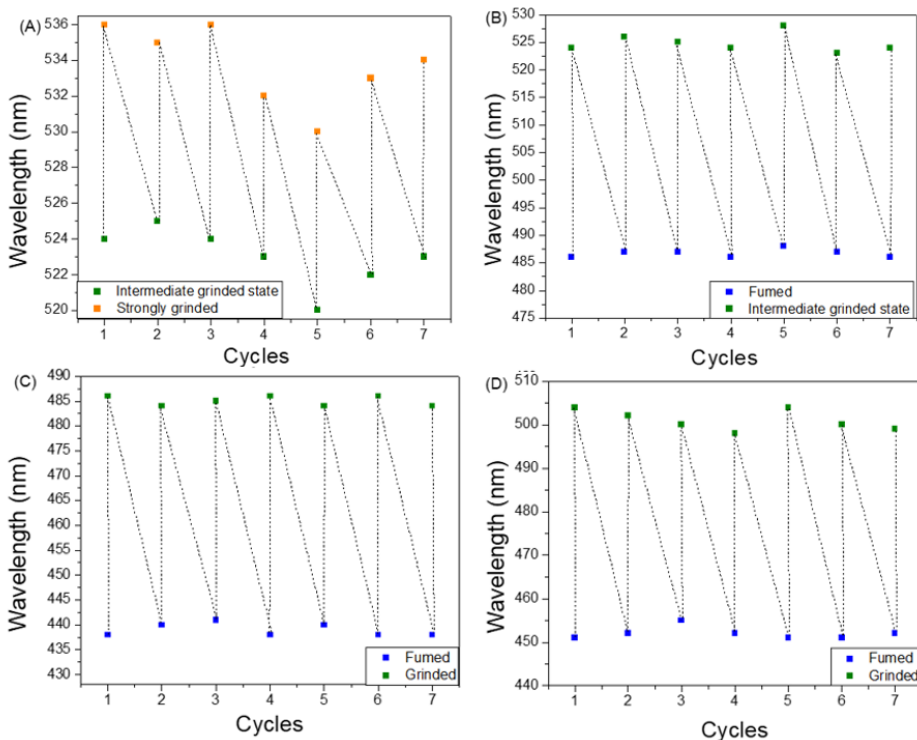


**Figure 6.13.** Repeated switching of the solid-state fluorescence of (A) *p*-PTZ in its intermediate and strongly grinded state and (B) *p*-PTZ, (C) *m*-PTZ and (D) *o*-PTZ by repeated grinding and fuming cycles.

The highest spectral shift initiated by grinding was observed in *o*-PTZ which is associated to a loosely packed structure. The *o*-PTZ isomer has absence of multiple C–H..... $\pi$  interactions and shows weak H-bonds which could be easily perturbed on grinding assuming a more planar structure resulting in higher bathochromic shift. The tightly packed crystal structure of *m*-PTZ driven by extensive C–H..... $\pi$  interactions makes it less susceptible to mechanical stimuli. The reversible mechanochromism by fumigation could be repeated upto many cycles for all the isomers (Figure 6.13.). The wavelength for pristine, grinded, fumed and self-reversible solids are given in Table 6.4. The PLQY of *p*-PTZ pristine powder and its

polymorphs ***p*-PTZ GC** and ***p*-PTZ YC** are 0.22, 0.26 and 0.21 respectively. The PLQY for ***p*-PTZ** at 524 nm is 0.19 and at 536 nm is 0.20. The fumed solid of ***p*-PTZ** has PLQY 0.24. The PLQY for pristine, grinded and fumed solids of ***m*-PTZ** is 0.02, 0.04 and 0.03 respectively. The PLQY for pristine, grinded and fumed solids of ***o*-PTZ** is 0.02, 0.01 and 0.01 respectively.

**Table 6.4.** Peak emission wavelengths ( $\lambda$ , in nm) of ***p*-PTZ**, ***m*-PTZ** and ***o*-PTZ** as pristine, grinded and fumed solids.

Compounds	Emission			
	$\lambda_{\text{pristine}}$ (nm)	$\lambda_{\text{ground}}$ (nm)	$\lambda_{\text{fumed}}$ (nm)	$\Delta\lambda^{\text{a}}$ (nm)
<b><i>p</i>-PTZ</b>	484	524 (intermediate state)	486	52
		536 (strong grinding)		
<b><i>m</i>-PTZ</b>	440	486	438	47
<b><i>o</i>-PTZ</b>	447	504	451	58

<sup>a</sup> Grinding-induced spectral shift,  $\Delta\lambda = \lambda_{\text{ground}} - \lambda_{\text{fumed/pristine}}$

## 6.8. Powder X-ray diffraction studies

The powder X-ray diffraction studies were carried out for the pristine, grinded and fumed solids of the isomers to find out the underlying mechanism for mechanochromic behaviour (Figure 6.14.). The ***p*-PTZ GC** and ***p*-PTZ YC** possess different diffraction patterns confirming its polymorphic nature. The sharp and intense diffraction patterns for pristine solids of all the isomers establish their crystalline nature. The intense peaks are lost on grinding and a wide diffused peak is observed for the grinded solids. The crystallinity is regained on fumigation which can be seen from the sharp patterns obtained for the fumed solids. The PXRD results prove that the crystalline pristine solids form an amorphous metastable state on grinding and the fumigation regenerates the crystallinity. The stimuli reactive colour change can therefore be related to a phase transition from

crystalline to amorphous caused by the disturbance in molecular packing on applying mechanical force.

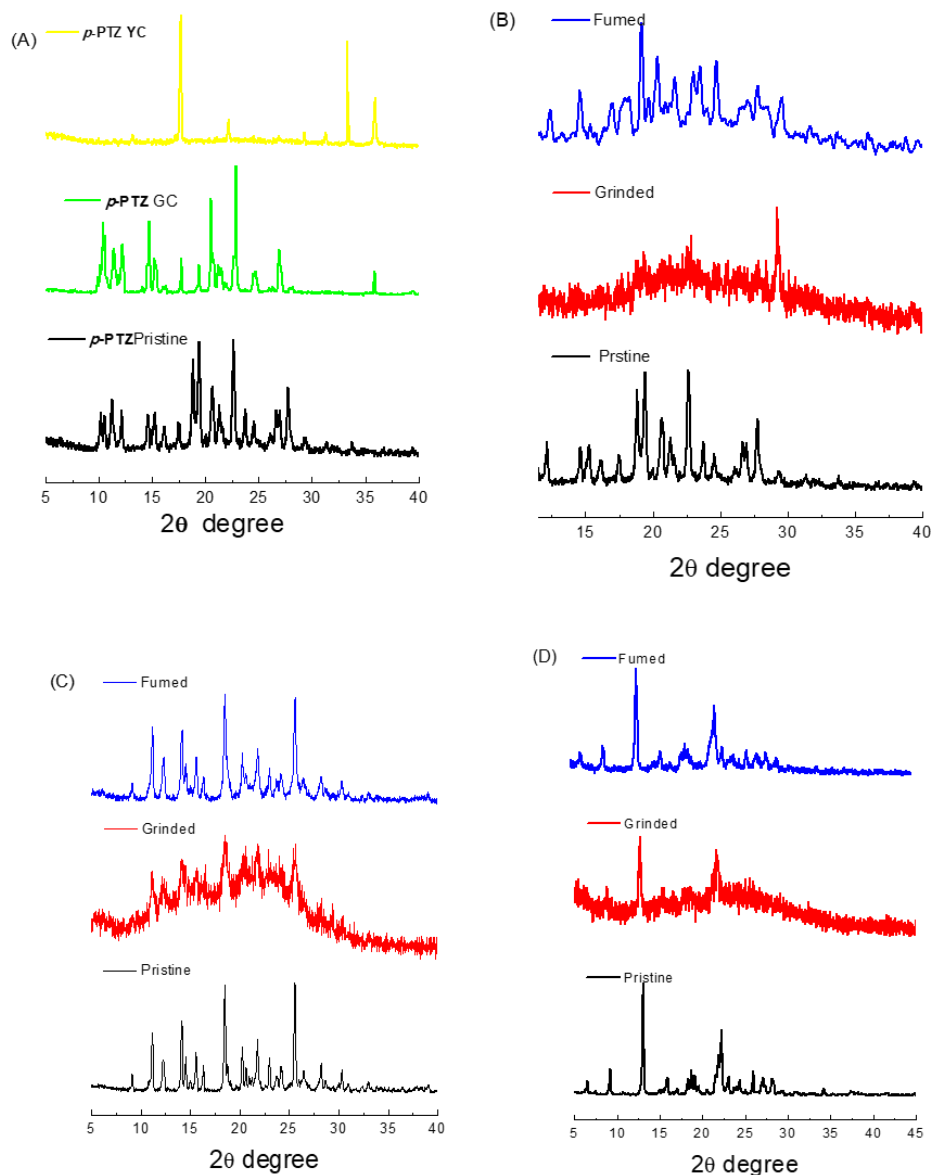


**Figure 6.14.** PXRD patterns of (A) *p*-PTZ pristine and its polymorphs *p*-PTZ GC and *p*-PTZ YC and (B) *p*-PTZ, (C) *m*-PTZ and (D) *o*-PTZ in its pristine, grinded and fumed forms.

## 6.9. Acidochromism

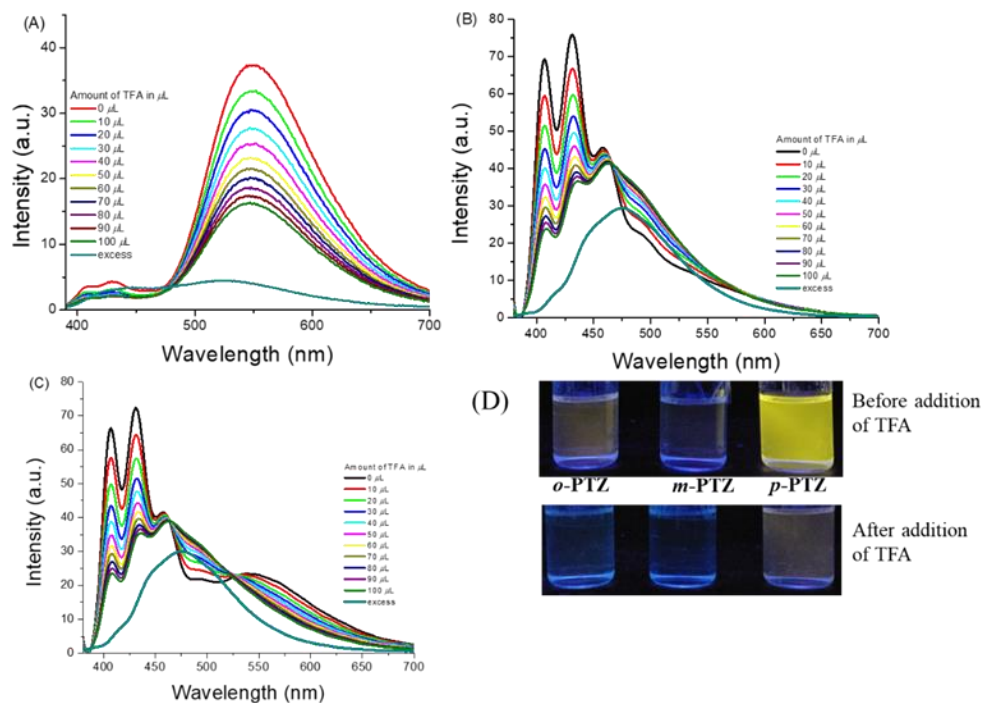


**Figure 6.15.** Emission spectra of (A) *p*-PTZ, (B) *m*-PTZ and (C) *o*-PTZ in  $\text{CHCl}_3$  on titration with known amounts of TFA ( $10\mu\text{L}$ - $100\mu\text{L}$ ), (Conc.  $2\times 10^{-5}$  M). (D) Emission photographs of *p*-PTZ, *m*-PTZ and *o*-PTZ in response to TFA.

The free N atom present in the **BT** moiety of the isomers are capable of protonation owing to which the response of isomers on treating with trifluoroacetic acid (TFA) was studied using fluorescence spectroscopy (Figure 6.15).<sup>[22]</sup> The experiment was carried out by titrating solution of the isomers in  $\text{CHCl}_3$  ( $2\times 10^{-5}$  M) against known amounts of TFA. The intensity emission maxima of *p*-PTZ at 549 nm due to ICT quenches on addition of TFA ( $10\mu\text{L}$ - $100\mu\text{L}$ ). On excess addition of TFA a low intensity blue shifted broad emission was observed at 524 nm. The addition of TFA ( $10\mu\text{L}$ - $100\mu\text{L}$ ) to the solution of *m*-PTZ isomer results in quenching of its localized emissions (407 nm, 431 nm and 458 nm) and a broad red shifted low intensity emission peak was seen at 475 nm on excess addition of TFA. The *o*-PTZ isomer in  $\text{CHCl}_3$  displays LE emission (407 nm, 432 nm and

458 nm) and CT emission at 539 nm. The addition of TFA ( $10\mu\text{L}$ - $100\mu\text{L}$ ) quenches the LE emissions and causes the CT emission to broaden and disappear. In excess TFA a broad emission is observed at 475 nm. The quenching efficiency of the emission maxima for *p*-PTZ, *m*-PTZ and *o*-PTZ is 87%, 61% and 58% respectively. The effective quenching of the emission of the isomers confirms that they are responsive to TFA and can act as potential TFA sensors.

### 6.10. Density functional theory calculations

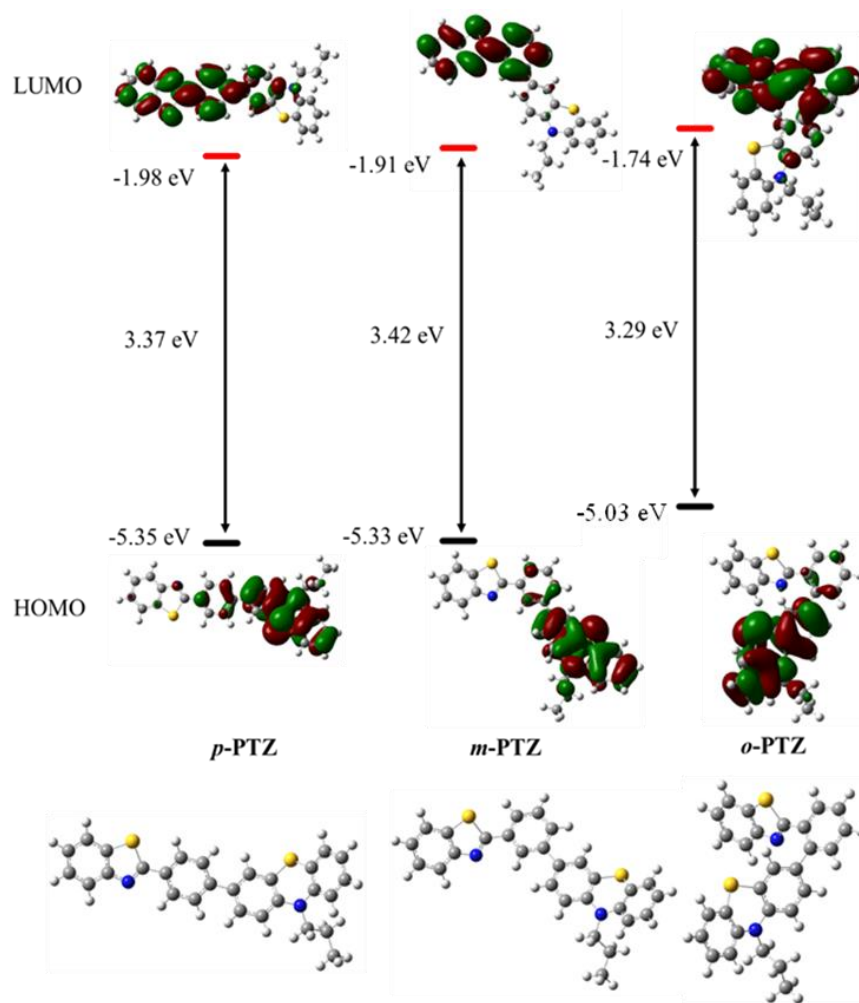


**Figure 6.16.** Energy level diagram showing the HOMO and LUMO energy levels of *p*-PTZ, *m*-PTZ and *o*-PTZ as determined at the B3LYP/6-31G+(d,p) level and their optimized structures.

The density functional theory calculations were done to analyse the geometries and the electronic distribution present in ground state for the isomers by utilizing the basis set B3LYP/631-G+ (d,p).<sup>[23]</sup> The optimized structures of the isomers are in accordance with the single crystal structure. The *o*-PTZ isomer has an extremely twisted structure as compared to the *m*-PTZ and *p*-PTZ isomer. Figure 6.16. depicts the optimized structures and calculated frontier orbitals whose values are listed in Table 6.5. The highest occupied molecular orbital (HOMO) is mainly concentrated on the donor PTZ moiety extending towards the phenyl ring while the lowest unoccupied molecular orbital (LUMO) is concentrated on the acceptor BT moiety. The calculated HOMO-LUMO gap for *p*-PTZ, *m*-PTZ and *o*-PTZ are 3.37 eV, 3.42 eV and 3.29 eV respectively.

**Table 6.5.** DFT calculations of *p*-PTZ, *m*-PTZ and *o*-PTZ.

Compounds	DFT calculations		
	HOMO <sup>a</sup> eV	LUMO <sup>a</sup> eV	HOMO-LUMO gap eV
<i>p</i> -PTZ	-5.35	-1.98	3.37
<i>m</i> -PTZ	-5.33	-1.91	3.42
<i>o</i> -PTZ	-5.03	-1.74	3.29

<sup>a</sup> Theoretical values at B3LYP/6-31G +(d,p) level.

## 6.11. Experimental details

### General methods

Chemicals were used as received unless otherwise indicated. All oxygen or moisture sensitive reactions were performed under nitrogen/argon atmosphere. <sup>1</sup>H NMR (400 MHz) and <sup>13</sup>C NMR (100 MHz) spectra were recorded on a Bruker Avance III instrument by using CDCl<sub>3</sub>. <sup>1</sup>H NMR chemical shifts are reported in parts per million (ppm) relative to the solvent

residual peak (CDCl<sub>3</sub>, 7.26 ppm). Multiplicities are given as s (singlet), d (doublet), t (triplet) and m (multiplet), and the coupling constants, *J*, are given in hertz. <sup>13</sup>C NMR chemical shifts are reported relative to the solvent residual peak (CDCl<sub>3</sub>, 77.0 ppm). UV–visible absorption spectra were recorded on a Perkin Elmer Lambda 35 UV–visible spectrophotometer. Emission spectra were taken in a The Fluoromax-4C, S/n.1579D-1417-FM Fluorescence software Ver 3.8.0.60. The relative quantum yields in solution were calculated using Quinine sulphate in 0.5 M H<sub>2</sub>SO<sub>4</sub> solution as standard. The quantum yields in solid state were measured using K-sphere Integrating sphere. The excitation and emission slits were 2/2 nm for the emission measurements and 3/3 for solid quantum yield measurements. All the measurements were done at 25 °C. HRMS were recorded on a Bruker-Daltonics micrOTOF-Q II mass spectrometer. Single-crystal X-ray structural studies of *p*-PTZ GC and *p*-PTZ YC were performed on a CCD equipped SUPERNOVA diffractometer from Agilent Technologies with Oxford Instruments low-temperature attachment under argon/nitrogen using standard Schlenk and vacuum-line techniques. Single-crystal X-Ray structural studies for *m*-PTZ was collected using (BRUKER KAPPA APEX II CCD Duo) with graphite monochromatic Mo K $\alpha$  radiation (0.71073 Å), on an Xcalibur, Eos, Gemini diffractometer. Single crystal X-ray structural studies for compound *o*-PTZ were collected on a Bruker D8 VENTURE diffractometer equipped with CMOS Photon 100 detector and MoK $\alpha$  ( $\lambda = 0.71073 \text{ \AA}$ ) radiation was used. The acidochromism was performed using 0.1 M stock solution of TFA in CHCl<sub>3</sub>. The PXRD studies were done using powdered samples on Rigaku SmartLab, Automated Multipurpose x-ray Diffractometer, equipped with a high-accuracy theta-theta goniometer featuring a horizontal sample mount. Scanning Electron Microscope (FE-SEM) was performed on Supra55 Zeiss, GEMINI Technology.

### Synthesis and characterization of *p*-PTZ, *m*-PTZ and *o*-PTZ.

General procedure for the synthesis of *p*-PTZ, *m*-PTZ and *o*-PTZ. **BT-1** (1.03 mmol), **PTZ-3** (1.03 mmol) and K<sub>2</sub>CO<sub>3</sub> (5.16 mmol) were dissolved in a mixture of tetrahydrofuran (20.0 mL)/ H<sub>2</sub>O (4.0 mL) and the solution was degassed. Pd(PPh<sub>3</sub>)<sub>4</sub> (0.10 mmol) was added to the resulting mixture and was stirred at 80 °C for 24 h under an argon atmosphere. After cooling, the mixture was evaporated to dryness and the residue was subjected to column chromatography on silica (hexane–DCM 70:30 in vol) to yield the desired product *p*-PTZ as a green powder. The same procedure was employed using intermediates **PTZ-3** and **BT-2** to obtain product *m*-PTZ as white powder. The product *o*-PTZ was also obtained as white powder by applying the above procedure using intermediates **PTZ-3** and **BT-3**.

*p*-PTZ Yield: 73%; <sup>1</sup>H NMR (400 MHz, CDCl<sub>3</sub>, 25 °C): δ 8.13 (d, *J* = 8.0 Hz, 2H), 8.08 (d, *J* = 8.0 Hz, 1H), 7.92 (d, *J* = 8.0 Hz, 1H), 7.66 (d, *J* = 8.0 Hz, 2H), 7.50 (t, *J* = 8.0 Hz, 1H), 7.37–7.46 (m, 3H), 7.15 (d, *J* = 8.0 Hz, 2H), 6.87–6.94 (m, 3H), 3.86 (t, *J* = 8.0 Hz, 2H), 1.83–1.91 (m, 2H), 1.04 (t, *J* = 8.0 Hz, 3H); <sup>13</sup>C NMR (100 MHz, CDCl<sub>3</sub>, 25 °C): δ 167.7, 154.2, 145.1, 144.8, 142.4, 135.3, 135.0, 134.0, 132.1, 128.9, 128.0, 127.5, 127.3, 126.8, 126.3, 125.9, 125.7, 125.4, 125.1, 124.3, 123.1, 122.5, 121.6, 115.5, 115.4, 49.2, 20.1, 11.3, 0.0 ppm; HRMS (ESI): calcd. for C<sub>28</sub>H<sub>22</sub>N<sub>2</sub>S<sub>2</sub> [M + H]<sup>+</sup>: 451.1297. Found: 451.1296.

*m*-PTZ Yield: 71%; <sup>1</sup>H NMR (400 MHz, CDCl<sub>3</sub>, 25 °C): δ 8.27 (s, 1H), 8.11 (d, *J* = 8.0 Hz, 1H), 8.02 (d, *J* = 8.0 Hz, 1H), 7.93 (d, *J* = 8.0 Hz, 1H), 7.64–7.66 (m, 1H), 7.46–7.55 (m, 4H), 7.39–7.43 (m, 1H), 7.15–7.18 (m, 2H), 6.88–6.95 (m, 3H), 3.87 (t, *J* = 8.0 Hz, 2H), 1.83–1.92 (m, 2H), 1.04 (t, *J* = 8.0 Hz, 3H); <sup>13</sup>C NMR (100 MHz, CDCl<sub>3</sub>, 25 °C): δ 168.0, 154.1, 154.1, 144.9, 140.9, 135.1, 134.3, 134.1, 129.4, 129.0, 127.4, 127.3, 126.3, 126.1, 126.0, 125.8, 125.4, 125.4, 125.2, 124.4, 123.2, 122.5, 121.6, 115.5, 115.4, 49.2, 20.1, 11.3, 0.0 ppm; HRMS (ESI): calcd. for C<sub>28</sub>H<sub>22</sub>N<sub>2</sub>S<sub>2</sub> [M]<sup>+</sup>: 450.1219. Found: 450.1201.

***o*-PTZ** Yield: 79%;  $^1\text{H}$  NMR (400 MHz,  $\text{CDCl}_3$ , 25 °C):  $\delta$  8.05–8.07 (m, 2H), 7.75 (d,  $J = 8.0$  Hz, 1H), 7.43–7.52 (m, 3H), 7.30–7.38 (m, 2H), 7.10–7.16 (m, 3H), 6.99 (d,  $J = 8.0$  Hz, 1H), 6.91 (t,  $J = 8.0$  Hz, 1H), 6.85 (d,  $J = 8.0$  Hz, 1H), 6.73 (d,  $J = 8.0$  Hz, 1H), 3.79 (t,  $J = 8.0$  Hz, 2H), 1.76–1.88 (m, 2H), 1.01 (t,  $J = 8.0$  Hz, 3H);  $^{13}\text{C}$  NMR (100 MHz,  $\text{CDCl}_3$ , 25 °C):  $\delta$  167.7, 152.8, 144.9, 144.9, 140.6, 136.7, 134.1, 132.5, 130.8, 130.4, 130.0, 129.2, 128.3, 127.6, 127.4, 127.2, 125.8, 124.8, 124.7, 124.3, 123.2, 122.4, 121.4, 115.3, 114.9, 49.3, 20.0, 11.3, 0.0 ppm; HRMS (ESI): calcd. for  $\text{C}_{28}\text{H}_{22}\text{N}_2\text{S}_2$   $[\text{M} + \text{H}]^+$ : 451.1297. Found: 451.1228.

## 6.12. Conclusion

In conclusion, a series of D-A positional isomers ***p*-PTZ**, ***m*-PTZ** and ***o*-PTZ** were designed and synthesized using Suzuki cross-coupling reaction in order to regulate the donor-acceptor character as well as the intermolecular interactions in solid state. The functionalization of phenothiazine (**PTZ**) at *para*, *meta* and *ortho* positions of phenyl **BT** resulted in contrasting photophysical and electronic properties. The ***p*-PTZ** isomer displayed strong ICT characteristics owing to enhanced conjugation due to lower degree of twisting. In contrast, the ***m*-PTZ** and ***o*-PTZ** displayed quenching of emission in polar solvents due to formation of TICT state. The non-planar twisted structures of the isomers assist in intensity enhancement in aggregated state and endow them with reversible MFC characteristics. The MFC behaviour is associated with generation of metastable states and is reflected from the crystalline to amorphous phase transformation studied by PXRD. The isomers exhibit self-reversible colour switching owing to the conformational flexibility of PTZ moiety. The unique butterfly shape of PTZ moiety allows it to exist in different conformations namely quasi axial and quasi equatorial in ***p*-PTZ** isomer resulting in polymorphism, which was also explored using SEM, PXRD and SCXRD. The single crystal X-ray analysis of the ***m*-PTZ** reveals multiple C–H..... $\pi$  interactions driven tightly packed structure, which makes it less

susceptible to grinding as compared to *o*-PTZ which has weak H-bonds and absence of C–H... $\pi$  interactions thereby exhibiting highest grinding induced spectral shift. The DFT optimized structures are in accordance with the single crystal structures. The isomers due to the presence of free N atom display sensing of trifluoroacetic acid. The work is of great importance for designing MFC materials with self-recovering mechanism. The adaptable conformations of PTZ moiety can regulate the intermolecular interactions resulting in molecules with distinct photophysical properties. The chosen strategy opens new avenues for producing smart stimuli responsive materials with modulate solid state properties.

### 6.13. References

- [1] (a) Weder, C. (2011). Mechanoresponsive materials. *J. Mater. Chem.*, 21(23), 8235-8236 (DOI: 10.1039/C1JM90068D); (b) B Sagara, Y., Kato, T. (2009). Mechanically induced luminescence changes in molecular assemblies. *Nat. Chem.*, 1(8), 605-610 (DOI: 10.1038/nchem.411); (c) Davis, D. A., Hamilton, A., Yang, J., Cremer, L. D., Van Gough, D., Potisek, S. L., Ong, M.T., Braun, P.V., Martínez, T.J., White, S.R. Moore, J.S., Sottos, N. R. (2009). Force-induced activation of covalent bonds in mechanoresponsive polymeric materials. *Nature*, 459(7243), 68-72 (DOI: 10.1038/nature07970); (d) Hirata, S., Watanabe, T. (2006). Reversible thermoresponsive recording of fluorescent images (TRF). *Advanced Materials*, 18(20), 2725-2729 (DOI: 10.1002/adma.200600209); (e) Sagara, Y., Yamane, S., Mitani, M., Weder, C., Kato, T. (2016). Mechanoresponsive luminescent molecular assemblies: an emerging class of materials. *Adv. Mater.*, 28(6), 1073-1095 (DOI: 10.1002/adma.201502589); (f) Gallardo, I., Guirado, G., Hernando, J., Morais, S., Prats, G. (2016). A multi-stimuli responsive switch as a fluorescent molecular analogue of transistors. *Chem. Sci*, 7(3), 1819-1825 (DOI:

- 10.1039/C5SC03395K); (g) Hou, X., Ke, C., Bruns, C. J., McGonigal, P. R., Pettman, R. B., Stoddart, J. F. (2015). Tunable solid-state fluorescent materials for supramolecular encryption. *Nat. Commun.*, *6*(1), 1-9 (DOI: 10.1038/ncomms7884); (h) Sagara, Y., Yamane, S., Mutai, T., Araki, K., Kato, T. (2009). A stimuli-responsive, photoluminescent, anthracene-based liquid crystal: emission color determined by thermal and mechanical processes. *Adv. Funct. Mater.*, *19*(12), 1869-1875 (DOI: 10.1002/adfm.200801726); (i) Luo, X., Li, J., Li, C., Heng, L., Dong, Y. Q., Liu, Z., Bo, Z. Tang, B. Z. (2011). Reversible switching of the emission of diphenyldibenzofulvenes by thermal and mechanical stimuli. *Adv. Mater.*, *23*(29), 3261-3265 (DOI: 10.1002/adma.201101059); (j) Minkin, V. I. (2004). Photo-, thermo-, solvato-, and electrochromic spiroheterocyclic compounds. *Chem. Rev.*, *104*(5), 2751-2776 (DOI: 10.1021/cr020088u); (k) Zhang, X., Chi, Z., Li, H., Xu, B., Li, X., Zhou, W., Liu, S., Zhang, Y., Xu, J. (2011). Piezofluorochromism of an aggregation-induced emission compound derived from tetraphenylethylene. *Chem. Asian J.*, *6*(3), 808-811 (DOI: 10.1002/asia.201000802); (l) Kishimura, A., Yamashita, T., Yamaguchi, K., Aida, T. (2005). Rewritable phosphorescent paper by the control of competing kinetic and thermodynamic self-assembling events. *Nat. Mater.*, *4*(7), 546-549 (DOI: 10.1038/nmat1401); (m) Chi, Z., Zhang, X., Xu, B., Zhou, X., Ma, C., Zhang, Y., Liu, S., Xu, J. (2012). Recent advances in organic mechanofluorochromic materials. *Chem. Soc. Rev.*, *41*(10), 3878-3896 (DOI: 10.1039/C2CS35016E)
- [2] (a) Farinola, G. M., Ragni, R. (2011). Electroluminescent materials for white organic light emitting diodes. *Chem. Soc. Rev.*, *40*(7), 3467-3482 (DOI: 10.1039/C0CS00204F); (b) Ning, Z., Chen, Z., Zhang, Q., Yan, Y., Qian, S., Cao, Y., Tian, H. (2007). Aggregation-

induced emission (AIE)-active starburst triarylamine fluorophores as potential non-doped red emitters for organic light-emitting diodes and Cl<sub>2</sub> gas chemodosimeter. *Adv. Funct. Mater.*, *17*(18), 3799-3807 (DOI: 10.1002/adfm.200700649); (c) Sun, H., Liu, S., Lin, W., Zhang, K. Y., Lv, W., Huang, X., Huo, F., Yang, H., Jenkins, G., Zhao, Q., Huang, W. (2014). Smart responsive phosphorescent materials for data recording and security protection. *Nat. Commun.*, *5*(1), 1-9 (DOI: 10.1038/ncomms4601); (d) Samuel, I. D. W., Turnbull, G. A. (2007). Organic semiconductor lasers. *Chem. Rev.*, *107*(4), 1272-1295 (DOI: 10.1021/cr050152i); (e) Yuan, L., Lin, W., Zheng, K., He, L., Huang, W. (2013). Far-red to near infrared analyte-responsive fluorescent probes based on organic fluorophore platforms for fluorescence imaging. *Chem. Soc. Rev.*, *42*(2), 622-661 (DOI: 10.1039/C2CS35313J); (f) Xu, B., Xie, M., He, J., Xu, B., Chi, Z., Tian, W., L., Zhao, F., Liu, S., Zhang, Y., Xu, J. (2013). An aggregation-induced emission luminophore with multi-stimuli single-and two-photon fluorescence switching and large two-photon absorption cross section. *Chem. Commun.*, *49*(3), 273-275 (DOI: 10.1039/C2CC36806D); (g) Liang, J., Tang, B. Z., Liu, B. (2015). Specific light-up bioprobes based on AIEgen conjugates. *Chem. Soc. Rev.*, *44*(10), 2798-2811 (DOI: 10.1039/C4CS00444B); (h) Kaji, H., Suzuki, H., Fukushima, T., Shizu, K., Suzuki, K., Kubo, S., Komino, T., Oiwa, H., Suzuki, F., Wakamiya, A., Murata, Y., Adachi, C. (2015). Purely organic electroluminescent material realizing 100% conversion from electricity to light. *Nat. Commun.*, *6*(1), 1-8 (DOI: 10.1038/ncomms9476); (i) Zheng, R., Mei, X., Lin, Z., Zhao, Y., Yao, H., Lv, W., Ling, Q. (2015). Strong CIE activity, multi-stimuli-responsive fluorescence and data storage application of new diphenyl maleimide derivatives. *J. Mater. Chem. C*, *3*(39), 10242-10248 (DOI: 10.1039/C5TC02374B); (j) Balch, A. L. (2009).

Dynamic Crystals: Visually Detected Mechanochemical Changes in the Luminescence of Gold and Other Transition-Metal Complexes. *Angew. Chem. Int. Ed.*, 48(15), 2641-2644 (DOI: 10.1002/anie.200805602); (k) Chan, E. P., Walish, J. J., Urbas, A. M., Thomas, E. L. (2013). Mechanochromic photonic gels. *Adv. Mater.*, 25(29), 3934-3947 (DOI: 10.1002/adma.201300692); (l) Berkovic, G., Krongauz, V., Weiss, V. (2000). Spiropyrans and spirooxazines for memories and switches. *Chem. Rev.*, 100(5), 1741-1754 (DOI: 10.1021/cr9800715)

- [3] (a) Xu, J., Chi, Z. (Eds.). (2014). Mechanochromic Fluorescent Materials: Phenomena, Materials and Applications. *Royal Society of Chemistry*; (b) Ciardelli, F., Ruggeri, G., Pucci, A. (2013). Dye-containing polymers: methods for preparation of mechanochromic materials. *Chem. Soc. Rev.* 42(3), 857-870 (DOI: 10.1039/C2CS35414D); (c) Crenshaw, B. R., Burnworth, M., Khariwala, D., Hiltner, A., Mather, P. T., Simha, R., Weder, C. (2007). Deformation-induced color changes in mechanochromic polyethylene blends. *Macromolecules*, 40(7), 2400-2408 (DOI: 10.1021/ma062936j); (d) Zhang, X., Chi, Z., Zhang, Y., Liu, S., Xu, J. (2013). Recent advances in mechanochromic luminescent metal complexes. *J. Mater. Chem. C*, 1(21), 3376-3390 (DOI: 10.1039/C3TC30316K); (e) Luo, X., Li, J., Li, C., Heng, L., Dong, Y. Q., Liu, Z., Bo, Z., Tang, B. Z. (2011). Reversible switching of the emission of diphenyldibenzofulvenes by thermal and mechanical stimuli. *Adv. Mater.*, 23(29), 3261-3265 (DOI: 10.1002/adma.201101059); (f) Yoon, S. J., Chung, J. W., Gierschner, J., Kim, K. S., Choi, M. G., Kim, D., Park, S. Y. (2010). Multistimuli two-color luminescence switching via different slip-stacking of highly fluorescent molecular sheets. *J. Am. Chem. Soc.*, 132(39), 13675-13683 (DOI: 10.1021/ja1044665); (g) Xue, P., Ding, J., Wang, P., Lu, R. (2016). Recent progress in the

- mechanochromism of phosphorescent organic molecules and metal complexes. *J. Mater. Chem. C*, 4(28), 6688-6706 (DOI: 10.1039/C6TC01503D); (h) Ito, H., Saito, T., Oshima, N., Kitamura, N., Ishizaka, S., Hinatsu, Y., Wakeshima, M., Kato, M., Tsuge, K., Sawamura, M. (2008). Reversible mechanochromic luminescence of [(C6F5Au)<sub>2</sub>( $\mu$ -1, 4-diisocyanobenzene)]. *J. Am. Chem. Soc.*, 130(31), 10044-10045 (DOI: 10.1021/ja8019356)
- [4] (a) Yuan, W. Z., Tan, Y., Gong, Y., Lu, P., Lam, J. W., Shen, X. Y., Feng, C., Sung, H.H.Y., Lu, Y., Williams, I.D., Sun, J.Z., Tang, B. Z. (2013). Synergy between twisted conformation and effective intermolecular interactions: strategy for efficient mechanochromic luminogens with high contrast. *Adv. Mater.*, 25(20), 2837-2843 (DOI: 10.1002/adma.201205043); (b) Kwon, M. S., Gierschner, J., Yoon, S. J., Park, S. Y. (2012). Unique piezochromic fluorescence behavior of dicyanodistyrylbenzene based donor–acceptor–donor triad: mechanically controlled photo-induced electron transfer (eT) in molecular assemblies. *Adv. Mater.*, 24(40), 5487-5492 (DOI: 10.1002/adma.201202409); (c) Sagara, Y., Mutai, T., Yoshikawa, I., Araki, K. (2007). Material design for piezochromic luminescence: hydrogen-bond-directed assemblies of a pyrene derivative. *J. Am. Chem. Soc.*, 129(6), 1520-1521 (DOI: 10.1021/ja0677362); (d) Zong, L., Xie, Y., Wang, C., Li, J. R., Li, Q., Li, Z. (2016). From ACQ to AIE: the suppression of the strong  $\pi$ – $\pi$  interaction of naphthalene diimide derivatives through the adjustment of their flexible chains. *Chem. Commun*, 52(77), 11496-11499 (DOI: 10.1039/C6CC06176A); (e) Misra, R., Jadhav, T., Dhokale, B., Mobin, S. M. (2014). Reversible mechanochromism and enhanced AIE in tetraphenylethene substituted phenanthroimidazoles. *Chemical Communications*, 50(65), 9076-9078 (DOI: 10.1039/C4CC02824D); (f) Walters, D. T., Aghakhanpour, R. B., Powers, X. B., Ghiassi, K. B., Olmstead, M.

- M., Balch, A. L. (2018). Utilization of a Nonemissive Triphosphine Ligand to Construct a Luminescent Gold (I)-Box That Undergoes Mechanochromic Collapse into a Helical Complex. *J. Am. Chem. Soc.*, *140*(24), 7533-7542 (DOI: 10.1021/jacs.8b01666)
- [5] (a) J. B. Birks, *Photophysics of Aromatic Molecules*, Wiley, London, UK, 1970; (b) Ma, X., Sun, R., Cheng, J., Liu, J., Gou, F., Xiang, H., Zhou, X. (2016). Fluorescence aggregation-caused quenching versus aggregation-induced emission: a visual teaching technology for undergraduate chemistry students. *J. Chem. Educ.*, *93*(2), 345-350 (DOI: 10.1021/acs.jchemed.5b00483); (c) Jayanty, S., Radhakrishnan, T. P. (2004). Enhanced fluorescence of remote functionalized diaminodicyanoquinodimethanes in the solid state and fluorescence switching in a doped polymer by solvent vapors. *Chem. Eur. J.*, *10*(3), 791-797 (DOI: 10.1002/chem.200305123); (d) Tracy, H. J., Mullin, J. L., Klooster, W. T., Martin, J. A., Haug, J., Wallace, S., S., Rudloe, I., Watts, K. (2005). Enhanced photoluminescence from group 14 metalloles in aggregated and solid solutions. *Inorganic chemistry*, *44*(6), 2003-2011 (DOI: 10.1021/ic049034o); (e) Th. Forster and K. Z. Kasper, *Phys. Chem.*, (Munich) 1954, 1, 275-282; (f) Hong, Y., Lam, J. W., Tang, B. Z. (2011). Aggregation-induced emission. *Chem. Soc. Rev.*, *40*(11), 5361-5388 (DOI: 10.1039/C1CS15113D)
- [6] (a) Mei, J., Leung, N. L., Kwok, R. T., Lam, J. W., Tang, B. Z. (2015). Aggregation-induced emission: together we shine, united we soar!. *Chem. Rev.*, *115*(21), 11718-11940 (DOI: 10.1021/acs.chemrev.5b00263); (b) Luo, J., Xie, Z., Lam, J. W., Cheng, L., Chen, H., Qiu, C., Kwok, H.S., Zhan, X., Liu, Y., Zhu, D., Tang, B. Z. (2001). Aggregation-induced emission of 1-methyl-1, 2, 3, 4, 5-pentaphenylsilole. *Chem. Commun.*, (18), 1740-1741 (DOI: 10.1039/B105159H); (c) Liu, H., Xu, J., Li, Y., Li, Y. (2010). Aggregate nanostructures of organic molecular materials. *Accounts*

of *chemical research*, 43(12), 1496-1508 (DOI: 10.1021/ar100084y)

- [7] (a) Yagai, S., Okamura, S., Nakano, Y., Yamauchi, M., Kishikawa, K., Karatsu, T., Kitamura, A., Ueno, A., Kuzuhara, D., Yamada, H. and Seki, T., Ito, H. (2014). Design amphiphilic dipolar  $\pi$ -systems for stimuli-responsive luminescent materials using metastable states. *Nat. Commun.*, 5(1), 1-10 (DOI: 10.1038/ncomms5013); (b) Dong, Y., Xu, B., Zhang, J., Tan, X., Wang, L., Chen, J., Lv, H., Wen, S., Li, B., Ye, L. and Zou, B., Tian, W. (2012). Piezochromic luminescence based on the molecular aggregation of 9, 10-Bis ((E)-2-(pyrid-2-yl) vinyl) anthracene. *Angewandte Chemie International Edition*, 51(43), 10782-10785 (DOI: 10.1002/anie.201204660); (c) Varghese, S., Das, S. (2011). Role of molecular packing in determining solid-state optical properties of  $\pi$ -conjugated materials. *J. Phys. Chem. Lett.*, 2(8), 863-873 (DOI: 10.1021/jz200099p); (d) Ooyama, Y., Harima, Y. (2011). Molecular design of mechanofluorochromic dyes and their solid-state fluorescence properties. *J. Mater. Chem.*, 21(23), 8372-8380 (DOI: 10.1039/C0JM03601C); (e) Suzuki, T., Okada, H., Nakagawa, T., Komatsu, K., Fujimoto, C., Kagi, H., Matsuo, Y. (2018). A fluorenylidene-acridane that becomes dark in color upon grinding—ground state mechanochromism by conformational change. *Chem. Sci*, 9(2), 475-482 (DOI: 10.1039/C7SC03567E); (f) Wang, L., Wang, K., Zou, B., Ye, K., Zhang, H., Wang, Y. (2015). Luminescent chromism of boron diketonate crystals: distinct responses to different stresses. *Adv. Mater.*, 27(18), 2918-2922 (DOI: 10.1002/adma.201500589); (g) Misra, R., Jadhav, T., Dhokale, B., Mobin, S. M. (2014). Reversible mechanochromism and enhanced AIE in tetraphenylethene substituted phenanthroimidazoles. *Chem. Commun.*, 50(65), 9076-9078 (DOI: 10.1039/C4CC02824D)

- [8] (a) Sasaki, S., Suzuki, S., Sameera, W. M. C., Igawa, K., Morokuma, K., Konishi, G. I. (2016). Highly twisted N, N-dialkylamines as a design strategy to tune simple aromatic hydrocarbons as steric environment-sensitive fluorophores. *J. Am. Chem. Soc.*, *138*(26), 8194-8206 (DOI: 10.1021/jacs.6b03749); (b) S. Sekiguchi, K. Kondo, Y. Sei, M. Akita, M. Yoshizawa, *Angew. Chem., Int. Ed.*, 2016, *55*, 6906–6910; (c) Xue, S., Qiu, X., Sun, Q., Yang, W. (2016). Alkyl length effects on solid-state fluorescence and mechanochromic behavior of small organic luminophores. *J. Mater. Chem. C*, *4*(8), 1568-1578 (DOI: 10.1039/C5TC04358A); (d) Yamaguchi, M., Ito, S., Hirose, A., Tanaka, K., Chujo, Y. (2016). Modulation of sensitivity to mechanical stimulus in mechanofluorochromic properties by altering substituent positions in solid-state emissive diiodo boron diimines. *J. Mater. Chem. C*, *4*(23), 5314-5319 (DOI: 10.1039/C6TC01111J); (e) Morris, W. A., Liu, T., Fraser, C. L. (2015). Mechanochromic luminescence of halide-substituted difluoroboron  $\beta$ -diketonate dyes. *J. Mater. Chem. C*, *3*(2), 352-363 (DOI: 10.1039/C4TC02268H); (f) Xu, B., Wu, H., Chen, J., Yang, Z., Yang, Z., Wu, Y. C., Zhang, Y., Jin, C., Lu, P. Y., Chi, Z., Liu, S., Aldred, M. (2017). White-light emission from a single heavy atom-free molecule with room temperature phosphorescence, mechanochromism and thermochromism. *Chem. Sci*, *8*(3), 1909-1914 (DOI: 10.1039/C6SC03038F); (g) Jadhav, T., Choi, J. M., Dhokale, B., Mobin, S. M., Lee, J. Y., Misra, R. (2016). Effect of end groups on mechanochromism and electroluminescence in tetraphenylethylene substituted phenanthroimidazoles. *J. Phys. Chem. C*, *120*(33), 18487-18495 (DOI: 10.1021/acs.jpcc.6b06277).
- [9] (a) Wang, K., Zhang, H., Chen, S., Yang, G., Zhang, J., Tian, W., Su, Z., Wang, Y. (2014). Organic Polymorphs: One-Compound-Based Crystals with Molecular-Conformation-and Packing-Dependent Luminescent Properties. *Adv. Mater.*, *26*(35), 6168-

- 6173 (DOI: 10.1002/adma.201401114); (b) Zhang, G., Lu, J., Sabat, M., Fraser, C. L. (2010). Polymorphism and reversible mechanochromic luminescence for solid-state difluoroboron avobenzene. *J. Am. Chem. Soc.*, 132(7), 2160-2162 (DOI: 10.1021/ja9097719); (c) Luo, G. G., Xia, J. X., Fang, K., Zhao, Q. H., Wu, J. H., Dai, J. C. (2013). Discovery of polymorphism-dependent emission for crystalline boron-dipyrromethene dye. *Dalton Trans.*, 42(46), 16268-16271 (DOI: 10.1039/C3DT52325J)
- [10] (a) Gu, X., Yao, J., Zhang, G., Yan, Y., Zhang, C., Peng, Q., Liao, Q., Wu, Y., Xu, Z., Zhao, Y. and Fu, H., Zhang, D. (2012). Polymorphism-Dependent Emission for Di (p-methoxyphenyl) dibenzofulvene and Analogues: Optical Waveguide/Amplified Spontaneous Emission Behaviors. *Adv. Funct. Mater.*, 22(23), 4862-4872 (DOI: 10.1002/adfm.201201482); (b) Li, R., Xiao, S., Li, Y., Lin, Q., Zhang, R., Zhao, J., Yang, C., Zou, K., Li, D., Yi, T. (2014). Polymorphism-dependent and piezochromic luminescence based on molecular packing of a conjugated molecule. *Chem. Sci*, 5(10), 3922-3928 (DOI: 10.1039/C4SC01243G); (c) Liu, Q., Xie, M., Chang, X., Gao, Q., Chen, Y., Lu, W. (2018). Correlating thermochromic and mechanochromic phosphorescence with polymorphs of a complex gold (i) double salt with infinite aurophilicity. *Chem. Commun.*, 54(91), 12844-12847 (DOI: 10.1039/C8CC05210G)
- [11] (a) Zhao, B., Li, N., Wang, X., Chang, Z., Bu, X. H. (2017). Host-Guest Engineering of Coordination Polymers for Highly Tunable Luminophores Based on Charge Transfer Emissions. *ACS Appl. Mater. Interfaces*, 9(3), 2662-2668 (DOI: 10.1021/acsami.6b14554); (b) Gong, Y., Tan, Y., Liu, J., Lu, P., Feng, C., Yuan, W. Z., Lu, Y., Sun, J.Z., He, G., Zhang, Y. (2013). Twisted D- $\pi$ -A solid emitters: efficient emission and high contrast

mechanochromism. *Chem. Commun.*, *49*(38), 4009-4011 (DOI: 10.1039/C3CC39243K); (c) Li, Y., Liu, T., Liu, H., Tian, M. Z., Li, Y. (2014). Self-assembly of intramolecular charge-transfer compounds into functional molecular systems. *Acc. Chem. Res.*, *47*(4), 1186-1198 (DOI: 10.1021/ar400264e); (d) Jadhav, T., Dhokale, B., Patil, Y., Mobin, S. M., Misra, R. (2016). Multi-stimuli responsive donor–acceptor tetraphenylethylene substituted benzothiadiazoles. *J. Mater. Chem. C*, *120*(42), 24030-24040 (DOI: 10.1021/acs.jpcc.6b09015); (e) Zhu, H., Chen, P., Kong, L., Tian, Y., Yang, J. (2018). Twisted donor– $\pi$ –acceptor carbazole luminophores with substituent-dependent properties of aggregated behavior (Aggregation-Caused quenching to aggregation-enhanced emission) and mechanoresponsive luminescence. *J. Mater. Chem. C*, *122*(34), 19793-19800 (DOI: 10.1021/acs.jpcc.8b05638); (f) Wu, J., Cheng, Y., Lan, J., Wu, D., Qian, S., Yan, L., He, Z., Li, X., Wang, K., Zou, B., You, J. (2016). Molecular engineering of mechanochromic materials by programmed C–H arylation: making a counterpoint in the chromism trend. *J. Am. Chem. Soc.*, *138*(39), 12803-12812 (DOI: 10.1021/jacs.6b03890)

- [12] (a) Ekbote, A., Jadhav, T., Misra, R. (2017). T-Shaped donor–acceptor–donor type tetraphenylethylene substituted quinoxaline derivatives: aggregation-induced emission and mechanochromism. *New J. Chem.*, *41*(17), 9346-9353 (DOI: 10.1039/C7NJ01531C); (b) Desroches, M., Morin, J. F. (2018). Anthanthrene as a super-extended tetraphenylethylene for aggregation-induced emission. *Org. Lett.*, *20*(10), 2797-2801 (DOI: 10.1021/acs.orglett.8b00452); (c) Yin, Y., Zhao, F., Chen, Z., Liu, G., Pu, S. (2018). Aggregation-induced emission enhancement (AIEE)-active mechanofluorochromic tetraphenylethene derivative bearing a rhodamine

- unit. *Tetrahedron Lett*, 59(50), 4416-4419 (DOI: 10.1016/j.tetlet.2018.10.073); (d) Martínez-Abadía, M., Giménez, R., Ros, M. B. (2018). Self-Assembled  $\alpha$ -Cyanostilbenes for Advanced Functional Materials. *Adv. Mater.*, 30(5), 1704161 (DOI: 10.1002/adma.201704161); (e) Luo, J., Xie, Z., Lam, J. W., Cheng, L., Chen, H., Qiu, C., Kwok, H.S., Zhan, X., Liu, Y., Zhu, D., Tang, B. Z. (2001). Aggregation-induced emission of 1-methyl-1, 2, 3, 4, 5-pentaphenylsilole. *Chem. Commun.*, (18), 1740-1741 (DOI: 10.1039/B105159H); (f) Yu, G., Yin, S., Liu, Y., Chen, J., Xu, X., Sun, X., Ma, D., Zhan, X., Peng, Q., Shuai, Z. and Tang, B., (2005). Structures, electronic states, photoluminescence, and carrier transport properties of 1, 1-disubstituted 2, 3, 4, 5-tetraphenylsiloles. *J. Am. Chem. Soc.*, 127(17), 6335-6346 (DOI: 10.1021/ja044628b); (g) Kwon, M. S., Gierschner, J., Yoon, S. J., Park, S. Y. (2012). Unique piezochromic fluorescence behavior of dicyanodistyrylbenzene based donor–acceptor–donor triad: mechanically controlled photo-induced electron transfer (eT) in molecular assemblies. *Adv. Mater.*, 24(40), 5487-5492 (DOI: 10.1002/adma.201202409)
- [13] (a) Xue, P., Ding, J., Chen, P., Wang, P., Yao, B., Sun, J., Sun, J., Lu, R. (2016). Mechanical force-induced luminescence enhancement and chromism of a nonplanar D–A phenothiazine derivative. *J. Mater. Chem. C*, 4(23), 5275-5280 (DOI: 10.1039/C6TC01193D); (b) Zhang, G., Sun, J., Xue, P., Zhang, Z., Gong, P., Peng, J., Lu, R. (2015). Phenothiazine modified triphenylacrylonitrile derivatives: AIE and mechanochromism tuned by molecular conformation. *J. Mater. Chem. C*, 3(12), 2925-2932 (DOI: 10.1039/C4TC02925A); (c) Okazaki, M., Takeda, Y., Data, P., Pander, P., Higginbotham, H., Monkman, A. P., Minakata, S. (2017). Thermally activated delayed fluorescent phenothiazine–dibenzo [a, j] phenazine–phenothiazine triads exhibiting tricolor-

changing mechanochromic luminescence. *Chem. Sci*, 8(4), 2677-2686 (DOI: 10.1039/C6SC04863C); (d) Tian, H., Yang, X., Chen, R., Pan, Y., Li, L., Hagfeldt, A., Sun, L. (2007). Phenothiazine derivatives for efficient organic dye-sensitized solar cells. *Chem. Commun.*, (36), 3741-3743 (DOI: 10.1039/B707485A); (e) Xie, Z., Chen, C., Xu, S., Li, J., Zhang, Y., Liu, S., Xu, J., Chi, Z. (2015). White-Light Emission Strategy of a Single Organic Compound with Aggregation-Induced Emission and Delayed Fluorescence Properties. *Angew. Chem. Int. Ed.*, 127(24), 7287-7290 (DOI: 10.1002/anie.201502180); (f) Ramachandran, E., Dhamodharan, R. (2015). Rational design of phenothiazine (PTz) and ethylenedioxythiophene (EDOT) based donor-acceptor compounds with a molecular aggregation breaker for solid state emission in red and NIR regions. *J. Mater. Chem. C*, 3(33), 8642-8648 (DOI: 10.1039/C5TC01423A).

- [14] (a) Liu, Q., Jian, L., Liu, R., Yang, H., Kong, J., Zhang, X. (2020). Metal-Free Photoinduced Atom Transfer Radical Polymerization for Highly Sensitive Detection of Lung Cancer DNA. *Chem. Eur. J.*, 26(7), 1633-1639 (DOI: 10.1002/chem.201904271); (b) Shen, Y., Chen, P., Liu, J., Ding, J., Xue, P. (2018). Effects of electron donor on luminescence and mechanochromism of D- $\pi$ -A benzothiazole derivatives. *Dyes Pigm*, 150, 354-362 (DOI: 10.1016/j.dyepig.2017.12.034); (c) Zhan, Y., Zhao, J., Yang, P., Ye, W. (2016). Multi-stimuli responsive fluorescent behaviors of a donor- $\pi$ -acceptor phenothiazine modified benzothiazole derivative. *RSC Adv.*, 6(94), 92144-92151 (DOI: 10.1039/C6RA19791D); (d) Liu, X., Li, A., Xu, W., Ma, Z., Jia, X. (2019). An ESIPT-based fluorescent switch with AIEE, solvatochromism, mechanochromism and photochromism. *Mater. Chem. Front.*, 3(4), 620-625 (DOI: 10.1039/C8QM00633D).

- [15] (a) Ekbote, A., Mobin, S. M., Misra, R. (2018). Structure–property relationship in multi-stimuli responsive D–A–A' benzothiazole functionalized isomers. *J. Mater. Chem. C*, 6(40), 10888-10901 (DOI: 10.1039/C8TC04310H); (b) Jadhav, T., Dhokale, B., Mobin, S. M., Misra, R. (2015). Mechanochromism and aggregation induced emission in benzothiazole substituted tetraphenylethylenes: a structure function correlation. *RSC Adv.*, 5(38), 29878-29884 (DOI: 10.1039/C5RA04881H)
- [16] (a) Maleki, B., Salehabadi, H. (2010). Ammonium chloride; as a mild and efficient catalyst for the synthesis of some 2-arylbenzothiazoles and bisbenzothiazole derivatives. *European Journal of Chemistry*, 1(4), 377-380 (DOI: 10.5155/eurjchem.1.4.377-380.165); (b) Mao, M., Zhang, X., Cao, L., Tong, Y., Wu, G. (2015). Design of Bodipy based organic dyes for high-efficient dye-sensitized solar cells employing double electron acceptors. *Dyes Pigm*, 117, 28-36 (DOI: 10.1016/j.dyepig.2015.02.001)
- [17] (a) Misra, R., Jadhav, T., Dhokale, B., Gautam, P., Sharma, R., Maragani, R., Mobin, S. M. (2014). Carbazole-BODIPY conjugates: design, synthesis, structure and properties. *Dalton Trans.*, 43(34), 13076-13086 (DOI: 10.1039/C4DT00983E); (b) Lu, X., Fan, S., Wu, J., Jia, X., Wang, Z. S., Zhou, G. (2014). Controlling the charge transfer in D–A–D chromophores based on pyrazine derivatives. *J. Org. Chem.*, 79(14), 6480-6489 (DOI: 10.1021/jo500856k)
- [18] (a) Roy, B., Reddy, M. C., Hazra, P. (2018). Developing the structure–property relationship to design solid state multi-stimuli responsive materials and their potential applications in different fields. *Chem. Sci*, 9(14), 3592-3606 (DOI: 10.1039/C8SC00143J); (b) Sasaki, S., Drummen, G. P., Konishi, G. I. (2016). Recent advances in twisted intramolecular charge transfer (TICT)

- fluorescence and related phenomena in materials chemistry. *J. Mater. Chem. C*, 4(14), 2731-2743 (DOI: 10.1039/C5TC03933A); (c) Grabowski, Z. R., Rotkiewicz, K., Rettig, W. (2003). Structural changes accompanying intramolecular electron transfer: focus on twisted intramolecular charge-transfer states and structures. *Chem. Rev.*, 103(10), 3899-4032 (DOI: 10.1021/cr9407451); (d) Kundu, A., Karthikeyan, S., Sagara, Y., Moon, D., Anthony, S. P. (2019). Temperature-Controlled Locally Excited and Twisted Intramolecular Charge-Transfer State-Dependent Fluorescence Switching in Triphenylamine–Benzothiazole Derivatives. *ACS omega*, 4(3), 5147-5154 (DOI: 10.1021/acsomega.8b03099)
- [19] (a) Jadhav, T., Dhokale, B., Mobin, S. M., Misra, R. (2015). Aggregation induced emission and mechanochromism in pyrenoimidazoles. *J. Mater. Chem. C*, 3(38), 9981-9988 (DOI: 10.1039/C5TC02181B); (b) Wang, E., Lam, J. W., Hu, R., Zhang, C., Zhao, Y. S., Tang, B. Z. (2014). Twisted intramolecular charge transfer, aggregation-induced emission, supramolecular self-assembly and the optical waveguide of barbituric acid-functionalized tetraphenylethene. *J. Mater. Chem. C*, 2(10), 1801-1807 (DOI: 10.1039/C3TC32161D); (c) Zhang, G. F., Aldred, M. P., Gong, W. L., Li, C., Zhu, M. Q. (2012). Utilising tetraphenylethene as a dual activator for intramolecular charge transfer and aggregation induced emission. *Chem. Commun.*, 48(62), 7711-7713 (DOI: 10.1039/C2CC33218C); (d) Jadhav, T., Dhokale, B., Misra, R. (2015). Effect of the cyano group on solid state photophysical behavior of tetraphenylethene substituted benzothiadiazoles. *J. Mater. Chem. C*, 3(35), 9063-9068 (DOI: 10.1039/C5TC01871D)
- [20] Takeda, Y., Kaihara, T., Okazaki, M., Higginbotham, H., Data, P., Tohnai, N., Minakata, S. (2018). Conformationally-flexible and moderately electron-donating units-installed D–A–D triad enabling

- multicolor-changing mechanochromic luminescence, TADF and room-temperature phosphorescence. *Chem. Commun.*, 54(50), 6847-6850 (DOI: 10.1039/C8CC02365D)
- [21] (a) Zhao, R., Zhao, L., Zhang, M., Li, Z., Liu, Y., Han, T., Gao, K. (2019). Self-recovering mechanochromic luminescent material with aggregation-induced emission: Implication for pressure sensor. *Dyes Pigm.*, 167, 181-188 (DOI: 10.1016/j.dyepig.2019.04.036); (b) Kartha, K. K., Nair, V. S., Praveen, V. K., Takeuchi, M., Ajayaghosh, A. (2019). A self-recovering mechanochromic chiral  $\pi$ -gelator. *J. Mater. Chem. C*, 7(5), 1292-1297 (DOI: 10.1039/C8TC05159C)
- [22] (a) Ma, C., Xu, B., Xie, G., He, J., Zhou, X., Peng, B., Xu, J. (2014). An AIE-active luminophore with tunable and remarkable fluorescence switching based on the piezo and protonation–deprotonation control. *Chem. Commun.*, 50(55), 7374-7377 (DOI: 10.1039/C4CC01012D); (b) Sun, J., Xue, P., Sun, J., Gong, P., Wang, P., Lu, R. (2015). Strong blue emissive nanofibers constructed from benzothizole modified tert-butyl carbazole derivative for the detection of volatile acid vapors. *J. Mater. Chem. C*, 3(34), 8888-8894 (DOI: 10.1039/C5TC02012C); (c) Zhan, Y., Zhao, J., Yang, P., Ye, W. (2016). Multi-stimuli responsive fluorescent behaviors of a donor– $\pi$ –acceptor phenothiazine modified benzothiazole derivative. *RSC advances*, 6(94), 92144-92151 (DOI: 10.1039/C6RA19791D)
- [23] (a) M. J. Frisch, G. W. Trucks, G. W. Schlegel, G. E. Scuseria, M. A. Robb, J. R. Cheeseman, G. Scalmani, V. Barone, B. Mennucci, G. A. Petersson, et al., *Gaussian 09, revision A.02*; Gaussian, Inc.: Wallingford, CT: 2009; (b) Lee, C., Yang, W., Parr, R. G. (1988). Development of the Colle-Salvetti correlation-energy formula into a functional of the electron density. *Phys. Rev. B*, 37(2), 785 (DOI:

10.1103/PhysRevB.37.785); (c) A. D. Becke, *J. Chem. Phys.*,  
1993, 98, 1372–1377.

## Chapter 7

### Structure-property relationship in multi-stimuli responsive D-A-A' benzothiazole functionalized isomers

---

---

#### 7.1. Introduction

The solid state materials which are susceptible to changes by external stimuli (mechanical forces, solvent and acid vapors, heat and light) are beneficial.<sup>[1]</sup> following their utilization in a range of promising applications such as optical information storage, fluorescent switches, memory devices, deformation detectors, optical recording, fluorescent bio-probes, security systems, mechanical sensors and optoelectronic devices.<sup>[2]</sup> The category of solid state materials, that manifest change in emission as a response to mechanical force such as grinding or rubbing are known as mechanofluorochromic (MFC) materials.<sup>[3]</sup> A significant emission in the solid state is crucial for mechanofluorochromism and is primarily determined by the nature of molecular packing and intermolecular interactions in the solid state.<sup>[4]</sup> The response to mechanical forces is associated with phase transitions or the disturbance in the basic molecular stacking interactions, consequently producing metastable states.<sup>[5]</sup> The factors such as effective conjugation, donor-acceptor interaction, and incorporation of alkyl or aryl substituent, electronegative or heavy atoms and their position play a pivotal role in regulating the MFC properties.<sup>[6]</sup> The common organic dyes in their aggregated state quench their emission due to the aggregation caused quenching (ACQ) which restricts their usage as MFC materials.<sup>[7]</sup> Recently, the concept of aggregation-induced emission (AIE) contributed by Tang *et al.* has successfully resulted in materials with enhanced emission in aggregated state. The non-planar architecture of AIE luminogens diminishes  $\pi$ - $\pi$  stacking in aggregated state and by the virtue of restriction of intramolecular rotations (RIR) induces extensive emission in

aggregated state.<sup>[8]</sup> The ACQ fluorophores have been successfully converted into solid state emitting materials by attaching to well-known AIEgens.<sup>[9]</sup> Tetraphenylethylene (TPE) is one of the widely used AIEgen because of its easy synthesis, bulky size and propeller shape. The TPE has been used as a weak electron donor in donor-acceptor systems resulting in highly emissive solid materials with a range of applications in material chemistry and electronics.<sup>[10]</sup>

It is familiar that organic molecules constituting of donor and acceptor fragments allowing fine tuning of the MFC properties. Organic molecules with D-A, D-A-D, D- $\pi$ -A *etc.* serve as excellent candidates for MFC with applications in optoelectronics.<sup>[11]</sup> Benzothiazole (BT) and benzothiadiazole (BTD) are well established electron acceptors and have been successfully explored for the synthesis of AIE active MFC materials.<sup>[12]</sup> Both BT and BTD based materials have been successfully employed in organic light emitting diodes (OLEDs) and organic solar cells (OSCs) and can be combined for potential applications in a multichromophoric assembly.<sup>[13]</sup>

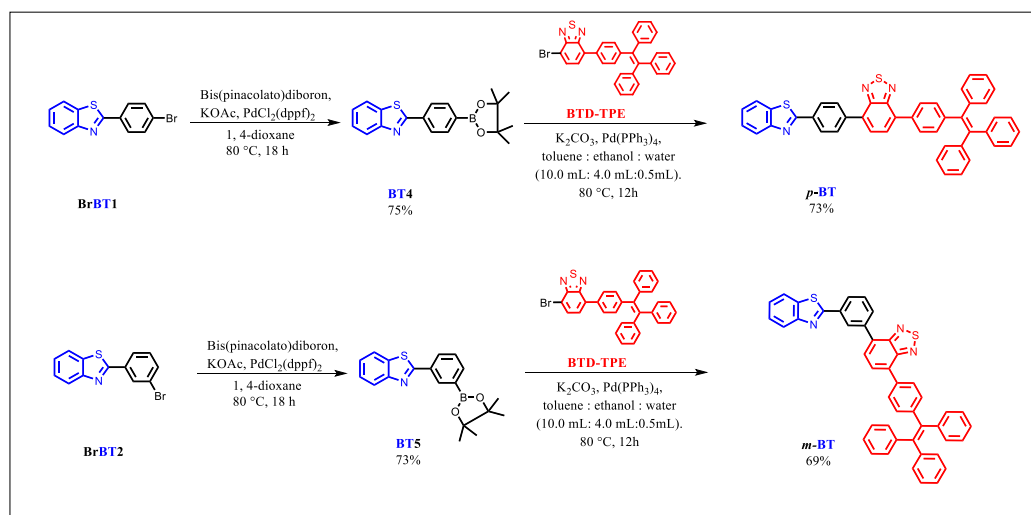
We were interested in design and synthesis of MFC materials. We have reported BT-TPE and BTD-TPE for MFC and successfully tuned their AIE and MFC behavior and have shown that MFC behavior can be tuned by controlling the strength of donor or acceptor.<sup>[11(c),14]</sup> Herein, we have designed and synthesized series of multichromophoric isomers ***p*-BT**, ***m*-BT** and ***o*-BT** based on BT, BTD and TPE with an aim of achieving high solid-state emission and MFC behavior. In this design strategy, we aim to control the acceptor strength and molecular packing by changing the position of BTD-TPE unit *ortho*, *meta* and *para* to BT unit. The variation of the position with respect to BT unit is expected in modulating the acceptor strength and molecular packing. The BT unit was selected because of moderate electron accepting behavior and presence of two hetero atoms “S and N”, as S-atom is well known for its strong supramolecular

interactions. The comparative study of the change in the photophysical, AIE and MFC properties of isomers with position has been carried out using crystal analysis and theoretical calculations. The photophysical, thermal, electrochemical, solvatochromic, mechanochromic, AIE and acidochromic properties of *p*-BT, *m*-BT and *o*-BT have been investigated. The isomers exhibit enhanced emission on aggregation with distinct MFC and acid sensing.

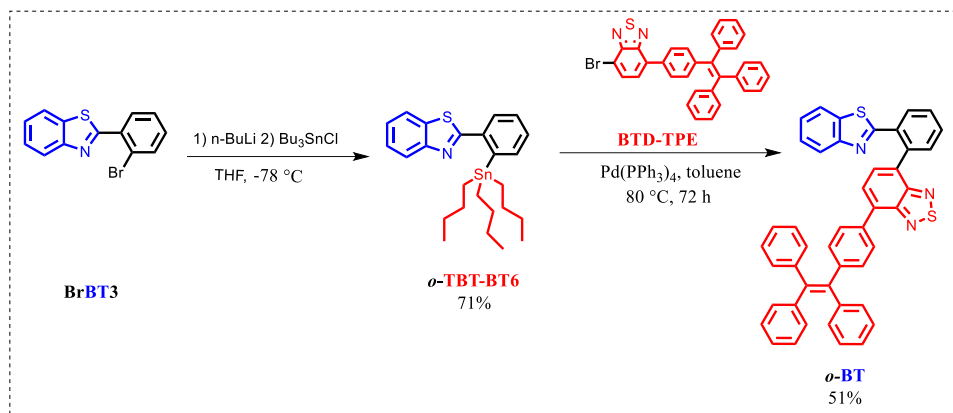
## 7.2. Results and discussions

### Synthesis

The *p*-BT, *m*-BT and *o*-BT are D-A-A' type molecules and were designed to evaluate the change in the photophysical and electronic properties as a result of altering the position of attachment of the BTD-TPE unit to the Ph-BT moiety. The synthetic route to the isomers *p*-BT and *m*-BT is given in Scheme 7.1 and for *o*-BT is as outlined in Scheme 7.2. The benzothiadiazole-tetraphenylethylene (BTD-TPE) moiety was attached at the 4-position, 3-position and 2-position of the phenyl ring of benzothiazole to furnish the para (*p*-BT), meta (*m*-BT) and ortho (*o*-BT) isomers respectively.

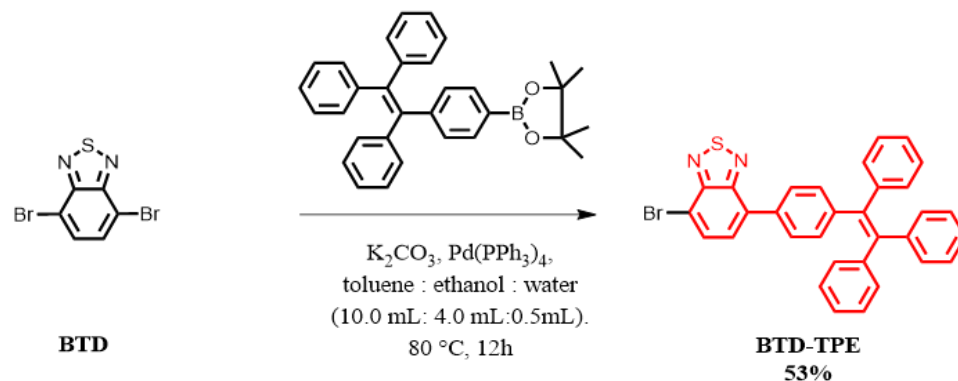


**Scheme 7.1.** Synthetic routes for *p*-BT and *m*-BT.



**Scheme 7.2.** Synthetic route for *o*-BT

To achieve this, firstly the tetraphenylethylene was selectively coupled to one side of 4,7-dibromobenzo[*c*][1,2,5]thiadiazole using the Suzuki cross-coupling reaction to yield intermediate **BTD-TPE** (Scheme 7.3).<sup>[14]</sup>



**Scheme 7.3.** Synthetic route to **BTD-TPE**.

Further, the benzothiazole intermediates **BT 4** and **BT 5** required for coupling with **BTD-TPE** were synthesized. 2-(4-bromophenyl)benzo[*d*]thiazole (**BrBT1**), 2-(3-bromophenyl)benzo[*d*]thiazole (**BrBT2**) and 2-(2-bromophenyl)benzo[*d*]thiazole (**BrBT3**) were obtained by the condensation reaction of 2-aminothiophenol and respective bromobenzaldehydes using literature procedures.<sup>[15]</sup> The Miyaura borylation reaction of **BrBT1** and **BrBT2** with bis(pinacolato)diboron

using [1,1'-bis(diphenylphosphino)ferrocene]palladium(II) dichloride as catalyst generated the boronate esters of benzothiazole at 4 position (**BT4**) and 3 position (**BT5**) respectively.<sup>[16]</sup> However, the Miyaura Borylation reaction of **BrBT3** did not proceed successfully to yield the boronate ester; alternatively the Stille intermediate *o*-**TBT-BT6** was synthesized. The in-situ anion formation of **BrBT3** using n-BuLi followed by addition of tributyltin chloride supplied the intermediate *o*-**TBT-BT6** in 71% yield. The Suzuki cross coupling reaction of **BTD-TPE** with **BT4** and **BT5** using Pd(PPh<sub>3</sub>)<sub>4</sub> as catalyst afforded *para* and *meta* isomers *p*-**BT** and *m*-**BT** with a yield of 73% and 69% respectively. The Stille cross-coupling reaction of **BTD-TPE** with *o*-**TBT-BT6** and Pd(PPh<sub>3</sub>)<sub>4</sub> as a catalyst resulted in the *ortho* isomer *o*-**BT** with a yield of 51%. All the target compounds (*p*-**BT**, *m*-**BT** and *o*-**BT**) and the newly synthesized intermediate *o*-**TBT-BT6** were characterized with <sup>1</sup>H, <sup>13</sup>C NMR spectra and HR-ESI mass spectroscopy. The *para* (*p*-**BT**) and *ortho* (*o*-**BT**) isomers produced good crystals for single crystal X-ray analysis. The synthesized isomers are highly soluble in common organic solvents such as dichloromethane (DCM), tetrahydrofuran (THF), chloroform *etc.*, although insoluble in ethanol, methanol, water and acetonitrile.

### 7.3. Thermogravimetric analysis

High thermal stability is essential for molecules to be utilized in solid state applications. The thermal properties of *p*-**BT**, *m*-**BT** and *o*-**BT** were evaluated by thermogravimetric analysis (TGA). The TGA curves are shown in Figure 7.1. and the decomposition temperature (*T<sub>d</sub>*) are listed in Table 7.1. The isomer *p*-**BT** exhibits the highest decomposition temperature of 405 °C corresponding to 5% weight loss. The isomer *m*-**BT** and *o*-**BT** show thermal decomposition temperatures of 398 °C and 363 °C respectively for 5% weight loss. The *p*-**BT** molecule has a lower twisting as compared to *m*-**BT** and *o*-**BT** and exhibits an extended conjugated structure. The *p*-**BT** isomer due to a planar conjugated structure engages in higher

intermolecular interactions in its crystal packing lattice leading to a densely packed structure which could be a reason for the higher thermal stability as compared to *m*-BT and *o*-BT.

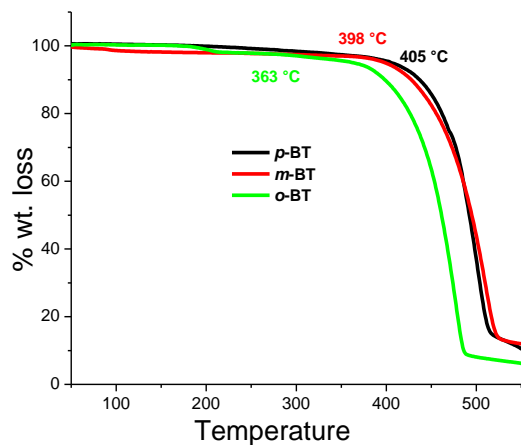


**Figure 7.1.** TGA curves of *p*-BT, *m*-BT and *o*-BT at a heating rate of  $10^{\circ}\text{C min}^{-1}$  under a nitrogen atmosphere.

#### 7.4. Photophysical properties

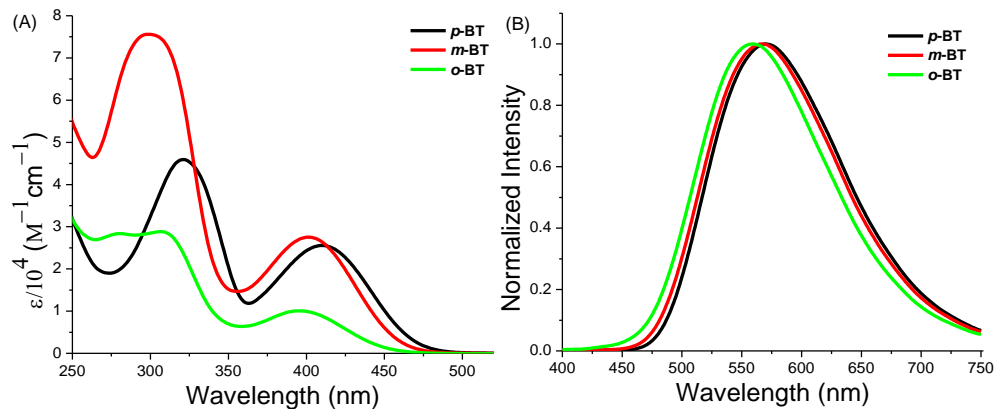


**Figure 7.2.** (A) UV-vis absorption spectra and (B) normalized emission spectra of *p*-BT, *m*-BT and *o*-BT in THF ( $2 \times 10^{-5}$  M).

The optical properties of *p*-BT, *m*-BT and *o*-BT were analyzed in THF by UV-vis absorption (Figure 7.2 (A)) and fluorescence spectroscopy (Figure

7.2 (B)) and the results are compiled in Table 7.1. The isomers possess two major absorption bands arising from  $\pi$ - $\pi^*$  transitions in lower wavelength region (250–330nm) and intramolecular-charge transfer (ICT) transitions between the donor-acceptor strands in higher wavelength region (390–415nm) with a high extinction coefficient. The emission maxima of the isomers are in the range of 555–575nm with blue shifted emission for ***o*-BT** as a result of the decrease in the conjugation induced by the highly twisted structure.

**Table 7.1** Photophysical and thermal properties of ***p*-BT**, ***m*-BT** and ***o*-BT**.

Compounds	$\lambda_{ab}$ [nm] ( $\epsilon$ [Lmol <sup>-1</sup> cm <sup>-1</sup> ]) <sup>a</sup>	$\lambda_{em}$ (nm) <sup>b</sup>	$T_d$ (°C) <sup>c</sup>
<b><i>p</i>-BT</b>	321(45939), 411(25544)	570	405 °C
<b><i>m</i>-BT</b>	300(75575), 402(27525)	567	398 °C
<b><i>o</i>-BT</b>	279(28335) 307(28838), 396(10068)	559	363 °C

<sup>a,b</sup> Recorded in tetrahydrofuran, <sup>c</sup> Decomposition temperature.

### 7.5. Density functional theory calculations

The density functional theory (DFT) calculations were conducted at the B3LYP-6-31G(d,p) level for further accurate examination of the ground state electronic structures and geometries of the isomers ***p*-BT**, ***m*-BT** and ***o*-BT**.<sup>[17]</sup> The calculated frontier molecular orbitals are depicted in Figure 7.3 and the values are compiled in Table 7.2. The DFT optimized structures of the ***p*-BT** and ***o*-BT** isomers are in well accordance with the crystal structures. The isomers have propeller shaped geometry for TPE moiety and twisted structures with highest twisting in ***o*-BT**. The highest occupied molecular orbital (HOMO) is localized on the weakly donating TPE moiety whereas the lowest unoccupied molecular orbital (LUMO) resides on the benzothiadiazole moiety which confirms its higher electron accepting nature over benzothiazole. The HOMO-LUMO gap for ***p*-BT**, ***m*-BT** and ***o*-BT** are 2.79 eV, 2.89 eV and 2.99 eV respectively. The HOMO and LUMO

are well separated allowing a distinct intramolecular charge transfer (ICT) from the donor to acceptor.

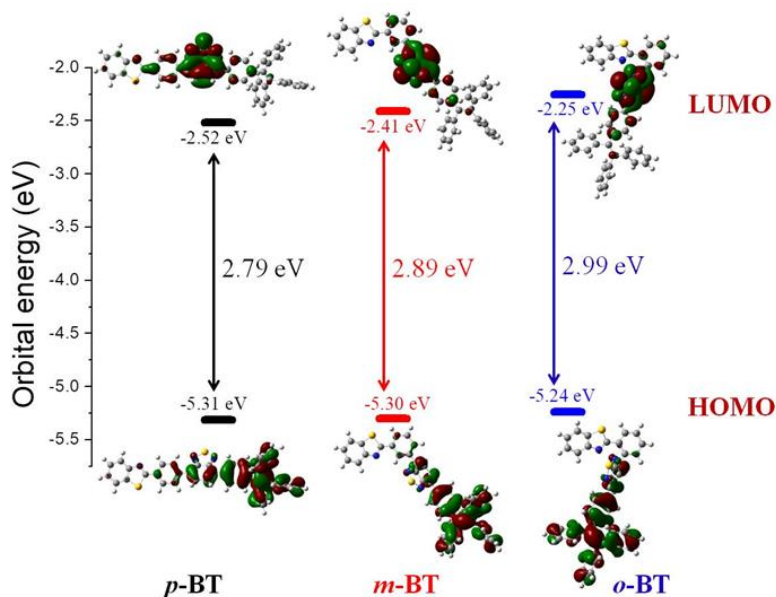


**Figure 7.3.** Energy level diagram showing the HOMO and LUMO energy levels of *p*-BT, *m*-BT and *o*-BT as determined at the B3LYP/6-31G(d,p) level.

	Electrochemical properties			DFT calculations		
	HOMO <sup>a</sup> eV	LUMO <sup>a</sup> eV	HOMO -LUMO gap eV	HOMO <sup>b</sup> eV	LUMO <sup>b</sup> eV	HOMO -LUMO gap eV
<i>p</i> -BT	-5.54	-3.62	1.92	-5.31	-2.52	2.79
<i>m</i> -BT	-5.56	-3.62	1.94	-5.30	-2.41	2.89
<i>o</i> -BT	-5.58	-3.68	1.90	-5.24	-2.25	2.99

**Table 7.2.** Electrochemical properties and DFT calculations of *p*-BT, *m*-BT and *o*-BT.

<sup>a</sup> Calculated from CV: Reference electrode- Ag/AgCl <sup>b</sup> Theoretical values at B3LYP/6-31g(d,p) level.

## 7.6. Electrochemical properties

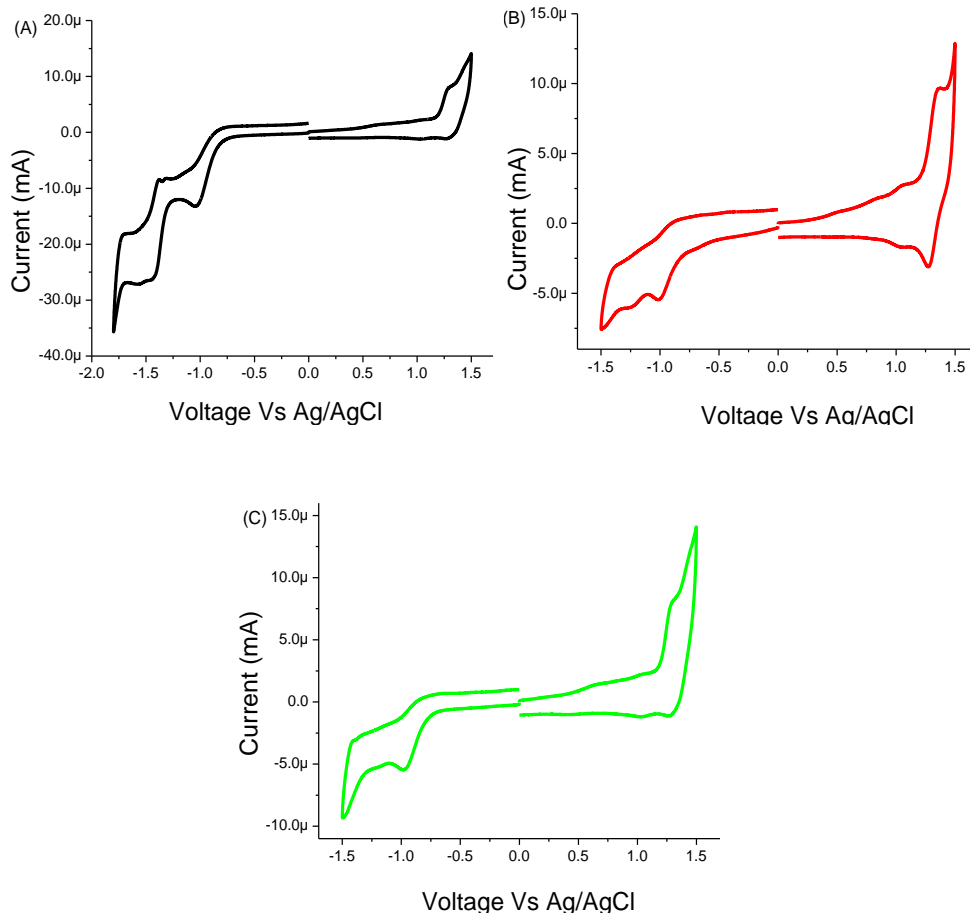


**Figure 7.4.** Cyclic voltammetry (CV) plots of (A) *p*-BT, (B) *m*-BT and (C) *o*-BT.

The energy levels and electrochemical properties were examined by employing cyclic voltammometry using tetrabutylammonium hexafluorophosphate (TBAPF<sub>6</sub>) as supporting electrolyte for a solution of the isomers in DCM. Figure 7.4. shows the irreversible nature of the cyclic voltammograms and Table 7.2. lists the corresponding data for the electrochemical study of *p*-BT, *m*-BT and *o*-BT. The HOMO and LUMO values were calculated from the onset value of oxidation or reduction wave ( $E_{\text{onset}}$ ) utilizing the equation  $\text{HOMO/LUMO} = - (E_{\text{onset}} + 4.4) \text{ eV}$ .<sup>[18]</sup> The

values for HOMO levels of *p*-BT, *m*-BT and *o*-BT are -5.54 eV, -5.56 eV and -5.58 eV respectively and the values of LUMO levels are -3.62 eV, -3.62 eV and -3.68 eV respectively. The electrochemical HOMO-LUMO gaps for *p*-BT, *m*-BT and *o*-BT are 1.92 eV, 1.94 eV and 1.90 eV respectively. The CV graphs exhibit one oxidation wave and two reduction waves corresponding to a donor TPE and acceptors BTD and BT respectively.

## 7.7. Solvatochromism

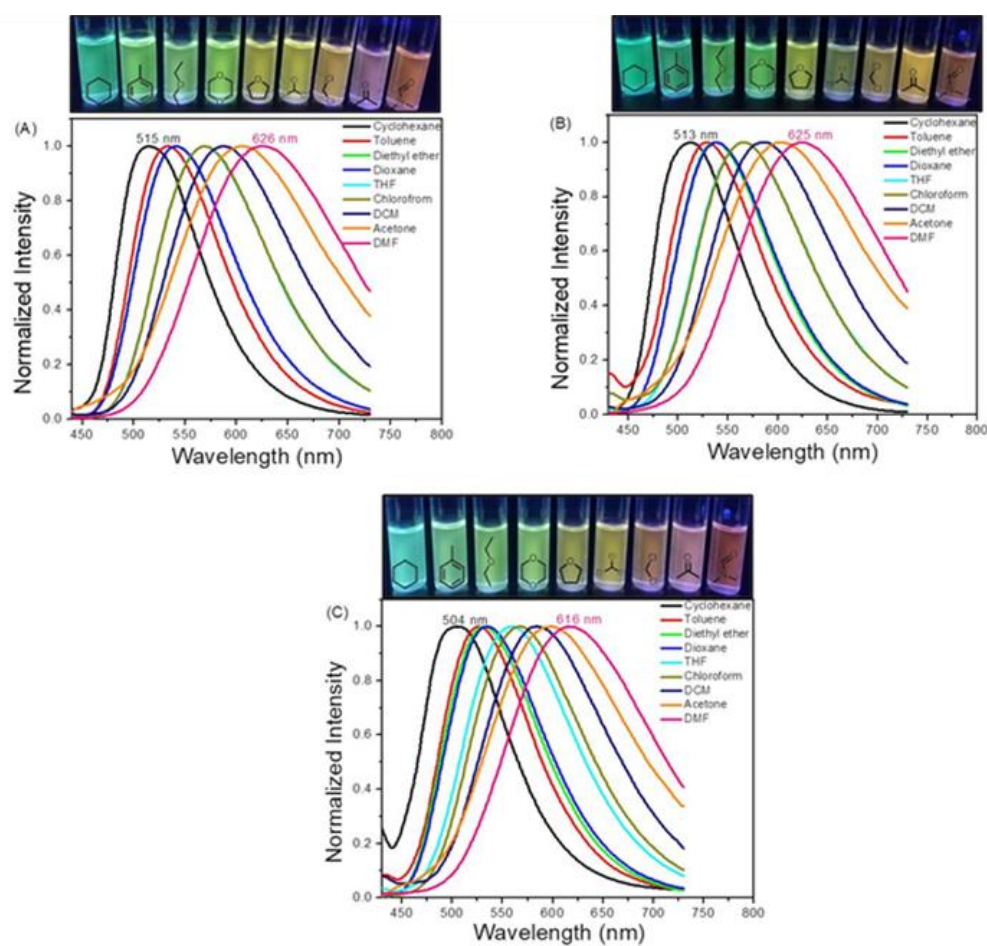


**Figure 7.5.** Emission spectra of the isomers (A) *p*-BT, (B) *m*-BT and (C) *o*-BT (excitation wavelength or  $\lambda_{\text{ex}}=370$  nm) in solvents of different polarities. (Photographs taken under 365 nm illumination, from left to right- cyclohexane, toluene, diethyl ether, 1,4-dioxane, THF, chloroform, DCM, acetone, DMF.)

The intramolecular charge transfer (ICT) transition is greatly influenced by change in solvent polarity and is a distinct feature in donor-acceptor molecule.<sup>[19]</sup> The target isomers are comprised of a D-A-A' structural unit owing to which the result of change in the solvent polarity was investigated using fluorescence spectroscopy (Figure 7.5.) and electronic absorption spectroscopy (Figure 7.6.) in a range of solvents from non-polar to polar (cyclohexane, toluene, diethyl ether, 1,4-dioxane, THF, chloroform, dichloromethane(DCM), acetone and N,N-dimethylformamide(DMF)).

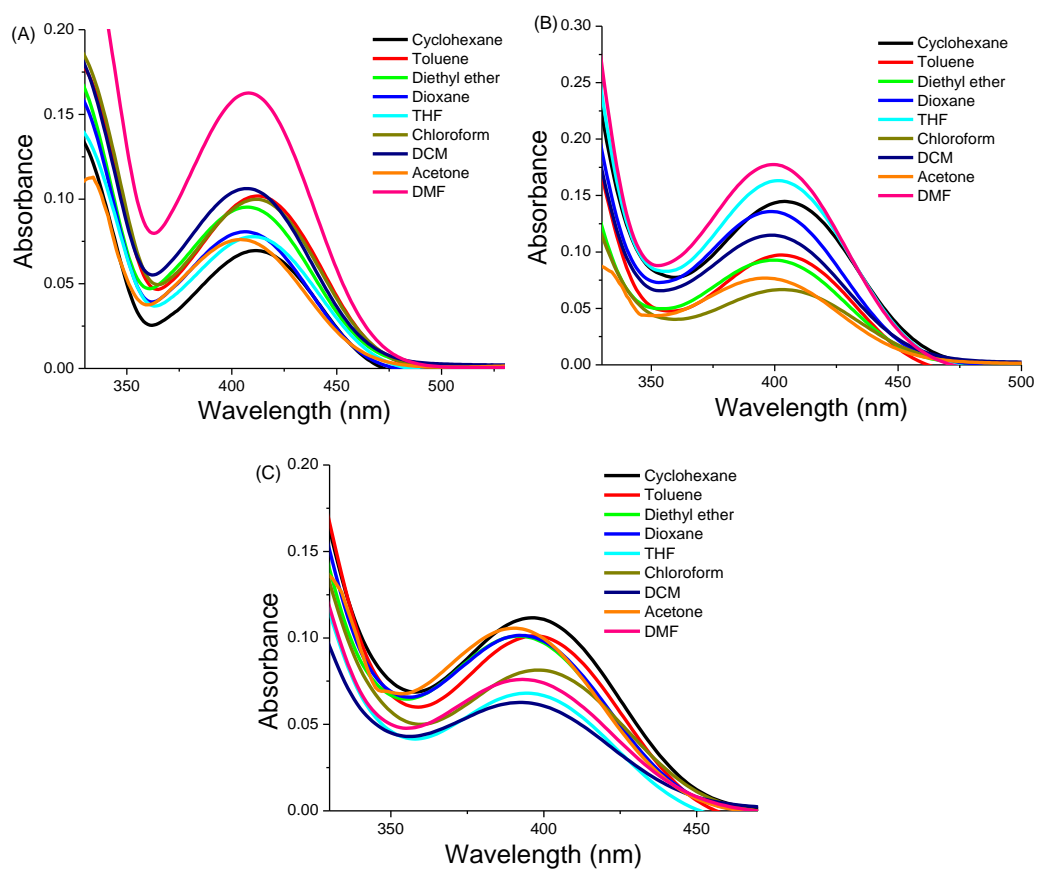


**Figure 7.6.** Electronic absorption spectra of the isomers (A) *p*-BT, (B) *m*-BT and (C) *o*-BT (excitation wavelength or  $\lambda_{ex}$ =370 nm) in solvents of different polarities.

In comparison to the fluorescence spectra, the absorption spectra exhibited minor changes on changing the polarity of solvent which suggests the presence of more polarized excited states than the ground electronic states.

The *p*-BT and *m*-BT isomers manifest a bright green fluorescence in cyclohexane at 515 nm and 513 nm respectively whereas the *o*-BT isomer emits at 504 nm in cyclohexane with a bluish green fluorescence. The isomers *p*-BT, *m*-BT and *o*-BT emit a yellow fluorescence in moderate polar solvents like 1,4-dioxane, THF, CHCl<sub>3</sub>. In polar solvent like DMF, a bright orange fluorescence was observed at 626 nm, 625 nm and 616 nm respectively enabling the isomers to achieve a wide range of colours in the visible region. The isomers *p*-BT, *m*-BT and *o*-BT exhibit similar changes in emission on gradually increasing the solvent polarity and a bathochromic shift of 111 nm, 112 nm and 112 nm respectively was observed (Figure 7.5.). In all the isomers, the HOMO mainly resides on the weak donor TPE and LUMO mainly resides on the BT unit and does not involve the benzothiazole unit as observed by the DFT calculations. The ICT transition occurs from TPE unit to the BT unit and does not involve the BT unit owing to which the positional isomerism does not have a significant effect on the ICT transition. The transfer of electron from donor to acceptor causes charge separation in the excited state resulting in polarized excited state possessing an enhanced transition dipole moment which can be stabilized by the reorganization of polar solvent molecules resulting in reduced energy of the excited state leading to noteworthy bathochromic changes in the emission spectra.

### 7.8. Aggregation-induced emission

The isomers were designed with tetraphenylethylene core to accomplish solid-state emission induced by aggregation. The formation of nanoaggregates was initiated by progressive addition of non-solvent (water) to the solvent system (DMF) and the AIE character of the isomers was measured using fluorescence (Figure 7.7.) and absorption spectroscopy (Figure 7.8.). The isomers *p*-BT, *m*-BT and *o*-BT emit at 626 nm, 627 nm and 618 nm respectively with a pink fluorescence at 0% water fraction or pure DMF solution due to significant ICT transition, unlike other TPE

containing molecules that are non-emissive in solution. The relative quantum yields (QY) for *p*-BT, *m*-BT and *o*-BT at 0% water fraction are 0.37, 0.20 and 0.21 respectively. The *o*-BT isomer shows reduction of intensity up to 40% while *m*-BT and *o*-BT isomer exhibit reduction of intensity up to 30% water fraction. This behavior can be attributed to the stabilized CT states resulting from increase in solvent polarity. The *p*-BT, *m*-BT and *o*-BT isomers display sharp intensity enhancement and a blue shift in wavelength (bright green emission) above 40-50% water fraction due to formation of nanoaggregates. The relative QY for *p*-BT, *m*-BT and *o*-BT at 90% water fraction are 0.60, 0.34 and 0.26 respectively. It can be concluded that the emission at lower water percentage is governed by ICT; however greatly influenced by aggregate formation at higher water percentage. Above 70% water fraction, a slight drop in emission intensity is observed due to the formation of the large-sized aggregates, which decreases the effective dye concentration in the solution and are less exposed to radiation as compared to smaller aggregates.<sup>[20]</sup>

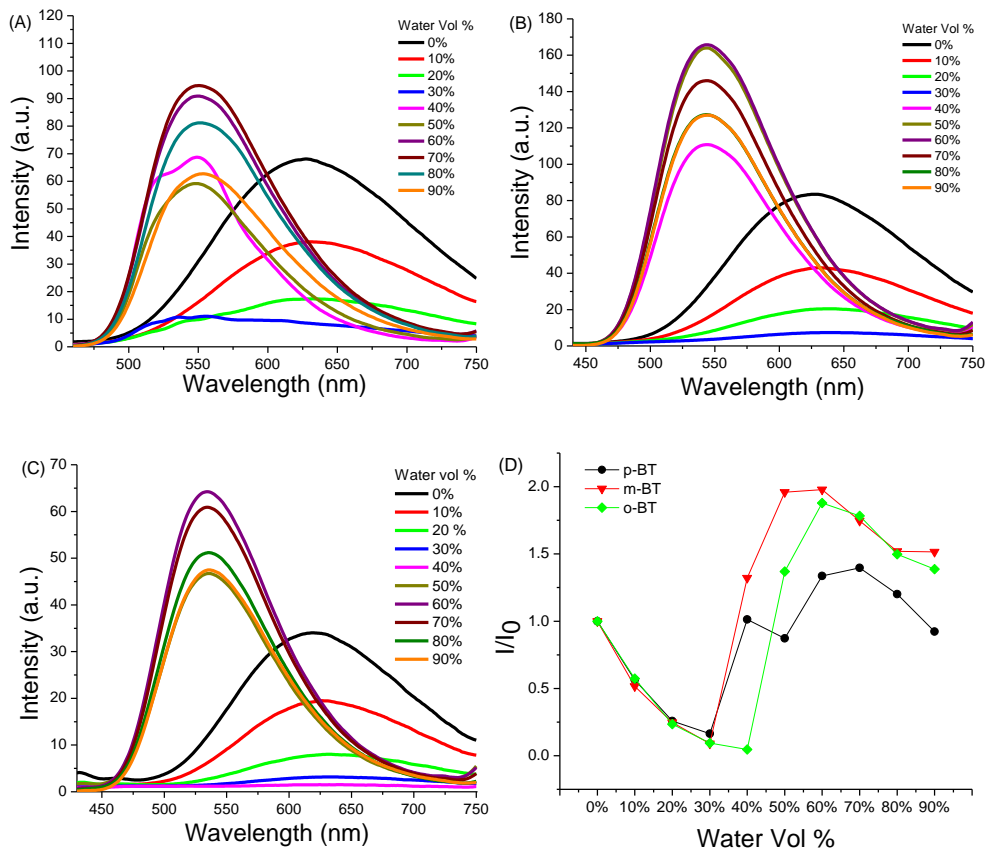


**Figure 7.7.** Emission spectra of (A) *p*-BT, (B) *m*-BT and (C) *o*-BT in DMF-water mixtures (0%–90% water), (D) Plot of fluorescence intensity vs. % of water fraction ( $f_w$ ). Luminogen concentration: 10  $\mu$ M; intensity calculated at  $\lambda_{max}$ .

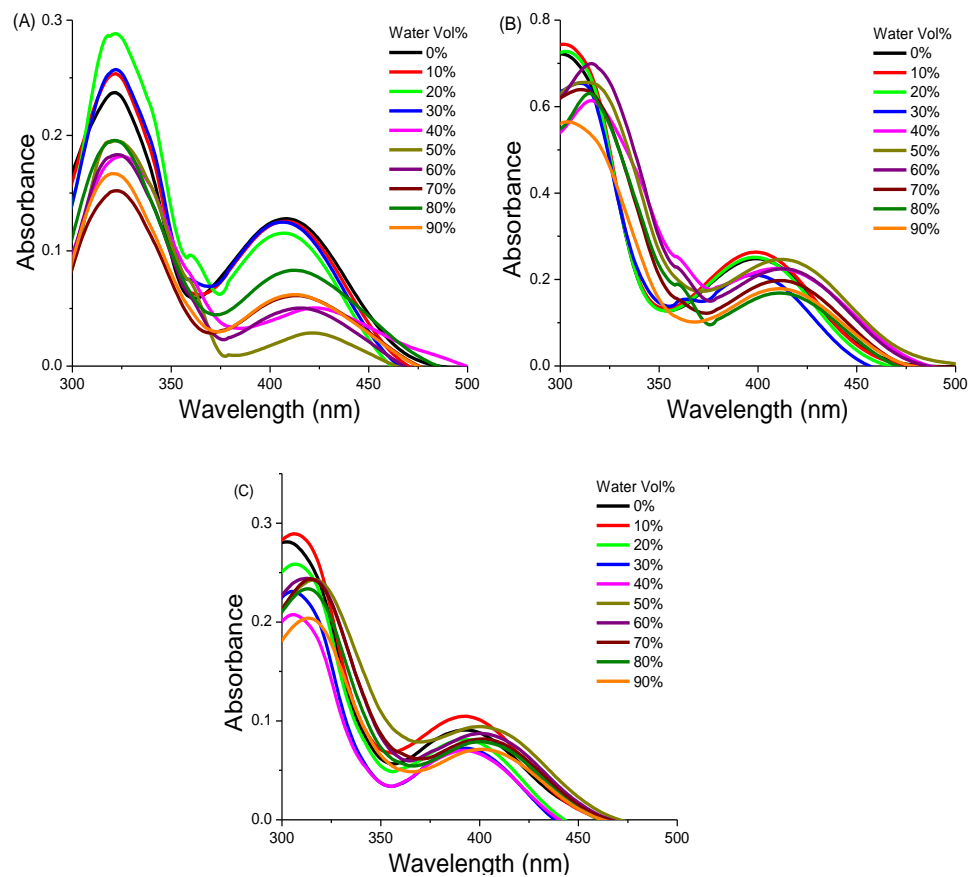


**Figure 7.8.** Electronic absorption spectra of (A) *p*-BT, (B) *m*-BT and (C) *o*-BT in DMF-water mixtures (0% to 90% water), Luminogen concentration: 10  $\mu$ M; intensity calculated at  $\lambda_{max}$ .



**Figure 7.9.** Photograph of (A) *p*-BT (B) *m*-BT and (C) *o*-BT in THF-water mixtures with different water fractions (10  $\mu$ M) (0% water to 90% water from left to right) under 365 nm UV illumination.

The Mie scattering effect of light can be witnessed in the electronic absorption spectra (Figure 7.8.) of *p*-BT, *m*-BT and *o*-BT as a consequence of nano-aggregate formation at 40% water fraction for the isomers.<sup>[21]</sup> The recorded AIE phenomenon can be visualized from the photographs given in Figure 7.9.

### 7.9. Single crystal X-ray analysis

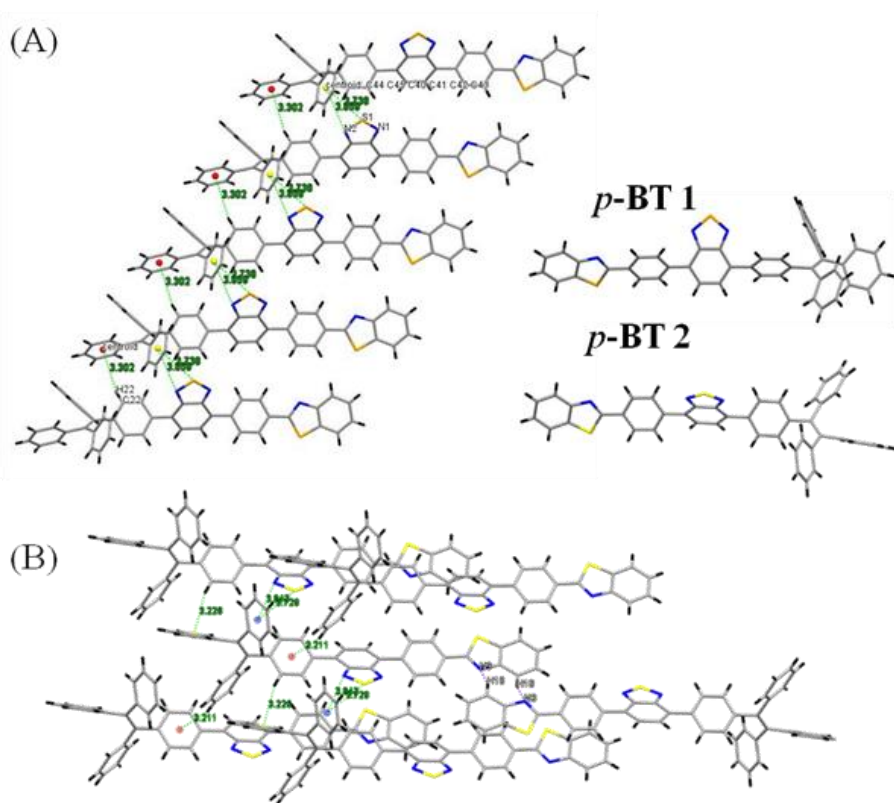


**Figure 7.10.** Crystal structure of *p*-BT 1 and *p*-BT 2; (A) Intermolecular interactions in (C-H $\cdots$  $\pi$  depicted by red centroid, N $\cdots$  $\pi$  and S $\cdots$  $\pi$  depicted by yellow centroid) in the crystal packing diagram of *p*-BT 1 (1-D ladder), (B) Intermolecular interactions (C-H $\cdots$  $\pi$  depicted by red and yellow centroid, N $\cdots$  $\pi$  and S $\cdots$  $\pi$  depicted by blue centroid, C-H $\cdots$ N weak hydrogen bonding interactions depicted by purple lines) in the crystal packing diagram of *p*-BT 2 (2-D framework).

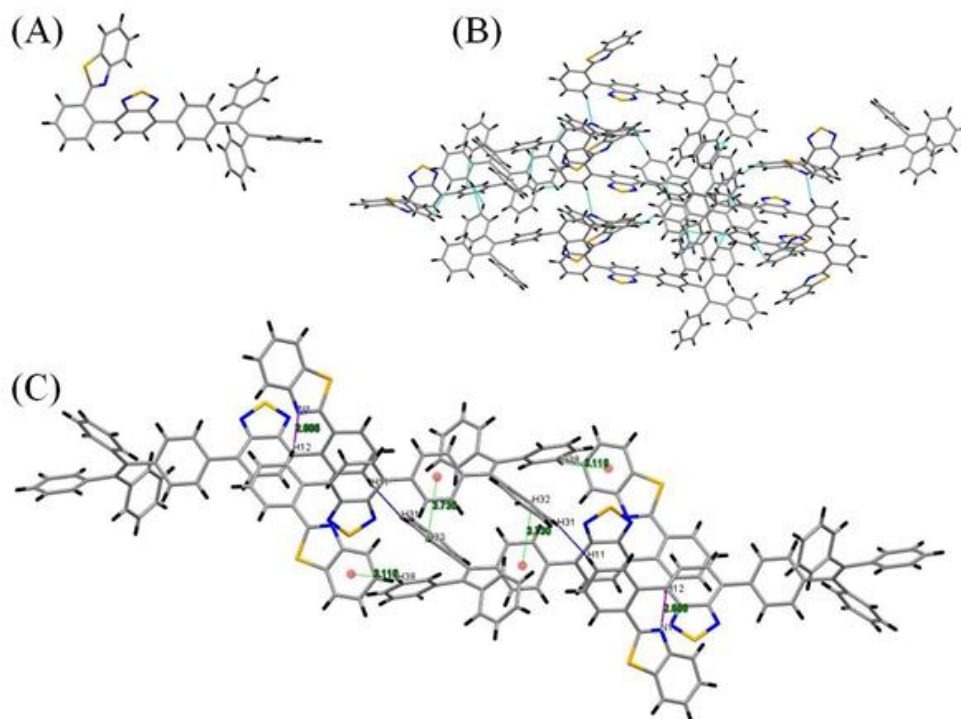


**Figure 7.11.** (A) Crystal structure of *o*-BT. (B) Crystal packing diagram of *o*-BT (anti-parallel arrangement and 3-D framework) (C) Intermolecular interactions (C-H... $\pi$  depicted by red centroid and green line, C-H...N weak hydrogen bonding interactions depicted by purple lines) in the crystal packing diagram of *o*-BT.

The successful interpretation of the observed properties can be achieved by deducing the structural information achieved from single crystal X-ray analysis. The slow evaporation of dichloromethane (DCM)/hexane and chloroform/hexane solvent mixtures was used to grow good quality crystals for *p*-BT (fluorescent green) and *o*-BT (yellow) respectively. However, the crystallization of *p*-BT isomer in different batches using the same solvent system by slow evaporation serendipitously resulted in two different crystal forms namely *p*-BT 1 and *p*-BT 2. The *o*-BT isomer belongs to monoclinic crystal system and P21/n space group. The two crystalline forms of *p*-BT isomer belong to the triclinic crystal system with P-1 space group but differ from each other in orientation of the TPE moiety and degree of twisting

resulting in different crystal packing diagrams. The difference in the crystal packing of *p*-BT 1 and *p*-BT 2 results in interesting emission properties. The crystal structures of *p*-BT 1, *p*-BT 2 (Figure 7.10.) and *o*-BT (Figure 7.11. (A)) revealed twisted geometries for the tetraphenylethylene moiety as predicted and extensive twisting was observed in *o*-BT as compared to *p*-BT 1 and *p*-BT 2. The unit cell of *o*-BT crystal (Figure 7.12. (C)) consists of four molecules arranged anti-parallel with multiple intermolecular interactions in contrast to the unit cell of *p*-BT 1 and *p*-BT 2 (Figure 7.12. (A, B)) having absence of interactions between two anti-parallel arranged molecules.

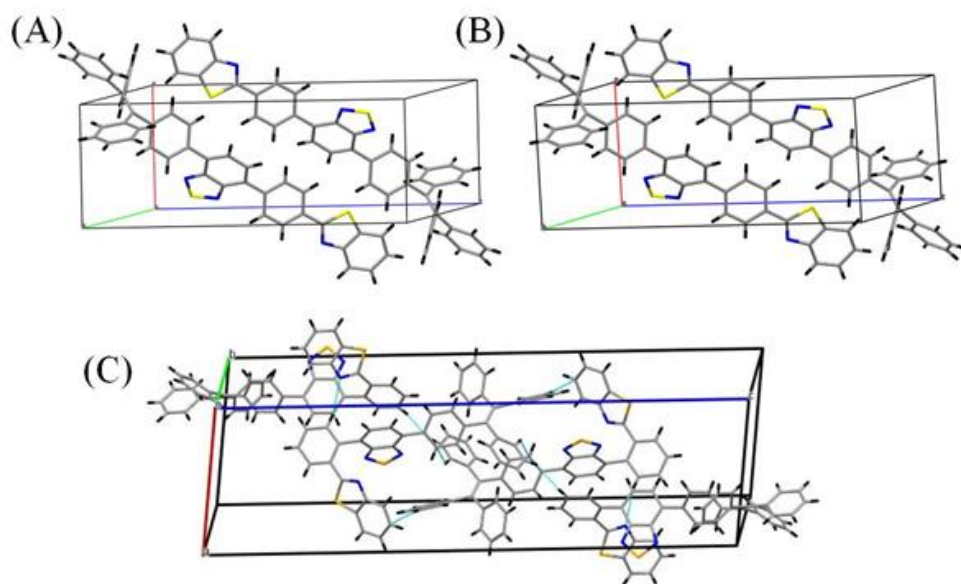


**Figure 7.12.** Unit cell diagrams for the crystal of (A) *p*-BT 1, (B) *p*-BT 2 and (C) *o*-BT.

The crystal packing diagram of *p*-BT 1 (Figure 7.10. (A)) reveals C(22)–H(22)⋯ $\pi$  (red centroid-C34–C35–C36–C37–C38–C39, 3.302 Å) and lone-pair⋯ $\pi$  i.e. N(2)⋯ $\pi$ (3.859 Å) and S(1)⋯ $\pi$  (3.738 Å) ( $\pi$  depicted by yellow centroid- C40–C41–C42–C43–C44–C45) leading to 1-D ladder type formation. The *p*-BT 2 (Figure 7.10. (B)) contrarily displays extensive intermolecular interactions leading to a densely packed 2-D framework. The

interactions observed in ***p*-BT 2** are C(20)–H(31)⋯ $\pi$  (red centroid-C20–C21–C22–C23–C24–C25, 3.211 Å), C(35)–H(24)⋯ $\pi$  (yellow centroid-C34–C35–C36–C37–C38–C39, 3.226 Å), lone-pair⋯ $\pi$  i.e. N(1)⋯ $\pi$ (3.842 Å) and S(1)⋯ $\pi$  (3.729 Å) ( $\pi$  depicted by blue centroid- C40–C41–C42–C43–C44–C45) and weak H-bonding with N of the benzothiazole moiety C–H(18)⋯N(3) 2.748 Å. The crystal packing diagram of ***o*-BT** (Figure 7.11. (C)) confirms C–H(38) ⋯ $\pi$  3.118 Å, C–H(32) ⋯ $\pi$  3.730 Å ( $\pi$ -red centroid) and weak H-bonding with N of the benzothiazole moiety C–H(12) ⋯N(1) 2.686 Å. The presence of abundant intermolecular interactions in ***o*-BT** constructs a head to tail driven 3-D framework. The highly twisted structure of ***o*-BT** a 3D framework of the crystal lattice makes the isomer resistant to physical structural changes caused by mechanical stimuli.<sup>[22]</sup> The top view and side views of the crystal packing diagrams for ***p*-BT 1**, ***p*-BT 2** and ***o*-BT** are given in Figure 7.13., Figure 7.14. and Figure 7.15. respectively. The crystallographic data is summarized in Table 7.3.

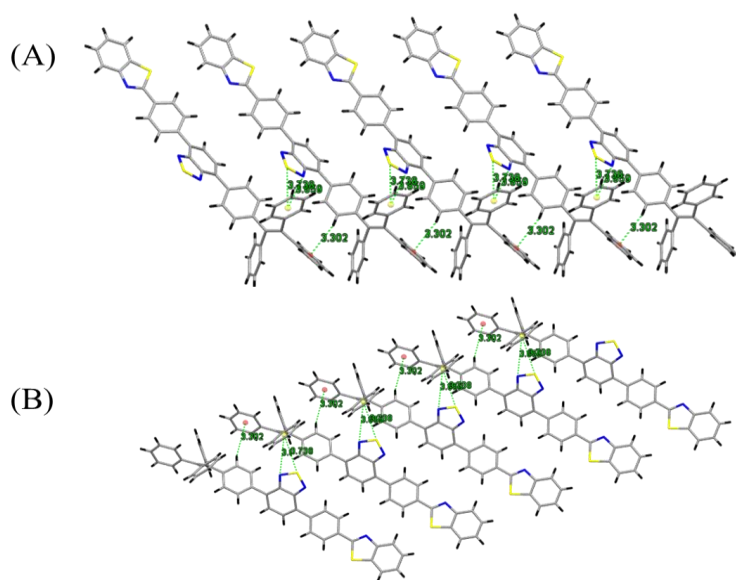


**Figure 7.13.** Crystal packing diagram of ***p*-BT 1** (A) side view and (B) top view.



**Table 7.3.** Crystal data and structure refinement for *p*-BT 1, *p*-BT 2 and *o*-BT

Identification code	rm211	rm262	rm241
Empirical formula	C45 H29 N3 S2	C45 H29 N3 S2	C45 H29 N3 S2
Formula weight	675.83	675.83	675.83
Temperature	293(2) K	293(2) K	293(2) K
Wavelength	1.54184 Å	0.71073 Å	0.71073 Å
Crystal system, space group	Triclinic, P -1	Triclinic, P -1	Monoclinic, P 21/n
a/(Å)	7.6932(3)	7.6440(8)	11.0588(10)
b/(Å)	9.9070(2)	9.8294(8)	8.5477(7)
c/(Å)	22.3507(6)	22.3403(19)	36.929(3)
Alpha/(°)	88.016(2)	87.824(7)	90
Beta/(°)	83.522(3)	83.835(8)	98.260(7)
Gamma/(°)	83.631(2)	83.258(7)	90
Volume	1681.75(9) Å <sup>3</sup>	1656.8(3) Å <sup>3</sup>	3454.6(5) Å <sup>3</sup>
Z, Calculated density	2, 1.335 mg/m <sup>-3</sup>	2, 1.355 mg/m <sup>-3</sup>	4, 1.299 mg/m <sup>-3</sup>
Absorption coefficient	1.727 mm <sup>-1</sup>	0.200 mm <sup>-1</sup>	0.192 mm <sup>-1</sup>
F(000)	704	704	1408
Crystal size	0.230 x 0.180 x 0.140 mm	0.230 x 0.180 x 0.130 mm	0.230 x 0.180 x 0.130 mm
Θ range for data collection/(°)	3.982 to 71.221	2.938 to 29.320	3.026 to 29.143
Reflections collected / unique	10875 / 6398 [R(int) = 0.0207]	20784 / 7817 [R(int) = 0.1927]	29511 / 8224 [R(int) = 0.1475]
Completeness to theta	Θ = 67.684 99.8 %	Θ = 25.242 99.8 %	Θ = 25.242 99.8 %
Absorption correction	Semi-empirical from equivalents	Semi-empirical from equivalents	Semi-empirical from equivalents

Max. and min. transmission	1.00000 and 0.42833	-	1.00000 and 0.52239
Refinement method	Full-matrix least-squares on F <sup>2</sup>	Full-matrix least-squares on F <sup>2</sup>	Full-matrix least-squares on F <sup>2</sup>
Data /restraints / parameters	6398 / 0 / 451	7817 / 0 / 451	8224 / 0 / 451
Goodness-of-fit on F <sup>2</sup>	1.043	0.944	1.041
Final R indices [I>2sigma(I)]	R1 = 0.0467, wR2 = 0.1336	R1 = 0.0985, wR2 = 0.2157	R1 = 0.0897, wR2 = 0.2097
R indices (all data)	R1 = 0.0483, wR2 = 0.1378	R1 = 0.2544, wR2 = 0.3547	R1 = 0.1470, wR2 = 0.2435
Extinction coefficient	n/a	n/a	n/a
Largest diff. peak and hole (e.Å <sup>-3</sup> )	0.229 and -0.393	0.607 and -0.737	0.332 and -0.407

## 7.10. Mechanochromism

The *p*-BT, *m*-BT and *o*-BT were predicted to exhibit mechano-responsive solid-state emission taking in account the non-planar framework and AIE nature of TPE. The *para*, *meta* and *ortho* attachment of BT-D-TPE to benzothiazole moiety could vary the mechanochromic nature owing to the amount of twisting and/or acceptor strength in these isomers. The isomers were subjected to mechanical stimuli by grinding with mortar and pestle and the behaviour was explored using solid-state emission spectroscopy (Figure 7.16.) and the data are tabulated in Table 7.4. The crystals of *p*-BT isomer (*p*-BT 1 and *p*-BT 2) and *o*-BT isomer were considered as pristine samples while the *m*-BT isomer did not form any crystal owing to which the as-synthesized sample was considered as pristine.

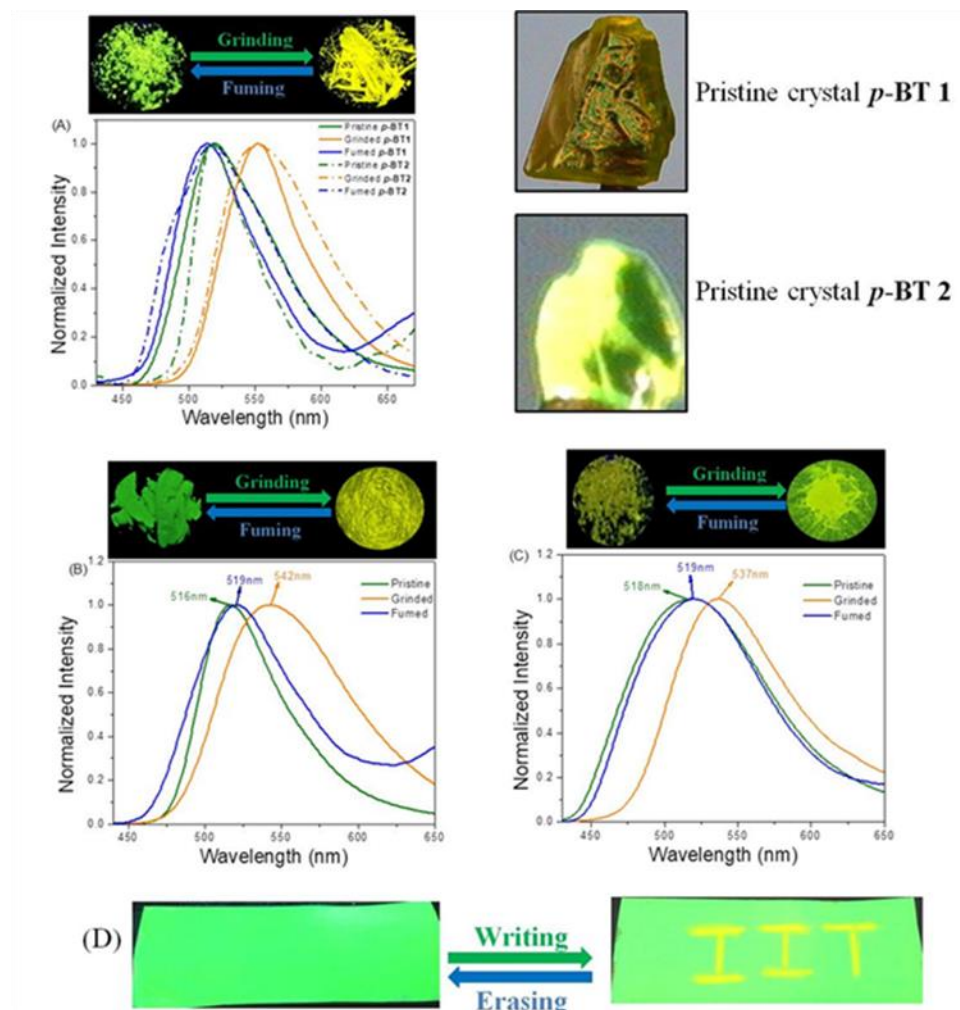


**Figure 7.16.** Solid-state emission spectra of pristine, grinded and fumed solids of (A) *p*-BT 1 and *p*-BT 2, (B) *m*-BT and (C) *o*-BT (D) writing and erasing on a filter paper coated with *p*-BT, illustrating ink free rewritable system. (Photographs taken under 365 nm UV light) (Inset: Pristine crystals *p*-BT 1 and *p*-BT 2).

The *p*-BT 1 and *p*-BT 2 crystals have same structure but differ in their orientation in space resulting in different crystal packing. The pristine crystals *p*-BT 1 and *p*-BT 2 exhibit a bright green emission at same wavelength of 519 nm. Grinding of the *p*-BT 1 and *p*-BT 2 bathochromically shifts the wavelength to 552 nm with a yellow emission. The fumigation of the grinded forms of *p*-BT 1 and *p*-BT 2 using DCM-hexane for 15-20 minutes reverted the emission to 513 nm and 516 nm

respectively. The reversibility by fumigation for *p*-BT 1 and *p*-BT 2 was repeated up to 7 times and obtain wavelength of the fumed samples in the range of 513-518 nm (Figure 7.17.).

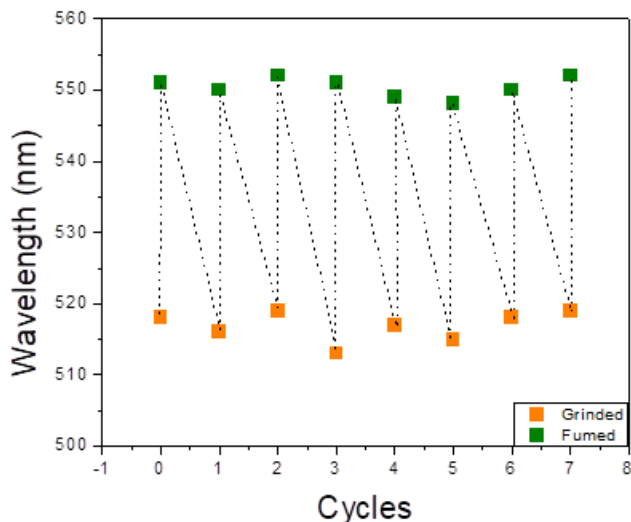


**Figure 7.17.** Repeated switching of the solid-state fluorescence of *p*-BT by repeated grinding and fuming cycles.

**Table 7.4.** Peak emission wavelengths ( $\lambda$ , in nm) of *p*-BT, *m*-BT and *o*-BT as pristine, grinded and fumed solids.

Compounds	Emission			
	$\lambda_{\text{pristine}}$ (nm)	$\lambda_{\text{ground}}$ (nm)	$\lambda_{\text{fumed}}$ (nm)	$\Delta\lambda^a$ (nm)
<i>p</i> -BT 1	519	552	513	39
<i>p</i> -BT 2	519	552	516	36
<i>m</i> -BT	516	542	519	26
<i>o</i> -BT	519	537	518	19

<sup>a</sup> Grinding-induced spectral shift,  $\Delta\lambda = \lambda_{\text{ground}} - \lambda_{\text{fumed/pristine}}$

The pristine solid of *m*-BT and *o*-BT exhibit a bright green emission at 518 nm and dark green emission at 519 nm respectively. The grinded forms of *m*-BT and *o*-BT display yellow and greenish yellow fluorescence at 542 nm

and 537 nm respectively. The fumed (DCM and hexane) solids of *m*-BT and *o*-BT emit at 519 nm and 518 nm, respectively. The spectral shift generated due to grinding in *p*-BT 1, *p*-BT 2, *m*-BT and *o*-BT is 39 nm, 36 nm, 26 nm and 19 nm respectively and follows the order *p*-BT > *m*-BT > *o*-BT.

### 7.11. Powder X-ray diffraction studies

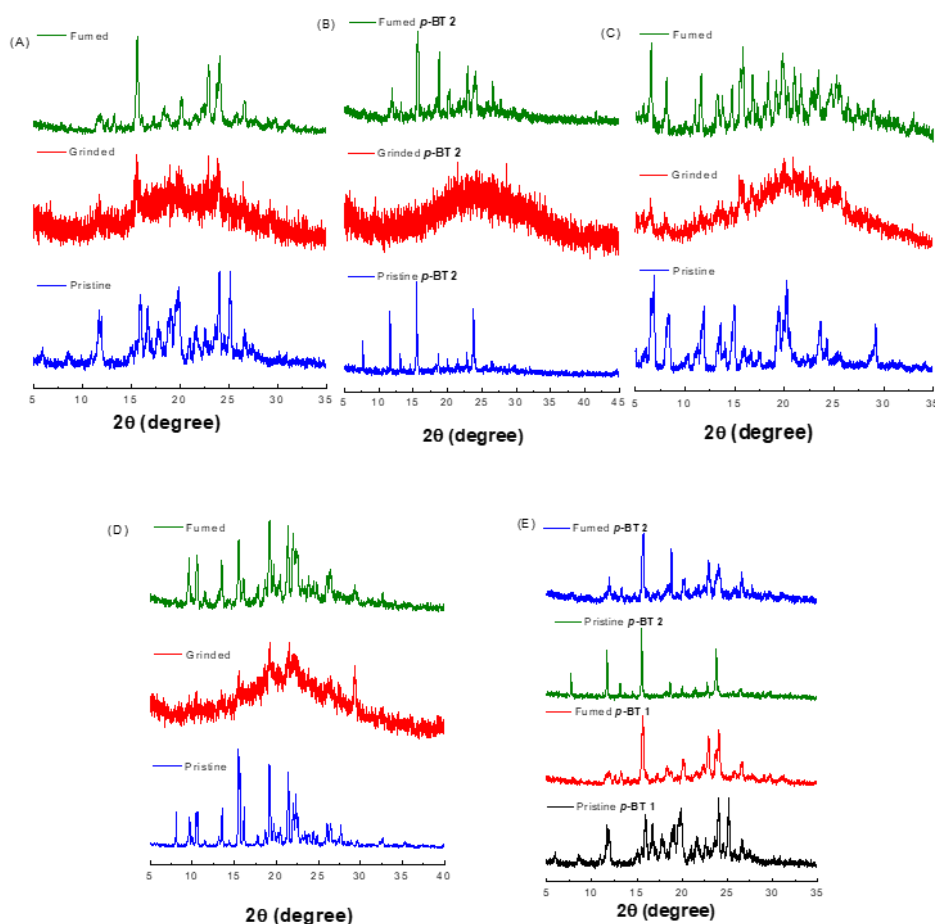


**Figure 7.18.** PXRD patterns of pristine, grinded and fumed solids of (A) *p*-BT 1 (B) *p*-BT 2 (C) *m*-BT and (D) *o*-BT, (E) Fumed patterns of *p*-BT 1 and *p*-BT 2.

The powder X-ray diffraction technique was used for interpretation of the reversible mechanochromic behavior. The PXRD patterns (Figure 7.18.) for the pristine solids of the isomers reveal sharp diffraction patterns due to the

crystalline nature. The grinded solids exhibit broad diffused PXRD pattern due to its amorphous nature. However, the sharp diffraction patterns reappeared on solvent fumigation indicating reversion to crystalline nature. The reversible mechanochromism can be assigned to morphology change from crystalline to amorphous caused due to modification of molecular arrangement on grinding. The different crystalline pristine forms ***p*-BT 1** and ***p*-BT 2** exhibit similar mechanochromic behavior but difference in their absolute quantum yields. The absolute quantum yields for the crystalline pristine forms ***p*-BT 1** and ***p*-BT 2** are 0.33 and 0.51 respectively. The absolute quantum yields of the grinded and fumed form for ***p*-BT 1** are 0.53 and 0.65 respectively and for ***p*-BT 2** are 0.51 and 0.63 respectively. The grinded and fumed forms of ***p*-BT 1** and ***p*-BT 2** exhibit similar quantum yields but a noticeable difference can be seen in the quantum yields of the pristine forms. The ***p*-BT 1** pristine crystal has very low quantum yield as compared to the pristine crystal ***p*-BT 2** and the grinded and fumed forms of ***p*-BT 1** and ***p*-BT 2**. The difference in the quantum yields of the two pristine crystals could be a consequence of their crystal packing.<sup>[23]</sup> The ***p*-BT 2** crystal confirms presence of abundant intermolecular interactions and weak H-bonding forming a tightly packed 2-D framework. On the other hand, the crystal packing of ***p*-BT 1** possesses a loosely packed 1-D structure which may result in the loss of excited state energy in terms of vibrational relaxation, lowering the quantum yield substantially. The two crystals exhibit difference in packing due to different orientation of TPE in space resulting in distinct PXRD patterns and absolute quantum yields. The fumed forms ***p*-BT 1** and ***p*-BT 2** are also crystalline in nature and possess similar PXRD patterns and quantum yields, however exhibit higher quantum yields as compared to pristine crystals of ***p*-BT 1** and ***p*-BT 2**. The fumigation of the sample is done over a short period of time which does not allow the molecule to orient in different ways resulting in similar quantum yields. The fumed forms of ***p*-BT 1** and ***p*-BT 2** exhibit highest quantum yields and blue shifted emission as compared to the two pristine crystalline

states which may possibly be an outcome of highest twisting of TPE in these crystalline forms resulting in a densely packed crystal structure. The absolute quantum yield of *m*-BT in its pristine, grinded and fumed forms is 0.74, 0.65 and 0.76 respectively. The absolute quantum yield of *o*-BT in its pristine, grinded and fumed forms is 0.34, 0.40 and 0.33 respectively.

## 7.12. Structure-property relationship

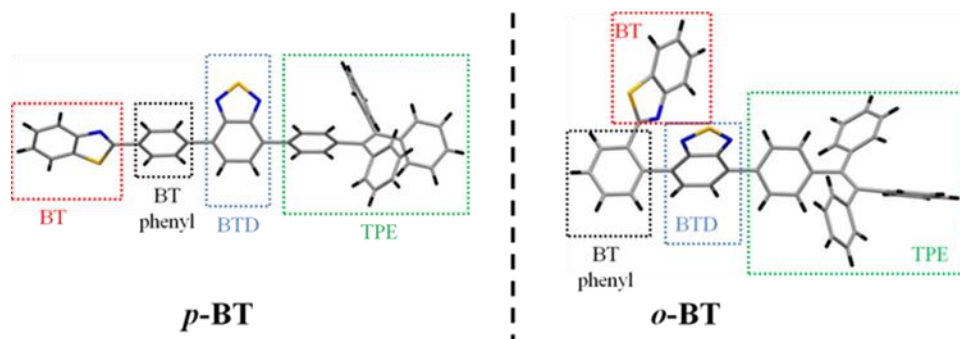


**Figure 7.19.** Schematic diagram for measurement of dihedral angles.

The difference in the mechano-responsive nature of the isomers can be inferred from the crystal analysis. The aromatic fragments in the *p*-BT and *o*-BT isomers were depicted as **BT** (benzothiazole), **BT phenyl** (phenyl attached to benzothiazole), **BTD** (benzothiadiazole) and **TPE** (tetraphenylethylene) as shown in Figure 7.19. for the measurement of dihedral angles. The dihedral angle between the **BT** plane and **BT phenyl** plane for *p*-BT 1, *p*-BT 2 and *o*-BT is 8.26°, 8.14° and 37.80° respectively and between **BT phenyl** and **BTD** for *p*-BT 1, *p*-BT 2 and *o*-BT is 35.09°, 34.42° and 62.25° respectively. The higher values of dihedral angle for *o*-BT over *p*-BT 1, *p*-BT 2 suggests an extremely twisted structure for *o*-BT reducing its susceptibility towards higher bathochromic shift on grinding. The highly twisted structure of *o*-BT makes it difficult in achieving planarity or furnishing meta-stable states after grinding thereby leading to poor mechanochromism. The twisting of donor moiety is essential for mechanochromism but higher twisting between the donor-acceptor moieties makes the structure rigid to move towards a planar structure. The dihedral

angle between **BT** plane and **TPE** plane in **p-BT 1**, **p-BT 2** is 44.13°, 46.22° and in **o-BT** is 40.53°. The higher twisting of the donor moiety in **p-BT** can also be one of the reasons for increased mechanochromism. The combined effect of the twisting and flexibility of the D-A moieties varies the degree of mechanochromism in the isomers.

### 7.13. Acidochromism

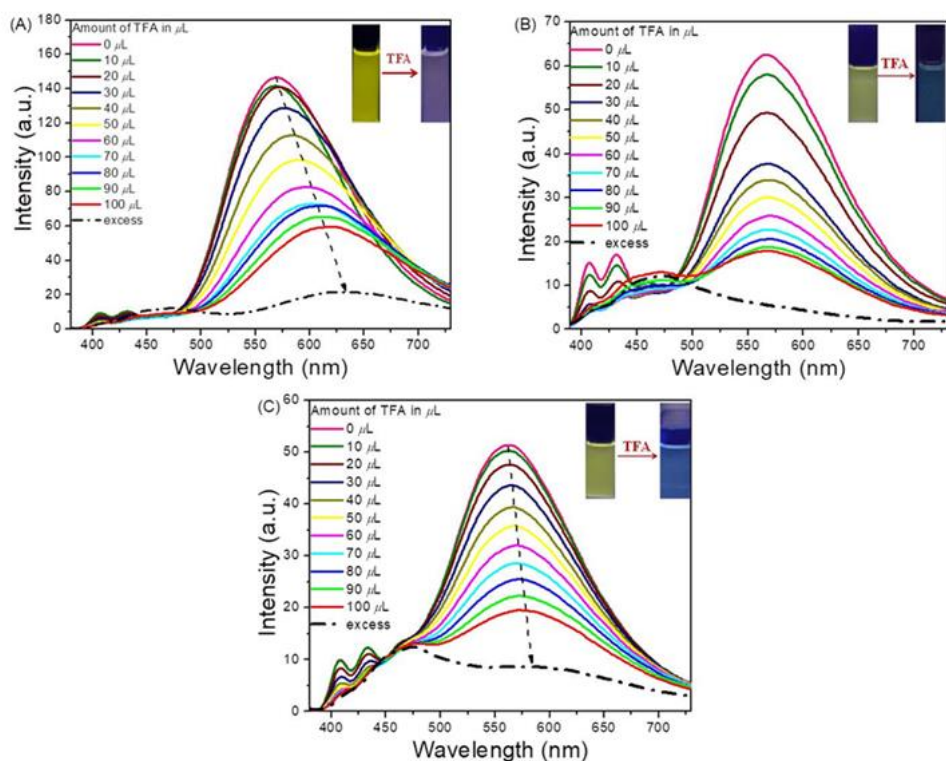


**Figure 7.20.** Emission spectra of (A) **p-BT**, (B) **m-BT** and (C) **o-BT** in response to known amounts of TFA in  $\text{CHCl}_3$ . (Conc.  $2 \times 10^{-5}$  M in  $\text{CHCl}_3$ ).

The spectral behavior of the isomers towards acid was analyzed taking in account the lone pair of N atoms which are susceptible to protonation.<sup>[24]</sup>

The solutions of the isomers **p-BT**, **m-BT** and **o-BT** in  $\text{CHCl}_3$  ( $2 \times 10^{-5}$  M) were titrated against known amounts of trifluoroacetic acid (TFA in  $\text{CHCl}_3$  stock solution) and studied using emission spectroscopy (Figure 7.20.). The emission maxima for the isomers **p-BT**, **m-BT** and **o-BT** at 569 nm, 566

nm and 562 nm respectively display quenching in emission intensity on gradual addition of TFA from 10 $\mu$ L to 100 $\mu$ L. The emission intensity at maximum wavelength quenched upto 91%, 90 % and 51% for ***p*-BT**, ***m*-BT** and ***o*-BT** respectively on excess addition of TFA. The ***p*-BT** isomer shows highest red shift of the emission maxima from 569 nm to 613 nm with reduced intensity on addition of 100 $\mu$ L TFA. Similarly, ***o*-BT** exhibits a bathochromic shift for the emission maxima from 562 nm to 576 nm on addition of 100 $\mu$ L. However, in case of ***m*-BT**, the excess addition of acid only resulted in extensive decrease of emission maxima. The peak between 460-465 nm was unaffected and appeared prominently on excess addition of TFA for all the isomers. The reduction in intensity for emission maxima confirms the response of isomers towards acid. The increased acceptor strength due to protonation of N atom by acid could result in a higher donor-acceptor interaction consequently causing a bathochromic shift. The isomers were exposed towards TFA vapors to further explore the changes in its solid-state emission. The emission intensity of ***p*-BT**, ***m*-BT** and ***o*-BT** was extensively decreased on fumigation with TFA (Figure 7.21.) for few minutes. The quenching of intensity can also be visualized by the color change of the fluorescent green solids to pale yellow. The absolute quantum yield of ***p*-BT**, ***m*-BT** and ***o*-BT** in its pristine form is 0.33, 0.74 and 0.34 respectively which on fumigation with TFA decreases to 0.01, 0.05 and 0.09 respectively. The isomers are highly reactive towards TFA in solution as well as solid state allowing its use as a fluorescent sensor for TFA.

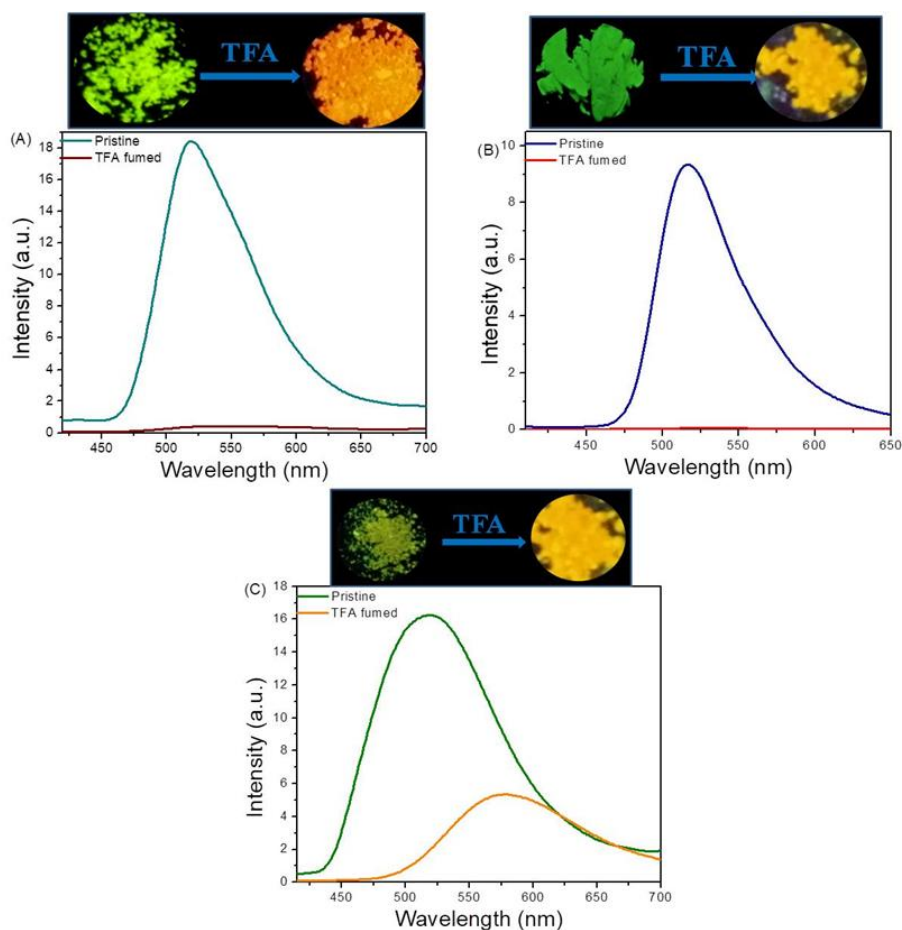


**Figure 7.21.** Emission spectra of the pristine and TFA fumed solids of (A) *p*-BT, (B) *m*-BT and (C) *o*-BT.

## 7.14. Experimental details

### General methods

Chemicals were used as received unless otherwise indicated. All oxygen or moisture sensitive reactions were performed under nitrogen/argon atmosphere.  $^1\text{H}$  NMR (400 MHz) and  $^{13}\text{C}$  NMR (100 MHz) spectra were recorded on a Bruker Avance III instrument by using  $\text{CDCl}_3$ .  $^1\text{H}$  NMR chemical shifts are reported in parts per million (ppm) relative to the solvent residual peak ( $\text{CDCl}_3$ , 7.26 ppm). Multiplicities are given as s (singlet), d (doublet), t (triplet) and m (multiplet), and the coupling constants,  $J$ , are given in hertz.  $^{13}\text{C}$  NMR chemical shifts are reported relative to the solvent

residual peak (CDCl<sub>3</sub>, 77.0 ppm). Thermogravimetric analyses were performed on the Mettler Toledo thermal analysis system. UV–visible absorption spectra were recorded on a Cary-100 Bio UV–visible spectrophotometer. Emission spectra were taken in a The Fluoromax-4C, S/n.1579D-1417-FM Fluorescence software Ver 3.8.0.60. The quantum yields in solid state were measured using K-sphere Integrating sphere. The excitation and emission slits were 2/2 nm for the emission measurements and 3/3 for solid quantum yield measurements. All of the measurements were done at 25 °C. HRMS were recorded on a Bruker-Daltonics micrOTOF-Q II mass spectrometer. The voltammograms were recorded on a CHI620D electrochemical analyzer in dichloromethane solvent and 0.1 M TBAF<sub>6</sub> as the supporting electrolyte. The electrodes used were glassy carbon as a working electrode, Pt wire as a counter electrode and Ag/AgCl as a reference electrode. Single-crystal X-ray structural studies of **1** and **4** were performed on a CCD equipped SUPERNOVA diffractometer from Agilent Technologies with Oxford Instruments low-temperature attachment under argon/nitrogen using standard Schlenk and vacuum-line techniques. The acidochromism was performed using 0.1 M stock solution of TFA in CHCl<sub>3</sub>. The rewritable-ink free paper was prepared using Whatman filter paper. The compound *p*-BT was dissolved in DCM, and then the filter paper was coated with *p*-BT. After drying, an ink-free plastic tip was used to write “IIT” on the *p*-BT loaded paper.

### Synthesis and characterization of *p*-BT and *m*-BT

General procedure for synthesis of *p*-BT and *m*-BT. Pd(PPh<sub>3</sub>)<sub>4</sub> (0.04 mmol) was added to a well degassed solution of BT4 (0.4 mmol), BTD-TPE (0.4 mmol), K<sub>2</sub>CO<sub>3</sub> (2.0 mmol) in a mixture of toluene (24.0 mL)/ethanol (8.0 mL)/H<sub>2</sub>O (4.0 mL). The resulting mixture was stirred at 80 °C for 24 h under an argon atmosphere. After cooling, the mixture was evaporated to dryness and the residue was subjected to column chromatography on silica (Hexane–DCM 30:70 in vol.) to yield the desired product *p*-BT as a green

crystals. The same procedure was employed using **BT5** and **BT-D-TPE** to obtain the desired product **m-BT** as a yellowish green powder.

**p-BT**: Yield: 73%;  $^1\text{H NMR}$  (400 MHz,  $\text{CDCl}_3$ , 25 °C):  $\delta$  8.27 (d,  $J = 8.0$  Hz, 2H), 8.11-8.14 (m, 3H), 7.94 (d,  $J = 8.0$  Hz, 1H), 7.85 (d,  $J = 8.0$  Hz, 1H), 7.80 (d,  $J = 8.0$  Hz, 3H), 7.52 (t,  $J = 8.0$  Hz, 1H), 7.41 (t,  $J = 8.0$  Hz, 1H), 7.22 (d,  $J = 8.0$  Hz, 2H), 7.05-7.15 (m, 15H);  $^{13}\text{C NMR}$  (100 MHz,  $\text{CDCl}_3$ , 25 °C):  $\delta$  167.5, 154.3, 154.0, 144.0, 143.7, 143.6, 141.6, 140.4, 139.9, 135.2, 135.1, 133.5, 133.3, 131.9, 131.6, 131.5, 131.4, 131.3, 129.8, 128.4, 128.3, 127.8, 127.6, 126.6, 126.5, 126.4, 125.3, 123.3, 121.6, 0.0 ppm; HRMS (ESI): Calcd. for  $\text{C}_{45}\text{H}_{29}\text{N}_3\text{S}_2$   $[\text{M} + \text{Na}]^+$ : 698.1695. Found: 698.1690.

**m-BT**: Yield: 69%;  $^1\text{H NMR}$  (400 MHz,  $\text{CDCl}_3$ , 25 °C):  $\delta$  8.69 (s, 1H), 8.17 (d,  $J = 8.0$  Hz, 1H), 8.12 (t,  $J = 8.0$  Hz, 2H), 7.94 (d,  $J = 8.0$  Hz, 1H), 7.89 (d,  $J = 8.0$  Hz, 1H), 7.81 (d,  $J = 8.0$  Hz, 3H) 7.68 (t,  $J = 8.0$  Hz, 1H), 7.52 (t,  $J = 8.0$  Hz, 1H), 7.41 (t,  $J = 8.0$  Hz, 1H), 7.22 (d,  $J = 8.0$  Hz, 2H), 7.06-7.14 (m, 15H);  $^{13}\text{C NMR}$  (100 MHz,  $\text{CDCl}_3$ , 25 °C):  $\delta$  167.8, 154.2, 154.0, 153.9, 144.0, 143.7, 143.6, 141.5, 140.5, 138.3, 135.1, 134.1, 133.4, 132.0, 131.8, 131.6, 131.5, 131.4, 131.3, 129.3, 128.4, 128.2, 127.8, 127.7, 127.6, 127.4, 126.6, 126.5, 126.4, 125.3, 123.3, 121.6, 0.0 ppm; HRMS (ESI): Calcd. for  $\text{C}_{45}\text{H}_{29}\text{N}_3\text{S}_2$   $[\text{M} + \text{Na}]^+$ : 698.1695. Found: 698.1687.

**Synthesis and characterization of o-BT**: The mixture of **BT-D-TPE** (0.4 mmol) and **o-TBT-BT6** (0.4 mmol) in toluene (15 mL) was degassed and  $\text{Pd}(\text{PPh}_3)_4$  (0.01 mmol) was added to it. The resulting mixture was heated at 80 °C for 72 h. The reaction was monitored using thin-layer chromatography. The mixture was cooled and the solvent was evaporated to dryness. The residue was subjected to column chromatography on silica (Hexane-DCM 20:80 in vol.) to yield the desired product **o-BT** as orange-yellow crystals. Yield: 51%;  $^1\text{H NMR}$  (400 MHz,  $\text{CDCl}_3$ , 25 °C):  $\delta$  8.20-8.22 (m, 1H), 7.88 (d,  $J = 8.0$  Hz, 1H), 7.80-7.83 (m, 2H), 7.73 (d,  $J = 8.0$  Hz, 1H), 7.60-7.64 (m, 5H), 7.37 (dt,  $J = 8.0$  Hz, 1H), 7.26-7.27 (m, 1H),

7.23-7.25 (m, 1H), 7.20 (d,  $J = 8.0$  Hz, 2H), 7.09-7.15 (m, 12H), 7.04-7.06 (m, 2H);  $^{13}\text{C}$  NMR (100 MHz,  $\text{CDCl}_3$ , 25 °C):  $\delta$  167.1, 165.1, 153.2, 152.8, 144.0, 143.7, 143.6, 141.5, 140.4, 137.0, 136.0, 135.0, 133.5, 132.6, 131.6, 131.5, 131.4, 131.3, 130.6, 130.5, 130.2, 128.8, 128.4, 129.3, 128.4, 127.8, 127.7, 127.6, 126.6, 126.5, 125.9, 124.9, 123.2, 121.2, 0.0 ppm; HRMS (ESI): Calcd. for  $\text{C}_{45}\text{H}_{29}\text{N}_3\text{S}_2$   $[\text{M} + \text{H}]^+$ : 676.1876. Found: 676.1874.

**Synthesis and characterization of *o*-TBT-BT6:** n-BuLi 1.6 M (1.89 mmol) was added dropwise to a stirred solution of **BrBT3** dissolved in THF under argon atmosphere at -78 °C (10.0 ml). The solution was stirred for 1 h at -78 °C. To this solution, tributyltin chloride (1.89 mmol) was added dropwise and the reaction was left overnight. The reaction mixture was neutralized using aqueous  $\text{NH}_4\text{Cl}$  and the aqueous layer was extracted using dichloromethane. The combined extracts were dried over anhydrous sodium sulphate. The solvent was removed under reduced pressure and the product was isolated by column chromatography on silica (Hexane-DCM 50:50 in volume) to give desired product ***o*-TBT-BT6** as colourless oil. Yield: 71%;  $^1\text{H}$  NMR (400 MHz,  $\text{CDCl}_3$ , 25 °C):  $\delta$  8.01 (d,  $J = 8.0$  Hz, 1H), 7.88-7.92 (m, 2H), 7.75 (d,  $J = 8.0$  Hz, 1H), 7.38-7.53 (m, 4H), 1.45-1.55 (m, 6H), 1.23-1.32 (m, 6H), 1.09 (t,  $J = 8.0$  Hz, 6H), 0.82 (t,  $J = 8.0$  Hz, 9H);  $^{13}\text{C}$  NMR (100 MHz,  $\text{CDCl}_3$ , 25 °C):  $\delta$  170.2, 153.1, 144.0, 139.1, 137.8, 135.1, 129.9, 129.0, 128.4, 126.1, 125.0, 122.6, 121.6, 29.2, 27.4, 13.6, 12.6, 0.0 ppm; HRMS (ESI): Calcd. for  $\text{C}_{21}\text{H}_{26}\text{NSn}$   $[\text{M} - \text{nBu}]^+$ : 444.0804. Found: 444.0803.

### 7.15. Conclusion

In conclusion, we have designed and synthesized multichromophoric D-A-A' isomers incorporating benzothiazole (BT) and benzothiadiazole (BTD) as acceptors and tetraphenylethylene (TPE) as donor. The acceptor strength was varied by changing the position of BTD-TPE with respect to the *ortho*, *meta* and *para* positions of BT. A comparative study about the structure-property relationship has been established for the isomers. The ***p*-BT**, ***m*-**

**BT** and ***o*-BT** isomers were synthesized by coupling BTD-TPE with BT using the Suzuki and Stille cross-coupling reactions. The isomers exhibit high thermal stability essential for fabrication in solid state devices. The isomers display distinct solvatochromic behavior in various polarity solvents with emission ranging from blue to orange with high bathochromic shifts. The non-planar framework of the isomers results in enhancement of intensity in the aggregated state. The ***p*-BT**, ***m*-BT** and ***o*-BT** exhibit reversible mechanochromism between green to yellow in the order ***p*-BT**>***m*-BT**>***o*-BT** and has been exploited for the development of ink-free rewritable papers. The PXRD studies reveal that a morphological conversion from crystalline to amorphous state is responsible for mechanochromism and leads to formation of metastable states. The single crystal X-ray analysis shows that the ***o*-BT** isomer has an extensively twisted structure and tightly packed 3-D framework as compared to ***p*-BT**, which explains the reason of lower response to mechanical stimuli. The higher twisting and tight packing of ***o*-BT** reduces the flexibility of the donor moiety to achieve planarization on grinding. The DFT studies reveal good separation of HOMO and LUMO supporting a distinct ICT transition. The isomers display changes in emission wavelength and intensity in solution and solid state in response to trifluoroacetic acid and can act as potential sensors for its detection. The combination of the three chromophores helps in achieving enhanced emission in solid state suitable for mechanochromic materials. The positional changes allow fine tuning of acceptor strength and molecular packing inducing changes in the mechano-responsive behaviour. The opted strategy provides a new pathway in design of AIE active mechanochromic materials suitable for application as mechano-sensors, security paper, light emitting devices and other optoelectronic applications.

## 7.16. References

- [1] (a) Sagara, Y., Yamane, S., Mutai, T., Araki, K., Kato, T. (2009). A stimuli-responsive, photoluminescent, anthracene-based liquid crystal: emission color determined by thermal and mechanical processes. *Adv. Funct. Mater.*, 19(12), 1869-1875 (DOI: [10.1002/adfm.200801726](https://doi.org/10.1002/adfm.200801726)); (b) Luo, X., Li, J., Li, C., Heng, L., Dong, Y. Q., Liu, Z., Bo, Z., Tang, B. Z. (2011). Reversible switching of the emission of diphenyldibenzofulvenes by thermal and mechanical stimuli. *Adv. Mater.*, 23(29), 3261-3265 (DOI: [10.1002/adma.201101059](https://doi.org/10.1002/adma.201101059)); (c) Toal, S. J., Jones, K. A., Magde, D., Trogler, W. C. (2005). Luminescent silole nanoparticles as chemoselective sensors for Cr (VI). *J. Am. Chem. Soc.* 127(33), 11661-11665 (DOI: [10.1021/ja052582w](https://doi.org/10.1021/ja052582w)); (d) Xu, J., Chi, Z. (Eds.). (2014). *Mechanochromic Fluorescent Materials: Phenomena, Materials and Applications*. Royal Society of Chemistry (DOI: [10.1039/9781782623229-00001](https://doi.org/10.1039/9781782623229-00001)); (e) Zheng, R., Mei, X., Lin, Z., Zhao, Y., Yao, H., Lv, W., Ling, Q. (2015). Strong CIE activity, multi-stimuli-responsive fluorescence and data storage application of new diphenyl maleimide derivatives. *J. Mater. Chem. C*, 3(39), 10242-10248 (DOI: [10.1039/C5TC02374B](https://doi.org/10.1039/C5TC02374B)); (f) Zhang, X., Chi, Z., Zhang, Y., Liu, S., Xu, J. (2013). Recent advances in mechanochromic luminescent metal complexes. *J. Mater. Chem. C*, 1(21), 3376-3390 (DOI: [10.1039/C3TC30316K](https://doi.org/10.1039/C3TC30316K)); (g) Butler, T., Morris, W. A., Samonina-Kosicka, J., Fraser, C. L. (2016). Mechanochromic luminescence and aggregation induced emission of dinaphthoylemethane  $\beta$ -diketones and their boronated counterparts. *ACS Appl. Mater. Interfaces*, 8(2), 1242-1251 (DOI: [10.1021/acsami.5b09688](https://doi.org/10.1021/acsami.5b09688)); (h) Genovese, D., Aliprandi, A., Prasetyanto, E. A., Mauro, M., Hirtz, M., Fuchs, H., & De Cola, L. (2016). Mechano- and Photochromism from Bulk to Nanoscale: Data Storage on Individual Self-Assembled Ribbons. *Adv. Funct. Mater.*, 26(29), 5271-5278 (DOI: [10.1002/adfm.201601269](https://doi.org/10.1002/adfm.201601269)). (i) Natansohn, A., Rochon, P. (2002). Photoinduced motions in azo-containing

- polymers. *Chem. Rev.*, *102*(11), 4139-4176 (DOI: 10.1021/cr970155y); (j) Minkin, V. I. (2004). Photo-, thermo-, solvato-, and electrochromic spiroheterocyclic compounds. *Chem. rev.*, *104*(5), 2751-2776. (DOI: <https://doi.org/10.1021/cr020088u>); (k) Wenger, O. S. (2013). Vapochromism in organometallic and coordination complexes: chemical sensors for volatile organic compounds. *Chem. rev.*, *113*(5), 3686-3733. (DOI: <https://doi.org/10.1021/cr300396p>).
- [2] (a) Weder, C. (2011). Mechanoresponsive materials. *J. Mater. Chem.*, *21*(23), 8235-8236 (DOI: 10.1039/C1JM90068D); (b) Farinola, G. M., Ragni, R. (2011). Electroluminescent materials for white organic light emitting diodes. *Chem. Soc. Rev.*, *40*(7), 3467-3482 (DOI: 10.1039/C0CS00204F); (c) Sagara, Y., Kato, T. (2009). Mechanically induced luminescence changes in molecular assemblies. *Nat. Chem.*, *1*(8), 605-610 (DOI: 10.1038/nchem.411); (d) Davis, D. A., Hamilton, A., Yang, J., Cremer, L. D., Van Gough, D., Potisek, S. L., Ong, M. T., Braun, P. V., Martinez, T. J., White, S., Moore, J., Sottos, N. R. (2009). Force-induced activation of covalent bonds in mechanoresponsive polymeric materials. *Nature*, *459*(7243), 68-72 (DOI: 10.1038/nature07970); (e) Ning, Z., Chen, Z., Zhang, Q., Yan, Y., Qian, S., Cao, Y., Tian, H. (2007). Aggregation-induced emission (AIE)-active starburst triarylamine fluorophores as potential non-doped red emitters for organic light-emitting diodes and Cl<sub>2</sub> gas chemodosimeter. *Adv. Funct. Mater.*, *17*(18), 3799-3807 (DOI: 10.1002/adfm.200700649); (f) Hirata, S., Watanabe, T. (2006). Reversible thermoresponsive recording of fluorescent images (TRF). *Adv. Mater.*, *18*(20), 2725-2729 (DOI: 10.1002/adma.200600209); (g) Sun, H., Liu, S., Lin, W., Zhang, K. Y., Lv, W., Huang, X., Huang, W. (2014). Smart responsive phosphorescent materials for data recording and security protection. *Nat. Commun.*, *5*(1), 1-9 (DOI: 10.1038/ncomms4601); (h) Samuel, I. D. W., Turnbull, G. A. (2007). Organic semiconductor

lasers. *Chem. Rev.*, *107*(4), 1272-1295 (DOI: 10.1021/cr050152i); (i) Sagara, Y., Yamane, S., Mitani, M., Weder, C., Kato, T. (2016). Mechanoresponsive luminescent molecular assemblies: an emerging class of materials. *Adv. Mater.*, *28*(6), 1073-1095 (DOI: 10.1002/adma.201502589); (j) Ito, H., Saito, T., Oshima, N., Kitamura, N., Ishizaka, S., Hinatsu, Y., Wakeshima, M., Kato, M., Tsuge, K., Sawamura, M. (2008). Reversible mechanochromic luminescence of [(C<sub>6</sub>F<sub>5</sub>Au)<sub>2</sub>(μ-1,4-diisocyanobenzene)]. *J. Am. Chem. Soc.*, *130*(31), 10044-10045 (DOI: 10.1021/ja8019356); (k) Yuan, L., Lin, W., Zheng, K., He, L., Huang, W. (2013). Far-red to near infrared analyte-responsive fluorescent probes based on organic fluorophore platforms for fluorescence imaging. *Chem. Soc. Rev.*, *42*(2), 622-661 (DOI: 10.1039/C2CS35313J); (l) Xu, B., Xie, M., He, J., Xu, B., Chi, Z., Tian, W., Jiang, L., Zhao, F., Liu, S., Zhang, Y., Xu, Z., Xu, J. (2013). An aggregation-induced emission luminophore with multi-stimuli single- and two-photon fluorescence switching and large two-photon absorption cross section. *Chem. Commun.*, *49*(3), 273-275 (DOI: 10.1039/C2CC36806D); (m) Gallardo, I., Guirado, G., Hernando, J., Morais, S., Prats, G. (2016). A multi-stimuli responsive switch as a fluorescent molecular analogue of transistors. *Chem. Sci.*, *7*(3), 1819-1825 (DOI: 10.1039/C5SC03395K); (n) Zhang, Y. J., Chen, C., Tan, B., Cai, L. X., Yang, X. D., Zhang, J. (2016). A dual-stimuli responsive small molecule organic material with tunable multi-state response showing turn-on luminescence and photocoloration. *Chem. Commun.*, *52*(13), 2835-2838 (DOI: [10.1039/C5CC09799A](https://doi.org/10.1039/C5CC09799A)); (o) Zheng, R., Mei, X., Lin, Z., Zhao, Y., Yao, H., Lv, W., Ling, Q. (2015). Strong CIE activity, multi-stimuli-responsive fluorescence and data storage application of new diphenyl maleimide derivatives. *J. Mater. Chem. C*, *3*(39), 10242-10248 (DOI: [doi.org/10.1039/C5TC02374B](https://doi.org/10.1039/C5TC02374B)); (p) Liang, J., Tang, B. Z., Liu, B. (2015). Specific light-up bioprobes based on AIEgen conjugates. *Chem. Soc. Rev.*, *44*(10), 2798-2811 (DOI: 10.1039/C5CS00000A)

- 10.1039/C4CS00444B); (q) Hou, X., Ke, C., Bruns, C. J., McGonigal, P. R., Pettman, R. B., Stoddart, J. F. (2015). Tunable solid-state fluorescent materials for supramolecular encryption. *Nat. Commun.*, 6(1), 1-9 (DOI: 10.1038/ncomms7884); (r) Kaji, H., Suzuki, H., Fukushima, T., Shizu, K., Suzuki, K., Kubo, S., Komino, T., Oiwa, H., Suzuki, F., Wakamiya, A., Murata, Y., Adachi, C. (2015). Purely organic electroluminescent material realizing 100% conversion from electricity to light. *Nat. Commun.*, 6(1), 1-8 (DOI: 10.1038/ncomms9476).
- [3] (a) Kishimura, A., Yamashita, T., Yamaguchi, K., Aida, T. (2005). Rewritable phosphorescent paper by the control of competing kinetic and thermodynamic self-assembling events. *Nat. Mater.*, 4(7), 546-549 (DOI: 10.1038/nmat1401); (b) Ciardelli, F., Ruggeri, G., Pucci, A. (2013). Dye-containing polymers: methods for preparation of mechanochromic materials. *Chem. Soc. Rev.*, 42(3), 857-870 (DOI: 10.1039/C2CS35414D); (c) Chi, Z., Zhang, X., Xu, B., Zhou, X., Ma, C., Zhang, Y., Liu, S., Xu, J. (2012). Recent advances in organic mechanofluorochromic materials. *Chem. Soc. Rev.*, 41(10), 3878-3896 (DOI: 10.1039/C2CS35016E); (d) Crenshaw, B. R., Burnworth, M., Khariwala, D., Hiltner, A., Mather, P. T., Simha, R., Weder, C. (2007). Deformation-induced color changes in mechanochromic polyethylene blends. *Macromolecules*, 40(7), 2400-2408 (DOI: 10.1021/ma062936j); (e) Zhang, X., Chi, Z., Zhang, Y., Liu, S., Xu, J. (2013). Recent advances in mechanochromic luminescent metal complexes. *J. Mater. Chem. C*, 1(21), 3376-3390 (DOI: 10.1039/C3TC30316K); (f) Luo, X., Li, J., Li, C., Heng, L., Dong, Y. Q., Liu, Z., Tang, B. Z. (2011). Reversible switching of the emission of diphenyldibenzofulvenes by thermal and mechanical stimuli. *Adv. Mater.*, 23(29), 3261-3265 (DOI: 10.1002/adma.201101059); (g) Yoon, S. J., Chung, J. W., Gierschner, J., Kim, K. S., Choi, M. G., Kim, D., Park, S. Y. (2010). Multistimuli two-color luminescence switching via

- different slip-stacking of highly fluorescent molecular sheets. *J. Am. Chem. Soc.*, *132*(39), 13675-13683 (DOI: 10.1021/ja1044665); (h) Wu, X., Guo, J., Cao, Y., Zhao, J., Jia, W., Chen, Y., Jia, D. (2018). Mechanically triggered reversible stepwise tricolor switching and thermochromism of anthracene-*o*-carborane dyad. *Chem. Sci.*, *9*(23), 5270-5277 (DOI: 10.1039/C8SC00833G).
- [4] (a) Sagara, Y., Mutai, T., Yoshikawa, I., Araki, K. (2007). Material design for piezochromic luminescence: hydrogen-bond-directed assemblies of a pyrene derivative. *J. Am. Chem. Soc.*, *129*(6), 1520-1521 (DOI: 10.1021/ja0677362); (b) Wu, H., Hang, C., Li, X., Yin, L., Zhu, M., Zhang, J., Zhou, Y., Ågren, H., Zhang, Q., Zhu, L., (2017). Molecular stacking dependent phosphorescence–fluorescence dual emission in a single luminophore for self-recoverable mechanoconversion of multicolor luminescence. *Chem. Commun.*, *53*(18), 2661-2664 (DOI: 10.1039/C6CC04901J); (c) Zhang, G., Lu, J., Sabat, M., Fraser, C. L. (2010). Polymorphism and reversible mechanochromic luminescence for solid-state difluoroboron avobenzene. *J. Am. Chem. Soc.*, *132*(7), 2160-2162 (DOI: 10.1021/ja9097719); (d) Sasaki, S., Suzuki, S., Sameera, W. M. C., Igawa, K., Morokuma, K., Konishi, G. I. (2016). Highly twisted N, N-dialkylamines as a design strategy to tune simple aromatic hydrocarbons as steric environment-sensitive fluorophores. *J. Am. Chem. Soc.*, *138*(26), 8194-8206 (DOI: 10.1021/jacs.6b03749); (e) Zong, L., Xie, Y., Wang, C., Li, J. R., Li, Q., Li, Z. (2016). From ACQ to AIE: the suppression of the strong  $\pi$ – $\pi$  interaction of naphthalene diimide derivatives through the adjustment of their flexible chains. *Chem. Commun.*, *52*(77), 11496-11499 (DOI: 10.1039/C6CC06176A); (f) Sekiguchi, S., Kondo, K., Sei, Y., Akita, M., Yoshizawa, M. (2016). Engineering Stacks of V-Shaped Polyaromatic Compounds with Alkyl Chains for Enhanced Emission in the Solid State. *Angewandte Chemie*, *128*(24), 7020-7024 (DOI: 10.1002/ange.201602502); (g)

- Mutai, T., Satou, H., Araki, K. (2005). Reproducible on–off switching of solid-state luminescence by controlling molecular packing through heat-mode interconversion. *Nat. Mater.*, 4(9), 685-687 (DOI: 10.1038/nmat1454); (h) Yuan, W.Z., Tan, Y., Gong, Y., Lu, P., Lam, J.W., Shen, X.Y., Feng, C., Sung, H.H.Y., Lu, Y., Williams, I.D. and Sun, J.Z., Zhang, Y., Tang, B. Z. (2013). Synergy between twisted conformation and effective intermolecular interactions: strategy for efficient mechanochromic luminogens with high contrast. *Adv. Mater.*, 25(20), 2837-2843 (DOI: 10.1002/adma.201205043); (i) Misra, R., Jadhav, T., Dhokale, B., Mobin, S. M. (2014). Reversible mechanochromism and enhanced AIE in tetraphenylethene substituted phenanthroimidazoles. *Chem. Commun.*, 50(65), 9076-9078 (DOI: 10.1039/C4CC02824D); (j) Walters, D. T., Aghakhanpour, R. B., Powers, X. B., Ghiassi, K. B., Olmstead, M. M., Balch, A. L. (2018). Utilization of a Nonemissive Triphosphine Ligand to Construct a Luminescent Gold (I)-Box That Undergoes Mechanochromic Collapse into a Helical Complex. *J. Am. Chem. Soc.*, 140(24), 7533-7542 (DOI: 10.1021/jacs.8b01666).
- [5] (a) Dong, Y., Xu, B., Zhang, J., Tan, X., Wang, L., Chen, J., Lv, H., Wen, S., Li, B., Ye, L., Zou, B., Tian, W. (2012). Piezochromic luminescence based on the molecular aggregation of 9, 10-Bis ((E)-2-(pyrid-2-yl) vinyl) anthracene. *Angew. Chem., Int. Ed.*, 51(43), 10782-10785 (DOI: 10.1002/anie.201204660); (b) Meng, X., Qi, G., Zhang, C., Wang, K., Zou, B., Ma, Y. (2015). Visible mechanochromic responses of spiropyrans in crystals via pressure-induced isomerization. *Chem. Commun.*, 51(45), 9320-9323 (DOI: 10.1039/C5CC01064K); (c) Wang, L., Wang, K., Zou, B., Ye, K., Zhang, H., Wang, Y. (2015). Luminescent chromism of boron diketonate crystals: distinct responses to different stresses. *Adv. Mater.*, 27(18), 2918-2922 (DOI: 10.1002/adma.201500589); (d) Sun, H., Liu, S., Lin, W., Zhang, K.Y., Lv, W., Huang, X., Huo, F., Yang, H., Jenkins,

- G., Zhao, Q. and Huang, W., (2014). Smart responsive phosphorescent materials for data recording and security protection. *Nat. Commun.*, 5(1), 1-9 (DOI: 10.1038/ncomms4601); (e) Li, W., Wang, L., Zhang, J. P., Wang, H. (2014). Bis-pyrene-based supramolecular aggregates with reversibly mechanochromic and vapo-chromic responsiveness. *J. Mater. Chem. C*, 2(10), 1887-1892 (DOI: 10.1039/C3TC31974A); (f) Jadhav, T., Choi, J. M., Dhokale, B., Mobin, S. M., Lee, J. Y., Misra, R. (2016). Effect of end groups on mechanochromism and electroluminescence in tetraphenylethylene substituted phenanthroimidazoles. *J. Phys. Chem. C*, 120(33), 18487-18495 (DOI: 10.1021/acs.jpcc.6b06277).
- [6] Jadhav, T., Dhokale, B., Mobin, S. M., Misra, R. (2015). Aggregation induced emission and mechanochromism in pyrenoimidazoles. *J. Mater. Chem. C*, 3(38), 9981-9988 (DOI: 10.1039/C5TC02181B); (b) Yoshii, R., Hirose, A., Tanaka, K., Chujo, Y. (2014). Functionalization of boron diiminates with unique optical properties: multicolor tuning of crystallization-induced emission and introduction into the main chain of conjugated polymers. *J. Am. Chem. Soc.*, 136(52), 18131-18139 (DOI: 10.1021/ja510985v); (c) Nguyen, N. D., Zhang, G., Lu, J., Sherman, A. E., Fraser, C. L. (2011). Alkyl chain length effects on solid-state difluoroboron  $\beta$ -diketonate mechanochromic luminescence. *J. Mater. Chem. C*, 21(23), 8409-8415 (DOI: 10.1039/C1JM00067E); (d) Ning, Z., Chen, Z., Zhang, Q., Yan, Y., Qian, S., Cao, Y., Tian, H. (2007). Aggregation-induced emission (AIE)-active starburst triarylamine fluorophores as potential non-doped red emitters for organic light-emitting diodes and Cl<sub>2</sub> gas chemodosimeter. *Adv. Funct. Mater.*, 17(18), 3799-3807 (DOI: 10.1002/adfm.200700649); (e) He, Z., Zhao, W., Lam, J. W., Peng, Q., Ma, H., Liang, G., Shuai, Z., Tang, B. Z. (2017). White light emission from a single organic molecule with dual phosphorescence at room temperature. *Nat. Commun.*, 8(1), 1-8 (DOI: 10.1038/s41467-017-00362-5);

- [7] (a) Birks, J. B. (1970). *Photophysics of aromatic molecules*. Wiley, London, UK, 1970; (b) Jayanty, S., & Radhakrishnan, T. P. (2004). Enhanced fluorescence of remote functionalized diaminodicyanoquinodimethanes in the solid state and fluorescence switching in a doped polymer by solvent vapors. *Chem. Eur. J.*, *10*(3), 791-797 (DOI: 10.1002/chem.200305123); (c) Tracy, H.J., Mullin, J.L., Klooster, W.T., Martin, J.A., Haug, J., Wallace, S., Rudloe, I., Watts, K., (2005). Enhanced photoluminescence from group 14 metalloles in aggregated and solid solutions. *Inorg. Chem.*, *44*(6), 2003-2011 (DOI: 10.1021/ic049034o); (d) Forster, T., Kasper, K. Z., *Phys. Chem.*, (Munich) 1954, 1, 275-282.
- [8] (a) Luo, J., Xie, Z., Lam, J. W., Cheng, L., Chen, H., Qiu, C., Kwok, H.S., Zhan, X., Liu, Y., Zhu, D., Tang, B. Z. (2001). Aggregation-induced emission of 1-methyl-1, 2, 3, 4, 5-pentaphenylsilole. *Chemical communications*, (18), 1740-1741. (DOI: 10.1039/B105159H); (b) Li, Y., Liu, T., Liu, H., Tian, M. Z., Li, Y. (2014). Self-assembly of intramolecular charge-transfer compounds into functional molecular systems. *Acc. Chem. Res.*, *47*(4), 1186-1198 (DOI: 10.1021/ar400264e); (c) Liu, H., Xu, J., Li, Y., Li, Y. (2010). Aggregate nanostructures of organic molecular materials. *Acc. Chem. Res.*, *43*(12), 1496-1508 (DOI: 10.1021/ar100084y); (d) Hong, Y., Lam, J. W., Tang, B. Z. (2011). Aggregation-induced emission. *Chem. Soc. Rev.*, *40*(11), 5361-5388, (DOI: 10.1039/C1CS15113D).
- [9] (a) Liang, J., Tang, B. Z., Liu, B. (2015). Specific light-up bioprobes based on AIEgen conjugates. *Chem. Soc. Rev.*, *44*(10), 2798-2811 (DOI: 10.1039/C4CS00444B); (b) Hu, R., Leung, N. L., Tang, B. Z. (2014). AIE macromolecules: syntheses, structures and functionalities. *Chem. Soc. Rev.*, *43*(13), 4494-4562 (DOI: 10.1039/C4CS00044G); (c) Yuan, W. Z., Gong, Y., Chen, S., Shen, X. Y., Lam, J. W., Lu, P., Lu, Y., Wang, Z., Hu, R., Xie, N. and Kwok, H.S., Zhang, Y., Sun., J. Z., Tang, B. Z. (2012). Efficient solid emitters

with aggregation-induced emission and intramolecular charge transfer characteristics: molecular design, synthesis, photophysical behaviors, and OLED application. *Chem. Mater.*, 24(8), 1518-1528 (DOI: 10.1021/cm300416y); (d) Dong, Y., Lam, J. W., Qin, A., Liu, J., Li, Z., Tang, B. Z., Sun, J., Kwok, H. S. (2007). Aggregation-induced emissions of tetraphenylethene derivatives and their utilities as chemical vapor sensors and in organic light-emitting diodes. *Appl. Phys. Lett.*, 91(1), 011111 (DOI: 10.1063/1.2753723); (e) Huang, J., Yang, X., Wang, J., Zhong, C., Wang, L., Qin, J., Li, Z. (2012). New tetraphenylethene-based efficient blue luminophores: aggregation induced emission and partially controllable emitting color. *J. Mater. Chem. C*, 22(6), 2478-2484 (DOI: 10.1039/C1JM14054J); (f) Gong, Y., Tan, Y., Liu, J., Lu, P., Feng, C., Yuan, W. Z., Lu, Y., Sun, J.Z., He, G., Zhang, Y. (2013). Twisted D- $\pi$ -A solid emitters: efficient emission and high contrast mechanochromism. *Chem. Commun.*, 49(38), 4009-4011 (DOI: 10.1039/C3CC39243K); (g) Imoto, H., Fujii, R., Naka, K. (2018). 3, 4-Diaminomaleimide Dyes-Simple Luminophores with Efficient Orange-Red Emission in the Solid State. *Eur. J. Org. Chem.*, 2018(6), 837-843 (10.1002/ejoc.201701479); (h) Chen, C., Li, R. H., Zhu, B. S., Wang, K. H., Yao, J. S., Yin, Y. C., Yao, M.M., Yao, H.B., Yu, S.H., (2018). Highly Luminescent Inks: Aggregation-Induced Emission of Copper-Iodine Hybrid Clusters. *Angew. Chem. Int. Ed.*, 57(24), 7106-7110 (DOI: 10.1002/anie.201802932); (i) Jadhav, T., Choi, J. M., Shinde, J., Lee, J. Y., Misra, R. (2017). Mechanochromism and electroluminescence in positional isomers of tetraphenylethylene substituted phenanthroimidazoles. *J. Mater. Chem. C*, 5(24), 6014-6020 (DOI: 10.1039/C7TC00950J); (j) Jiang, M., Gu, X., Kwok, R. T., Li, Y., Sung, H. H., Zheng, X., Zhang, Y., Lam, J.W., Williams, I.D., Huang, X., Wong, K.S., Tang, B. Z. (2018). Multifunctional AIEgens: ready synthesis, tunable emission, mechanochromism, mitochondrial,

and bacterial imaging. *Adv. Funct. Mater.*, 28(1), 1704589 (DOI: 10.1002/adfm.201704589).

- [10] (a) Zhu, Y. X., Wei, Z. W., Pan, M., Wang, H. P., Zhang, J. Y., Su, C. Y. (2016). A new TPE-based tetrapodal ligand and its Ln (III) complexes: multi-stimuli responsive AIE (aggregation-induced emission)/ILCT (intraligand charge transfer)-bifunctional photoluminescence and NIR emission sensitization. *Dalton Trans.*, 45(3), 943-950 (DOI: 10.1039/C5DT03640B); (b) Xu, B., Li, W., He, J., Wu, S., Zhu, Q., Yang, Z., Bryce, M. R. (2016). Achieving very bright mechanoluminescence from purely organic luminophores with aggregation-induced emission by crystal design. *Chem. Sci.*, 7(8), 5307-5312 (DOI: 10.1039/C6SC01325B); (c) Ekbote, A., Jadhav, T., Misra, R. (2017). T-Shaped donor-acceptor-donor type tetraphenylethylene substituted quinoxaline derivatives: aggregation-induced emission and mechanochromism. *New J. Chem.*, 41(17), 9346-9353 (DOI: 10.1039/C7NJ01531C); (d) Yang, Z., Chi, Z., Mao, Z., Zhang, Y., Liu, S., Zhao, J., Aldred, M.P., Chi, Z. (2018). Recent advances in mechano-responsive luminescence of tetraphenylethylene derivatives with aggregation-induced emission properties. *Mater. Chem. Front.*, 2(5), 861-890 (DOI: 10.1039/C8QM00062J); (e) Umar, S., Jha, A. K., Purohit, D., Goel, A. (2017). A tetraphenylethene-naphthyridine-based AIEgen TPEN with dual mechanochromic and chemosensing properties. *J. Org. Chem.*, 82(9), 4766-4773 (DOI: 10.1021/acs.joc.7b00456); (f) Desroches, M., Morin, J. F. (2018). Anthanthrene as a super-extended tetraphenylethylene for aggregation-induced emission. *Organic letters*, 20(10), 2797-2801 (DOI: 10.1021/acs.orglett.8b00452). (g) Biswas, S., Jana, D., Kumar, G. S., Maji, S., Kundu, P., Ghorai, U. K., Giri, R.P., Das, B., Chattopadhyay, N., Ghorai, B.K., Acharya, S. (2018). Supramolecular aggregates of tetraphenylethene-cored AIEgen toward mechanoluminescent and electroluminescent devices. *ACS applied materials & interfaces*, 10(20), 17409-17418. (DOI:

- <https://doi.org/10.1021/acsami.8b00165>); (h) Xiong, J., Wang, K., Yao, Z., Zou, B., Xu, J., Bu, X. H. (2018). Multi-stimuli-responsive fluorescence switching from a pyridine-functionalized tetraphenylethene AIEgen. *ACS Appl. Mater. Interfaces*, *10*(6), 5819-5827 (DOI: 10.1021/acsami.7b18718).
- [11](a) Zhang, M., Xue, S., Dong, W., Wang, Q., Fei, T., Gu, C., Ma, Y. (2010). Highly-efficient solution-processed OLEDs based on new bipolar emitters. *Chem. Commun.*, *46*(22), 3923-3925 (DOI: [doi.org/10.1039/C001170C](https://doi.org/10.1039/C001170C)); (b) Ishi-i, T., Ikeda, K., Ogawa, M., Kusakaki, Y. RSC Adv. 2015, 5, 89171. *Crossref, CAS* (DOI: 10.1021/cr020088u); (c) Jadhav, T., Dhokale, B., Patil, Y., Mobin, S. M., Misra, R. (2016). Multi-stimuli responsive donor–acceptor tetraphenylethylene substituted benzothiadiazoles. *J. Phys. Chem. C.*, *120*(42), 24030-24040 (DOI: 10.1021/acs.jpcc.6b09015); (d) Xu, B., Li, W., He, J., Wu, S., Zhu, Q., Yang, Z., Wu, Y.C., Zhang, Y., Jin, C., Lu, P.Y., Chi, Z., Liu, S., Xu, J., Bryce, M. R. (2016). Achieving very bright mechanoluminescence from purely organic luminophores with aggregation-induced emission by crystal design. *Chem. Sci.*, *7*(8), 5307-5312 (DOI: 10.1039/C6SC01325B); (e) Wu, J., Cheng, Y., Lan, J., Wu, D., Qian, S., Yan, L., He, Z., Li, X., Wang, K., Zou, B., You, J. (2016). Molecular engineering of mechanochromic materials by programmed C–H arylation: making a counterpoint in the chromism trend. *J. Am. Chem. Soc.*, *138*(39), 12803-12812 (DOI: 10.1021/jacs.6b03890); (f) Kwon, M. S., Gierschner, J., Yoon, S. J., Park, S. Y. (2012). Unique piezochromic fluorescence behavior of dicyanodistyrylbenzene based donor–acceptor–donor triad: mechanically controlled photo-induced electron transfer (eT) in molecular assemblies. *Adv. Mater.*, *24*(40), 5487-5492 (DOI: 10.1002/adma.201202409); (g) Li, W., Liu, D., Shen, F., Ma, D., Wang, Z., Feng, T., Xu, Y., Yang, B., Ma, Y., (2012). A twisting donor-acceptor molecule with an intercrossed excited state for highly

- efficient, deep-blue electroluminescence. *Adv. Funct. Mater.*, 22(13), 2797-2803 (DOI: 10.1002/adfm.201200116); (h) Zhao, B., Li, N., Wang, X., Chang, Z., Bu, X. H. (2017). Host–Guest Engineering of Coordination Polymers for Highly Tunable Luminophores Based on Charge Transfer Emissions. *ACS Appl. Mater. Interfaces*, 9(3), 2662-2668 (DOI: 10.1021/acsami.6b14554).
- [12](a) Ito, S., Taguchi, T., Yamada, T., Ubukata, T., Yamaguchi, Y., Asami, M. (2017). Indolylbenzothiadiazoles with varying substituents on the indole ring: a systematic study on the self-recovering mechanochromic luminescence. *RSC Adv.*, 7(28), 16953-16962 (DOI: 10.1039/C7RA01006K); (b) Naeem, K. C., Neenu, K., Nair, V. C. (2017). Effect of differential self-assembly on mechanochromic luminescence of fluorene-benzothiadiazole-based fluorophores. *ACS omega*, 2(12), 9118-9126 (DOI: 10.1021/acsomega.7b01339); (c) Zhang, X., Ma, Z., Yang, Y., Zhang, X., Jia, X., Wei, Y. (2014). Fine-tuning the mechanofluorochromic properties of benzothiadiazole-cored cyano-substituted diphenylethene derivatives through D–A effect. *J. Mater. Chem. C*, 2(42), 8932-8938 (DOI: 10.1039/C4TC01457J); (d) Chen, J., Li, D., Chi, W., Liu, G., Liu, S. H., Liu, X., Zhang, C., Yin, J. (2018). A Highly Reversible Mechanochromic Difluorobenzothiadiazole Dye with Near-Infrared Emission. *Chem. Eur. J.*, 24(15), 3671-3676 (DOI: 10.1002/chem.201705780).
- [13](a) Wang, L., Cui, M., Tang, H., Cao, D. (2018). Synthesis of a BODIPY–2-(2'-hydroxyphenyl) benzothiazole conjugate with solid state emission and its application as a fluorescent pH probe. *Anal. Methods*, 10(14), 1633-1639 (DOI: 10.1039/C8AY00053K); (b) Wang, Y., Xin, X., Lu, Y., Xiao, T., Xu, X., Zhao, N., Hu, X., Ong, B.S., Ng, S. C. (2013). Substituent effects on physical and photovoltaic properties of 5, 6-difluorobenzo [c][1, 2, 5] thiadiazole-based D–A polymers: toward a donor design for high performance polymer solar cells. *Macromolecules*, 46(24), 9587-9592 (DOI:

10.1021/ma401709r); (c) Pathak, A., Justin Thomas, K. R., Singh, M., Jou, J. H. (2017). Fine-tuning of photophysical and electroluminescence properties of benzothiadiazole-based emitters by methyl substitution. *J. Org. Chem.*, 82(21), 11512-11523 (DOI: 10.1021/acs.joc.7b02127); (d) Maragani, R., Gautam, P., Mobin, S. M., Misra, R. (2016). C 2-Symmetric ferrocenyl bithiazoles: synthesis, photophysical, electrochemical and DFT studies. *Dalton Trans.*, 45(11), 4802-4809 (DOI: 10.1039/C5DT04988A); (e) Ni, F., Wu, Z., Zhu, Z., Chen, T., Wu, K., Zhong, C., An, K., Wei, D., Ma, D., Yang, C. (2017). Teaching an old acceptor new tricks: rationally employing 2, 1, 3-benzothiadiazole as input to design a highly efficient red thermally activated delayed fluorescence emitter. *J. Mater. Chem. C*, 5(6), 1363-1368 (DOI: 10.1039/C7TC00025A); (f) Sun, Y., Duan, L., Wei, P., Qiao, J., Dong, G., Wang, L., Qiu, Y. (2009). An ambipolar transporting naphtho [2, 3-c][1, 2, 5] thiadiazole derivative with high electron and hole mobilities. *Org. Lett.*, 11(10), 2069-2072 (DOI: 10.1021/o1900431a).

- [14](a) Jadhav, T., Dhokale, B., Mobin, S. M., & Misra, R. (2015). Mechanochromism and aggregation induced emission in benzothiazole substituted tetraphenylethylenes: a structure function correlation. *RSC Adv.*, 5(38), 29878-29884. (DOI: 10.1039/C5RA04881H); (b) Jadhav, T., Dhokale, B., Misra, R. (2015). Effect of the cyano group on solid state photophysical behavior of tetraphenylethene substituted benzothiadiazoles. *J. Mater. Chem. C*, 3(35), 9063-9068 (DOI: 10.1039/C5TC01871D); (c) Gautam, P., Maragani, R., Mobin, S. M., Misra, R. (2014). Reversible mechanochromism in dipyrindylamine-substituted unsymmetrical benzothiadiazoles. *RSC Adv.*, 4(94), 52526-52529 (DOI: 10.1039/C4RA09921D).
- [15](a) Maleki, B., Salehabadi, H. (2010). Ammonium chloride; as a mild and efficient catalyst for the synthesis of some 2-arylbenzothiazoles

- and bisbenzothiazole derivatives. *Eur. J. Chem.* 1(4), 377-380 (DOI: 10.5155/eurjchem.1.4.377-380.165);
- [16] (a) Wang, G., Pu, K. Y., Zhang, X., Li, K., Wang, L., Cai, L., Ding, D., Lai, Y.H., Liu, B. (2011). Star-shaped glycosylated conjugated oligomer for two-photon fluorescence imaging of live cells. *Chem. Mater.*, 23(20), 4428-4434 (DOI: 10.1021/cm201377u); (b) Bai, Y., Wei, B., Ouyang, X., Liu, Z., Jiang, W., Li, W., Zhang, L., Hong, L., He, G., Chen, Y. Ge, Z. (2016). Tunable crystal packing for enhanced electroluminescent properties based on novel thiazole derivatives with different connecting positions of carbazole. *Dyes and Pigments*, 130, 319-326 (DOI: 10.1016/j.dyepig.2016.03.031).
- [17] (a) Frisch, M. J. E. A., Trucks, G. W., Schlegel, H. B., Scuseria, G. E., Robb, M. A., Cheeseman, J. R., *et.al.*, (2009). gaussian 09, Revision d. 01, Gaussian. Inc., Wallingford CT, 201.; (b) Lee, C., Yang, W., Parr, R. G. (1988). *Phys. Rev. B: Condens. Matter Mater. Phys.*, (DOI: 10.1103/PhysRevB.37.785); (c) Becke, A. D. (1993). A new mixing of Hartree–Fock and local density-functional theories. *J. Chem. Phys.*, 98(2), 1372-1377 (DOI: 10.1063/1.464304).
- [18] Janietz, S., Bradley, D. D. C., Grell, M., Giebeler, C., Inbasekaran, M., Woo, E. P. (1998). Electrochemical determination of the ionization potential and electron affinity of poly (9, 9-dioctylfluorene). *Appl. Phys. Lett.*, 73(17), 2453-2455 (DOI: 10.1063/1.122479).
- [19] (a) Jadhav, T., Maragani, R., Misra, R., Sreeramulu, V., Rao, D. N., Mobin, S. M. (2013). Design and synthesis of donor–acceptor pyrazabole derivatives for multiphoton absorption. *Dalton Trans.*, 42(13), 4340-4342 (DOI: 10.1039/C3DT33065F); (b) Lu, X., Fan, S., Wu, J., Jia, X., Wang, Z. S., Zhou, G. (2014). Controlling the charge transfer in D–A–D chromophores based on pyrazine derivatives. *J. Org. Chem.*, 79(14), 6480-6489 (DOI: 10.1021/cm301520z).
- [20] Wang, E., Lam, J. W., Hu, R., Zhang, C., Zhao, Y. S., Tang, B. Z. (2014). Twisted intramolecular charge transfer, aggregation-induced

- emission, supramolecular self-assembly and the optical waveguide of barbituric acid-functionalized tetraphenylethene. *J. Mater. Chem. C*, 2(10), 1801-1807 (DOI: 10.1039/C3TC32161D); (b) Zhang, G. F., Aldred, M. P., Gong, W. L., Li, C., Zhu, M. Q. (2012). Utilising tetraphenylethene as a dual activator for intramolecular charge transfer and aggregation induced emission. *Chem. Commun.*, 48(62), 7711-7713 (DOI: 10.1039/C2CC33218C).
- [21] (a) Sun, Q., Lam, J. W., Xu, K., Xu, H., Cha, J. A., Wong, P. C., Wen G., Zhang, X., Jing, X., Wang, F., Tang, B. Z. (2000). Nanocluster-containing mesoporous magnetoceramics from hyperbranched organometallic polymer precursors. *Chem. Mater.*, 12(9), 2617-2624 (DOI: <https://doi.org/10.1021/cm000094b>); (b) Tang, B. Z., Xu, H., Lam, J. W., Lee, P. P., Xu, K., Sun, Q., Cheuk, K. K. (2000). C60-containing poly (1-phenyl-1-alkynes): synthesis, light emission, and optical limiting. *Chem. Mater.*, 12(5), 1446-1455 (DOI: 10.1002/9783527629787); (c) Tang, B. Z., Geng, Y., Lam, J. W. Y., Li, B., Jing, X., Wang, X., Wang, F., Pakhomov, A.B., Zhang, X. X. (1999). Processible nanostructured materials with electrical conductivity and magnetic susceptibility: preparation and properties of maghemite/polyaniline nanocomposite films. *Chem. Mater.*, 11(6), 1581-1589 (DOI: 10.1021/cm9900305).
- [22] Roy, B., Reddy, M. C., Hazra, P. (2018). Developing the structure–property relationship to design solid state multi-stimuli responsive materials and their potential applications in different fields. *Chem. Sci.*, 9(14), 3592-3606. (DOI: 10.1039/C8SC00143J).
- [23] Katoh, R., Suzuki, K., Furube, A., Kotani, M., Tokumaru, K. (2009). Fluorescence quantum yield of aromatic hydrocarbon crystals. *J. Phys. Chem. C*, 113(7), 2961-2965 (DOI: 10.1021/jp807684m).
- [24] (a) Ma, C., Xu, B., Xie, G., He, J., Zhou, X., Peng, B., Jiang, L., Xu, B., Tian, W., Chi, Z., Liu, S., Zhang, Y., Xu, J. (2014). An AIE-active luminophore with tunable and remarkable fluorescence switching

based on the piezo and protonation–deprotonation control. *Chem. Commun.*, 50(55), 7374–7377 (DOI: 10.1039/C4CC01012D); (b) Sun, J., Xue, P., Sun, J., Gong, P., Wang, P., Lu, R. (2015). Strong blue emissive nanofibers constructed from benzothizole modified tert-butyl carbazole derivative for the detection of volatile acid vapors. *J. Mater. Chem. C*, 3(34), 8888–8894 (DOI: 10.1039/C5TC02012C); (c) Zhan, Y., Zhao, J., Yang, P., Ye, W. (2016). Multi-stimuli responsive fluorescent behaviors of a donor– $\pi$ –acceptor phenothiazine modified benzothiazole derivative. *RSC Adv.*, 6, 92144–92151. (DOI: <https://doi.org/10.1039/C6RA19791D>).

## Chapter 8

### Conclusions and future scope

---

---

#### 8.1. Conclusion

The development of organic molecules with tunable solid-state emission is of great importance owing to their wide range of applications such as organic light emitting diodes (OLEDs), sensors, bioimaging, stimuli-responsive materials and other optoelectronic devices.<sup>[1]</sup> Organic molecules exhibiting changes in their optical properties as a response to various external stimuli (such as pressure, light, pH, temperature) are known as stimuli-responsive materials.<sup>[2]</sup> Mechanochromic materials have emerged as one of the most promising stimuli-responsive materials owing to their potential applications in pressure sensors, rewritable inks, photo modulation, memory devices, luminescent switches, fluorescent probes, data storage materials.<sup>[3]</sup> The application of external stimuli for most of the stimuli-responsive materials has been successfully exploited in their solid state. Hence, stimuli-responsive materials essentially require solid-state emission which can be achieved by the phenomenon of aggregation-induced emission (AIE) discovered by Tang *et. al.*<sup>[4]</sup> The introduction of (AIE) active luminogens in conventional organic fluorophores that are usually non-emissive in solid state has proved to be a useful technique for furnishing solid-state emissive stimuli responsive materials.<sup>[5]</sup> The well-known AIE active molecules such as tetraphenylethylene, triphenylamine, phenothiazine have been utilized for the development of mechanochromic materials.<sup>[6]</sup> The solid-state emission majorly depends on the molecular packing modes and intermolecular interaction in the solid state.<sup>[6]</sup> Hence, tunable emission can be achieved by subtle changes in the molecular packing which are dependent on twisting or planarity in the structures, steric hindrance, inclusion of alkyl chains or heavy atoms, intermolecular interactions due to heteroatom or halogen effects, positional

isomerization.<sup>[6]</sup> Organic molecules utilizing different donor-acceptor frameworks such as D-A, D-A-D, D- $\pi$ -A *etc.* serve as excellent candidates for stimuli-responsive materials with applications in optoelectronics.<sup>[7]</sup> The incorporation of various heterocyclic acceptors and AIE donors can further allow modulation of the electronic, photophysical and stimuli-responsive properties. We have designed and synthesized donor-acceptor functionalized organic molecules and investigated the photophysical, electronic and stimuli-responsive properties such as mechanochromism, solvatochromism and acidochromism of these systems.

In Chapter 3, we have synthesized set of novel T-shaped donor-acceptor-donor type luminophores employing phenanthrene-quinoxaline (**PQ**) as acceptor **A** and acenaphthene-quinoxaline (**AQ**) as acceptor **A'** as central units substituted with phenothiazine (**PTZ**) as donor **D** and tetraphenylethylene (**TPE**) as donor **D'**. The D-A-D based symmetrical quinoxaline luminophores display intramolecular charge transfer (ICT) transitions which is confirmed by solvatochromism. In comparison to the TPE substituted luminophores, the PTZ based symmetrical luminophores possess higher donor-acceptor character to the owing to the higher donor character of PTZ. All the symmetrical quinoxaline luminophores exhibit emission enhancement induced by aggregation (AIE) due to the incorporation of AIEgens PTZ and TPE which makes them suitable solid-state emitters. The symmetrical quinoxaline luminophores display reversible mechanochromic behavior with a good color contrast and a morphological change from crystalline to amorphous is responsible for mechanochromism. The AIEgen PTZ exhibits better stimuli-responsive behavior as compared to AIEgen TPE owing to the better conformational flexibility of butterfly shaped PTZ unit. The contrasting donor-acceptor interaction between the two set of symmetrical quinoxaline luminophores can be exploited to tune the photophysical and electronic properties of these materials. The attachment of AIEgens PTZ and TPE to quinoxaline results in efficient solid-state emission with stimuli-responsive properties.<sup>[8]</sup>

In Chapter 4, we have designed and synthesized phenanthrene-quinoxaline (PQ) (acceptor A) and acenaphthene-quinoxaline (AQ) (acceptor A') based D-A-D'/D-A'-D' quinoxaline derivatives substituted with three different donors namely phenothiazine (PTZ), tetraphenylethylene (TPE) and N-substituted PTZ in an unsymmetrical fashion. The quinoxaline derivatives exhibit contrasting photophysical properties due to the unsymmetrical substitution of different donors which majorly affects the D-A character, structural geometries and intermolecular interactions in the solid state. The set of unsymmetrical derivatives using donors PTZ and TPE exhibit intense ICT emissions originating from both the TPE and PTZ donors which are highly solvent-dependent. The ICT emission corresponding to PTZ donor are highly polarized and stabilized in polar solvents as compared to the TPE due to the stronger donating ability of PTZ in comparison to TPE. In contrast, the unsymmetrical quinoxaline derivatives having N-PTZ substitution along with PTZ display reduced or quenched CT emissions in polar solvents owing to the formation of a twisted intramolecular charge transfer (TICT) state originating from the almost perpendicular positioned N-PTZ unit. The presence of AIEgens PTZ and TPE in one set of unsymmetrical derivatives allows intense emission in the aggregated state; however the unsymmetrical derivatives containing N-PTZ unit display quenching of emission in their aggregated state. The PTZ-TPE based unsymmetrical derivatives derivative display reversible emission switching on grinding with very high grinding induced spectral shift making them suitable stimuli-responsive materials and the mechanochromic performance is related to crystalline to amorphous phase change. The PTZ and N-PTZ based quinoxaline derivatives possess non-fluorescent solids although exhibit grinding induced color-switching. The donors PTZ and TPE turn out to be favorable in developing AIE active stimuli-responsive materials as compared to N-PTZ donor. The work gives a detailed analysis of utilizing donors with different strengths in unsymmetrical fashion with heterocyclic

$\pi$ -conjugated acceptor unit and its effect on the photophysical and electronic properties, solid-state emission and stimuli-responsive properties.<sup>[8]</sup>

In Chapter 5, we have designed and synthesized phenanthroimidazole (PI) functionalized positional isomers comprising of a weak donor tetraphenylethylene TPE and a strong donor triphenylamine TPA. The PI based positional isomers exhibit high thermal stability making them suitable for practical applications. The single crystal analysis reveals a propeller orientation of the TPA unit and TPE unit which endows the derivatives with strong AIE characteristics making the derivatives excellent solid-state emitters. The PI positional isomers display reversible emission changes in response to mechanical stimuli with a good colour contrast corresponding to a morphological change from amorphous state to crystalline state. The positional change alters the sensitivity of PI isomers towards mechanical stimuli. The combination of phenanthroimidazole, TPA and TPE synergistically result in high stimuli responsive solid-state emission.<sup>[9]</sup>

In Chapter 6, a series of D-A positional isomers were designed and synthesized by the functionalization of phenothiazine (**PTZ**) at *para*, *meta* and *ortho* positions of phenyl **BT**. The isomers were designed to regulate the donor-acceptor character as well as the intermolecular interactions in solid state and resulted in contrasting photophysical and electronic properties. The *para* isomer displayed strong ICT characteristics owing to enhanced conjugation due to lower degree of twisting compared to the *meta* and *ortho* isomers which displayed emission quenching in polar solvents due to formation of TICT state. All the isomers exhibit intensity enhancement in aggregated state and reversible mechanochromic characteristics owing to their non-planar twisted structures. The mechanochromic behaviour is associated with generation of metastable states and the crystalline to amorphous phase transformation. The isomers exhibit self-reversible colour switching owing to the conformational flexibility of PTZ moiety. The *para* isomer exhibits polymorphism owing

to the unique butterfly shape of PTZ moiety. The *meta* isomer has tightly packed crystal structure, which makes it less susceptible to grinding as compared to *ortho* isomer which has loosely packed structure, thereby exhibiting highest grinding induced spectral shift. The isomers are employed for sensing of trifluoroacetic acid. The adaptable conformations of PTZ moiety can regulate the intermolecular interactions resulting in molecules with distinct photophysical properties and stimuli-responsive materials with self-recovering mechanism.<sup>[10]</sup>

In Chapter 8, we have designed and synthesized multichromophoric D-A-A' isomers using benzothiazole (BT) and benzothiadiazole (BTD) as acceptors and tetraphenylethylene (TPE) as donor. The change of position of BTD-TPE with respect to the *ortho*, *meta* and *para* positions of BT also varies the acceptor strength. The isomers possess high thermal stability essential for fabrication in solid state devices. The isomers display distinct solvatochromic behavior in various polarity solvents with emission ranging from blue to orange with high bathochromic shifts. The non-planar framework of the isomers results in enhancement of intensity in the aggregated state. The isomers exhibit reversible mechanochromism between green to yellow in the order *para*>*meta*> *ortho* which has been exploited for the development of ink-free rewritable papers. A morphological conversion from crystalline to amorphous state is responsible for mechanochromism and leads to formation of metastable states. The highly twisted structure and tightly packed 3-D framework in *ortho* isomer results in lower response to mechanical stimuli as compared to *para*. The higher twisting and tight packing of *ortho* isomer reduces the flexibility of the donor moiety to achieve planarization on grinding. The isomers act as potential sensors for trifluoroacetic acid in solution and solid state. The combination of the three chromophores helps in developing effective solid-state emitters and stimuli-responsive materials. The positional changes allow fine tuning of acceptor strength and molecular packing inducing changes in the mechano-responsive behaviour.<sup>[11]</sup>

## 8.2. Future scope

The thesis highlights design strategies for development of donor-acceptor based stimuli-responsive materials. The use of various heterocyclic acceptors and AIE donors of different strengths in different donor-acceptor frameworks resulted in efficient solid-state emitters and stimuli-responsive materials. Further, the use of donor-acceptor systems, positional changes, different substitutions and incorporation of conformationally flexible moieties further helps in effective modulation of the photophysical, electronic and stimuli-responsive properties which was achieved by subtle changes in the molecular packing and intermolecular interactions. The solid-state emission and mechanochromic properties were explored and tuned depending upon the conjugation length and strength of donor-acceptor interaction. We have proposed that the change from twisted to planar structures is responsible for reversible mechanochromism and is associated with morphological transition from crystalline to amorphous forms. The donor-acceptor systems can also be successfully employed as sensors for acid detection and as rewritable inks. The work is of great importance and provides insights for designing different donor-acceptor functionalized solid-state emitters with reversible stimuli-responsive properties which can be finely tuned with physical structural changes. The opted strategy provides a new pathway in design of AIE active stimuli-responsive materials suitable for application as mechano-sensors, security paper, light emitting devices and other optoelectronic applications.

## 8.3. References

- [1] (a) Weder, C. (2011). Mechanoresponsive materials. *J. Mater. Chem.*, 21(23), 8235-8236 (DOI: 10.1039/C1JM90068D); (b) Kishimura, A., Yamashita, T., Yamaguchi, K., Aida, T. (2005). Rewritable phosphorescent paper by the control of competing kinetic and thermodynamic self-assembling events. *Nat. Mater.*, 4(7), 546-549 (DOI: 10.1038/nmat1401); (c) Farinola, G. M., Ragni, R. (2011).

- Electroluminescent materials for white organic light emitting diodes. *Chem. Soc. Rev.*, 40(7), 3467-3482 (DOI: 10.1039/C0CS00204F).
- [2] (a) Hirata, S., Watanabe, T. (2006), Reversible thermoresponsive recording of fluorescent images (TRF), *Adv. Mater.*, 18(20), 2725-2729 (DOI: <https://doi.org/10.1002/adma.200600209>); (b) Sagara, Y., Mutai, T., Yoshikawa, I., Araki, K. (2007), Material design for piezochromic luminescence: hydrogen-bond-directed assemblies of a pyrene derivative, *J. Am. Chem. Soc.*, 129(6), 1520-1521 (DOI: <https://doi.org/10.1021/ja0677362>); (c) Zhou, X., Wang, L., Wei, Z., Weng, G., He, J. (2019), An Adaptable Tough Elastomer with Moisture-Triggered Switchable Mechanical and Fluorescent Properties, *Adv. Funct. Mater.*, 29(34), 1903543 (DOI: <https://doi.org/10.1002/adfm.201903543>).
- [3] (a) Zhang, X., Chi, Z., Zhang, Y., Liu, S., Xu, J. (2013). Recent advances in mechanochromic luminescent metal complexes. *J. Mater. Chem. C*, 1(21), 3376-3390 (DOI: 10.1039/C3TC30316K).
- [4] (a) Mei, J., Leung, N. L., Kwok, R. T., Lam, J. W., Tang, B. Z. (2015). Aggregation-induced emission: together we shine, united we soar!. *Chem. Rev.*, 115(21), 11718-11940 (DOI: 10.1021/acs.chemrev.5b00263); (b) Luo, J., Xie, Z., Lam, J. W., Cheng, L., Chen, H., Qiu, C., Kwok, H.S., Zhan, X., Liu, Y., Zhu, D., Tang, B. Z. (2001). Aggregation-induced emission of 1-methyl-1, 2, 3, 4, 5-pentaphenylsilole. *Chem. Commun.*, (18), 1740-1741 (DOI: 10.1039/B105159H).
- [5] (a) Hu, R., Leung, N. L., Tang, B. Z. (2014). AIE macromolecules: syntheses, structures and functionalities. *Chem. Soc. Rev.*, 43(13), 4494-4562 (DOI: 10.1039/C4CS00044G); (b) Dong, Y., Lam, J. W., Qin, A., Liu, J., Li, Z., Tang, B. Z., Sun, J., Kwok, H. S. (2007). Aggregation-induced emissions of tetraphenylethene derivatives and their utilities as chemical vapor sensors and in organic light-emitting

- diodes. *Appl. Phys. Lett.*, *91*(1), 011111 (DOI: 10.1063/1.2753723); (c) Gong, Y., Tan, Y., Liu, J., Lu, P., Feng, C., Yuan, W. Z., Lu, Y., Sun, J.Z., He, G., Zhang, Y. (2013). Twisted D- $\pi$ -A solid emitters: efficient emission and high contrast mechanochromism. *Chem. Commun.*, *49*(38), 4009-4011 (DOI: 10.1039/C3CC39243K); (d) Chen, C., Li, R. H., Zhu, B. S., Wang, K. H., Yao, J. S., Yin, Y. C., Yao, M.M., Yao, H.B., Yu, S.H., (2018). Highly Luminescent Inks: Aggregation-Induced Emission of Copper-Iodine Hybrid Clusters. *Angew. Chem. Int. Ed.*, *57*(24), 7106-7110 (DOI: 10.1002/anie.201802932).
- [6] (a) Sasaki, S., Suzuki, S., Sameera, W. M. C., Igawa, K., Morokuma, K., Konishi, G. I. (2016). Highly twisted N, N-dialkylamines as a design strategy to tune simple aromatic hydrocarbons as steric environment-sensitive fluorophores. *J. Am. Chem. Soc.*, *138*(26), 8194-8206 (DOI: 10.1021/jacs.6b03749); (b) Xue, S., Qiu, X., Sun, Q., Yang, W. (2016). Alkyl length effects on solid-state fluorescence and mechanochromic behavior of small organic luminophores. *J. Mater. Chem. C*, *4*(8), 1568-1578 (DOI: 10.1039/C5TC04358A); (c) Yamaguchi, M., Ito, S., Hirose, A., Tanaka, K., Chujo, Y. (2016). Modulation of sensitivity to mechanical stimulus in mechanofluorochromic properties by altering substituent positions in solid-state emissive diiodo boron diimines. *J. Mater. Chem. C*, *4*(23), 5314-5319 (DOI: 10.1039/C6TC01111J); (d) Xu, B., Wu, H., Chen, J., Yang, Z., Yang, Z., Wu, Y. C., Zhang, Y., Jin, C., Lu, P.Y., Chi, Z., Liu, S., Aldred, M. (2017). White-light emission from a single heavy atom-free molecule with room temperature phosphorescence, mechanochromism and thermochromism. *Chem. Sci*, *8*(3), 1909-1914 (DOI: 10.1039/C6SC03038F).
- [7] (a) Zhang, Y., Chen, Z., Song, J., He, J., Wang, X., Wu, J., Chen, S., Qu, J., Wong, W. Y. (2019), Rational design of high efficiency green to deep red/near-infrared emitting materials based on isomeric donor-acceptor chromophores, *J. Mater. Chem. C*, *7*(7), 1880-1887 (DOI: 10.1039/C8TC05383A); (b) Tsujimoto, H., Ha, D. G., Markopoulos, G.,

- Chae, H. S., Baldo, M. A., Swager, T. M. (2017), Thermally activated delayed fluorescence and aggregation induced emission with through-space charge transfer, *J. Am. Chem. Soc.*, 139(13), 4894-4900 (DOI: <https://doi.org/10.1021/jacs.7b00873>); (c) Nakae, T., Nishio, M., Usuki, T., Ikeya, M., Nishimoto, C., Ito, S., Nishihara, H., Hattori, M., Hayashi, S., Yamada, T., Yamanoi, Y. (2021), Luminescent Behavior Elucidation of a Disilane-Bridged D–A–D Triad Composed of Phenothiazine and Thienopyrazine, *Angew. Chem. Int. Ed.*, 60(42), 22871-22878 (<https://doi.org/10.1002/anie.202108089>).
- [8] Ekbote, A., Jadhav, T., Misra, R. (2017) T-Shaped donor–acceptor–donor type tetraphenylethylene substituted quinoxaline derivatives: aggregation-induced emission and mechanochromism. *New J. Chem.*, 41, 9346–9353 (DOI: 10.1039/C7NJ01531C)
- [9] Ekbote, A., Han, S. H., Jadhav, T., Mobin, S. M., Lee, J. Y., Misra, R. (2018) Stimuli responsive AIE active positional isomers of phenanthroimidazole as non-doped emitters in OLEDs, *J. Mater. Chem. C*, 6, 2077–2087 (DOI:10.1039/C7TC05450E).
- [10] Ekbote, A., Mobin, S. M., Misra, R. (2020) Stimuli-responsive phenothiazine-based donor–acceptor isomers: AIE, mechanochromism and polymorphism, *J. Mater. Chem. C*, 8, 3589–3602 (DOI: 10.1039/C9TC05192A).
- [11] Ekbote, A., Mobin, S. M., Misra, R. (2018) Structure–property relationship in multi-stimuli responsive D–A–A' benzothiazole functionalized isomers, *J. Mater. Chem. C*, 6, 10888–10901.